

第48回 フラーレン・ナノチューブ・グラフェン 総合シンポジウム講演要旨集

平成27年2月21日～23日

第 48 回 フラーレン・ナノチューブ・グラフェン 総合シンポジウム

The 48th Fullerenes–Nanotubes–Graphene General Symposium



講演要旨集 Abstracts

2015 年 2 月 21 日(土)～ 23 日(月)
東京大学 伊藤国際学術研究センター

The University of Tokyo, ITO INTERNATIONAL RESEARCH CENTER

主催 フラーレン・ナノチューブ・グラフェン学会

The Fullerenes, Nanotubes and Graphene Research Society

共催

社会構想マネジメントを先導するグローバルリーダー養成プログラム(GSDM)

「社会構想構築のためのナノテクノロジー科学技術シンポジウム」

Global Leader Program for Social Design and Management (GSDM)

“Nanotechnology Symposium for Social Design and Management”

日本化学会

The Chemical Society of Japan

JST 戦略的国際共同研究プロジェクト IRENA

IRENA Project by JST-EC DG RTD,

Strategic International Collaborative Research Program, SICORP

東京大学 GMSI

The University of Tokyo

Graduate Program for Mechanical Systems Innovation (GMSI)

協賛

日本物理学会

The Physical Society of Japan

応用物理学会

The Japan Society of Applied Physics

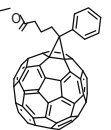
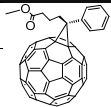
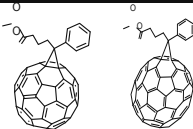
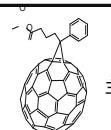
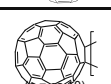
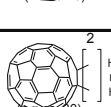
高分子学会

The Society of Polymer Science, Japan

電気化学会

The Electrochemical Society of Japan

nanom フロンティアカーボンのフラーレン製品

銘柄	分子構造	純度(HPLC面積%、代表値) 内容他	最低数量 (g)
nanom purple フラーレンC60		99	10
		99.5	2
		99.5/昇華精製品	2
		99.9/昇華精製品	1
		99.9/昇華精製/単結晶品	1
nanom orange フラーレンC70		97	1
		98/昇華精製品	0.5
nanom mix 混合フラーレン		C60,C70,その他高次 フラーレンの混合物 ※微粒化品(ST-F)もあります	50
nanom spectra [60]PCBM (phenyl C61-butylric acid methyl ester)		99	1
		99.5	1
		99.9	0.5
nanom spectra E400 bis[60]PCBM (bis-phenyl C61-butylric acid methyl ester)		98/異性体トータル ※位置異性体の混合物	1
nanom spectra E124 [60,70]PCBM		[60]PCBM、[70]PCBMの混合物	1
nanom spectra [70]PCBM (phenyl C71-butylric acid methyl ester)		99/異性体トータル ※位置異性体の混合物	0.5
		99.5/異性体トータル ※位置異性体の混合物	0.5
nanom spectra Q100 [60]インデン付加体		99	0.5
nanom spectra Q400 [60]インデン2付加体		99/異性体トータル ※位置異性体の混合物	1
nanom spectra D100 水酸化フラーレン		C ₆₀ OH _n n=10を主成分とする混合物	1
nanom spectra A100 水素化フラーレン		C ₆₀ H _n n=30を主成分とする混合物	1

※銘柄、取扱数量等は予告無く変更する場合がございます。 ※試験研究用途向けです。

当社製品は、下記から購入いただけます。直接お問い合わせください。

・関東化学株式会社 試薬事業本部

〒103-0022 東京都中央区日本橋室町2-2-1 TEL:03-6214-1090 FAX:03-3241-1047
http://www.kanto.co.jp E-mail:reag-info@gms.kanto.co.jp

・中山商事株式会社 筑波営業所 (担当 落合敬宝)

〒300-2651茨城県つくば市鬼ヶ窪1139-1 TEL:029-847-7355 FAX:029-847-1923
E-mail:nst15@nakayama-co.jp

<本資料に関するお問い合わせ先>

フロンティアカーボン株式会社【担当:梶原】

〒100-8086 東京都千代田区丸の内2-6-1丸の内パークビルディング24階

TEL:03-3210-2620 FAX:03-3210-4606 <http://www.f-carbon.com>

※弊社へのお問い合わせはHPよりお願いいたします。

Abstract of The 48th Fullerenes-Nanotubes-Graphene General Symposium

Sponsored by : The Fullerenes, Nanotubes and Graphene Research Society

Co-Sponsored by : Global Leader Program for Social Design and Management (GSDM)
“Nanotechnology Symposium for Social Design and Management”
The Chemical Society of Japan
IRENA Project by JST-EC DG RTD,
Strategic International Collaborative Research Program, SICORP
The University of Tokyo
Graduate Program for Mechanical Systems Innovation (GMSI)

Supported by : The Physical Society of Japan
The Japan Society of Applied Physics
The Society of Polymer Science, Japan
The Electrochemical Society of Japan

Date : February 21st (Sat) – 23rd (Mon), 2015

Place : The University of Tokyo, ITO INTERNATIONAL RESEARCH CENTER
7-3-1 Hongo, Bunkyo-ku, Tokyo 113-8656

Presentation Time : Special Lecture (25 min presentation + 5 min discussion)
General Lecture (10 min presentation + 5 min discussion)
Poster Preview (1 min presentation without discussion)

第 48 回フラーレン・ナノチューブ・グラフェン総合シンポジウム 講演要旨集

主催 : フラーレン・ナノチューブ・グラフェン学会

共催 : 社会構想マネジメントを先導するグローバルリーダー養成プログラム (GSDM)
「社会構想構築のためのナノテクノロジー科学技術シンポジウム」
日本化学会
JST 戦略的国際共同研究プロジェクト IRENA
東京大学大学院工学系研究科
「機械システム・イノベーション」プログラム (GMSI)

協賛 : 日本物理学会、応用物理学会、高分子学会、電気化学会

日時 : 平成 27 年 2 月 21 日 (土) ~ 23 日 (月)

場所 : 東京大学 伊藤国際学術研究センター 伊藤謝恩ホール
〒113-8656 東京都文京区本郷 7-3-1

発表時間 : 特別講演 (発表 25 分 + 質疑応答 5 分)
一般講演 (発表 10 分 + 質疑応答 5 分)
ポスタープレビュー (発表 1 分・質疑応答 なし)

展示団体御芳名 (五十音順、敬称略)

アイクストロン(株)
(株)アド・サイエンス
オックスフォード・インストゥルメンツ(株)
QuantumWise Japan(株)
共立出版(株)
サイバネットシステム(株)
シグマ アルドリッチ ジャパン(同)
(株)島津製作所
東京ダイレック(株)
ナカライテスク(株)
ナノフoton(株)
日本カンタム・デザイン(株)
(株)ニューメタルスエンドケミカルスコーポレーション
日立工機(株)
(株)堀場製作所
(株)名城ナノカーボン
レニショー(株)
ワケンビーテック(株)

広告掲載団体御芳名 (五十音順、敬称略)

アイクストロン(株)
WITec(株)
エクセルソフト(株)
(株)エリオニクス
共立出版(株)
(株)コロナ社
サーモフィッシャーサイエンティフィック(株)
ナカライテスク(株)
フロンティアカーボン(株)
(株)堀場製作所

Contents

Time Table	• • • • •	i
Chairperson	• • • • •	iii
Program	Japanese • • • • •	iv
	English • • • • •	xix
Abstracts	Special Lecture • • • • •	1
	General Lecture • • • • •	11
	Poster Preview • • • • •	45
Author Index	• • • • •	177

目次

早見表	• • • • •	i
座長一覧	• • • • •	iii
プログラム	和文 • • • • •	iv
	英文 • • • • •	xix
講演予稿	特別講演 • • • • •	1
	一般講演 • • • • •	11
	ポスター発表 • • • • •	45
発表索引	• • • • •	177

プログラム早見表

2月21日 (土)	
	受付開始 8:30~ 講演開始 9:30~
9:30	特別講演 (Yan Li) 9:30-10:00
10:00	一般講演 2件 10:00-10:30 (ナノチューブの生成と精製・内包ナノチューブ)
10:30	休憩 10:30-10:45
10:45	特別講演 (今津直樹) 10:45-11:15
11:15	一般講演 3件 (ナノチューブの生成と精製・ ナノチューブの応用) 11:15-12:00
12:00	昼食 (幹事会) 12:00-13:15
13:15	特別講演 (斉木幸一郎) 13:15-13:45
13:45	一般講演 4件 (グラフェンの応用・ ナノホーン・ナノ炭素粒子) 13:45-14:45
14:45	ポスタープレビュー (1P-1 ~ 1P-44) 14:45-15:45
15:45	ポスターセッション (多目的スペース) 15:45-17:30
17:30	休憩 17:30-18:00
18:00	チュートリアル 講師: 末永和知 産業技術総合研究所 (伊藤謝恩ホール) 18:00-19:30

19:30

2月22日 (日)	
	受付開始 8:30~ 講演開始 9:00~
9:00	特別講演 (Esko I. Kauppinen) 9:00-9:30
9:30	一般講演 3件 (ナノチューブの生成と精製・ ナノチューブの応用) 9:30-10:15
10:15	休憩 10:15-10:30
10:30	特別講演 (山田容子) 10:30-11:00
11:00	一般講演 4件 (フラーレンの化学・ 金属内包フラーレン・フラーレン) 11:00-12:00
12:00	昼食 12:00-13:15
13:15	授賞式 13:15-14:00
14:00	ポスタープレビュー (2P-1 ~ 2P-44) 14:00-15:00
15:00	ポスターセッション (多目的スペース) 15:00-16:45
16:45	特別講演 (加藤雄一郎) 16:45-17:15
17:15	一般講演 6件 (ナノチューブの物性) 17:15-18:45
18:45	懇親会 (多目的スペース) 18:45-20:45

20:45

2月23日 (月)	
	受付開始 8:30~ 講演開始 9:00~
9:00	特別講演 (長汐晃輔) 9:00-9:30
9:30	一般講演 4件 (グラフェンの物性・その他) 9:30-10:30
10:30	休憩 10:30-10:45
10:45	特別講演 (松田一成) 10:45-11:15
11:15	一般講演 3件 (グラフェンの物性・その他) 11:15-12:00
12:00	昼食 12:00-13:15
13:15	ポスタープレビュー (3P-1 ~ 3P-43) 13:15-14:15
14:15	ポスターセッション (多目的スペース) 14:15-16:00
16:00	特別講演 (北浦 良) 16:00-16:30
16:30	一般講演 4件 (グラフェン生成・その他・ グラフェンの応用) 16:30-17:30

17:30

特別講演 発表25分・質疑5分
一般講演 発表10分・質疑5分
ポスタープレビュー 発表1分・質疑なし

Time table

February 21 (Sat.)	
	Registration begins at 8:30
	Lectures begin at 9:30
9:30	Special Lecture (Yan Li) 9:30-10:00
10:00	General Lectures [2] (Formation and purification of nanotubes · Endohedral nanotubes) 10:00-10:30
10:30	Coffee Break 10:30-10:45
10:45	Special Lecture (Naoki Imazu) 10:45-11:15
11:15	General Lectures [3] (Formation and purification of nanotubes · Applications of nanotubes) 11:15-12:00
12:00	Lunch (Administrative meeting) 12:00-13:15
13:15	Special Lecture (Koichiro Saiki) 13:15-13:45
13:45	General Lectures [4] (Applications of graphene · Carbon nanoparticles · Nanohorns) 13:45-14:45
14:45	Poster Preview (1P-1 through 1P-44) 14:45-15:45
15:45	Poster Session (Event Space) 15:45-17:30
17:30	Coffee Break 17:30-18:00
18:00	Tutorial Lecturer: Kazutomo Suenaga AIST (Ito Hall) 18:00-19:30

19:30

February 22 (Sun.)	
	Registration begins at 8:30
	Lectures begin at 9:00
9:00	Special Lecture (Esko I. Kauppinen) 9:00-9:30
9:30	General Lectures [3] (Applications of nanotubes · Formation and purification of nanotubes) 9:30-10:15
10:15	Coffee Break 10:15-10:30
10:30	Special Lecture (Hiroko Yamada) 10:30-11:00
11:00	General Lectures [4] (Chemistry of fullerenes · Endohedral metallofullerenes · Fullerenes) 11:00-12:00
12:00	Lunch 12:00-13:15
13:15	Award Ceremony 13:15-14:00
14:00	Poster Preview (2P-1 through 2P-44) 14:00-15:00
15:00	Poster Session (Event Space) 15:00-16:45
16:45	Special Lecture (Yuichiro K. Kato) 16:45-17:15
17:15	General Lectures [6] (Properties of nanotubes) 17:15-18:45
18:45	Banquet (Event Space) 18:45-20:45

20:45

February 23 (Mon.)	
	Registration begins at 8:30
	Lectures begin at 9:00
9:00	Special Lecture (Kosuke Nagashio) 9:00-9:30
9:30	General Lectures [4] (Properties of graphene · Other topics) 9:30-10:30
10:30	Coffee Break 10:30-10:45
10:45	Special Lecture (Kazunari Matsuda) 10:45-11:15
11:15	General Lectures [3] (Properties of graphene · Other topics) 11:15-12:00
12:00	Lunch 12:00-13:15
13:15	Poster Preview (3P-1 through 3P-43) 13:15-14:15
14:15	Poster Session (Event Space) 14:15-16:00
16:00	Special Lecture (Ryo Kitaura) 16:00-16:30
16:30	General Lectures [4] (Graphene synthesis · Applications of graphene · Other topics) 16:30-17:30

17:30

Special Lecture: 25 min (Presentation) + 5 min (Discussion)
General Lecture: 10 min (Presentation) + 5 min (Discussion)
Poster Preview: 1 min (Presentation)

座長一覧 (Chairpersons)

2月21日(土)

(敬称略)

セッション	時 間	座 長
特別講演(Yan Li)	9:30 ~ 10:00	丸山 茂夫
一般講演	10:00 ~ 10:30	野田 優
特別講演(今津 直樹)	10:45 ~ 11:15	中嶋 直敏
一般講演	11:15 ~ 12:00	大野 雄高
特別講演(斉木 幸一郎)	13:15 ~ 13:45	吾郷 浩樹
一般講演	13:45 ~ 14:45	菅井 俊樹
ポスタープレビュー	14:45 ~ 15:45	長谷川 馨 小林 慶太
チュートリアル(末永 和知)	18:00 ~ 19:30	丸山 茂夫

2月22日(日)

セッション	時 間	座 長
特別講演(Esko I. Kauppinen)	9:00 ~ 9:30	篠原 久典
一般講演	9:30 ~ 10:15	岡崎 俊也
特別講演(山田 容子)	10:30 ~ 11:00	長汐 晃輔
一般講演	11:00 ~ 12:00	松尾 豊
ポスタープレビュー	14:00 ~ 15:00	宮田 耕充 項 榮
特別講演(加藤 雄一郎)	16:45 ~ 17:15	松田 一成
一般講演	17:15 ~ 18:45	小鍋 哲

2月23日(月)

セッション	時 間	座 長
特別講演(長汐 晃輔)	9:00 ~ 9:30	山本 貴博
一般講演	9:30 ~ 10:30	高井 和之
特別講演(松田 一成)	10:45 ~ 11:15	加藤 雄一郎
一般講演	11:15 ~ 12:00	北浦 良
ポスタープレビュー	13:15 ~ 14:15	宮内 雄平 井ノ上 泰輝
特別講演(北浦 良)	16:00 ~ 16:30	齋藤 弥八
一般講演	16:30 ~ 17:30	齋藤 晋

2月21日(土)

特別講演 発表 25分・質疑応答 5分
一般講演 発表 10分・質疑応答 5分
ポスタープレビュー 発表 1分・質疑応答 なし

特別講演 (9:30-10:00)

- 1S-1 What we know about chirality-controlled growth of single-walled carbon nanotubes 1
* Yan Li

一般講演 (10:00-10:30)

ナノチューブの生成と精製・内包ナノチューブ

- 1-1 Rh/Pd触媒下で共存する二つのチューブ成長メカニズム 11
* 阿知波 洋次, 児玉 拓也, 児玉 健, 橋本 健朗, 城丸 春夫
- 1-2 Ionic atomic chains inside carbon nanotubes 12
* 千賀 亮典, 末永 和知

>>>>>>> 休憩 (10:30-10:45) <<<<<<<<

特別講演 (10:45-11:15)

- 1S-2 次世代フレキシブルデバイス向け2層カーボンナノチューブ透明導電フィルム 2
* 今津 直樹, 大井 亮, 西野 秀和, 佐藤 謙一, 渡邊 修, 本田 史郎, 鈴木 基之

一般講演 (11:15-12:00)

ナノチューブの生成と精製・ナノチューブの応用

- 1-3 Selective Separation of Semiconducting Single-Walled Carbon Nanotubes Using Flavin Compounds 13
* 福澤 将史, 利光 史行, 加藤 雄一, 中嶋 直敏
- 1-4 単層カーボンナノチューブの構造選択におけるコール酸塩の役割 14
* 蓬田 陽平, 都築 真由美, 魏 小均, 平野 篤, 藤井 俊治郎, 田中 丈士, 片浦 弘道
- 1-5 コバルトセン内包CNTを用いた熱電材料の開発 15
* 藤ヶ谷 剛彦, 福丸 貴弘, 中嶋 直敏

>>>>>>> 昼食 (12:00-13:15) <<<<<<<<

特別講演 (13:15-13:45)

- 1S-3 熱放射顕微法によるグラフェン成長のリアルタイム観察 3
* 斉木 幸一郎, 寺澤 知潮, 加藤 頌

一般講演 (13:45-14:45)

グラフェンの応用・ナノホーン・ナノ炭素粒子

- 1-6 イオン照射による炭素材料の局所的な構造の制御およびワンステップ電着法によるPtナノ粒子の担持特性 16
* 早瀬 勝平, 吉竹 晴彦, 西村 智朗, 王 志朋, 緒方 啓典

2月21日(土)

1-7	中性子線捕捉療法のためのBNナノホーンの作製 * 飯泉 陽子, 岡崎 俊也, 張 民芳, 弓削 亮太, 市橋 鋭也, 中村 真紀, 池原 譲, 飯島 澄男, 湯田坂 雅子	17
1-8	ガン療法のための多機能性カーボンナノホーン複合体の開発 * Eijiro Miyako, Svetlana Chechetka, Benoit Pichon, Minfang Zhang, Masako Yudasaka, Sylvie Bégin-Colin, Alberto Bianco	18
1-9	爆轟法および太陽系外起源炭素隕石中ナノダイヤのLDI比較分析 * 田中 利彦, 山野井 亮子, 大澤 映二	19
ポスタープレビュー (14:45-15:45)		
ポスターセッション (15:45-17:30) (☆) 若手奨励賞候補		
その他		
1P-1	移動度測定による粒子帯電量の解析 * 菅井 俊樹, 廣芝 泰祐, 松林 広延, 三室 和暉, 陣内 涼太	45
ナノ環境と安全評価		
1P-2	Exciton-photon interaction in tip enhanced Raman spectroscopy of single wall carbon nanotubes * Thomas Czank, Pourya Airya, Riichiro Saito	46
ナノチューブの物性		
1P-3	(5,4)(6,4)(6,5)(8,6)カーボンナノチューブ酸化過程の第一原理計算 * 大淵 真理	47
1P-4	Bias-voltage induced absorption peaks in individual suspended carbon nanotubes ☆ * Takushi Uda, Masahiro Yoshida, Akihiro Ishii, Yuichiro K. Kato	48
1P-5	Photoluminescence studies on individual small-diameter carbon nanotubes * Shun Aota, Naoto Akizuki, Shinichiro Mouri, Xiaojun Wei, Takeshi Tanaka, Hiromichi Kataura, Kazunari Matsuda, Yuhei Miyauchi	49
1P-6	Assigning (n, m) of Random Single-Walled Carbon Nanotubes on Silicon Substrates by Resonant Raman Spectroscopy * Daqi Zhang, Feng Yang, Yan Li, Juan Yang	50
1P-7	Trions in individual air-suspended carbon nanotubes * Alexander Popert, Masahiro Yoshida, Yuichiro K. Kato	51
1P-8	電界下におけるCNT薄膜の電子物性 ☆ * 石山 佑, 岡田 晋	52
ナノチューブの応用		
1P-9	高密度CNTフォレストの面内伝導による隣接CNTの電氣的接触評価 * 稲葉 優文, 李 智宇, 鈴木 和真, 平野 優, 渋谷 恵, 明道 三穂, 乗松 航, 楠 美智子, 川原田 洋	53

2月21日(土)

1P-10	Overcoming the Quality-Quantity Trade-Off in Printing Carbon Nanotubes by Repetitive Dispersion-Extraction Process	54
☆	* <i>Hiroyuki Shirae, Dong Young Kim, Kei Hasegawa, Taishi Takenobu, Yutaka Ohno, Suguru Noda</i>	
1P-11	基板上の単層カーボンナノチューブナノギャップの制御形成と電界放出	55
	* <i>大塚 慶吾, 下村 勇貴, 井ノ上 泰輝, 千足 昇平, 丸山 茂夫</i>	
1P-12	ベンジル誘導体からの光誘起ラジカル生成を利用したカーボンナノチューブの表面修飾	56
	* <i>高田 知哉, 阿部 薫明</i>	
1P-13	ナノプレミキサーを利用したCNT, VGCFの新しい分散法	57
	* <i>生田 太郎, 高塚 隆之</i>	

ナノチューブの生成と精製

1P-14	単一構造単層カーボンナノチューブ光学異性体の光学特性	58
☆	* <i>魏 小均, 都築 真由美, 平川 琢也, 蓬田 陽平, 平野 篤, 藤井 俊治郎, 田中 丈士, 片浦 弘道</i>	
1P-15	サブミリメートル長カーボンナノチューブの小粒径セラミックス担体上での流動層合成	59
☆	* <i>川端 孝祐, 陳 忠明, 長谷川 馨, 大沢 利男, 野田 優</i>	
1P-16	Controlled Growth of Single-Walled Carbon Nanotubes Using W-Co Catalyst at Different Temperatures and Carbon Feedings	60
	* <i>Feng Yang, Xiao Wang, Daqi Zhang, Juan Yang, Yan Li</i>	
1P-17	アセチレンブラック粒子上でのカーボンナノチューブ合成による複合化と、秒スケールでの反応制御	61
☆	* <i>栗谷 匡明, 長谷川 馨, 原田 祐作, 野田 優</i>	
1P-18	FT-ICRによるエタノール分子およびアセトニトリル分子と遷移金属クラスターの反応分析	62
	* <i>小笠原 一樹, 戸張 雄太, 佐藤 仁紀, 斎藤 真琴, 千足 昇平, 菅井 俊樹, 丸山 茂夫</i>	
1P-19	単層カーボンナノチューブの火炎合成と、温度場・反応制御	63
☆	* <i>山口 麻衣, 長谷川 馨, 大沢 利男, 野田 優</i>	
1P-20	An Effective Method for the Production of Single Walled Carbon Nanotubes by the Bipolar Pulsed Arc Discharge Method	64
	* <i>Kazi Haniun Maria, Tetsu Mieno</i>	

グラフェン生成

1P-21	SiO ₂ 上h-BNの上面および周囲への数層～多層グラフェンの選択的析出	65
☆	* <i>山口 航太郎, 長谷川 馨, 野田 優</i>	
1P-22	WS ₂ /MoS ₂ ヘテロ構造の二段階成長と評価	66
☆	* <i>森 勝平, 真庭 豊, 宮田 耕充</i>	
1P-23	分子蛍光性を持つグラフェン量子ドットの生成	67
	* <i>高橋 未咲, 菅井 俊樹</i>	

2月21日(土)

1P-24	2層グラフェンの作製及び電気特性	68
☆	* 星野 峻, 木村 諒也, 今井 健太郎, 林 佑太郎, 永田 知子, 岩田 展幸, 山本 寛	
1P-25	WドープNbS ₂ 原子層の成長と評価	69
☆	* 佐々木 将悟, 真庭 豊, 宮田 耕充	
グラフェンの応用		
1P-26	パイ共役高分子マイクロ球体の酸化グラフェンによる被覆	70
	* 愛敬 雄介, 田畑 顕一, 榎田 創, ダニエル ブラーム, 桑原 純平, 神原 貴樹, 近藤 剛弘, 中村 潤児, タン ダオ デュイ, 石井 智, 長尾 忠昭, アクセル ロルケ, 山本 洋平	
1P-27	Direct and real-time TEM observation of aqueous solution sandwiched by graphene layers	71
☆	* Yuki Sasaki, Ryo Kitaura, Hisanori Shinohara	
1P-28	グラフェンの近接効果における基板表面構造の影響	72
	泉山 彰里, * 高井 和之	
グラフェンの物性		
1P-29	単層遷移金属カルコゲナイドで構成されるファンデルワールスヘテロ構造の発光特性	73
	* 毛利 真一郎, 小澤 大知, 江田 剛輝, 宮内 雄平, 松田 一成	
1P-30	Crossover between Localization and Delocalization in Edge-Disordered Graphene Nanoribbons	74
☆	* 高島 健悟, 山本 貴博	
1P-31	G* band Raman spectra of single layer graphene revisited	75
	* シレガール シヤハリル, ハスデオ ヘスキ, ヌグラハ アフマド, リウ ハシアン, 齋藤 理一郎	
1P-32	コランニユレンポリマーの構造と電子構造	76
☆	* 成田 康平, 岡田 晋	
1P-33	微量水素終端したグラフェンにおけるスピン軌道相互作用と電子波位相破壊の抑制	77
	上條 潤一, * 片桐 勇人, 加藤 建彰, 中村 壮智, 勝本 信吾, 江澤 雅彦, Barbaros Özyilmaz, 春山 純志	
その他		
1P-34	黒リン単原子層の特異な電子物性	78
	片桐 勇人, 牧野 竜也, * 大島 智佳, 中村 壮智, 勝本 信吾, 江澤 雅彦, 篠原 久典, 春山 純志	
1P-35	黒リン単原子層のエッジ磁性	79
	* 中西 雄大, 大島 智佳, 岩城 稜磨, 野村 くみ子, 江澤 雅彦, 篠原 久典, 春山 純志	
ナノチューブの物性		
1P-36	イオン化ゲルゲートを配した金属伝導カーボンナノチューブ膜の電子物性	80
	* 本間 友大, 菊地 涼, 山田 俊矢, 大島 智佳, 小谷田 美保, 春山 純志, Apparao Rao	

2月21日(土)

ナノ炭素粒子

- 1P-37 カーボンナノポットの生成に対する酸化グラフェンの光還元効果 81
* 横井 裕之, 畠山 一翔, 松本 正吾, 上田 茉莉, 谷口 貴章, 鯉沼 陸央, 松本 泰道
- 1P-38 ナノダイヤモンドの電子物性と構造及びそのフッ素化効果 82
☆ * 黄金 健太, 東原 秀和, 服部 義之, 高井 和之
- 1P-39 自己摩耗法によるマイクロダイヤモンドの球形化:予備的結果 83
* 山野井 亮子, 大澤 映二

その他

- 1P-40 The Topological Structure of Starfish Nanocarbon 84
* Natsuki Namba, Yukihiro Takada, Kyoko Nakada
- 1P-41 Double resonance Raman modes in mono- and few-layer MoTe₂ 85
* Huaihong Guo, Teng Yang, Mahito Yamamoto, Lin Zhou, Ryo Ishikawa, Keiji Ueno, Kazuhito Tsukagoshi, Zhidong Zhang, M. S. Dresselhaus, R. Saito
- 1P-42 Improving the property of electric double layer capacitor by using activated carbon nanoballoon 86
* Akitaka Mizutani, Yoshiyuki Suda, Hirofumi Takikawa, Hitoshi Ue, Kazuki Shimizu, Yoshito Umeda
- 1P-43 Spontaneous antiferromagnetism in the α -graphyne single layer 87
* Teng Yang, Baojuan Dong, Huaihong Guo, R. Saito, Zhidong Zhang
- 1P-44 亜鉛をドーピングした酸化鉄ナノチューブと有機金属ハライドペロブスカイト複合膜の分光感度特性 88
* 小杉 優太, 楠田 寛之, 斉木 彩乃, 坂東 俊治

>>>>>>> 休憩 (17:30-18:00) <<<<<<<<

チュートリアル (18:00-19:30)

- 電子顕微鏡によるナノカーボン構造評価
* 末永 和知

2月22日(日)

特別講演 発表 25分 ・ 質疑応答 5分
一般講演 発表 10分 ・ 質疑応答 5分
ポスタープレビュー 発表 1分 ・ 質疑応答 なし

特別講演 (9:00-9:30)

2S-4 STUDIES ON SWNT BUNDLING 4
* Esko I. Kauppinen

一般講演 (9:30-10:15)

ナノチューブの応用 ・ ナノチューブの生成と精製

- 2-1 フレキシブル有機太陽電池のための電子ブロック透明電極としての酸化モリブデンでドーピングした直接・乾式堆積による単層カーボンナノチューブ膜 20
* 田 日, Kehang Cui, 千葉 孝昭, Anton Anisimov, Albert Nasibulin, Esko Kauppinen, 丸山 茂夫, 松尾 豊
- 2-2 単層カーボンナノチューブカソードを用いたペロブスカイト型太陽電池の評価 21
* 千葉 孝昭, 坂口 貴寛, Nasibulin Albert, Kauppinen Esko, 項 榮, 千足 昇平, 丸山 茂夫
- 2-3 SiC表面分解法により形成したカーボンナノチューブフォレストからの無触媒CVD成長 22
* 平野 優, 稲葉 優文, 渋谷 恵, 鈴木 和真, 李 智宇, 明道 三穂, 平岩 篤, 乗松 航, 楠 美智子, 川原田 洋

>>>>>>> 休憩 (10:15-10:30) <<<<<<<<<

特別講演 (10:30-11:00)

2S-5 グラフェンナノリボンの戦略的 ボトムアップ合成への提案 5
* 山田 容子, 林 宏暢

一般講演 (11:00-12:00)

フラーレンの化学 ・ 金属内包フラーレン ・ フラーレン

- 2-4 分子性フラーライド塩[lucigenin]C₆₀の構造と電子状態 23
* 森山 広思, 山本 翔平, 森 初果, 与座 健治, 原 英之
- 2-5 電子ドナー性物質および極性溶媒を用いた金属内包フラーレン分離法 24
* 千葉 和喜, 秋山 和彦, 久富木 志郎
- 2-6 C₆₀への多段階環化付加反応の振電相互作用密度解析 25
* 春田 直毅, 佐藤 徹, 田中 一義
- 2-7 レーザー蒸発条件下における直線炭素分子からフラーレンまで 26
* 若林 知成, 和田 資子, 森澤 勇介, 遠藤 瞳, 田口 裕貴, 松本 淳, 兒玉 健, 阿知波 洋次, 城丸 春夫

>>>>>>> 昼食 (12:00-13:15) <<<<<<<<<

大澤賞・飯島賞・若手奨励賞の授賞式 (13:15-14:00)

2月22日(日)

ポスタープレビュー (14:00-15:00)

ポスターセッション (15:00-16:45) (☆) 若手奨励賞候補

フラーレンの化学

- 2P-1 (5,6)-および(6,6)-[Li⁺@C₆₁Ph₂]NTf₂⁻のそれぞれの異性体についての単離とキャラクターゼーション 89
* 岡田 洋史, 川上 裕貴, 青柳 忍, 松尾 豊
- 2P-2 オキサゾリノ[70]フラーレン誘導体の構造変化を利用した有機太陽電池における開放電圧向上へのアプローチ 90
* 松尾 豊, Shu-Hui Li, Zong-Jun Li, 中川 貴文, James Ryan, Xiang Gao
- 2P-3 固体¹H-NMR分光法による水酸化フラーレン固体のプロトンダイナミクスに与える水分子の影響 91
* 佐野 喜章, 緒方 啓典

金属内包フラーレン

- 2P-4 Photoinduced Electron Transfer from Anionic Phthalocyanines to Li⁺@C₆₀ and Light-Energy Conversion 92
☆ * Yuki Kawashima, Kei Ohkubo, Vicente Manuel Blas-Ferrando, Hayato Sakai, Enrique Font-Sanchis, Javier Ortíz, Fernando Fernández-Lázaro, Taku Hasobe, Angela Sastre-Santos, Shunichi Fukuzumi
- 2P-5 Addition Reactions of Trimetallic Nitride Template Endohedral Metallofullerenes with Disilirane and Digermirane 93
* 宮部 恭輔, 加固 昌寛, 佐藤 久美子, 鈴木 光明, 溝呂木 直美, Marilyn M. Olmstead, Alan L. Balch, Wei-Wei Wang, 永瀬 茂, 赤坂 健

フラーレン

- 2P-6 ナノサターのエネルギー論 94
☆ * 木暮 聖太, 大町 遼, 篠原 久典, 岡田 晋
- 2P-7 電場下における水内包フラーレンのエネルギー論 95
* 反町 純也, 岡田 晋
- 2P-8 Absolute yield of fullerene formed by graphite laser ablation at room temperature 96
☆ * Hitomi Endo, Yuki Taguchi, Jun Matsumoto, Tomonari Wakabayashi, Takeshi Kodama, Yohji Achiba, Haruo Shiromaru

ナノチューブの物性

- 2P-9 カイラリティ分離したDNA修飾ナノチューブを用いた薄膜トランジスタの作製と評価 97
* 桑原 有紀, 二瓶 史行, 大森 滋和, 斎藤 毅
- 2P-10 潰れたカーボンナノチューブの安定性と電子構造 98
* 西川 潤平, 斎藤 晋
- 2P-11 単層カーボンナノチューブの化学修飾による電子準位への影響(1): 実験による解明 99
☆ * 白石 智也, 秋月 直人, 宮内 雄平, 松田 一成, 中嶋 直敏

2月22日(日)

2P-12	Effect of Chemical Doping on the Electronic States of Single-Walled Carbon Nanotubes: Theory * <i>Gergely Juhasz</i> , 白石 智也, 中嶋 直敏	100
2P-13	Ab initio calculation for electronic bands of CNT in which the chain of sulphur is inserted * <i>Yuhei Natsume</i>	101
ナノチューブの応用		
2P-14	電気二重層キャリア注入により極性制御された半導体型単層カーボンナノチューブ熱電デバイスの作製 * 大島 侑己, 北村 典雅, 神田 翔平, 河合 英輝, 中井 祐介, 真庭 豊, 柳 和宏	102
2P-15	医療応用にむけた単層カーボンナノチューブの水溶化と細胞毒性評価 ☆ * 中村 圭祐, 趙 利, 秦 紅梅, 青沼 秀児, 木村 隆英, 小松 直樹	103
2P-16	Gate-controlled generation of optical pulse trains using individual carbon nanotubes <i>Ming Jiang, Yusuke Kumamoto</i> , * <i>Akihiro Ishii, Masahiro Yoshida, Takashi Shimada, Yuichiro K. Kato</i>	104
2P-17	Electroluminescence from individual air-suspended carbon nanotubes within split-gate structures * <i>Noriyuki Higashide, Ming Jiang, Takushi Uda, Masahiro Yoshida, Akihiro Ishii, Yuichiro K. Kato</i>	105
ナノチューブの生成と精製		
2P-18	ゲルを用いた単層カーボンナノチューブの分離における酸化剤の効果 * 平野 篤, 田中 丈士, 片浦 弘道	106
2P-19	Optimization of the synthesis parameters of Carbon Nanotube (CNT) forest using the Taguchi Method ☆ * <i>パンダー アダム, 古田 寛, 八田 章光</i>	107
2P-20	木質バイオエタノールからの単層カーボンナノチューブの合成 * 荒木 拓馬, 本田 淳, 藪下 侑平, 村上 俊也, 木曾田 賢治, 山口 真範, 伊東 千尋	108
2P-21	Nitrogen doping of single-walled carbon nanotubes prepared from fluorinated SWCNTs using ammonia gas ☆ * <i>Koji Yokoyama, Yoshinori Sato, Kazutaka Hirano, Kenichi Motomiya, Kazuyuki Tohji, Yoshinori Sato</i>	109
2P-22	欠陥のない単層カーボンナノチューブ成長の分子動力学シミュレーション * 吉川 亮, 高木 勇海, 千足 昇平, 丸山 茂夫	110
2P-23	Automatic Gradient Elution Gel Filtration for Separation of Metal and Semiconducting Single-Wall Carbon Nanotubes ☆ * <i>Boanerges Thendie, Haruka Omachi, Ryo Kitaura, Yasumitsu Miyata, Hisanori Shinohara</i>	111
2P-24	超分子ポリマーによる半導体性カーボンナノチューブの選択的かつ可逆的抽出 * 利光 史行, 中嶋 直敏	112

2月22日(日)

内包ナノチューブ

- 2P-25 Structural transformation of tellurium encapsulated in the inner space of carbon nanotubes depending on tube diameter 113
* 小林 慶太, 保田 英洋
- 2P-26 カーボンナノチューブの内部空間を鋳型にしたダイヤモンド分子鎖の合成 114
☆ * 中西 勇介, 大町 遼, Fokina Natalie A., 北浦 良, Schreiner Peter R., Dahl Jeremy E. P., Carlson Robert M. K., 篠原 久典
- 2P-27 カーボンナノチューブに内包された複数パイ共役系オリゴマーの特性に関する量子化学計算 115
* 湯村 尚史, 山下 裕生

グラフェン生成

- 2P-28 エピタキシャル銅表面における単層グラフェン成長のダイナミクス 116
☆ * 太田 勇二郎, 水野 清義, 日比野 浩樹, 河原 憲治, 滝沢 里奈, 辻 正治, 吾郷 浩樹
- 2P-29 微小酸化グラフェンの作製とそのバイオ分野への応用可能性 117
* 張 民芳, 岡崎 俊也, 飯泉 陽子, 都 英二郎, 飯島 澄男, 湯田坂 雅子
- 2P-30 金属融解によるCVDグラフェンの絶縁性基板上への直接転写 118
☆ * 井上 凌介, 真庭 豊, 宮田 耕充
- 2P-31 反応性指標としての振電相互作用密度: グラフェンフラグメントのDiels-Alder反応への応用 119
春田 直毅, * 佐藤 徹, 田中 一義
- 2P-32 グラファイト上における高品質単層WS₂の成長 120
☆ * 小林 佑, 佐々木 将悟, 森 勝平, 日比野 浩樹, 渡邊 賢司, 谷口 尚, 真庭 豊, 宮田 耕充

グラフェンの物性

- 2P-33 アームチェア型グラフェンナノリボンによる光電場振幅変調: 第一原理計算による研究 121
* Yoshiyuki Miyamoto, Hong Zhang
- 2P-34 Spectroscopic studies of single layer molybdenum ditelluride 122
* Sandhaya Koirala, Daichi Kozawa, Shinichiro Mouri, Yuhei Miyauchi, Kazunari Matsuda
- 2P-35 単層遷移金属ダイカルコゲナイドのゼーベック効果 123
* 金橋 魁利, 蒲 江, Nguyen Thanh Cuoug, Lain-Jong Li, 岡田 晋, 太田 裕道, 竹延 大志
- 2P-36 金属電極間に架橋されたグラフェンの電気伝導特性 124
* 實宝 秀幸, 岡田 晋, 大淵 真理
- 2P-37 グラフェンにおけるフォノンの非調和性と熱伝導 125
* 水野 将志, 齋藤 理一郎
- 2P-38 エピタキシャルグラフェンの構造と電子物性および分子吸着効果 126
* 中本 圭亮, 赤津 隆, 高井 和之

2月22日(日)

2P-39	欠陥グラフェン吸着によるグラフェンのバンドギャップ形成 * 岸本 健, 岡田 晋	127
2P-40	Fabrication and In-situ TEM Characterization of Freestanding Graphene Nanoribbons Devices ☆ * Qing Wang, Ryo Kitaura, Shoji Suzuki, Hisanori Shinohara	128
その他		
2P-41	グラファイト面に垂直なガスフローによって運ばれるグラファイトレーザーアブレーション生成物 * 田口 裕貴, 遠藤 瞳, 阿部 百合香, 松本 淳, 若林 知成, 兒玉 健, 阿知波 洋次, 城丸 春夫	129
2P-42	二次元結晶の相転移制御と新機能 ☆ * 吉田 将郎, 張 奕勁, 叶 劍挺, 鈴木 龍二, 今井 康彦, 木村 滋, 藤原 明比古, 岩佐 義宏	130
2P-43	Structure and Spectra of Polyyne-Iodine Complex * 長島 大, 佐藤 徹, 岩原 直也, 田中 一義, 和田 資子, 若林 知成	131
2P-44	Ambipolar transistor and superconductivity in transition metal dichalcogenides * Wu Shi, Jianting Ye, Yijing Zhang, Ryuji Suzuki, Masaro Yoshida, Naoko Inoue, Yu Saito, Yoshihiro Iwasa	132

特別講演 (16:45-17:15)

2S-6	Single carbon-nanotube photonics and optoelectronics * 加藤 雄一郎	6
------	--	---

一般講演 (17:15-18:45)

ナノチューブの物性

2-8	単層カーボンナノチューブの光学遷移における塩基配列に依存したDNAの吸着効果 * 伊藤 雅浩, 伊藤 悠介, 加藤 大樹, 梅村 和夫, 本間 芳和	27
2-9	ドーピングされた原子層物質における電子構造と極性 * 斎藤 晋, 是常 隆, 藤本 義隆	28
2-10	Electronic States of Flattened Carbon Nanotubes: Effects of tube chirality and displacement * 中西 毅, 安藤 恒也	29
2-11	Coherent and squeezed phonons in single wall carbon nanotubes * ヌグラハ アフマド, ハスデオ エッドウィ, 齋藤 理一郎	30
2-12	Stark effect of excitons in individual air-suspended carbon nanotubes * Masahiro Yoshida, Yusuke Kumamoto, Akihiro Ishii, Akio Yokoyama, Yuichiro K. Kato	31
2-13	Exciton diffusion, end quenching, and exciton-exciton annihilation in individual air-suspended carbon nanotubes * Akihiro Ishii, Masahiro Yoshida, Yuichiro K. Kato	32

2月23日(月)

特別講演 発表 25分 ・ 質疑応答 5分
一般講演 発表 10分 ・ 質疑応答 5分
ポスタープレビュー 発表 1分 ・ 質疑応答 なし

特別講演 (9:00-9:30)

- 3S-7 グラフェン電界効果トランジスタ —コンダクタンス法によるギャップ内準位解析— 7
* 長汐 晃輔

一般講演 (9:30-10:30)

グラフェンの物性 ・ その他

- 3-1 電極接合に起因する二層グラフェンのバンドギャップ 33
* 野内 亮
- 3-2 還元した酸化グラフェン薄膜のバンドライク伝導 34
* 根岸 良太, 赤堀 誠志, 山田 省二, 伊藤 孝寛, 渡辺 義夫, 小林 慶裕
- 3-3 Circularly polarized luminescence from lateral TMD *p-i-n* junctions 35
* Yijin Zhang, Masaru Onga, Yoshihiro Iwasa
- 3-4 Mechanical exfoliation and van der Waals assembly of layered ferromagnetic dichalcogenide Fe_xTaS_2 36
* 荒井 美穂, 守谷 頼, 矢吹 直人, 増淵 寛, 上野 啓司, 町田 友樹

>>>>>>> 休憩 (10:30-10:45) <<<<<<<<

特別講演 (10:45-11:15)

- 3S-8 ナノカーボン物質・原子層物質のナノ光科学とその応用 8
* 松田 一成

一般講演 (11:15-12:00)

グラフェンの物性 ・ その他

- 3-5 単層黒リン”phosphorene”の光学特性 37
* 中村 隆, 小澤 大知, 毛利 真一郎, 松田 一成
- 3-6 遷移金属ダイカルコゲナイドにおけるバレー分極緩和の理論的研究 38
* 小鍋 哲, 岡田 晋
- 3-7 3R-MoS₂の励起子 39
* 鈴木 龍二, Sandor Bordacs, 明石 遼介, 越智 正之, 有田 亮太郎, 十倉 好紀, 岩佐 義宏

>>>>>>> 昼食 (12:00-13:15) <<<<<<<<

2月23日(月)

ポスタープレビュー (13:15-14:15)

ポスターセッション (14:15-16:00) (☆) 若手奨励賞候補

フラーレンの応用

- 3P-1 Solid-State NMR Studies on the Aggregated Structures of Organic Bulk Heterojunction Solar Cells with Solvent Additives(II) 133
* Saki Kawano, Hironori Ogata
- 3P-2 低いLUMO準位を有するスピロ-1,3-ジオキソラノフラーレンの開発とローバンドギャップポリマーを用いた有機薄膜太陽電池への応用 134
☆ * 三木江 翼, 佐伯 昭紀, 伊熊 直彦, 小久保 研, 関 修平
- 3P-3 スタック構造を用いた半透明タンデム有機薄膜太陽電池の作製 135
* 藤井 俊治郎, 田中 丈士, 片浦 弘道

金属内包フラーレン

- 3P-4 [5,6]-pyrrolidino-Sc₃N@I_h-C₈₀ジアステレオマーの単離とキャラクタリゼーション 136
* 前田 優, 木村 仁士, 上田 ちひろ, 鈴木 光明, 山田 道夫, Nikolaos Karousis, Nikos Tagmatarchis, Marilyn M Olmstead, Alan L Balch, Wei-Wei Wang, 永瀬 茂, 赤坂 健
- 3P-5 Reactions of Trimetallic Nitride Template Endohedral Metallofullerenes with Silacyclopropanes 137
* 南 和也, 杉浦 健, 加固 昌寛, 佐藤 久美子, 永瀬 茂, 赤坂 健
- 3P-6 Ionic Donor-Acceptor Supramolecules: Complexation of Molecular Nanocarbons with Cationic Li⁺@C₆₀ 138
* Hiroshi Ueno, Taishi Nishihara, Katsuma Matsui, Yasutomo Segawa, Kenichiro Itami

ナノチューブの物性

- 3P-7 単層カーボンナノチューブの特性に対する純度の量的重要性 139
* 松本 尚之, Chen Guohai, 湯村 守雄, フタバドン, 畠 賢治
- 3P-8 バンドルしたSWNTのRBM周波数に関する分子動力学計算 140
☆ * 紅谷 篤史, 本間 直樹, 千足 昇平, 本間 芳和, 山本 貴博
- 3P-9 Molecular structure of chalcogen encapsulated in single-walled carbon nanotubes studied by molecular dynamics simulations 141
* Yutaka Sato, Yosuke Kataoka, Hironori Ogata
- 3P-10 分子動力学シミュレーションによる単層カーボンナノチューブに内包されたアルカリハライドの局所構造と特性 142
* 横倉 瑛太, 片岡 洋右, 緒方 啓典

ナノチューブの応用

- 3P-11 Ultralow mode-volume photonic crystal nanobeam cavities for high-efficiency coupling to individual carbon nanotube emitters 143
* Hidenori Machiya, Ryohei Miura, Saneyuki Imamura, Ryuichi Ohta, Akihiro Ishii, Xuqing Liu, Takashi Shimada, Satoshi Iwamoto, Yasuhiko Arakawa, Yuichiro K. Kato

2月23日(月)

- 3P-12 Characteristic variation of thin-film transistors based on purified semiconducting carbon nanotubes 144
☆ * *Jun Hirotsu, Ryotaro Matsui, Shigeru Kishimoto, Yutaka Ohno*
- 3P-13 Thermoelectric power of carbon nanotubes from first principles 145
* *グエン タン フン, 齋藤 理一郎*
- 3P-14 Effect of TiO₂ coating on field emission properties of carbon nanotube by in-situ transmission electron microscopy 146
☆ * *松田 薫洋, 中原 仁, 安坂 幸師, 齋藤 弥八*
- 3P-15 Light-emitting Electrochemical Cell with Few-Walled Carbon-Nanotube Electrodes 147
* *中山 航, 白江 宏之, 野田 優, 坂上 知, 竹延 大志*

ナノチューブの生成と精製

- 3P-16 高真空アルコールガスソース法によるRh触媒からの単層カーボンナノチューブ成長 148
* *小澤 顕成, 才田 隆広, 成塚 重弥, 丸山 隆浩*
- 3P-17 Relationship between Chirality Control of Single-Walled Carbon Nanotube and Wavelength of the Irradiated Free Electron Laser 149
☆ * *吉田 圭佑, 津田 悠作, 川口 大貴, 永田 知子, 岩田 展幸, 山本 寛*
- 3P-18 Synthesis of single walled carbon nanotubes by using sputtered Co/Cu and Co/W as catalyst 150
* *Hua An, Kehang Cui, Rong Xiang, Taiki Inoue, Shohei Chiashi, Shigeo Maruyama*
- 3P-19 ホットウォール型化学気相成長装置と自由電子レーザーを用いた単層カーボンナノチューブカーボンの面内配向成長とカイラリティ制御 151
☆ * *川口 大貴, 吉田 圭介, 永田 知子, 岩田 展幸, 山本 寛*
- 3P-20 FT-ICR質量分析器によるH₂Oとの反応におけるコバルトクラスター上の水素原子の効果の解析 152
* *戸張 雄太, 小笠原 一樹, 佐藤 仁紀, 斎藤 真琴, 千足 昇平, 丸山 茂夫, 菅井 俊樹*
- 3P-21 Synthesis of carbon nanotubes by means of “molecular template epitaxial growth” approach 153
☆ * *Liu Hong, Akira Takakura, Lawrence Scott, Yuhei Miyauchi, Kenichiro Itami*
- 3P-22 フラーレンを有するカルバゾールフルオレン共重合体による半導体性単層カーボンナノチューブの可溶化および複合化 154
* *利光 史行, 小澤 寛晃, 中嶋 直敏*

ナノホーン

- 3P-23 Cytotoxicity of Carbon Nanohorns Enhanced by Too Much PLPEG 155
* *Maki Nakamura, Yoshio Tahara, Shinsuke Fukata, Minfang Zhang, Sumio Iijima, Masako Yudasaka*
- 3P-24 ホウ素と窒素をドーピングしたカーボンナノホーン集合体の電気化学特性 156
* *弓削 亮太, 坂東 俊治, 湯田坂 雅子, 當山 清彦, 飯島 澄男, 田村 宜之, 眞子 隆志*

2月23日(月)

グラフェン生成

- 3P-25 グラフェンの亀裂におけるジグザグ端の選択的な形成 157
☆ * 藤原 美帆, 井上 凌介, 真庭 豊, 篠原 久典, 宮田 耕充
- 3P-26 炭素含有ガス不使用の熱CVD法によるグラフェン生成法 158
* 森迫 詩陽, 辻本 茉里奈, 橘 勝
- 3P-27 Cu-Ni合金薄膜上における非常に均一な二層グラフェン 159
☆ * 竹崎 悠一郎, 日比野 浩樹, 辻 正治, 吾郷 浩樹
- 3P-28 Al₂O₃バリア層、Auキャップ層を用いた高品質多層グラフェンの析出法におけるアニール温度依存性 160
* 山田 純平, 鈴木 学, 上田 悠貴, 丸山 隆浩, 成塚 重弥

グラフェンの応用

- 3P-29 酸化グラフェン/ナノグラフェンにおける磁気的評価 161
☆ * 山科 智貴, 井坂 琢也, 井上 和美, 松尾 吉晃, 高井 和之
- 3P-30 水溶液中でシリコン酸化膜上グラフェンの不要ひずみとドーピングを抑える前処理法 162
増田 祥也, * 佐野 正人
- 3P-31 単層WSe₂を用いた電気二重層発光ダイオード 163
☆ * 蒲 江, 藤本 太陽, Huang Jing-Kai, Li Lain-Jong, 坂上 知, 竹延 大志

グラフェンの物性

- 3P-32 グラフェンFETにおけるヒドラジン分子吸着効果 164
* 梅原 太一, 高井 和之
- 3P-33 Kohn anomaly meets Fano resonance in G and G' bands Raman spectra of graphene 165
* ハスデオ エツドウイ, ヌグラハ アフマド, 齋藤 理一郎
- 3P-34 Surface plasmon excitations in graphene 166
* Shoufie Ukhtary, Eddwi Hasdeo, Ahmad Nugraha, Riichiro Saito
- 3P-35 Interlayer exciton in atomically thin heterostructures of transition metal dichalcogenides 167
☆ * Daichi Kozawa, Ivan Verzhbitskiy, Alexandra Carvalho, A. H. Castro Neto, Kazunari Matsuda, Goki Eda
- 3P-36 Optical characteristic of CVD grown monolayer WSe₂ under high-density carrier doping 168
* 松木 啓一郎, Jiang Pu, 松田 一成, Lain-Jong Li, 竹延 大志
- 3P-37 Photon energy dependence of angle resolved photoemission spectroscopy in graphene 169
* アイリヤ ポウルヤ, ハスデオ ヘスキ, ヌグラハ アフマド, 田中 慎一郎, 齋藤 理一郎
- 3P-38 グラフェンナノリボンのNFE状態に対する局所電界効果 170
☆ * 山中 綾香, 岡田 晋

2月23日(月)

- 3P-39 Evaluation of Graphene Quality by Raman Rapid Chemical Imaging 171
*Mamoru Komatsu, Kaori Umeyama, * Noriaki Nishikawa, Mark Wall*

その他

- 3P-40 ヘテロ積層デバイスを目指した高品質h-BNシートのCVD成長 172
** 内田 勇氣, 祝迫 佑, 辻 正治, 吾郷 浩樹*
- 3P-41 WSe₂における熱電特性の電界制御 173
☆ ** 飯塚 貴彦, 吉田 将郎, 清水 直, 岩佐 義宏*
- 3P-42 CVD合成された多層MoS₂・WS₂薄膜の光電気化学特性 174
** 本間 光太郎, 河合 英輝, 柳 和宏*

ナノ環境と安全評価

- 3P-43 Preparation of Nb₂O₅- Graphene Nanocomposites and Kinetics for Photocatalytic Degradation of Organic Dyes 175
*Hae Soo Park, * Jeong Won Ko, Weon Bae Ko*

特別講演 (16:00-16:30)

- 3S-9 高品質原子層のCVD成長と機能開拓 9
** 北浦 良*

一般講演 (16:30-17:30)

グラフェン生成・その他・グラフェンの応用

- 3-8 CVD synthesis of single-crystal single-layer graphene and bi-layer graphene from ethanol 40
** Xiao Chen, Kohei Tsushima, Masaki Sota, Rong Xiang, Shohei Chiashi, Shigeo Maruyama*
- 3-9 Magnetic Ordering of Two-dimensional Networks of Fused C₃₆ Polyhedra under an Electric Field 41
** 丸山 実那, 岡田 晋*
- 3-10 炭素材料へのPt-Ru金属ナノ粒子の担持および電着条件の違いにおける電極触媒特性の評価 42
** 吉竹 晴彦, 早瀬 勝平, 王 志朋, 緒方 啓典*
- 3-11 Hexahydroxytriphenylene and its derivatives for graphene exfoliation in aqueous and organic media 43
** 劉 剛, 木村 隆英, 小松 直樹*

February 21st, Sat.

Special Lecture : 25 min (Presentation) + 5 min (Discussion)

General Lecture : 10 min (Presentation) + 5 min (Discussion)

Poster Preview : 1 min (Presentation)

Special Lecture (9:30–10:00)

- 1S-1 What we know about chirality-controlled growth of single-walled carbon nanotubes 1
* *Yan Li*

General Lecture (10:00–10:30)

Formation and purification of nanotubes ▪ Endohedral nanotubes

- 1-1 Co-existence of two tube-growth processes by Rh/Pd catalyst 11
* *Yohji Achiba, Takuya Kodama, Takeshi Kodama, Kenro Hashimoto, Haruo Shiromaru*
- 1-2 Ionic atomic chains inside carbon nanotubes 12
* *Ryosuke Senga, Kazu Suenaga*

>>>>>>> Coffee Break (10:30–10:45) <<<<<<<<

Special Lecture (10:45–11:15)

- 1S-2 Double-walled carbon nanotube transparent conductive film for next generation flexible device 2
* *Naoki Imazu, Takashi Oi, Hidekazu Nishino, Kenichi Sato, Osamu Watanabe, Shiro Honda, Motoyuki Suzuki*

General Lecture (11:15–12:00)

Formation and purification of nanotubes ▪ Applications of nanotubes

- 1-3 Selective Separation of Semiconducting Single-Walled Carbon Nanotubes Using Flavin Compounds 13
* *Masashi Fukuzawa, Fumiyuki Toshimitsu, Yuichi Kato, Naotoshi Nakashima*
- 1-4 Role of cholate for chirality selection of SWCNTs 14
* *Yohei Yomogida, Mayumi Tsuzuki, Xiaojun Wei, Atsushi Hirano, Shunjiro Fujii, Takeshi Tanaka, Hiromichi Kataura*
- 1-5 Development of thermoelectric device using cobaltocene-encapsulated carbon nanotubes 15
* *Tsuyohiko Fujigaya, Takahiro Fukumaru, Naotoshi Nakashima*

>>>>>>> Lunch Time (12:00–13:15) <<<<<<<<

Special Lecture (13:15–13:45)

- 1S-3 Real-time observation of graphene growth by thermal emission microscopy 3
* *Koichiro Saiki, Tomo-o Terasawa, Sho Kato*

February 21st, Sat.

General Lecture (13:45–14:45)

Applications of graphene ▪ Nanohorns ▪ Carbon nanoparticles

- 1-6 Modification of the local structure of carbon materials by ion irradiation and the support properties of Pt nanoparticles by one-step electro deposition method 16
* Shohei Hayase, Haruhiko Yoshitake, Tomoaki Nishimura, Wang Zhipeng, Hironori Ogata
- 1-7 Preparation of Boron Nitride Containing Carbon Nanohorn for Boron Neutron Capture Therapy 17
* Yoko Iizumi, Toshiya Okazaki, Minfanf Zhang, Ryota Yuge, Toshinari Ichihashi, Maki Nakamura, Yuzuru Ikehara, Sumio Iijima, Masako Yudasaka
- 1-8 Multifunctional carbon nanohorn complexes for cancer treatment 18
* Eijiro Miyako, Svetlana Chechetka, Benoit Pichon, Minfang Zhang, Masako Yudasaka, Sylvie Bégin-Colin, Alberto Bianco
- 1-9 Comparative LDI analysis of nanodiamonds from detonation synthesis and pre-solar carbonaceous meteorites 19
* Toshihiko Tanaka, Ryoko Yamanoi, Eiji Osawa

Poster Preview (14:45–15:45)

Poster Session (15:45–17:30) (★)Candidates for the Young Scientist Poster Award

Other topics

- 1P-1 Charge analyses on particles by Ion Mobility Measurement 45
* Toshiki Sugai, Yasuhiro Hiroshiba, Matsubayashi Hironobu, Kazuki Mimuro, Ryota Jinnouchi

Environmental/Safety characterization of nanomaterials

- 1P-2 Exciton-photon interaction in tip enhanced Raman spectroscopy of single wall carbon nanotubes 46
* Thomas Czank, Pourya Airya, Riichiro Saito

Properties of nanotubes

- 1P-3 *Ab Initio* Study on Oxidation of (5,4), (6,4), (6,5), and (8,6) Carbon Nanotubes 47
* Mari Ohfuchi
- 1P-4 Bias-voltage induced absorption peaks in individual suspended carbon nanotubes 48
☆ * Takushi Uda, Masahiro Yoshida, Akihiro Ishii, Yuichiro K. Kato
- 1P-5 Photoluminescence studies on individual small-diameter carbon nanotubes 49
* Shun Aota, Naoto Akizuki, Shinichiro Mouri, Xiaojun Wei, Takeshi Tanaka, Hiromichi Kataura, Kazunari Matsuda, Yuhei Miyauchi
- 1P-6 Assigning (n,m) of Random Single-Walled Carbon Nanotubes on Silicon Substrates by Resonant Raman Spectroscopy 50
* Daqi Zhang, Feng Yang, Yan Li, Juan Yang
- 1P-7 Trions in individual air-suspended carbon nanotubes 51
* Alexander Popert, Masahiro Yoshida, Yuichiro K. Kato

February 21st, Sat.

1P-8	Electronic properties of CNT thin films under an electric field	52
☆	* <i>U Ishiyama, Susumu Okada</i>	
Applications of nanotubes		
1P-9	Electrical contact of parallel adjacent CNTs estimated from in-plane conductivity of dense CNT forest on silicon carbide	53
	* <i>Masafumi Inaba, Chih-Yu Lee, Kazuma Suzuki, Yu Hirano, Megumi Shibuya, Miho Myodo, Wataru Norimatsu, Michiko Kusunoki, Hiroshi Kawarada</i>	
1P-10	Overcoming the Quality-Quantity Trade-Off in Printing Carbon Nanotubes by Repetitive Dispersion-Extraction Process	54
☆	* <i>Hiroyuki Shirae, Dong Young Kim, Kei Hasegawa, Taishi Takenobu, Yutaka Ohno, Suguru Noda</i>	
1P-11	Controlled formation of nanogaps of single-walled carbon nanotubes on substrates and field emission from the nanogaps	55
	* <i>Keigo Otsuka, Yuuki Shimomura, Taiki Inoue, Shohei Chiashi, Shigeo Maruyama</i>	
1P-12	Surface modification of carbon nanotubes utilizing photo-induced radical formation from benzyl derivatives	56
	* <i>Tomoya Takada, Shigeaki Abe</i>	
1P-13	The new method for CNT and VGCF dispersion by Nano Premixer	57
	* <i>Taro Ikuta, Takayuki Takatsuka</i>	
Formation and purification of nanotubes		
1P-14	Optical Properties of Optical Isomer of Single-Chirality SWCNTs	58
☆	* <i>Xiaojun Wei, Mayumi Tsuzuki, Takuya Hirakawa, Yohei Yomogida, Atsushi Hirano, Shunjiro Fujii, Takeshi Tanaka, Hiromichi Kataura</i>	
1P-15	Synthesis of Submillimeter-Long Carbon Nanotubes on Small Ceramic Powders by Fluidized Bed	59
☆	* <i>Kosuke Kawabata, Zhongming Chen, Kei Hasegawa, Toshio Osawa, Suguru Noda</i>	
1P-16	Controlled Growth of Single-Walled Carbon Nanotubes Using W-Co Catalyst at Different Temperatures and Carbon Feedings	60
	* <i>Feng Yang, Xiao Wang, Daqi Zhang, Juan Yang, Yan Li</i>	
1P-17	Growing carbon nanotubes on acetylene black particles to form their hybrid and controlling the reaction on a few second time scale	61
☆	* <i>Masaaki Kuriya, Kei Hasegawa, Yusaku Harada, Suguru Noda</i>	
1P-18	FT-ICR study of chemical reaction of ethanol and acetonitrile molecules on transition metal clusters	62
	* <i>Kazuki Ogasawara, Yuta Tobari, Yoshinori Sato, Makoto Saito, Shohei Chiashi, Toshiki Sugai, Shigeo Maruyama</i>	

February 21st, Sat.

1P-19	Flame Synthesis of Single-Wall Carbon Nanotube and Control over the Temperature Field and Reactions	63
☆	* <i>Mai Yamaguchi, Kei Hasegawa, Toshio Osawa, Suguru Noda</i>	
1P-20	An Effective Method for the Production of Single Walled Carbon Nanotubes by the Bipolar Pulsed Arc Discharge Method	64
	* <i>Kazi Hanium Maria, Tetsu Mieno</i>	
Graphene synthesis		
1P-21	Selective precipitation of few/multi-layer graphene on/around h-BN on SiO ₂ from metal-carbon films	65
☆	* <i>Kohtaro Yamaguchi, Kei Hasegawa, Suguru Noda</i>	
1P-22	Two-step growth and characterization of WS ₂ /MoS ₂ heterostructures	66
☆	* <i>Shohei Mori, Yutaka Maniwa, Yasumitu Miyata</i>	
1P-23	Production of graphene quantum dots with molecule-like fluorescence	67
	* <i>Misaki Takahashi, Toshiki Sugai</i>	
1P-24	Growth of bilayer graphene and its electric property	68
☆	* <i>Ryo Hoshino, Ryoya Kimura, Kentaro Imai, Yutaro Hayashi, Tomoko Nagata, Nobuyuki Iwata, Hiroshi Yamamoto</i>	
1P-25	Growth and characterization of W-doped NbS ₂ atomic layers	69
☆	* <i>Shogo Sasaki, Yutaka Maniwa, Yasumitsu Miyata</i>	
Applications of graphene		
1P-26	π -Conjugated Polymer Microspheres Covered by Graphene Oxide	70
	* <i>Yusuke Aikyo, Kenichi Tabata, Soh Kushida, Daniel Braam, Junpei Kuwabara, Takaki Kanbara, Takahiro Kondo, Junji Nakamura, Thang Dao Duy, Satoshi Ishii, Tadaaki Nagao, Axel Lorke, Yohei Yamamoto</i>	
1P-27	Direct and real-time TEM observation of aqueous solution sandwiched by graphene layers	71
☆	* <i>Yuki Sasaki, Ryo Kitaura, Hisanori Shinohara</i>	
1P-28	Influence of the surface structure of substrate for proximity effect on Graphene	72
	<i>Akinori Izumiyama, * Kazuyuki Takai</i>	
Properties of graphene		
1P-29	Photoluminescence Properties of van der Waals Hetero Structure Composed of Monolayer Transition Metal Dichalcogenides	73
	* <i>Shinichiro Mouri, Daichi Kozawa, Goki Eda, Yuhei Miyauchi, Kazunari Matsuda</i>	
1P-30	Crossover between Localization and Delocalization in Edge-Disordered Graphene Nanoribbons	74
☆	* <i>Kengo Takashima, Takahiro Yamamoto</i>	

February 21st, Sat.

1P-31	G* band Raman spectra of single layer graphene revisited * Syahril Siregar, Hesky Hasdeo, Ahmad Nugraha, Hsiang Liu, Riichiro Saito	75
1P-32	Geometric and Electronic Structures of Corannulene Polymers ☆ * Kohei Narita, Susumu Okada	76
1P-33	Electron-wave dephasing suppressed by spin-orbit interaction in slightly hydrogenated graphene within a topological insulating regime Junichi Kamijo, * Yuto Katagiri, Tateaki Kato, Taketomo Nakamura, Shingo Katumoto, Motohiko Ezawa, Barbaros Özyilmaz, Junji Haruyama	77
Other topics		
1P-34	Anomalous electronic properties of mono-atomic layer of black phosphorus Yoto Katagiri, Tatyua Makino, * Tika Ohata, Taketomo Nakamura, Shingo Katumoto, Motohiko Ezawa, Hisanori Shinohara, Junji Haruyama	78
1P-35	Magnetism of Edges of single-layer black phosphorus * Yudai Nakanishi, Tika Ohata, Ryoma Iwaki, Kumiko Nomura, Motohiko Ezawa, Hisanori Shinohara, Junji Haruyama	79
Properties of nanotubes		
1P-36	Electronic properties of thin films of all-metallic carbon nanotubes with ionized gel-gate * Tomohiro Honma, Ryo Kikuchi, Syunya Yamada, Chika Ohata, Miho Koyata, Junji Haruyama, Apparao Rao	80
Carbon nanoparticles		
1P-37	Photo-reduction of graphene oxide for improvement of the purity of carbon nanopot * Hiroyuki Yokoi, Kazuto Hatakeyama, Shogo Matsumoto, Mako Ueda, Takaaki Taniguchi, Michio Koinuma, Yasumichi Matsumoto	81
1P-38	Structure and electronic properties of nanodiamond and its fluorination effect ☆ * Kennta Kogane, Hidekazu Touhara, Yoshiyuki Hattori, Kazuyuki Takai	82
1P-39	Spheroidization of microdiamond by self-ablation: preliminary results * Ryoko Yamanoi, Eiji Ōsawa	83
Other topics		
1P-40	The Topological Structure of Starfish Nanocarbon * Natsuki Namba, Yukihiro Takada, Kyoko Nakada	84
1P-41	Double resonance Raman modes in mono- and few-layer MoTe ₂ * Huaihong Guo, Teng Yang, Mahito Yamamoto, Lin Zhou, Ryo Ishikawa, Keiji Ueno, Kazuhito Tsukagoshi, Zhidong Zhang, M. S. Dresselhaus, R. Saito	85

February 21st, Sat.

- 1P-42 Improving the property of electric double layer capacitor by using activated carbon nanoballoon 86
** Akitaka Mizutani, Yoshiyuki Suda, Hirofumi Takikawa, Hitoshi Ue, Kazuki Shimizu, Yoshito Umeda*
- 1P-43 Spontaneous antiferromagnetism in the α -graphyne single layer 87
** Teng Yang, Baojuan Dong, Huaihong Guo, R. Saito, Zhidong Zhang*
- 1P-44 Characteristic of spectral sensitivity for the composite film of Zn doped iron oxide nanotubes and organometal halide perovskite 88
** Yuta Kosugi, Hiroyuki Kusuda, Ayano Saiki, Shunji Bandow*

>>>>>>> **Coffee Break (17:30-18:00)** <<<<<<<<

Tutorial (18:00-19:30)

TEM characterization of carbon nanomaterials

** Kazutomo Suenaga*

February 22nd, Sun.

Special Lecture : 25 min (Presentation) + 5 min (Discussion)

General Lecture : 10 min (Presentation) + 5 min (Discussion)

Poster Preview : 1 min (Presentation)

Special Lecture (9:00–9:30)

- 2S-4 STUDIES ON SWNT BUNDLING 4
* *Esko I. Kauppinen*

General Lecture (9:30–10:15)

Applications of nanotubes ▪ Formation and purification of nanotubes

- 2-1 Direct- and Dry-Deposited Single-Walled Carbon Nanotube Films Doped with MoO_x as Electron-Blocking Transparent Electrodes for Efficient Flexible Organic Solar Cells 20
* *Il Jeon, Kehang Cui, Takaaki Chiba, Anton Anisimove, Albert Nasibulin, Esko Kauppinen, Shigeo Maruyama, Yutaka Matsuo*
- 2-2 Evaluation of perovskite solar cells with single-walled carbon nanotube cathodes 21
* *Takaaki Chiba, Takahiro Sakaguchi, Albert G. Nasiblin, Esko I. Kauppinen, Rong Xiang, Shohei Chiashi, Shigeo Maruyama*
- 2-3 Non-catalytic CVD growth from carbon nanotube forest formed by SiC surface decomposition 22
* *Yu HIRANO, Masafumi INABA, Megumi SHIBUYA, Kazuma SUZUKI, Chih-Yu LEE, Miho MYODO, Atsushi HIRAIWA, Wataru NORIMATSU, Michiko KUSUNOKI, Hiroshi KAWARADA*

>>>>>>> Coffee Break (10:15–10:30) <<<<<<<<<

Special Lecture (10:30–11:00)

- 2S-5 A Proposal of New Strategy for Bottom-up Synthesis of Graphene Nanoribbons 5
* *Hiroko Yamada, Hironobu Hayashi*

General Lecture (11:00–12:00)

Chemistry of fullerenes ▪ Endohedral metallofullerenes ▪ Fullerenes

- 2-4 Structure and electronic state of [lucigenin]C₆₀ molecular fulleride salt 23
* *Hiroshi Moriyama, Shohei Yamamoto, Hatsumi Mori, Kenji Yoza, Hideyuki Hara*
- 2-5 Method of Separating Endohedral Metallofullerenes using Electron Donor and Polar Solvent 24
* *Kazuki Chiba, Kazuhiko Akiyama, Shiro Kubuki*
- 2-6 Vibronic Coupling Density Analysis for Multiple Cycloadditions to C₆₀ 25
* *Naoki Haruta, Tohru Sato, Kazuyoshi Tanaka*
- 2-7 From linear carbon molecules to fullerenes under laser vaporization 26
* *Tomonari Wakabayashi, Yoriko Wada, Yusuke Morisawa, Hitomi Endo, Yuki Taguchi, Jun Matsumoto, Takeshi Kodama, Yohji Achiba, Haruo Shiromaru*

>>>>>>> Lunch Time (12:00–13:15) <<<<<<<<<

February 22nd, Sun.

Awards Ceremony (13:15–14:00)

Poster Preview (14:00–15:00)

Poster Session (15:00–16:45) (☆) Candidates for the Young Scientist Poster Award

Chemistry of fullerenes

- 2P-1 Isolation and Characterization for Each Isomer of (5,6)- and (6,6)-[Li⁺@C₆₁Ph₂]NTf₂⁻ 89
* Hiroshi Okada, Hiroki Kawakami, Shinobu Aoyagi, Yutaka Matsuo
- 2P-2 Approach to High Open-circuit Voltage in Organic Solar Cells Utilizing Structural Change of Oxazolino-C₇₀ Derivative 90
* Yutaka Matsuo, Shu-Hui Li, Zong-Jun Li, Takafumi Nakagawa, James Ryan, Xiang Gao
- 2P-3 Effects of water molecules on the proton dynamics in fullerene solids investigated by solid-state ¹H NMR 91
* Yoshiaki Sano, Hironori Ogata

Endohedral metallofullerenes

- 2P-4 Photoinduced Electron Transfer from Anionic Phthalocyanines to Li⁺@C₆₀ and Light-Energy Conversion 92
☆ * Yuki Kawashima, Kei Ohkubo, Vicente Manuel Blas-Ferrando, Hayato Sakai, Enrique Font-Sanchis, Javier Ortíz, Fernando Fernández-Lázaro, Taku Hasobe, Ángela Sastre-Santos, Shunichi Fukuzumi
- 2P-5 Addition Reactions of Trimetallic Nitride Template Endohedral Metallofullerenes with Disilirane and Digermirane 93
* Kyosuke Miyabe, Masahiro Kako, Kumiko Sato, Mitsuaki Suzuki, Naomi Mizorogi, Marilyn M. Olmstead, Alan L. Balch, Wei-Wei Wang, Shigeru Nagase, Takeshi Akasaka

Fullerenes

- 2P-6 Energetics of the Nano-Saturn 94
☆ * Shota Kigure, Haruka Omachi, Hisanori Shinohara, Susumu Okada
- 2P-7 Energetics of H₂O encapsulated in fullerenes under an electric field 95
* Jun-ya Sorimachi, Susumu Okada
- 2P-8 Absolute yield of fullerene formed by graphite laser ablation at room temperature 96
☆ * Hitomi Endo, Yuki Taguchi, Jun Matsumoto, Tomonari Wakabayashi, Takeshi Kodama, Yohji Achiba, Haruo Shiromaru

Properties of nanotubes

- 2P-9 Fabrication and characterization of SWCNT-TFTs using chirality separated DNA-wrapped SWCNTs 97
* Yuki Kuwahara, Fumiyuki Nihey, Shigekazu Ohmori, Takeshi Saito
- 2P-10 Energetics and electronic structure of deformed carbon nanotubes 98
* Jumpei Nishikawa, Susumu Saito

February 22nd, Sun.

2P-11	Effect of Chemical Doping on the Electronic States of Single-Walled Carbon Nanotubes (1) : Experiment	99
☆	* <i>Tomonari Shiraishi, Naoto Akizuki, Yuhei Miyauchi, Kazunari Matsuda, Naotoshi Nakashima</i>	
2P-12	Effect of Chemical Doping on the Electronic States of Single-Walled Carbon Nanotubes: Theory	100
	* <i>Gergely Juhasz, Tomonari Shiraishi, Naotoshi Nakashima</i>	
2P-13	Ab initio calculation for electronic bands of CNT in which the chain of sulphur is inserted	101
	* <i>Yuhei Natsume</i>	
Applications of nanotubes		
2P-14	Fabrication of Thermoelectric Device using P- and N-Type Controlled Single Wall Carbon Nanotubes by Electric Double Layer Carrier Injections	102
	* <i>Yuki Oshima, Yoshimasa Kitamura, Shouhei Kanda, Hideki Kawai, Yusuke Nakai, Yutaka Maniwa, Kazuhiro Yanagi</i>	
2P-15	Polyglycerol-functionalized SWNTs: size separation, toxicological study and biomedical application	103
☆	* <i>Keisuke Nakamura, Li Zhao, Hongmei Qin, Shuji Aonuma, Takahide Kimura, Naoki Komatsu</i>	
2P-16	Gate-controlled generation of optical pulse trains using individual carbon nanotubes	104
	<i>Ming Jiang, Yusuke Kumamoto, * Akihiro Ishii, Masahiro Yoshida, Takashi Shimada, Yuichiro K. Kato</i>	
2P-17	Electroluminescence from individual air-suspended carbon nanotubes within split-gate structures	105
	* <i>Noriyuki Higashide, Ming Jiang, Takushi Uda, Masahiro Yoshida, Akihiro Ishii, Yuichiro K. Kato</i>	
Formation and purification of nanotubes		
2P-18	Redox-dependent separation of single-wall carbon nanotubes in hydrogels	106
	* <i>Atsushi Hirano, Takeshi Tanaka, Hiromichi Kataura</i>	
2P-19	Optimization of the synthesis parameters of Carbon Nanotube (CNT) forest using the Taguchi Method	107
☆	* <i>Adam Pander, Hiroshi Furuta, Akimitsu Hatta</i>	
2P-20	Synthesis of single-walled carbon nanotubes from woody bioethanol	108
	* <i>Takuma Araki, Atsushi Honda, Yuhei Yabushita, Toshiya Murakami, Kenji Kisoda, Masanori Yamaguchi, Chihiro Itoh</i>	
2P-21	Nitrogen doping of single-walled carbon nanotubes prepared from fluorinated SWCNTs using ammonia gas	109
☆	* <i>Koji Yokoyama, Yoshinori Sato, Kazutaka Hirano, Kenichi Motomiya, Kazuyuki Tohji, Yoshinori Sato</i>	

February 22nd, Sun.

2P-22	Molecular Dynamic Simulation of Defect Free Growth of Single-Walled Carbon Nanotube * <i>Ryo Yoshikawa, Yukai Takagi, Shohei Chiashi, Shigeo Maruyama</i>	110
2P-23	Automatic Gradient Elution Gel Filtration for Separation of Metal and Semiconducting Single-Wall Carbon Nanotubes ☆ * <i>Boanerges Thendie, Haruka Omachi, Ryo Kitaura, Yasumitsu Miyata, Hisanori Shinohara</i>	111
2P-24	Facile sorting and release of semiconducting single-walled carbon nanotubes based on dynamic formation of supramolecular polymers * <i>Fumiyuki Toshimitsu, Naotoshi Nakashima</i>	112
Endohedral nanotubes		
2P-25	Structural transformation of tellurium encapsulated in the inner space of carbon nanotubes depending on tube diameter * <i>Keita Kobayashi, Hidehiro Yasuda</i>	113
2P-26	Synthesis of Diamantane Chains inside Carbon Nanotubes from Bridgehead-halogenated Diamantanes ☆ * <i>Yusuke Nakanishi, Haruka Omachi, Natalie A. Fokina, Ryo Kitaura, Peter R. Schreiner, Jeremy E. P. Dahl, Robert M. K. Carlson, Hisanori Shinohara</i>	114
2P-27	A Computational Study on Properties of Multimeric Pi Conjugated Oligomers inside Carbon Nanotubes * <i>Takashi Yumura, Hiroki Yamashita</i>	115
Graphene synthesis		
2P-28	Growth Dynamics of Single-Layer Graphene on Epitaxial Cu surfaces ☆ * <i>Yujiro Ohta, Seigi Mizuno, Hiroki Hibino, Kenji Kawahara, Rina Takizawa, Masaharu Tsuji, Hiroki Ago</i>	116
2P-29	Preparation of Small-Sized Nano-Graphene Oxide for Biological Application * <i>Minfang Zhang, Toshiya Okazaki, Yoho Iizumi, Eijiro Miyako, Sumio Iijima, Masako Yudasaka</i>	117
2P-30	Direct transfer of CVD graphene to insulating substrates by metal melting ☆ * <i>Ryosuke Inoue, Yutaka Maniwa, Yasumitsu Miyata</i>	118
2P-31	Vibronic Coupling Density as a Reactivity Index: Applications for Diels-Alder Reactions of Graphene Fragments <i>Naoki Haruta, * Tohru Sato, Kazuyoshi Tanaka</i>	119
2P-32	Growth of high-quality monolayer WS ₂ on graphite ☆ * <i>Yu Kobayashi, Shogo Sasaki, Shohei Mori, Hiroki Hibino, Kenji Watanabe, Takashi Taniguchi, Yutaka Maniwa, Yasumitsu Miyata</i>	120
Properties of graphene		
2P-33	Amplitude modulation of optical field by arm-chair graphene nanoribbons:A First-principles Study * <i>Yoshiyuki Miyamoto, Hong Zhang</i>	121

February 22nd, Sun.

2P-34	Spectroscopic studies of single layer molybdenum ditelluride <i>* Sandhaya Koirala, Daichi Kozawa, Shinichiro Mouri, Yuhei Miyauchi, Kazunari Matsuda</i>	122
2P-35	Seebeck effect of monolayer transition metal dichalcogenides <i>* Kaito Kanahashi, Jiang Pu, Nguyen Thanh Cuoug, Lain-Jong Li, Susumu Okada, Hiromichi Ohta, Taishi Takenobu</i>	123
2P-36	Electronic transport properties of graphene between metal electrode <i>* Hideyuki Jippo, Susumu Okada, Mari Ohfuchi</i>	124
2P-37	Anharmonicity of Phonons and Thermal Conduction in Graphene <i>* Masashi Mizuno, Riichiro Saito</i>	125
2P-38	Structure and electronic properties of epitaxial graphene and its molecular adsorption effect <i>* Keisuke Nakamoto, Takashi Akatsu, Kazuyuki Takai</i>	126
2P-39	Bandgap Opening in Graphene Adsorbed on Defective Graphene <i>* Ken Kishimoto, Susumu Okada</i>	127
2P-40	Fabrication and In-situ TEM Characterization of Freestanding Graphene Nanoribbons Devices ☆ <i>* Qing Wang, Ryo Kitaura, Shoji Suzuki, Hisanori Shinohara</i>	128
Other topics		
2P-41	Graphite laser ablation products carried by coaxial gas flow <i>* Yuuki Taguchi, Hitomi Endo, Yurika Abe, Jun Matsumoto, Tomonari Wakabayashi, Takeshi Kodama, Yohji Achiba, Haruo Shiromaru</i>	129
2P-42	Controlling and functionalizing phase transitions in two-dimensional crystals ☆ <i>* Masaro Yoshida, Yijin Zhang, Jianting Ye, Ryuji Suzuki, Yasuhiko Imai, Shigeru Kimura, Akihiko Fujiwara, Yoshihiro Iwasa</i>	130
2P-43	Structure and Spectra of Polyynes-Iodine Complex <i>* Dai Nagashima, Tohru Sato, Naoya Iwahara, Kazuyoshi Tanaka, Yoriko Wada, Tomonari Wakabayashi</i>	131
2P-44	Ambipolar transistor and superconductivity in transition metal dichalcogenides <i>* Wu Shi, Jianting Ye, Yijing Zhang, Ryuji Suzuki, Masaro Yoshida, Naoko Inoue, Yu Saito, Yoshihiro Iwasa</i>	132

February 22nd, Sun.

Special Lecture (16:45–17:15)

- 2S-6 Single carbon-nanotube photonics and optoelectronics 6
* *Yuichiro K. Kato*

General Lecture (17:15–18:45)

Properties of nanotubes

- 2-8 The effect of DNA adsorption on optical transitions in single-walled carbon nanotube depending on base sequence 27
* *Masahiro Ito, Yusuke Ito, Hiroki Kato, Kazuo Umemura, Yoshikazu Homma*
- 2-9 Electronic properties and polarities of atomic-layer materials: Doped graphene, hexagonal BN layers, and carbon nanotubes 28
* *Susumu Saito, Takashi Koretsune, Yoshitaka Fujimoto*
- 2-10 Electronic States of Flattened Carbon Nanotubes: Effects of tube chirality and displacement 29
* *Takeshi Nakanishi, Tsuneya Ando*
- 2-11 Coherent and squeezed phonons in single wall carbon nanotubes 30
* *Ahmad R. T. Nugraha, Eddwi H. Hasdeo, Riichiro Saito*
- 2-12 Stark effect of excitons in individual air-suspended carbon nanotubes 31
* *Masahiro Yoshida, Yusuke Kumamoto, Akihiro Ishii, Akio Yokoyama, Yuichiro K. Kato*
- 2-13 Exciton diffusion, end quenching, and exciton-exciton annihilation in individual air-suspended carbon nanotubes 32
* *Akihiro Ishii, Masahiro Yoshida, Yuichiro K. Kato*

February 23rd, Mon.

Special Lecture : 25 min (Presentation) + 5 min (Discussion)

General Lecture : 10 min (Presentation) + 5 min (Discussion)

Poster Preview : 1 min (Presentation)

Special Lecture (9:00–9:30)

- 3S-7 Graphene field-effect transistors -Analysis on gap states by conductance method- 7
* *Kosuke Nagashio*

General Lecture (9:30–10:30)

Properties of graphene ▪ Other topics

- 3-1 Bandgap opening in bilayer graphene at metal contacts 33
* *Ryo Nouchi*
- 3-2 Band-like transport in reduced graphene oxide films 34
* *Ryota Negishi, Masashi Akabori, Shoji Yamada, Takahiro Ito, Yoshio Watanabe, Yoshihiro Kobayashi*
- 3-3 Circularly polarized luminescence from lateral TMD *p-i-n* junctions 35
* *Yijin Zhang, Masaru Onga, Yoshihiro Iwasa*
- 3-4 Mechanical exfoliation and van der Waals assembly of layered ferromagnetic dichalcogenide Fe_xTaS_2 36
* *Miho Arai, Rai Moriya, Naoto Yabuki, Satoru Masubuchi, Keiji Ueno, Tomoki Machida*

>>>>>>> Coffee Break (10:30–10:45) <<<<<<<<<

Special Lecture (10:45–11:15)

- 3S-8 Nano-optical science and application of nano-carbon materials and atomically thin layered materials 8
* *Kazunari Matsuda*

General Lecture (11:15–12:00)

Properties of graphene ▪ Other topics

- 3-5 Optical Properties of Single-layer Black Phosphorus, “Phosphorene” 37
* *Takashi Nakamura, Daichi Kozawa, Shinichiro Mouri, Kazunari Matsuda*
- 3-6 Relaxation of Valley Polarization in Transition Metal Dichalcogenides 38
* *Satoru Konabe, Susumu Okada*
- 3-7 Exciton spectroscopy of 3R-MoS₂ 39
* *Ryuji Suzuki, Sandor Bordacs, Ryosuke Akashi, Masayuki Ochi, Ryotaro Arita, Yoshinori Tokura, Yoshihiro Iwasa*

>>>>>>> Lunch Time (12:00–13:15) <<<<<<<<<

February 23rd, Mon.

Poster Preview (13:15–14:15)

Poster Session (14:15–16:00) (★) Candidates for the Young Scientist Poster Award

Applications of fullerenes

- 3P-1 Solid-State NMR Studies on the Aggregated Structures of Organic Bulk Heterojunction Solar Cells with Solvent Additives(II) 133
* *Saki Kawano, Hironori Ogata*
- 3P-2 Application of spiro-1, 3-dioxolanofullerenes with low-lying LUMO level to low bandgap polymer based organic photovoltaic cell 134
☆ * *Tsubasa Mikie, Akinori Saeki, Naohiko Ikuma, Ken Kokubo, Shu Seki*
- 3P-3 Fabrication of semitransparent tandem organic solar cells using multiple-device stacked structure 135
* *Shunjiro Fujii, Takeshi Tanaka, Hiromichi Kataura*

Endohedral metallofullerenes

- 3P-4 Isolation and characterization of [5,6]-pyrrolidino-Sc₃N@I_h-C₈₀ diastereomers 136
* *Yutaka Maeda, Masato Kimura, Chihiro Ueda, Mitsuaki Suzuki, Michio Yamada, Nikolaos Karousis, Nikos Tagmatarchis, Marilyn M Olmstead, Alan L Balch, Wei-Wei Wang, Shigeru Nagase, Takeshi Akasaka*
- 3P-5 Reactions of Trimetallic Nitride Template Endohedral Metallofullerenes with Silacyclopropanes 137
* *Kazuya Minami, Takeshi Sugiura, Masahiro Kako, Kumiko Sato, Shigeru Nagase, Takeshi Akasaka*
- 3P-6 Ionic Donor-Acceptor Supramolecules: Complexation of Molecular Nanocarbons with Cationic Li⁺@C₆₀ 138
* *Hiroshi Ueno, Taishi Nishihara, Katsuma Matsui, Yasutomo Segawa, Kenichiro Itami*

Properties of nanotubes

- 3P-7 The Quantitative Importance of Purity on the Properties of Single Wall Carbon Nanotubes 139
* *Naoyuki Matsumoto, Guohai Chen, Motoo Yumura, Don Futaba, Kenji Hata*
- 3P-8 MD simulation on RBM frequency of bundled SWNTs 140
☆ * *Atsushi Beniya, Naoki Homma, Shohei Chiashi, Yoshikazu Homma, Takahiro Yamamoto*
- 3P-9 Molecular structure of chalcogen encapsulated in single-walled carbon nanotubes studied by molecular dynamics simulations 141
* *Yutaka Sato, Yosuke Kataoka, Hironori Ogata*
- 3P-10 Local structure and properties of the alkali halides encapsulated in single-walled carbon nanotubes studied by molecular dynamics simulations 142
* *Eita Yokokura, Yosuke Kataoka, Hironori Ogata*

Applications of nanotubes

- 3P-11 Ultralow mode-volume photonic crystal nanobeam cavities for high-efficiency coupling to individual carbon nanotube emitters 143
* *Hidenori Machiya, Ryohei Miura, Saneyuki Imamura, Ryuichi Ohta, Akihiro Ishii, Xuqing Liu, Takashi Shimada, Satoshi Iwamoto, Yasuhiko Arakawa, Yuichiro K. Kato*

February 23rd, Mon.

3P-12	Characteristic variation of thin-film transistors based on purified semiconducting carbon nanotubes	144
☆	* <i>Jun Hirotani, Ryotaro Matsui, Shigeru Kishimoto, Yutaka Ohno</i>	
3P-13	Thermoelectric power of carbon nanotubes from first principles	145
	* <i>Nguyen Tuan Hung, Riichiro Saito</i>	
3P-14	Effect of TiO ₂ coating on field emission properties of carbon nanotube by in-situ transmission electron microscopy	146
☆	* <i>Masahiro Matsuda, Hitosi Nakahara, Koji Asaka, Yahachi Saito</i>	
3P-15	Light-emitting Electrochemical Cell with Few-Walled Carbon-Nanotube Electrodes	147
	* <i>Ko Nakayama, Hiroyuki Shirae, Suguru Noda, Tomo Sakanoue, Taishi Takenobu</i>	
Formation and purification of nanotubes		
3P-16	Synthesis of Single-Walled Carbon Nanotubes from Rh Catalysts by Alcohol Gas Source Method in high Vacuum	148
	* <i>Akinari Kozawa, Takahiro Saida, Shigeya Naritsuka, Takahiro Maruyama</i>	
3P-17	Relationship between Chirality Control of Single-Walled Carbon Nanotube and Wavelength of the Irradiated Free Electron Laser	149
☆	* <i>Keisuke Yoshida, Yusaku Tsuda, Daiki Kawaguchi, Tomoko Nagata, Nobuyuki Iwata, Hiroshi Yamamoto</i>	
3P-18	Synthesis of single walled carbon nanotubes by using sputtered Co/Cu and Co/W as catalyst	150
	* <i>Hua An, Kehang Cui, Rong Xiang, Taiki Inoue, Shohei Chiashi, Shigeo Maruyama</i>	
3P-19	Control of In-Plane Orientation and Chirality of Single-Walled Carbon Nanotubes using Hot-Walled Chemical Vapor Deposition Method and Free Electron Laser	151
☆	* <i>Daiki Kawaguchi, Keisuke Yoshida, Tomoko Nagata, Nobuyuki Iwata, Hiroshi Yamamoto</i>	
3P-20	The Effects of Hydrogen Atom on Cobalt Clusters in the Reaction with H ₂ O Investigated by FT-ICR Mass Spectrometer	152
	* <i>Yuta Tobari, Kazuki Ogasawara, Yoshinori Sato, Makoto Saito, Shohei Chiashi, Shigeo Maruyama, Toshiki Sugai</i>	
3P-21	Synthesis of carbon nanotubes by means of “molecular template epitaxial growth” approach	153
☆	* <i>Liu Hong, Akira Takakura, Lawrence Scott, Yuhei Miyauchi, Kenichiro Itami</i>	
3P-22	Hybridization of Semiconducting-Single-Walled Carbon Nanotubes and Fullerene-Carrying Carbazole-Fluorene Copolymers	154
	* <i>Fumiyuki Toshimitsu, Hiroaki Ozawa, Naotoshi Nakashima</i>	
Nanohorns		
3P-23	Cytotoxicity of Carbon Nanohorns Enhanced by Too Much PLPEG	155
	* <i>Maki Nakamura, Yoshio Tahara, Shinsuke Fukata, Minfang Zhang, Sumio Iijima, Masako Yudasaka</i>	

February 23rd, Mon.

3P-24	Electrochemical properties of boron- and nitrogen-doped carbon nanohorn aggregates * <i>Ryota Yuge, Shunji Bandow, Masako Yudasaka, Kiyohiko Toyama, Sumio Iijima, Noriyuki Tamura, Takashi Manako</i>	156
Graphene synthesis		
3P-25	Selective formation of zigzag edges in graphene cracks ☆ * <i>Miho Fujihara, Ryosuke Inoue, Yutaka Maniwa, Hisanori Shinohara, Yasumitsu Miyata</i>	157
3P-26	The synthesis of graphene by thermal CVD process without flowing gas containing carbon * <i>Shiyo Morisako, Marina Tsujimoto, Masaru Tachibana</i>	158
3P-27	Highly Uniform Bilayer Graphene on Cu-Ni Alloy Films ☆ * <i>Yuichiro Takesaki, Hiroki Hibino, Masaharu Tsuji, Hiroki Ago</i>	159
3P-28	Annealing time dependence of precipitation of high-quality multilayer graphene using Al ₂ O ₃ barrier and Au capping layers * <i>Jumpei Yamada, Manabu Suzuki, Yuki Ueda, Takahiro Maruyama, Shigeya Naritsuka</i>	160
Applications of graphene		
3P-29	Evaluation of magnetism of chemically active sites in graphene oxide / nanographene ☆ * <i>Tomoki Yamashina, Takuya Isaka, Kadumi Inoue, Yoshiaki Matsuo, Kazuyuki Takai</i>	161
3P-30	Acid-treatment minimizes unintentional strain and doping of single-layer graphene on SiO ₂ substrate in aqueous environments <i>Katsuya Masuda, * Masahito Sano</i>	162
3P-31	Electric Double Layer Light-emitting Diodes of Monolayer WSe ₂ ☆ * <i>Jiang Pu, Taiyo Fujimoto, Jing-Kai Huang, Lain-Jong Li, Tomo Sakanoue, Taishi Takenobu</i>	163
Properties of graphene		
3P-32	Effect of hydrazine adsorption on Graphene FET characteristic * <i>Taichi Umehara, Kazuyuki Takai</i>	164
3P-33	Kohn anomaly meets Fano resonance in G and G' bands Raman spectra of graphene * <i>Eddwi Hasdeo, Ahmad Nugraha, Riichiro Saito</i>	165
3P-34	Surface plasmon excitations in graphene * <i>Shoufie Ukhtary, Eddwi Hasdeo, Ahmad Nugraha, Riichiro Saito</i>	166
3P-35	Interlayer exciton in atomically thin heterostructures of transition metal dichalcogenides ☆ * <i>Daichi Kozawa, Ivan Verzhbitskiy, Alexandra Carvalho, A. H. Castro Neto, Kazunari Matsuda, Goki Eda</i>	167
3P-36	Optical characteristic of CVD grown monolayer WSe ₂ under high-density carrier doping * <i>Keiichiro Matsuki, Jiang Pu, Kazunari Matsuda, Lain-Jong Li, Taishi Takenobu</i>	168

February 23rd, Mon.

3P-37	Photon energy dependence of angle resolved photoemission spectroscopy in graphene <i>* Pourya Ayria, Hesky Hasdeo, Ahmad Nugraha, Shin-Ichiro Tanaka, Riichiro Saito</i>	169
3P-38	Local electric field effects on nearly free electron states of graphene nanoribbons ☆ <i>* Ayaka Yamanaka, Susumu Okada</i>	170
3P-39	Evaluation of Graphene Quality by Raman Rapid Chemical Imaging <i>Mamoru Komatsu, Kaori Umeyama, * Noriaki Nishikawa, Mark Wall</i>	171
Other topics		
3P-40	CVD synthesis of high-quality h-BN films for heterostructure devices <i>* Yuki Uchida, Tasuku Iwaizako, Masaharu Tsuji, Hiroki Ago</i>	172
3P-41	Electric field control of thermoelectric properties in WSe ₂ ☆ <i>* Takahiko Iizuka, Masaro Yoshida, Sunao Shimizu, Yoshihiro Iwasa</i>	173
3P-42	Influence of Electric Double Layer Carrier Injections on Optical Absorption Spectra of CVD synthesized Multi-layered MoS ₂ and WS ₂ thin films <i>* Kotaro Homma, Hideki Kawai, Kazuhiro Yanagi</i>	174
Environmental/Safety characterization of nanomaterials		
3P-43	Preparation of Nb ₂ O ₅ - Graphene Nanocomposites and Kinetics for Photocatalytic Degradation of Organic Dyes <i>Hae Soo Park, * Jeong Won Ko, Weon Bae Ko</i>	175
Special Lecture (16:00–16:30)		
3S-9	Characterization of CVD-grown high-quality atomic layers <i>* Ryo Kitaura</i>	9
General Lecture (16:30–17:30)		
Graphene synthesis ▪ Other topics ▪ Applications of graphene		
3-8	CVD synthesis of single-crystal single-layer graphene and bi-layer graphene from ethanol <i>* Xiao Chen, Kohei Tsushima, Masaki Sota, Rong Xiang, Shohei Chiashi, Shigeo Maruyama</i>	40
3-9	Magnetic Ordering of Two-dimensional Networks of Fused C ₃₆ Polyhedra under an Electric Field <i>* Mina Maruyama, Susumu Okada</i>	41
3-10	Effects of electrodeposition conditions on the states of Pt-Ru nanoparticles on carbon materials and their electrocatalytic properties toward methanol oxidation <i>* Haruhiko Yoshitake, Shohei Hayase, Zhipeng Wang, Hironori Ogata</i>	42
3-11	Hexahydroxytriphenylene and its derivatives for graphene exfoliation in aqueous and organic media <i>* Gang Liu, Takahide Kimura, Naoki Komatsu</i>	43

特別講演
Special Lecture

1S – 1 ~ 1S – 3

2S – 4 ~ 2S – 6

3S – 7 ~ 3S – 9

What we know about chirality-controlled growth of single-walled carbon nanotubes

○Yan Li

College of Chemistry and Molecular Engineering, Peking University, Beijing 100871, China

The chirality-controlled synthesis of single-walled carbon nanotubes (SWNTs) is a crucial issue for their advanced applications (e.g. carbon-based nanoelectronics) and has been a great challenge for about two decades. Recently, we realized the selective growth of (12,6) SWNTs at the content of >92%, and also showed the selective growth of (14,4) and (16,0) tubes. In this talk, I will start from our understanding on catalyzed growth of SWNTs in chemical vapor deposition (CVD), then discuss the important factors on the chirality control, and finally explain our design on the catalysts composition and structure as well as the CVD conditions.

[1] F. Yang *et al.* *Nature* **510**, 522-524 (2014).

[2] Y. Li *et al.*, *Adv. Mater* **22**, ,1508-1515 (2010)..

Corresponding Author: Y. Li

Tel & Fax: +86-10-6275-6773

E-mail: yanli@pku.edu.cn

Double-walled carbon nanotube transparent conductive film for next generation flexible device

○Naoki Imazu¹, Takashi Oi¹, Hidekazu Nishino², Kenichi Sato², Osamu Watanabe¹, Shiro Honda², Motoyuki Suzuki¹

¹ Film products development center, Toray Industries, Inc., Shiga 520-8558, Japan

² Chemicals research laboratories, Toray Industries, Inc., Aichi 455-8502, Japan

We have developed double-walled carbon nanotube (DWCNT) transparent conductive film (TCF). Our DWCNT TCF has very high transparent conductivity, which are currently among the top in the world. And it has great characteristics such as high flexibility (bending and stretching durability) and high environmental stability.

In order to improve transparent conductivity, we focus on DWCNT, and developed flexible, high transparent conductive DWCNT TCF. We already have established mass production system [1].

Combining this CNT dispersion and our fine wet coating technology, we have developed DWCNT TCF. Picture of our DWCNT TCF roll is shown in Fig. 1. We also have established mass production roll to roll technology for this DWCNT TCF. The width of mass production DWCNT TCF is over 1000 mm.

One example of our DWCNT TCF commercialized product is shown in Fig. 2. This figure is twist-ball type e-paper display. DWCNT TCF is used as upper transparent conductive electrode. DWCNT TCF's neutral color and high light transmittance contribute to showing clear image. And as this figure, large screen digital signage is realized using our DWCNT TCF.

Flexible touch screen using patterned Toray DWCNT TCF are shown in Fig. 3. Even if these devices are under bended situation, both work normally. Especially, touch screen detected the multi position across the folding line. These demonstrations are significant for future flexible device realization.

[1] Toray Industries, Inc., "Mass production technology development of CNT transparent conductive film for EPD" 9 February 2012, <<http://www.toray.co.jp/news/rd/nr120209.html>> (19 August 2012)

Corresponding Author: M. Suzuki

Tel: +81-77-533-8254, Fax: +81-77-533-8461,

E-mail: Motoyuki_Suzuki@nts.toray.co.jp

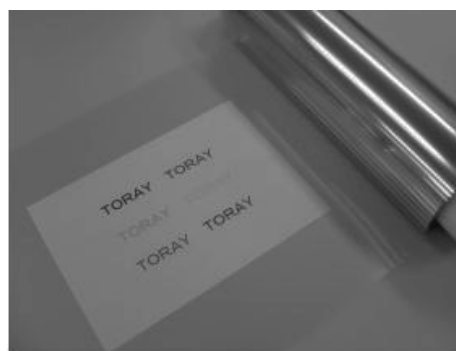


Fig.1 Toray DWCNT TCF roll sample



Fig.2 Commercialized product of E-paper using Toray DWCNT TCF

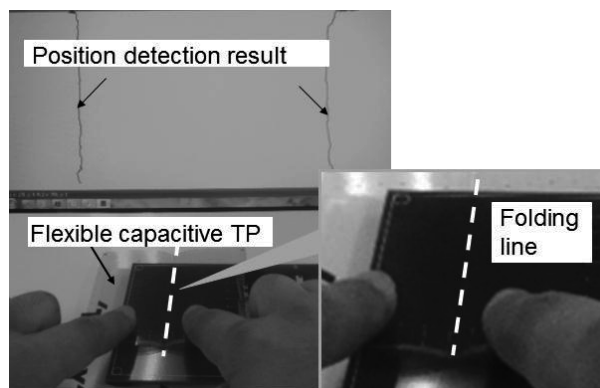


Fig.3 Flexible touch screen using patterned Toray DWCNT TCF (Prototype)

Real-time observation of graphene growth by thermal emission microscopy○Koichiro Saiki^{1,2}, Tomo-o Terasawa², and Sho Kato¹¹ *Department of Complexity Science & Engineering, The University of Tokyo*² *Department of Chemistry, The University of Tokyo, Chiba 277-8561, Japan*

Scalable synthesis of a large-area, high-quality graphene is indispensable to use the excellent nature of graphene for various industrial applications. Chemical vapor deposition (CVD) is considered the most promising synthesis method for that purpose and a large number of works on CVD growth of graphene have been carried out worldwide. Nevertheless, the property of CVD graphene has not yet reached that of exfoliated one. The optimization of CVD growth parameters has been done mostly based on the post-synthesis characterization by use of scanning electron microscopy, Raman spectroscopy, etc. If the intermediate state during the growth can be observed in situ and in real time, it will help to elucidate the growth mechanism and to optimize the growth parameters. In the case of CVD growth on Cu, the most popular substrate, however, conventional electron microscopy could not be used during the growth under gas ambience and at high temperatures.

Recently we have proved that the graphene could be distinguished optically from the metal substrate at elevated temperatures. The large difference in thermal emissivity between carbon materials and a certain kind of metal gives rise to the contrast between graphene and the metal substrate. By using optical microscopy we can observe the growing graphene from outside the furnace even under the gaseous condition of several thousand Pa. The spatial and time resolution was 1800 nm and 1 sec, respectively.[1]

Using this observation method we succeeded in analyzing the growth mechanism of graphene on the metal substrate. In the case of CVD growth of graphene on Cu, we evaluated the saturation nucleation density and growth rate for various methane flow rates and substrate temperatures. Both the growth rate and saturation nucleation density increased with the substrate temperature, indicating that the production on surface and attachment to graphene edge of growth precursors were enhanced at the substrate temperatures between 900 and 1000 °C. After the methane supply was stopped, the graphene started to shrink and finally disappeared. The shrinkage rate also depended on the substrate temperature, suggesting the enhanced detachment of C atoms from graphene edge.[1]

The effect of vapor phase oxygen on the CVD growth of graphene on Cu was studied. Oxygen has been found to decrease the saturation nucleation density and the growth rate. In the low partial pressure region, however, the growth rate increased with oxygen partial pressure. This increase might be ascribed to the decrease in the energy barrier for the attachment of precursor to the graphene edge by the surface oxygen.[2]

The graphene growth on Pd from graphene oxide was also observed by thermal emission microscopy. The graphene appeared at the boundary between Pd grains at high temperatures, while it also segregated from the center of Pd grains by decreasing the substrate temperature.

Thermal emission microscopy proved to be a powerful tool to observe the growth feature in the CVD condition and optimize the growth parameters.

[1] T. Terasawa and K. Saiki, submitted.

[2] T. Terasawa and K. Saiki, submitted.

Corresponding Author: K. Saiki

Tel: +81-4-7136-5526, Fax: +81-4-7136-3903,

E-mail: saiki@k.u-tokyo.ac.jp

STUDIES ON SWNT BUNDLING

Esko I. Kauppinen

Department of Applied Physics, Aalto University School of Science
Puumiehenkuja 2, P.O. Box 16100, FI-00076 Aalto, FINLAND**esko.kauppinen@aalto.fi**

SWNTs have the tendency to form bundles during the growth processes. However, much of the research on SWNT optical and transport properties has been focused on the individual tubes, i.e. the effect of bundling has received relatively minor efforts. In this paper, we discuss our recent work on the effect on SWNT bundling on the conductivity of SWNT thin film transparent conductors (TCF) as well as on the thin film field effect transistors (TFT-FET). In addition, we also explore how the bundling affects both the Raman as well as the optical absorption spectra of SWNTs.

To control the fraction of the bundled tubes formed during the floating catalyst CVD synthesis, we have developed a novel iron catalyst particle production method via physical vapor deposition, based on arc discharge between two electrodes i.e. the spark generator. This method allows us to control separately both the catalyst particle size and concentration when fed into the floating catalyst SWCNT synthesis reactor using CO as the carbon source gas. Our results show that when reducing the catalyst particle gas phase number concentration, the fraction of the bundled tubes can be reduced down to 20 %. When allowing the individual tubes to agglomerate i.e. form bundles in the gas phase downstream the reactor but prior thin film deposition, we form bundles in controlled manner from the individual primary tubes with given length distribution. The sheet resistance of TCF increases significantly with the bundling of the individual tubes with the very same length distribution. Similarly, the on-off ratio of TFT-FETs is reduced. We also explore the effect of bundling on the Raman and optical absorption spectra of SWNT thin films with varying degree of the tube bundling.

A Proposal of New Strategy for Bottom-up Synthesis of Graphene Nanoribbons

○Hiroko Yamada^{1,2}, Hironobu Hayashi¹

¹ Graduate School of Materials Science, Nara Institute of Science and Technology, Nara 630-0192, Japan

² CREST, JST, Saitama 102-0075, Japan

The electronic structure of graphene nanoribbon (GNR) is known to depend on the edge structures. Zigzag edge GNR is expected to be metallic while armchair edge GNR can be semiconducting. Therefore the bottom-up synthesis of armchair GNR with a fixed width has been sought widely. Cai *et al.* have reported the in-situ synthesis of anthracene nanoribbon by heating 9,10-dibromoanthracene at 400 °C in vacuo via radical coupling of anthracenes at 9,10-positions followed by the annelation [1]. However the synthesis of nanoribbons with higher acenes are difficult because higher acenes are insoluble and unstable to prepare dibromoacenes as starting materials and the reaction points of radical elongation will be disordered.

We have developed thermal and photochemical precursor methods, where acenes can be prepared from the corresponding precursors by heating or photoirradiation quantitatively (Figure 1). The diketone precursors can be converted to acenes in solution, film, and solid states by photoirradiation [2]. Bicyclo[2.2.2]octadiene (BCOD)-fused precursors can be converted to acenes in film and solid by heating [3]. Using this technique we have prepared organic semiconducting materials for solution process, employing the difference of solubility between precursors and acenes. These precursor methods are promising for the synthesis of nonoribbons of higher acenes. Here we will report the synthesis of the acene unit compounds for the bottom-up synthesis of GNRs.

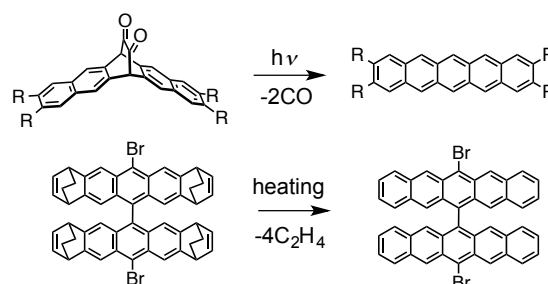


Fig. 1 Photoconversion from the precursor to pentacene (upper) and thermal conversion from the precursor to pentacene dimer (lower).

[1] J. Cai, P. Ruffieux *et al.*, *Nature* **466**, 470 (2010)

[2] M. Suzuki, H. Nakano, K. Nakayama, H. Yamada *et al.* *J. Photochem. Photobiol. C, Photochem. Rev.* **18**, 50 (2014).

[3] H. Yamada *et al.*, *RSC Adv.* **3**, 15310 (2013)

Corresponding Author: H. Yamada

Tel: +81-743-72-6041, Fax: +81-743-72-6042

E-mail: hyamada@ms.naist.jp

Single carbon-nanotube photonics and optoelectronics

Yuichiro K. Kato

Institute of Engineering Innovation, The University of Tokyo, Tokyo 113-8656, Japan

Single-walled carbon nanotubes have unique optical properties as a result of their one-dimensional structure. Not only do they exhibit strong polarization for both absorption and emission, large exciton binding energies allow for room-temperature excitonic luminescence. Furthermore, their emission is in the telecom-wavelengths and they can be directly synthesized on silicon substrates, providing new opportunities for nanoscale photonics and optoelectronics.

Here we discuss the use of individual single-walled carbon nanotubes for generation, manipulation, and detection of light on a chip. Their emission properties can be controlled by coupling to silicon photonic structures such as photonic crystal microcavities [1] and microdisk resonators [2]. Simultaneous photoluminescence and photocurrent measurements show that excitons can dissociate spontaneously [3], enabling photodetection at low bias voltages despite the large binding energies. More recently, we have found that alternating gate-voltages can generate optical pulse trains from individual nanotubes [4]. Ultimately, these results may be combined to achieve further control over photons at the nanoscale.

Work supported by KAKENHI (24340066, 24654084, 26610080, 26870167), SCOPE, The Canon Foundation, The Asahi Glass Foundation, KDDI Foundation, and JSPS Open Partnership Joint Projects, as well as Project for Developing Innovation Systems, the Nanotechnology Platform, and Photon Frontier Network Program of MEXT, Japan.

- [1] R. Miura, S. Imamura, R. Ohta, A. Ishii, X. Liu, T. Shimada, S. Iwamoto, Y. Arakawa, Y. K. Kato, *Nature Commun.* **5**, 5580 (2014).
- [2] S. Imamura, R. Watahiki, R. Miura, T. Shimada, Y. K. Kato, *Appl. Phys. Lett.* **102**, 161102 (2013).
- [3] Y. Kumamoto, M. Yoshida, A. Ishii, A. Yokoyama, T. Shimada, Y. K. Kato, *Phys. Rev. Lett.* **112**, 117401 (2014).
- [4] M. Jiang, Y. Kumamoto, A. Ishii, M. Yoshida, T. Shimada, Y. K. Kato, arXiv:1407.7086.

Corresponding Author: Y. K. Kato

Tel: +81-3-5841-7702, Fax: +81-3-5841-7772,

E-mail: ykato@sogo.t.u-tokyo.ac.jp

Graphene field-effect transistors -Analysis on gap states by conductance method-

K. Nagashio^{1,2}

¹ *Department of Materials Engineering, The University of Tokyo, Tokyo 113-8656, Japan*
² *PRESTO-JST*

The perspective to overcome the short channel effect based on the scaling length (λ) [1] attracts great attention to 2D layered channels. This is due to their rigidly-controllable few atomic thickness as well as low dielectric constant (~ 4) for 2D layered channel. Although old-but-new 2D channels such as transition metal dichalcogenides are intensively investigated [2], bilayer graphene has still advantage for high performance device from the viewpoint of mobility due to the smaller effective mass ($m_{\text{BLG}} \sim 0.037$ and $m_{\text{MoS}_2} \sim 0.5$).

The targeted issue for bilayer graphene is low $I_{\text{on}}/I_{\text{off}}$ at the room temperature, which is explained by the variable range hopping in “gap states” [3]. However, as the zero-order approximation, there will be intrinsically no interface states in bilayer graphene because there is no dangling bonds on the basal plane, compared with P_b centers in SiO_2/Si system. The origin for the gap states is still open question. In spite of this, the detailed measurements on D_{it} and time constant for gap states have not been reported yet. One of reasons could be the leakage current through the top gate insulator since robust methodology is not established.

Recently, we demonstrated a considerable suppression of the low-field leakage as well as the ultra-high displacement of ~ 8 V/nm ($n = \sim 4 \times 10^{13} \text{ cm}^{-2}$) in bilayer graphene by applying the high-pressure O_2 annealing to Y_2O_3 top gate insulator [4,5]. The reliable Y_2O_3 top gate insulator provides the access to the carrier response issue in the largely-opened band gap. In this talk, we focus on the conductance measurements for bilayer graphene to extract D_{it} and time constant. Based on these measurements, two possible origins for the gap states, (i) border traps at the edge of Y_2O_3 and (ii) the local breakdown of A-B stacking in bilayer graphene, are discussed.

Acknowledges

The Kish graphite was provided from Covalent Materials Corporation. This work was partly supported by a Grant-in-Aid for Scientific Research on Innovative Areas.

References

- [1] I. Ferain, C. A. Colinge, and J.-P. Colinge, *Nature*, 2011, **479**, 310.
- [2] R. Radisavljevic, A. Radenovic, J. Brivio, V. Giacometti, and A. Kis, *Nature nanotech.* 2011, **6**, 147.
- [3] J. B. Oostinga, H. B. Heersche, X. Liu, A. F. Morpurgo, and L. M. K. Vandersypen, *Nature Mater.* 2008, **7**, 151.
- [4] K. Nagashio, K. Kanayama, T. Nishimura, and A. Toriumi, *IEDM Tech. Dig.* 2013, 503.
- [5] K. Kanayama, K. Nagashio, T. Nishimura, and A. Troiumi, *APL*, 2014, **104**, 083519.

Corresponding Author: K. Nagashio

Tel&Fax: +81-3-5841-7161

E-mail: nagashio@material.t.u-tokyo.ac.jp

Nano-optical science and application of nano-carbon materials and atomically thin layered materials

○Kazunari Matsuda

Institute of Advanced Energy, Kyoto University, Uji, Kyoto 611-0011, Japan

Recently, nano-carbon materials (carbon nanotube, and graphene) and atomically thin layered materials (transition metal dichalcogenides) have attracted a great deal of attention from viewpoint of fundamental physics [1-7] and optical device application [8]. In nano-carbon materials, the single-walled carbon nanotubes have novel electronic properties, because of their degenerated band structures and enhanced Coulomb interaction with a 1-dimensional (1D) cylindrical structure. The enhanced Coulomb interaction in carbon nanotubes leads to the formation of stable excitons (bound electron-hole pairs) with extremely large binding energies of about several hundred meV by the optical excitation. It is anticipated that the excitons and exciton-complexes in carbon nanotubes show various interesting physical aspects such as mesoscopic quantum phenomena, efficient light-exciton conversion and so on. We studied the excitonic properties of carrier-doped carbon nanotubes [3-5] and found the positive and negative charged excitons (trions) at room temperature in the carbon nanotubes [3,5]. This is the first observation of room temperature stable trion (charged exciton) among various semiconductors, which will open the door to realize the spin manipulation in carbon based materials. We successfully improved the photoluminescence quantum efficiency of carbon nanotubes using 0D-1D hybrid nanostructure [6]. In atomically thin layered transition metal dichalcogenides such MoS₂, is also a promising platform to study the novel excitonic properties and optical applications [9,10]. The transition-metal dichalcogenides shows the strong light absorption (5-10%) even in an atomically thin material [10], which suggests the characteristics excitonic properties in the atomically-thin layered materials. We will discuss the novel optical properties of nano-carbon materials and atomically thin layered materials.

- [1] H. Hirori, K. Matsuda *et al.*, *Phys. Rev. Lett.* **97**, 257401 (2006).
- [2] R. Matsunaga, K. Matsuda *et al.*, *Phys. Rev. Lett.* **101**, 147404 (2008).
- [3] R. Matsunaga, K. Matsuda *et al.*, *Phys. Rev. Lett.* **106**, 037404 (2011).: *Physics Viewpoint; Physics* **4**, 5 (2011).
- [4] S. Konabe, K. Matsuda, and S. Okada, *Phys. Rev. Lett.* **109**, 187403 (2012).
- [5] J. S. Park, N. Nakashima, K. Matsuda *et al.*, *J. Am. Chem. Soc.* **134**, 14461 (2012).
- [6] Y. Miyauchi, K. Matsuda *et al.*, *Nature Photonics* **7**, 715 (2013).
- [7] M. Iwamura, Y. Miyauchi, K. Matsuda *et al.*, *ACS Nano* **8**, 11254 (2014).
- [8] F. Wang, K. Matsuda *et al.*, *submitted for publication*
- [9] S. Mouri, K. Matsuda *et al.*, *Nano Lett.* **13**, 5944 (2013).
- [10] D. Kozawa, K. Matsuda, G. Eda *et al.*, *Nature Commun.* **5**, 4543 (2014).

Corresponding Author: Kazunari Matsuda
Tel: +81-774-38-3460
Fax: +81-774-38-3460
E-mail: matsuda@iae.kyoto-u.ac.jp

Characterization of CVD-grown high-quality atomic layers

Ryo Kitaura

Department of Chemistry, Nagoya University, Nagoya 464-8602, Japan

The discovery of graphene has attracted significant research attention, leading to creation of the research field of atomic layer material^[1]. The family of atomic layers, including graphene, hexagonal boron nitrides (hBN, Fig. 1a) and transition metal dichalcogenides (TMDCs, Fig 1b), provides fundamental and wide-spread platform to explore materials science in two-dimensional (2D) systems. To explore this fascinating new field, preparation of high-quality sample to observe intrinsic properties of 2D atomic layers is essential. In addition to the high-crystallinity, the environmental effect is one of the most important factors to determine quality of sample. Recent studies have shown that environment such as substrates alter intrinsic properties of atomic layers. For example, carrier mobility of graphene is about 10 times smaller than that of graphene on hBN^[2].

For preparation of high-quality atomic layers, we have focused on chemical vapor deposition (CVD) method with various substrates, realizing successful growth of high-quality atomic layers including graphene, hBN and TMDCs. In this presentation, I would like to show our recent results on CVD growth and characterization of high-quality atomic layers: TMDCs on hBN (WS₂ grown on hBN, for example (Fig. 2)), large-area hBN etc.

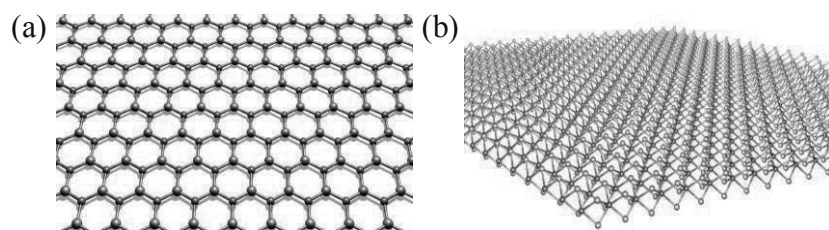


Fig.1 Structure representations of structure of (a) hexagonal boron nitride and (b) transition metal dichalcogenides.

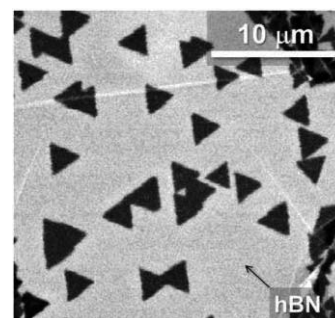


Fig.2 A SEM image of WS₂ grown on hBN

[1] K. S. Novoselov *et al.*, *Nature* **438**, 197 (2005).

[2] C. R. Dean *et al.*, *Nat Nanotechnol* **5**, 722 (2010).

Corresponding Author: R. Kitaura

Tel: +81-52-789-2482, Fax: +81-52-747-6442,

E-mail: r.kitaura@nagoya-u.jp

一般講演
General Lecture

1-1 ~ 1-9

2-1 ~ 2-13

3-1 ~ 3-11

Co-existence of two tube-growth processes by Rh/Pd catalyst

-What we learned about growth mechanism from Pd addition experiments-

○Yohji Achiba, Takuya Kodama, Takeshi Kodama, Kenro Hashimoto and Haruo Shiromaru

Department of Chemistry, Tokyo Metropolitan University, Hachioji, 192-0397, Japan

Metal nanoparticles definitely play an important role on controlling size and chirality distributions of carbon nanotubes, and thus a variety of atomic elements have so far been examined not only to establish an industrial scale production of carbon nanotubes but also to develop a selective generation of specific nanotubes with a single chirality. Particularly, for realizing the latter aim, so called “CoMoCAT” has been developed for a CVD tube production and Rh/Pd (1:1) bimetallic alloy for a laser vaporization method. Here, in the present work, we will show the experimental details of Rh/Pd system by placing an emphasis on how the difference in the concentration of Pd in the Rh/Pd alloy system give an effect on the yields as well as on the size and chirality distributions of the nanotubes and will discuss how the Pd catalyst plays a key role on the large enhancement in the formation of the tubes with a specific chirality.

Typical examples of the Pd effect on the yield of the tubes with specific (n,m) species are shown in Figure (a) and (b), where the Rh concentration to the carbon source was kept constant 1.2% (atomic ratio), while the amount of Pd was systematically changed from 0 to 4.8%. The furnace temperature of the laser vaporization method was also systematically changed from 900 to 1150°C. The resulting bimodal distribution of the tube-growth curves strongly suggests the presence of two different growth mechanisms governed by two parameters, temperature and Pd concentration.

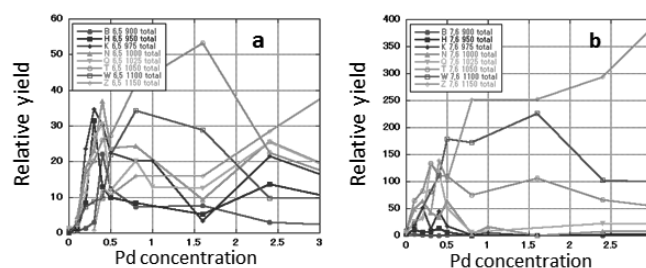


Figure: (a) the relative yield of (6,5) tubes prepared at different furnace temperature and different Pd concentration. (b) the same for (7,6) tubes.

Corresponding Author: Yohji Achiba

E-mail: achiba-yohji@tmu.ac.jp, Tel:+81-42-677-2534, Fax:+81-42-677-2525

Ionic atomic chains inside carbon nanotubes

○Ryosuke Senga¹, Kazu Suenaga¹

¹ Nanotube research center, AIST, Tsukuba 305-8565, Japan

Low-dimensional materials are attracting a wide range of interests in many research fields as their unique properties induced by their confined size and reduced dimensionality. The field of two-dimensional materials such as graphene, hexagonal boron nitride and transition metal dichalcogenides have been widely spread and deeply progressed over the past years. However the study of one-dimensional materials has been still limited and remained as scientific challenges. Especially, one-dimensional ionic crystals have not been well discussed because of the difficulties in their fabrication and assessment, even though more intriguing physical properties can be expected in such a diatomic linear lattice. Herein, we describe the successful synthesis of ionic atomic chains inside carbon nanotubes (CNTs) and their atomic structural analysis, based on scanning transmission electron microscopy (STEM) and electron energy loss spectroscopy (EELS) [1].

Figure 1(a) shows an annular dark-field (ADF) image of a CsI atomic chain encapsulated in a double walled CNT. From the EELS chemical maps (Fig.1 (b) and (c)), it is clear that two chemical elements, one being a cation (Cs^+) and the other an anion (I^-), align alternately inside the CNT as shown in Fig. 1(d). One of the unique phenomena of the CsI atomic chain is non-equivalent atomic vibrations for different atoms corresponding to the interactions of the atoms with the CNT. We have also found monovacancies at both Cs and I sites. They are of great importance because the properties of the atomic chains are strongly governed by such interrupted periodicities. Indeed, the theoretical studies show that these vacancy sites contribute as donor or acceptor states depending on the missing elements. These properties can be obviously distinguished from three-dimensional bulk structures and have a huge potential for future applications.

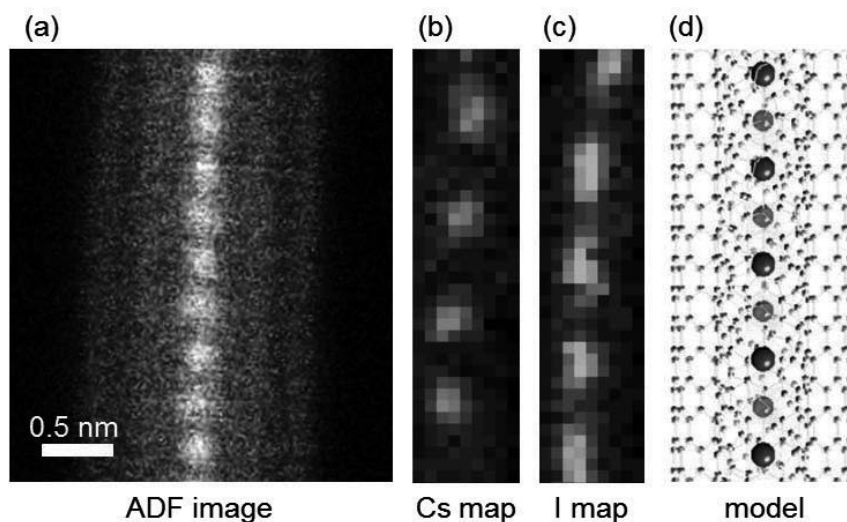


Fig. 1 The elemental analysis for a CsI atomic chain [1].

(a) An ADF image of a CsI atomic chain inside a double walled CNT. (b), (c) EELS chemical maps of Cs and I, respectively, corresponding to the ADF image as shown in (a). (d) A schematic model of the CsI atomic chain.

[1] R. Senga *et al.* Nature Mat. **13**, 1050 (2014).

Corresponding Author: R. Senga

Tel: +81-29-862-6518

E-mail: ryosuke-senga@aist.go.jp

Selective Separation of Single-Walled Carbon Nanotubes Using Flavin Compounds

○Masashi Fukuzawa¹, Fumiuyuki Toshimitsu¹, Yuichi Kato¹, Naotoshi Nakashima^{1,2,3}

¹ Department of Applied Chemistry, Kyushu University, Fukuoka 819-0395, Japan

² WPI-ICNER, Kyushu University, Fukuoka 819-0395, Japan

³ JST-CREST, Chiyoda-ku, Tokyo 102-0075, Japan

Single-walled carbon nanotubes (SWNTs) are classified into metallic or semiconducting tubes according to their chirality. These tubes coexist in the raw SWNT materials; thus the separation of metallic or semiconducting SWNTs is quite important for use of the materials in many applications. One of the key techniques for the chirality-sorting is a utilization of conjugated polymers such as poly(9,9-dialkylfluorene-2,7-diyl).^[1,2] Selective extraction of the semiconducting SWNTs (s-SWNTs) using such polymers is simple and powerful; however, removal of the used adsorbents from the polymer/SWNT composites is difficult due to the strong interaction between the polymers and the SWNTs. In addition, the preparation of these synthetic polymers is complicated. Therefore, it is eagerly demanded to develop an s-SWNT-selective solubilizer having features, such as facile preparation, efficient solubilizing ability and detachability from the SWNT surfaces.

We have found that a flavin compound (**1**,^[3] Fig. 1a) can selectively solubilize s-SWNTs with ~99% purity from raw SWNTs.^[4] In a systematical exploration for the efficient solubilizers, we here synthesized various flavin derivatives (Fig. 1), and examined their s-SWNT solubilization abilities. The absorption spectra of the HiPco-SWNTs dissolved in toluene using these compounds revealed that **1**, **2** and **3** are able to solubilize the s-SWNTs selectively. On the other hand, **4** and **5** did not solubilize any SWNTs. The selective extraction of s-SWNTs with **1**, **2** and **3** is also confirmed by Raman spectroscopy. These results strongly suggested that the imidyl hydrogen and methyl group(s) on the aromatic rings are essential for selective extraction of s-SWNTs. The use of such small molecules for the SWNT solubilization has an advantage not only in its preparation but also in post-processing after the SWNT solubilization. We examined the removal of these compounds from s-SWNTs after the selective solubilization, and found that just washing with chloroform take flavin compounds off from the s-SWNT surfaces. A possible mechanism for such selective separation will be presented at the meeting.

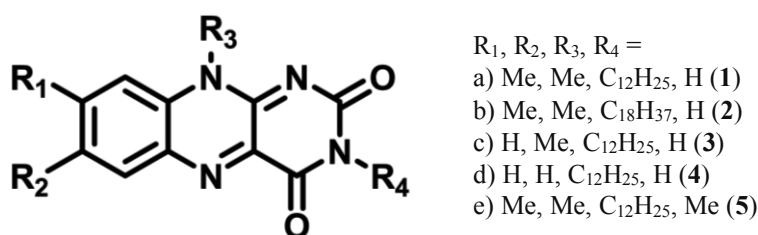


Fig. 1 Chemical structures of flavin derivatives.

[1] F. Chen, *et al.*, *Nano Lett.* **2007**, 7, 3013.

[2] A. Nish, *et al.*, *Nat. Nanotech.* **2007**, 2, 640.

[3] S. Y. Ju, *et al.*, *Science* **2009**, 323, 1319.

[4] Y. Kato *et al.*, *Chem. Lett.*, submitted.

Corresponding Author: N. Nakashima

Tel: +81-92-802-2840, Fax: +81-92-802-2840;

E-mail: nakashima-tcm@mail.cstm.kyushu-u.ac.jp

Role of cholate for chirality selection of SWCNTs

○Yohei Yomogida, Xiaojun Wei, Atsushi Hirano, Shunjiro Fujii, Takeshi Tanaka, and Hiromichi Kataura

Nanosystem Research Institute, National Institute of Advanced Industrial Science and Technology (AIST), Ibaraki 305-8562, Japan

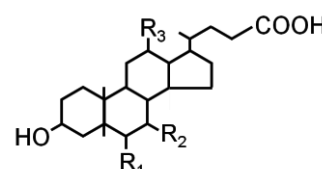
Chirality separation is highly desired to know chirality-dependent physical properties of single-wall carbon nanotubes (SWCNTs). Previously, we reported a milligram-scale separation of single chirality SWCNTs using a gel column and mixed surfactants of sodium dodecyl sulfate (SDS), sodium cholate (SC), and sodium deoxycholate (DOC) [1]. In the separation, chirality species have different affinities to the gel and are collected in the order of their affinities. We found that their affinities could be changed by introducing cholates and thus we demonstrated more efficient separation than that in single system of SDS [2] by using suitable cholate for the separation of specific species. However, the role of cholate in mixed surfactant system is still not well known.

In this work, we applied several cholate derivatives with different structure in the number, position, and orientation of hydroxyl groups to the column separation (Fig. 1). Their selectivities were evaluated by the elution order of chiral species in the separation. SWCNTs adsorbed to the gel in SC/SDS system were eluted by stepwise increase of the concentration of each derivative in the fixed concentration of SC/SDS. In this method, the species with low affinity to the gel are eluted first with low concentration of eluent. We observed that elution orders were strongly dependent on the used cholate derivatives. For example, the order eluted by DOC showed the trend from smaller diameter species to larger diameter species (Fig. 2, top), while the order eluted by SC showed countertrend (Fig. 2, bottom). Finally, we found that these different elution orders correlate with their hydrophobic/hydrophilic balance.

This work was supported by KAKENHI No. 25220602.

[1] Y. Yomogida *et al.* 47th FNTG General Symposium

[2] H. Liu *et al.* Nat. Commun. **2**, 309 (2011).



cholate	R ₁	R ₂	R ₃
ursodeoxycholate	H	βOH	H
hyodeoxycholate	αOH	H	H
cholate	H	αOH	αOH
chenodeoxycholate	H	αOH	H
deoxycholate	H	H	αOH
lithocholate	H	H	H

Fig.1 Molecular structure of cholate derivatives

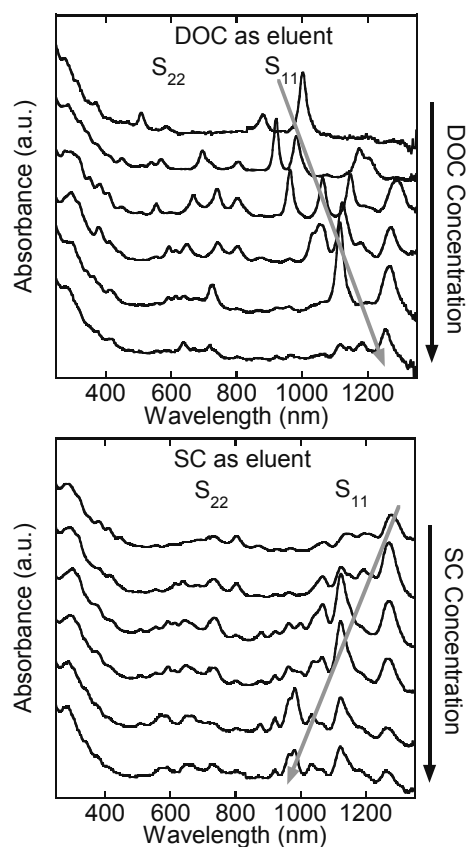


Fig.2 Optical absorption spectra of eluted SWCNTs with increasing DOC (top) and SC (bottom) concentration

Development of thermoelectric device using cobaltocene-encapsulated carbon nanotubes

○Tsuyohiko Fujigaya^{1,2}, Takahiro Fukumaru¹ and Naotoshi Nakashima^{1,2}.

1 Department of Applied Chemistry, Graduate School of Engineering,

Kyushu University, 744, Motoooka Nishi-ku Fukuoka, 819-0395, Japan

2 WPI PCNER, Kyushu University, 744 Motoooka, Nishi-ku, Fukuoka, 819-0395, Japan

Thermoelectric conversion is one of the key technologies to realize a sustainable society since large quantities of energy have been wasted as heat. A number of semiconducting materials especially, inorganic materials, such as Bi₂Te₃, Si/Ge and PbTe, have been intensively studied due to their high power factors originated from large Seebeck coefficients and high carrier conductivity. Recently, carbon nanotubes have attracted much attention as substitutes due to their lower cost, ease of fabrication, flexibility and light weight. Very recently, Maniwa et al. reported that a sorted semiconducting single-walled carbon nanotubes (s-SWNTs) film shows a very large Seebeck coefficient (170 $\mu\text{V K}^{-1}$ at 300 K) [1]. While SWNTs are promising p-type organic thermoelectric materials, the development of the flexible n-type thermoelectric materials is still challenging even at present, because n-type semiconducting organic materials are inherently unstable in air due to oxidation.

In this study, in order to tune the SWNTs to the n-type, we chose cobaltocene (CoCp₂) as the dopant for the encapsulation due to its strong reducibility (Fig. 1). Among the variety of doping approach, we focused on encapsulation of the dopant molecules inside the SWNTs, which show a superior doping stability due to the molecular shielding effect compared to the doping on the outside the tubes. Then, the SWNTs encapsulated with CoCp₂ (CoCp₂@SWNTs) were used to fabricate a p-n connected thermoelectric device without any air protective coating.

We prepared cobaltocene-encapsulated SWNTs (denoted CoCp₂@SWNTs) by evaporating the CoCp₂ under heating in the presence of the open-capped SWNTs. It was revealed that CoCp₂@SWNTs showed a negative-type (n-type) semiconducting behaviour (Seebeck coefficient: -41.8 $\mu\text{V K}^{-1}$ at 320 K). The CoCp₂@SWNT film was found to show a high electrical conductivity (43,200 S m⁻¹ at 320 K) and large power factor (75.4 $\mu\text{W m}^{-1} \text{K}^{-2}$) and the performance was remarkably stable under atmospheric conditions over a wide range of temperatures.

The thermoelectric figure of merit (ZT) value of the CoCp₂@SWNT film (0.157 at 320 K) was highest among the reported n-type organic thermoelectric materials due to the large power factor and low thermal conductivity (0.15 W m⁻¹ K⁻¹). These characteristics of the n-type CoCp₂@SWNTs allowed us to fabricate a p-n type thermoelectric device by combination with an empty SWNT-based p-type film. The fabricated device exhibited a highly efficient power generation close to the calculated values even without any air-protective coating due to the high stability of the SWNT-based materials under atmospheric conditions.[2]

[1] Y. Nakai, et al.. *Appl. Phys. Express* 7, 025103, (2014).

[2] T. Fukumaru, et al. *Sci. Rep.*, in press.

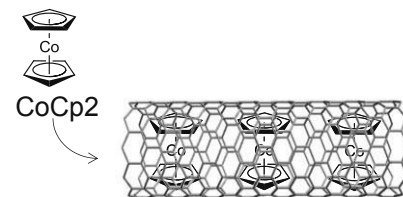


Fig. 1 Structure of CoCp₂@SWNT

Modification of the local structure of carbon materials by ion irradiation and the support properties of Pt nanoparticles by one-step electro deposition method

○¹Shohei Hayase, ¹Haruhiko Yoshitake, ²Tomoaki Nishimura, ⁴Wang Zhipeng and ^{1,2,3}Hironori Ogata

¹ Graduate School of Science and Engineering, Hosei University, Koganei 184-8584, Japan

² Research Center of Ion Beam Technology, Hosei University, Koganei 184-8584, Japan

³ Research Center for Micro-Nano Technology, Hosei University, Koganei 184-0003, Japan

⁴ Institute of Carbon Science and Technology, Shinshu University, Nagano 380-8553, Japan

Pt nanoparticles supported on the carbon materials are known to exhibit high methanol oxidation activity and it is expected use as anode materials of direct methanol fuel cell (DMFC). As is well-known, the highly dispersed Pt on carbon supports as well as catalyst particle size and shape plays a dominant role in the electrochemical performance for fuel cells¹⁾. We have explored the effects of ion-irradiation of carbon materials with different microstructures, including Carbon nanosheets(CNSs), Single-Walled Carbon Nanotubes (SWNTs) and HOPG on their support properties of Pt nanoparticles by one-step electro deposition method²⁾ and reported the improvement of the electrocatalytic activities by ion irradiation. In this study we investigated more detailed local structures of ion irradiated carbon materials and relationship between the local structures of carbon materials, the shape and dispersion state of Pt nanoparticles and the methanol oxidation activities. The ion beam accelerated with carbon ion source with 200 keV and 400keV were irradiated to the carbon materials with 1×10^{13} , 1×10^{14} , 1×10^{15} ions/cm². Figure.1 shows the one example of TEM images of HOPG before and after ion irradiation. The detailed results will be presented.

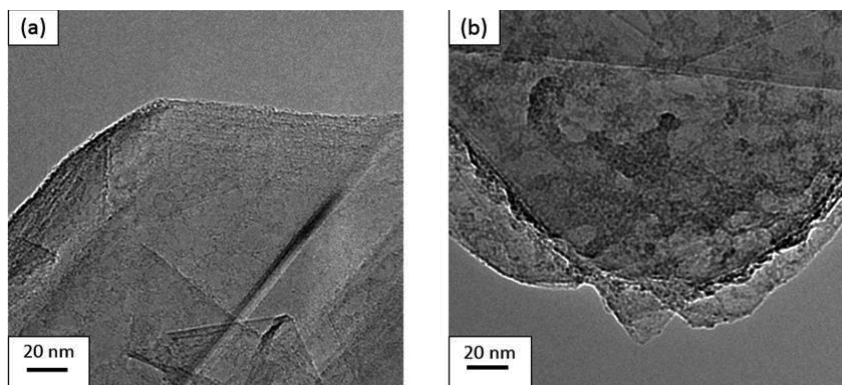


Figure. 1. TEM images (a) pristine of HOPG and (b) ion irradiated HOPG (400 keV, 1×10^{14} ions/cm²)

1) Zhipeng Wang, Mao Shoji and Hironori Ogata, *Appl. Surf. Sci.* **259**(2012)219-224.

2) S.Hayase *et al.*, Abstract of the 47th Fullerenes-Nanotubes-Graphene General Symposium(1P-19).

Corresponding Author: Hironori Ogata,

Tel: +81-42-387-6229, Fax: +81-42-387-6229, E-mail: hogata@hosei.ac.jp

Preparation of Boron Nitride Containing Carbon Nanohorn for Boron Neutron Capture Therapy

○Yoko Iizumi¹, Toshiya Okazaki¹, Minfang Zhang¹, Ryota Yuge², Toshinari Ichihashi², Maki Nakamura¹, Yuzuru Ikehara¹, Sumio Iijima^{1,2,3}, Masako Yudasaka¹

¹*Nanotube Research Center, National Institute of Advanced Science and Technology (AIST), Tsukuba, 305-8565, Japan*

²*Smart Energy Research Laboratories, NEC Corporation, Tsukuba 305-8501, Japan*

³*Faculty of Science & Technology, Meijo University, Nagoya 468-8502, Japan*

Boron neutron capture therapy (BNCT) has been tried to establish as a novel treatment for a malignant tumor of Brain, glioblastoma. The nuclear reaction between boron and low energy neutrons generate α beam and ${}^7\text{Li}$, which have short trajectory, about 10 micrometer, comparable to the cell sizes. When the boron compounds exist only in the tumor cells but not in the normal cells, the neutron beam can kill the tumor cells, while harmless to the normal cells. In other words, BNCT is feasible to use for the control of not only glioblastoma, but also the other solid tumors with dissemination, and massive invasion and metastasis if the boron compounds are properly delivered to cancer cells.

Various types of boron compounds and carriers have been studied to increase the BNCT efficacies, though the high and selective accumulation of boron compounds at tumor cells has not been well achieved. In this context, we have prepared the BN loaded single-walled carbon nanohorns aggregate (CNH) using a method of Nakanishi et al [1] modified for our purpose. And the obtained BN-CN H was functionalized with tumor targeting molecule, folic acid (FA).

Ammonia borane ($\text{H}_3\text{N}-\text{BH}_3$) and CNHs were sealed in a quartz glass ampoule, and heated at various temperatures (550-850 °C). An optimum production temperature was 800 °C in terms of the large BN quantities and stable BN structures. The XPS analysis showed that a number ratio of C:B:N was 5:2:2 in BN-CN H prepared at 800 °C. The BN had layer morphology, therefore they were hexagonal BN, which was confirmed also by EELS measurements. The BN sheets were found on the outside and inside of nanohorn tubule walls. The BN sheets were also deposited on the thin graphite sheets as confirmed by TEM observations and XRD measurements. Here, the thin graphite sheets mean those constructing CNHs together with nanohorn tubules.

Further, purposing the selective accumulation of BN-CN Hs in tumor cells, BN-CN Hs were coated with phospholipid polyethylene glycol having FA (BN-CN H/PLPEG-FA). The *in vitro* cell experiments indicated that BN-CN H/PLPEG-FA was selectively ingested by human tumor KB cells but not by human normal FHs 173We cells. BN-CN H/PLPEG (without FA) did not show such tumor cell selective uptake tendency. Thus BN-CN H is concluded to have high potential for BNCT application.

[1] R. Nakanishi, et al. Sci. Report. DOI:10.1038/srep01385.

Contact: t-okazaki@aist.go.jp, m-yudasaka@aist.go.jp

Multifunctional carbon nanohorn complexes for cancer treatment

○Eijiro Miyako¹, Svetlana A. Chechetka¹, Benoit Pichon², Minfang Zhang¹,
Masako Yudasaka¹, Sylvie Bégin-Colin², Alberto Bianco³

¹ *Nanotube Research Center (NTRC), National Institute of Advanced Industrial Science and Technology (AIST), Central 5, 1-1-1 Higashi, Tsukuba 305-8565, Japan*

² *Institut de Physique et Chimie des Matériaux de Strasbourg, UMR 7504 (CNRS-UdS-ECPM) 23, rue du Loess, BP 43, 67034 Strasbourg Cedex 2, France*

³ *CNRS, Institut de Biologie Moléculaire et Cellulaire, Immunopathologie et Chimie Thérapeutique, 15 Rue René Descartes, 67084 Strasbourg Cedex, France*

Multifunctional carbon nanohorn (CNH) complexes were synthesized using oxidized CNH, magnetite (MAG) nanoparticles, and polyethyleneimine (PEI). The ferromagnetic MAG nanoparticles were loaded onto CNH (MAG–CNH) using iron (II) acetate and a subsequent heat treatment. Chemical functionalization of the MAG–CNH complexes with PEI improved their water-dispersibility and allowed further conjugation with a fluorophore. The application of an external magnetic field significantly intensified the targeted vectorization of CNH complexes into human cervical cancer (HeLa) cells. Following cell uptake, laser irradiation of the cells showed a significant enhancement in the photothermal effects of CNHs leading to cell death. We have confirmed that the photothermal property and ferromagnetic characteristics of CNH complexes exhibit an efficient cell elimination. The present study is an essential step toward the development of an innovative cancer therapy and a highly sensitive detection of cancer cells at the single-cell level.

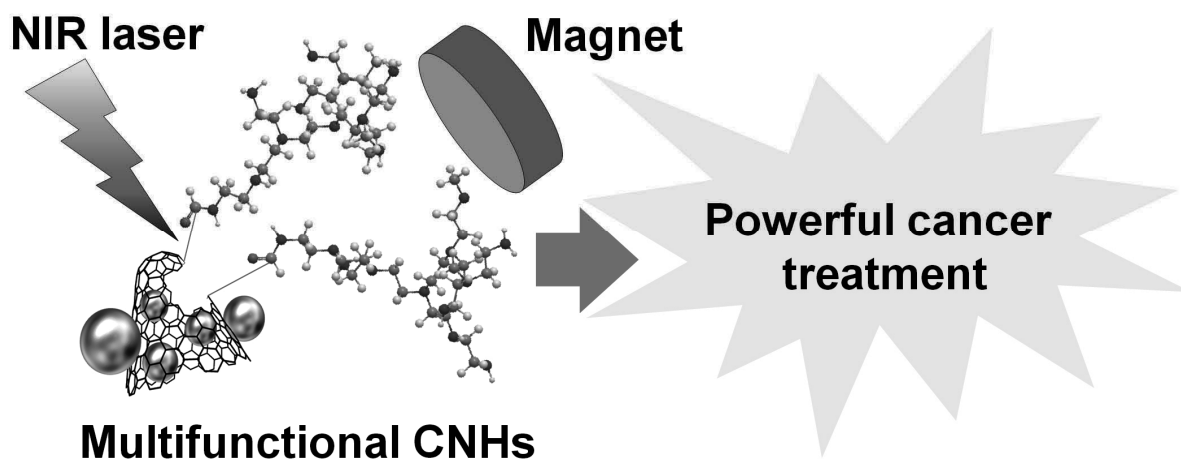
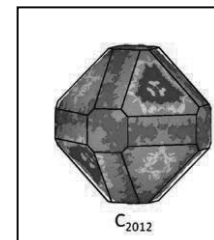


Fig. 1 Concept of the cancer treatment using multifunctional CNHs.

- [1] E. Miyako *et al.* *Angew. Chem. Int. Ed.* **53**, 13121 (2014).
 [2] E. Miyako *et al.* *Nature Communications* **3**, 1226 (2012).
 [3] E. Miyako *et al.* *Proc. Natl. Acad. Sci. USA* **109**, 7523 (2012).
 [4] E. Miyako *et al.* *Angew. Chem. Int. Ed.* **50**, 12266 (2011).

Corresponding Author: E. Miyako
 Tel: +81-87-869-3574, Fax: +81-29-861-6290,
 E-mail: e-miyako@aist.go.jp



Comparative LDI analysis of nanodiamonds from detonation synthesis and pre-solar carbonaceous meteorites

○Toshihiko Tanaka,¹ Ryoko Yamanoi² and Eiji Ōsawa^{2*}

¹ *Department of Chemistry and Biochemistry, National Institute of Technology, Fukushima College, Iwaki, Fukushima 970-8034, Japan.*

² *NanoCarbon Research Institute, AREC, Faculty of Fiber Science and Technology, Shinshu University, Ueda, Nagano 386-8567, Japan. *osawa@nano-carbon.jp, Tel: +81-268-75-8381*

Primary particles of detonation nanodiamond (PPDND) are the smallest known artificial diamond (diameter of 2.8~3nm), available in macroscopic quantities and well-studied¹. On the other hand, the smallest known natural diamonds, isolated from several pre-solar carbonaceous chondrites of Allende, Murchison and a few other meteorites, have been shown to have comparative sizes (2.4~2.8nm)^{2,3}. We recently found that LDI (Laser desorption ionization) MS of these two kinds of nanodiamond gave identical features as well regarding position and abnormal width of core diamond peak (**Fig. 1**). The purpose of this work is to analyze origin of the similarities.

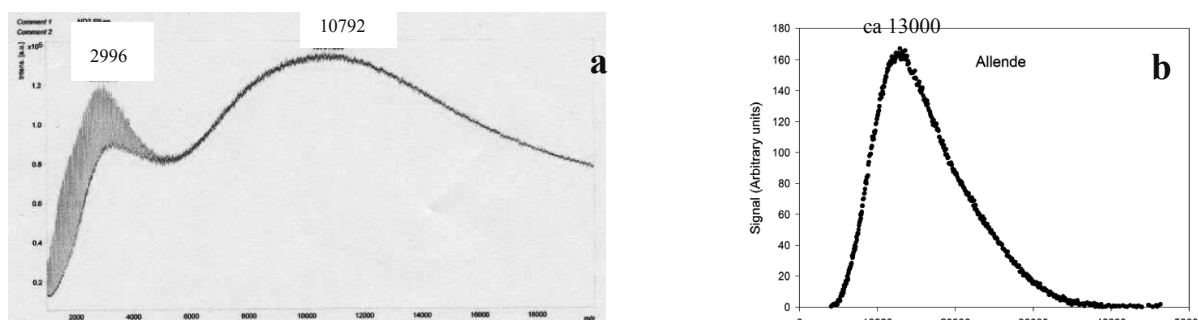


Fig. 1 (a) LDI MS of our primary particles of dispersed detonation nanodiamond. (b) MALDI MS Nanodiamond isolated from Allende meteorite, copied from ref. 2.

According to our modeling with SCC-DFTB level of theory, the 3nm PPDND is a bucky diamond having 2012 carbon atoms (24,144 Dalton) with the morphology of doubly truncated octahedron (inserted in the upper right corner)⁴. However, the observed LDI spectra show major diamond peak at ca. 11,000 Dalton (**Fig. 1a**), nearly one-half of the expected mass. One likely explanation for this observation would be to invoke the well-known macule formation process,⁵ which produced a pair of equal divisions during high-energy of laser desorption, but the two halves drifted apart while undergoing extensive fragmentation by excess energy.

Nanodiamond from Allende meteorite is considered consisting of ca. 1,000 carbon atoms based on MALDI spectra (**Fig. 1b**), but this mass contradicts with the size of ca. 2.8nm obtained by visual analysis of TEM images and comparable to that of PPDND!² Confusion is aggravated by very low reported density (2.22g/cm³)³, too low for a diamond crystal. We will present a comprehensive picture for the nanodiamonds based on information from detonation nanodiamond.

[1] A. Barnard, N. Mchedlov-Petrosyan, E. Ōsawa et al. manuscript in preparation. [2] I. C. Lyon, *Meteorit. Planet. Sci.* **40**, 981 (2005). [3] R. S. Lewis et al. *Nature*, **326**, 160 (1987). [4] A. S. Barnard, E. Ōsawa, *Nanoscale*, **6**, 1188 (2014). [5] R. Tappert & M. Tappert, 'Diamond in Nature', Springer, Berlin, 2011, p. 32.

Direct- and Dry-Deposited Single-Walled Carbon Nanotube Films Doped with MoO_x as Electron-Blocking Transparent Electrodes for Efficient Flexible Organic Solar Cells

○ Il Jeon¹, Kehang Cui², Takaaki Chiba², Anton Anisimov³, Albert G. Nasibulin^{4,5}, Esko I. Kauppinen⁴, Shigeo Maruyama^{2*}, and Yutaka Matsuo^{1*}

¹ Department of Chemistry, The University of Tokyo, Tokyo 113-0033, Japan

² Department of Mechanical Engineering, The University of Tokyo, Tokyo 113-8656, Japan

³ Canatu Ltd., Konalankuja 5, FI-00390 Helsinki, Finland

⁴ Department of Applied Physics, Aalto University School of Science, Aalto, Finland

⁵ Skolkovo Institute of Science and Technology, Moscow, 143025, Russia

As an alternative path to indium based organic solar cells (OSCs), carbon nanotubes (CNTs) and graphene with excellent mechanical flexibility and earth abundance have emerged as the next generation electrode¹. Single-walled CNTs (SWCNTs) have advantages in terms of stretchability², easier synthesis, direct roll-to-roll deposition onto substrates, and accordingly lower costs. There has been a vigorous research on SWCNTs and its application as transparent conductive film in photovoltaics to date.³ Here, we propose the most effectively composed ITO-free OSC and its flexible application by applying technologies that are state-of-the-art. Firstly, high quality direct- and dry-deposited aerosol SWCNT was used as anode for the first time. Secondly, MoO_x with poly-(3,4-ethylenedioxythiophene)-polystyrenesulfonic (PEDOT:PSS) on top functioning as both dopant and hole-transporting layer (HTL) was discovered and applied. Thirdly, using thieno[3,4-b]thiophene/benzodithiophene (PTB7), which is highly performing photoactive material with no annealing requirement, flexible application on films are demonstrated. Our record high SWCNT OSC shows a power conversion efficiency (PCE) of 6.04%, which is 83% to its ITO based counterpart with a PCE of 7.48%. (Fig. 1) We anticipate the methodology presented here is not only limited to OSCs but extends to other photovoltaic applications such as emerging perovskite solar cells too. Our finding paves toward fully carbon flexible solar cells by using a facile and stable process.

[1] D. Volder *et al.* Science **339**, 535 (2013).

[2] S. Won *et al.* Nanoscale **6**, 6057 (2014).

[3] J. Du *et al.* Adv. Mater. **26**, 1958 (2014).

Corresponding Author: S. Maruyama and Y. Matsuo

Tel: +81-3-123-4567, Fax: +81-3-123-4567,

E-mail: matsuo@chem.s.u-tokyo.ac.jp

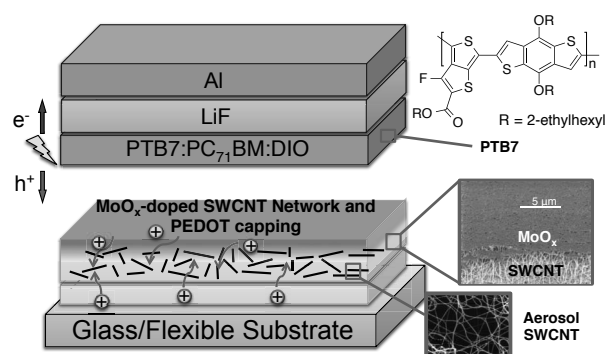


Fig.1 The schematics of our optimized device.

Evaluation of perovskite solar cells with single-walled carbon nanotube cathodes

○Takaaki Chiba ¹, Takahiro Sakaguchi ¹, Albert G. Nasiblin ^{2,3}, Esko I. Kauppinen ²,
Rong Xiang ¹, Shohei Chiashi ¹ and Shigeo Maruyama ¹

¹ Department of Mechanical Engineering, The University of Tokyo, Tokyo 113-8656, Japan

² Department of Applied Physics, Aalto University School of Science, Espoo 15100, Finland

³ Skolkovo Institute of Science and Technology, 100 Novaya str., Skolkovo, Moscow Region, 143025, Russia

Organic-inorganic metal halide perovskite solar cells, which were invented in 2009 ^[1], have been attracting much attention because of their high power conversion efficiency (PCE). Only in these 5 years, the PCE of perovskite solar cells has increased from 3.8 % to about 20 %. Beside this promising aspects, the stability is still a concern. As cathodes, hole transport material (HTM), usually spiro-OMeTAD, and gold electrode are used in conventional perovskite solar cells. The spiro-OMeTAD is expensive and gradually deteriorates. The gold electrode is also expensive, moreover, vacuum deposition process hinders the cost-effective manufacturing. Hence, for further low cost bulk production, it is desired to replace HTM and gold electrode to inexpensive and stable materials, which can be fabricated in ambient condition. Single-walled carbon nanotubes (SWNTs) are considered to be one of the promising candidates for the cathode, and there are a few reports on perovskite solar cells with SWNTs ^[2].

In this study, we employed vertically aligned-SWNT (VA-SWNT)/FTO cathodes and fabricated perovskite solar cells (Fig. 1). Perovskite crystals were prepared from PbI₂ and PbCl₂ in ambient conditions. The J-V characteristics show that the PCE of solar cells with SWNT/FTO from PbI₂ and PbCl₂ are 5.4 % and 4.0 %, respectively, while the PCE with HTM/Au are 8.9 % and 10.1 % (Fig. 2). Figure 3 shows the SEM images of perovskite crystal (a) from PbI₂ and (b) from PbCl₂. The surface coverage of perovskite crystal from PbI₂ is larger than that of perovskite crystal from PbCl₂, which indicates the surface coverage has significant effect. The solar cell system using the SWNT transparent conductive film by dry deposition process ^[3] will also be discussed.

[1] A. Kojima *et al.* JACS **131**, 6050 (2009). [2] Z. Li *et al.* ACS Nano **8**, 6797 (2014).

[3] A. G. Nasibulin *et al.* ACS Nano **5**, 3214 (2011).

Corresponding Author: S. Maruyama

Tel: +81-3-5841-6421, Fax: +81-3-5841-6421,

E-mail: maruyama@photon.t.u-tokyo.ac.jp

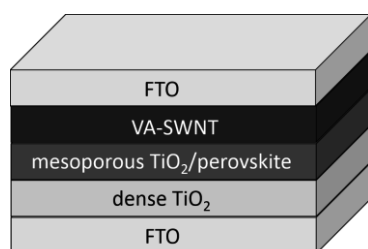


Fig. 1 Schematic image of perovskite solar cells with VA-SWNT.

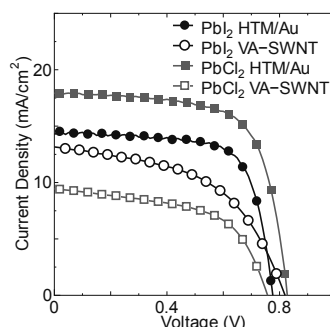


Fig. 2 J-V characteristics of perovskite solar cells.

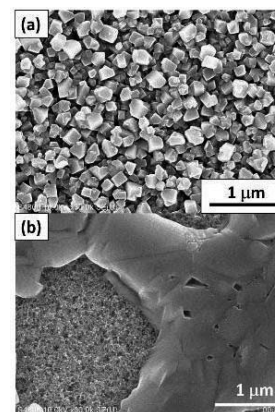


Fig. 3 SEM images of perovskite crystal (a) from PbI₂ and (b) PbCl₂.

Non-catalytic CVD growth from carbon nanotube forest formed by SiC surface decomposition

Yu Hirano¹, Masafumi Inaba¹, Megumi Shibuya¹, Kazuma Suzuki¹, Chih-Yu Lee¹, Miho Myodo¹, Atsushi Hiraiwa¹, Wataru Norimatsu², Michiko Kusunoki², Hiroshi Kawarada¹

¹ School of Science and Engineering, Waseda University, Tokyo 169-8555, Japan

² Eco Topia Science Institute, Nagoya University, Aichi 464-8603, Japan

We report the non-catalytic synthesis of carbon nanotubes by thermal CVD method from uncapped carbon nanotube forest as template. The uncapped CNT forest was formed by SiC surface decomposition (CNT forest on SiC) [1]. CNT forest on SiC consists of nearly ideally close-packed, well-aligned, and catalyst-free CNTs. We also report analysis of the synthesized CNTs by using Raman spectroscopy and SEM, and investigation of the chirality and the growth model.

CNT forest was formed on the C-face (000 $\bar{1}$) of n-type 4H-SiC substrate with SiC surface decomposition method. The length of CNT forest was about 30 nm. Then, this CNT forest was treated to uncap CNTs by mild oxidation with 15 wt%, 100°C H₂O₂ solution [2]. CNTs were grown from uncapped CNT surface by thermal CVD method with CH₄ and H₂ as source gases. Fig.1 shows the schematic image of this experimental.



Fig.1 Process image of this experimental

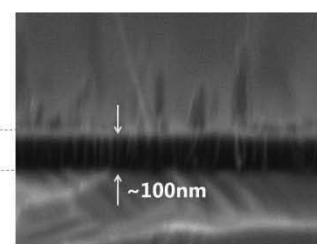


Fig.2 The SEM image after CVD (CH₄ 40%, 1000°C, 1h)

We explored the optimal proportion of these gases and temperature condition for growth. In thermal CVD method, CNTs were grown under wide range conditions; at 1000°C, CH₄ proportion of 10~100% (H₂ dilution, total flow 50 sccm). The best condition of these gases for non-catalytic CVD growth was CH₄ ratio of 40%, 1000°C. The CNT forest thickness increased homogeneously from 30 nm to about 100 nm in this condition, various diameters CNTs grew rapidly from the surface of CNT forest. The ratio of the rapidly grown CNTs was estimated to be about 1/1000 of uncapped CNT surface.

Raman spectra after uncap, CVD 1h, and CVD 4h (the treatment conditions were the same as the above) are shown in Fig.3. As the CVD growth time got longer, the intensity of G-band increased and G/D ratio became higher. Non-catalytic CNTs growth in CVD continued for a long period. Also, we can see enhanced RBM spectra after 4h CVD growth indicating high quality CNTs were synthesized.

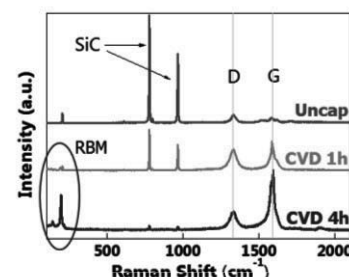


Fig.3 Raman spectra after uncap, CVD 1h, and 4h

[1] M. Kusunoki *et al.*, *Appl. Phys. Lett.* 87, 103105 (2005)

[2] R. Marega *et al.*, *Carbon* 47, 675 (2009).

Corresponding Author: Y. Hirano/Tel: 03-5286-3391, Fax: 03-5286-3391, E-mail: yu.-855@ruri.waseda.jp

Structure and electronic state of [lucigenin] C_{60} molecular fulleride salt

○Hiroshi Moriyama¹, Shohei Yamamoto¹, Hatsumi Mori², Kenji Yoza³, Hideyuki Hara⁴

¹Department of Chemistry, Toho University, Miyama 2-2-1, Funabashi 274-8510, Japan

²Institute for Solid State Physics, The University of Tokyo, Kashiwanoha 5-1-1, Kashiwa, 277-8581, Japan

³Bruker AXS, Moriyacho 3-9, Yokohama, 221-0022, Japan

⁴Bruker Biospin, Moriyacho 3-9, Yokohama, 221-0022, Japan

Fullerene C_{60} has high electron affinity, and is easily reduced to form fulleride anion radicals by accepting an electron. Electrocrystallization of C_{60} in the presence of appropriate counter cations affords relatively stable single crystals of radical salts. In this study, we used lucigenin (Fig. 1) as a counter cation for the preparation of fulleride salts because lucigenin has an intriguing charge state (+2, +1, 0) and its fulleride salts are obtained by electrocrystallization. We determined the crystal structure by single-crystal X-ray diffraction analysis and investigated the electronic state of the fulleride salt by ESR measurements.

Single-crystal X-ray analysis of the crystal structure revealed that in [lucigenin] C_{60} the ratio of lucigenin: C_{60} is 1:1 (Fig. 2). A columnar structure of C_{60} moieties was observed with a C_{60} - C_{60} distance of 9.993 Å (Fig. 2), within van der Waals interaction. Jahn-Teller distortion of the C_{60} cage was clearly observed; thus there was descent in symmetry of the C_{60} moiety from I_h to S_6 . The Jahn-Teller distortion causes orbital splitting of t_{1u} . Therefore, it was expected that the t_{1u} orbital would be split into e_u and a_u orbitals.

An ESR spectrum showed a weak signal assignable to a trace amount of $[C_{120}O]^{n-}$, but there was no broad signal characteristic of $C_{60}^{\cdot-}$. This result implies that the charge state of C_{60} was further reduced to C_{60}^{2-} from C_{60}^{1-} and the lucigenin cation remains 2^+ . It should be noted that the spin state of C_{60}^{2-} is not the degenerated spin-parallel triplet state (Fig. 3, left), but the singlet state (spin paired) of the a_u state caused by Jahn-Teller distortion. Therefore, the a_u orbital is occupied by two electrons, and hence the charge state of the salt was found to be ESR-silent $[lucigenin]^{2+}(C_{60})^{2-}$. However, spin singlet-triplet conversion should easily occur to give the triplet state, ESR-active parallel spins on the e_u orbital, because ΔEST (the singlet-triplet energy gap) was found to be rather small.

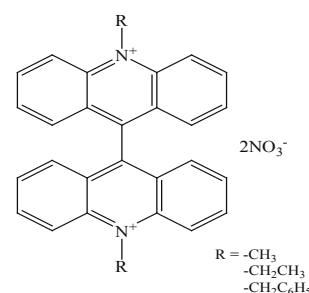


Fig. 1 Lucigenin and analogues

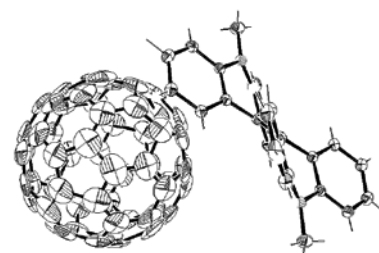


Fig. 2 ORTEP diagram of [lucigenin] C_{60}

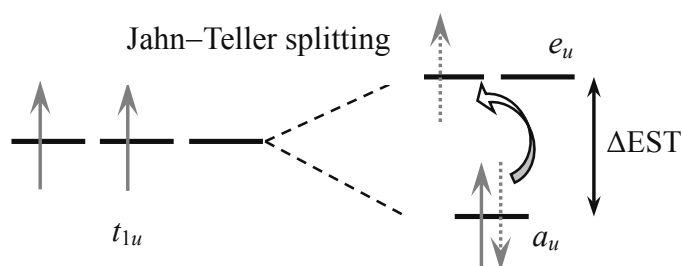


Fig. 3 Singlet-triplet splitting model

Method of Separating Endohedral Metallofullerenes using Electron Donor and Polar Solvent

○Kazuki Chiba, Kazuhiko Akiyama, and Shiro Kubuki

Department of Chemistry, Tokyo Metropolitan University, Hachioji 192-0397, Japan

Various methods for the separation of endohedral metallofullerene (EMF) have been developed and reported so far. One of the most efficient way is electrochemical separation making use of the difference in the redox potential between EMF and empty fullerene. In 2012, a method for the separation with TiCl_4 was reported [1]. EMF in fullerene crude extract is selectively oxidized with TiCl_4 , and efficiently separated as the precipitate. So the formation of precipitate composed of EMF- TiCl_4 aggregate and their particle size are found to be the most important parameters, this separation method could be effectively applied for the separation of the large amount of EMFs [2]. However, this method is not suitable for the separation of trace amount of EMF, such as carrier-free radioactive EMFs applicable for the nuclear medicine, because the formation of aggregate and their size are expected to be insufficient. Herein, we report a newly developed separation method without aggregation of EMFs using electron donor and polar solvent.

Fullerene crude extract was prepared by arc-discharge method using porous carbon rod containing La and radio-tracer of ^{139}Ce . Fivefold volume of 0.3 M triethylamine (TEA)/acetonitrile solution was added to the CS_2 solution of the fullerene crude extract for the reduction of EMF and to remove the empty fullerenes as a precipitate. After the shaking it for 5 minutes, this suspended solution was filtered. The filtrate was treated with dichloroacetic acid (DCA) to oxidize EMF to its neutral form and then analyzed with high performance liquid chromatography (HPLC). Figure 1(a) shows the HPLC chromatogram of the filtrate after removal of DCA. For the comparison, the chromatograms of the EMF rich fraction separated with TiCl_4 (b) and fullerene crude extract (c) are also indicated. The peak intensity of $\text{La}@C_{82}$ was almost same as those in crude extract and fraction separated with TiCl_4 . On the other hand, the intensities of C_{60} and C_{70} were decreased drastically compared to those in crude extract, though those of higher fullerenes such as C_{78} and C_{84} were still remained. The separation rate, which was defined as the percentage of the amount of EMF after separation to before, was determined from γ ray measurement using ^{139}Ce -EMF as a radio-tracer and was found to be $93 \pm 2\%$.

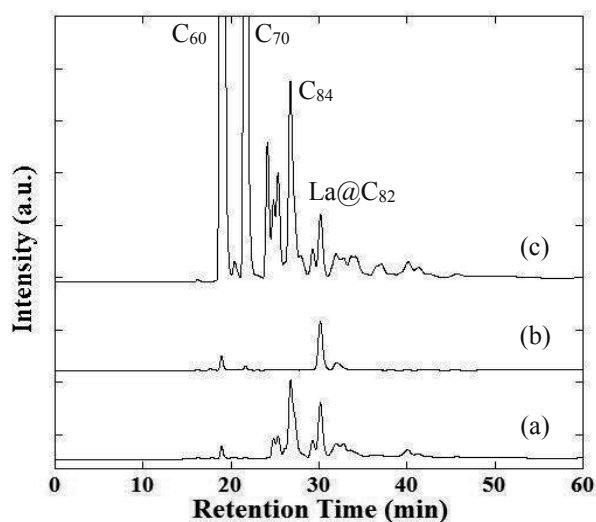


Fig.1 HPLC chromatograms of (a) filtrate of the separation with TEA, (b) EMF rich fraction separated with TiCl_4 and (c) fullerene crude extract. (column: 5PYE, eluent: chlorobenzene)

[1] K. Akiyama *et al.*, *J. Am. Chem. Soc.*, **134**, 9762-9767, (2012).

[2] K. Chiba *et al.*, 5th Asia-Pacific Symposium on Radiochemistry, 271p-24-APP-04 (Kanazawa, 2013).

Corresponding Author: K. Akiyama

Tel: +81-42-677-2525 (Ext. 3587), E-mail: kakiyama@tmu.ac.jp

Vibronic Coupling Density Analysis for Multiple Cycloadditions to C₆₀

○ Naoki Haruta¹, Tohru Sato^{1,2}, Kazuyoshi Tanaka¹

¹*Department of Molecular Engineering, Graduate School of Engineering,
Kyoto University, Kyoto, 615-8510, Japan*

²*Unit of Elements Strategy Initiative for Catalysts & Batteries, Kyoto University,
Nishikyo-ku, Kyoto 615-8510, Japan*

Much attention has been attracted to functionalizations of fullerenes because fullerene derivatives such as PCBM have been used in the field of material chemistry. Theoretical prediction for the regioselectivity of fullerenes and their derivatives would therefore be helpful to develop novel fullerene-based materials.

The frontier orbital theory is such a theory. However, the conventional frontier orbital theory sometimes fails to predict the regioselectivities of fullerenes because their frontier orbitals are strongly delocalized due to the large molecular size and high symmetry. To overcome this difficulty, we have proposed vibronic coupling density (VCD) as a reactivity index [1,2]. It can be formulated in the framework of Parr and Yang's conceptual density functional theory [3]. The VCD theory takes into consideration not only electronic states but also molecular deformations. This is in contrast to the frontier orbital theory, in which only the electronic states (frontier orbitals) are considered.

In our previous studies, we have explained the reactive sites of C₆₀ [2], C₇₀ [4], and La₂@C₈₀ [5] on the basis of the VCD theory. We found their reactive sites to have almost the same VCD distributions as a dienophile, ethylene (Fig. 1). This is consistent with experimental observations that fullerenes act like dienophiles in Diels–Alder reactions. The VCD analysis enabled us to extract a picture of the functional group, ethylene.

In this study, we applied the VCD theory to successive multiple cycloadditions of butadienes to C₆₀ [6]. C₆₀ *n*-adducts (*n* = 1, ⋯, 6) were experimentally reported to be synthesized [7-9]. We calculated the VCDs of C₆₀ adducts with *n* butadienes (*n* = 1, ⋯, 5) and analyzed their reactivities. Just like C₆₀, all the calculated C₆₀ multiadducts were found to have ethylene-like VCD distributions at their reactive sites. This is consistent with experimental observations that C₆₀ multiadducts behave as dienophiles in multiple cycloadditions. Furthermore, the VCD theory predicted that the hexakisadduct with a six-fold axis can be finally obtained, which is also consistent with experimental findings [8,9].

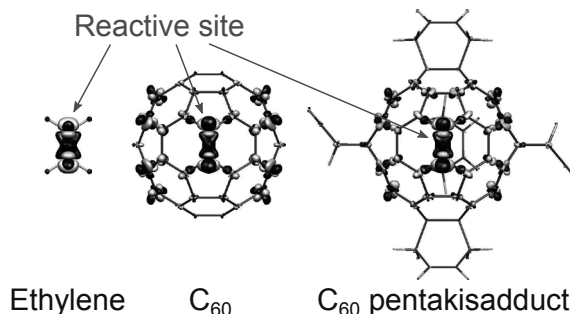


Fig. 1: VCDs of ethylene, C₆₀, and C₆₀ pentakisadduct for their effective modes in nucleophilic cycloadditions.

- [1] T. Sato *et al.*, *J. Phys. Chem. A* **112**, 758 (2008). [2] T. Sato *et al.*, *Chem. Phys. Lett.* **531**, 257 (2012). [3] R. G. Parr and W. J. Yang, *J. Am. Chem. Soc.* **106**, 4049 (1984). [4] N. Haruta *et al.*, *J. Org. Chem.* **77**, 9702 (2012). [5] N. Haruta *et al.*, *J. Org. Chem.* **80**, 141 (2015). [6] N. Haruta *et al.*, *Tetrahedron* **70**, 3510 (2014). [7] A. Hirsch *et al.*, *Angew. Chem., Int. Ed. Engl.* **33**, 437 (1994). [8] A. Hirsch *et al.*, *J. Am. Chem. Soc.* **116**, 9385 (1994). [9] B. Kräutler and J. Maynollo, *Angew. Chem., Int. Ed. Engl.* **34**, 87 (1995).

Corresponding Author: T. Sato

Tel: +81-75-383-2803, Fax: +81-75-383-2555

E-mail: tsato@moleng.kyoto-u.ac.jp

From linear carbon molecules to fullerenes under laser vaporization - Growth, annealing, and quenching -

○Tomonari Wakabayashi¹, Yoriko Wada², Yusuke Morisawa¹, Hitomi Endo², Yuki Taguchi²,
Jun Matsumoto², Takeshi Kodama², Yohji Achiba², Haruo Shiromaru²

¹ Department of Chemistry, Kinki University, Higashi-Osaka 577-8502, Japan

² Department of Chemistry, Tokyo Metropolitan University, Hachioji 192-0397, Japan

Laser vaporization of graphite has opened a wide variety of synthetic routes to novel carbon nanostructures, i.e., linear carbon molecules [1], monocyclic rings [2], fullerenes [3], and nanotubes [4]. It is essentially a high-temperature process, instantaneously heating target materials above 4,000 K, followed by ablation of layered carbons, which eventually fragment into scrambling small carbon molecules of sp hybridization. The sticky carbon molecules agglomerate rapidly, growing into spheroidal nanoparticles through self-annealing by latent heat of isomerization from sp to sp^2 as well as by heat of formation of chemical bonds [5].

When the cooling process is accompanied by subsidy annealing by the heat of an external source like a furnace, keeping the ambient temperature above $\sim 800^\circ\text{C}$ for more than a millisecond, the molecular carbon aggregates are efficiently converted to perfect symmetry of hollow, closed carbon cages of fullerenes [6]. Assisted by the presence of appropriate metal catalysts, carbon vapor molecules condense into a nano-sized metal particle then crystallize on the surface into nanotubes. Both, fullerenes and nanotubes, are based on sp^2 hybridization and thermodynamically stable allotropic forms of carbon at standard conditions.

Another form of carbon, amongst those appeared in the context of allotropy of carbon, naturally be a linearly organized solid form of sp carbon atoms, namely carbyne. A number of attempts have been made but thwarted in characterizing the material in a crystallographic sense [7]. It is in one part by metastable nature in thermodynamics and in another by highly reactive nature of unsaturated chemical bonds in the sp form of carbon. Again, under the condition of laser vaporization, such a transient species of sp carbon atoms can be quenched chemically as hydrogen-end-capped linear carbon molecules, namely polyynes [8,9], or as a self-terminated monocyclic ring of carbon, cyclic- C_{10} [10]. In a balance of competitive reactions between growth and quenching, possibly with annealing, polyynes and fullerenes are formed simultaneously under laboratory conditions. We discuss our recent finding on the process of laser vaporization forming polyynes, fullerenes, and monocyclic carbon rings.

[1] J. R. Heath *et al.* J. Am. Chem. Soc. **109**, 359 (1987).

[2] S. Yang *et al.* Chem. Phys. Lett. **144**, 431 (1988).

[3] H. W. Kroto *et al.* Nature **318**, 162 (1985).

[4] S. Iijima *et al.* Nature **363**, 603 (1993).

[5] T. Wakabayashi *et al.* J. Phys. Chem. B **108**, 3686 (2004).

[6] R. E. Haufler *et al.* Proc. Mat. Res. Soc. Symp. **206**, 627 (1991).

[7] F. Diederich *et al.* Acetylene Chemistry, Wiley, Chap. 9 (2005).

[8] M. Tsuji *et al.* Chem. Phys. Lett. **355**, 101 (2002).

[9] H. Tabata *et al.* Carbon. **44**, 522 (2006).

[10] Y. Kato *et al.* Chem. Phys. Lett. **386**, 279 (2004).

Corresponding Author: T. Wakabayashi

Tel: +81-6-4307-3408, Fax: +81-6-6723-2721,

E-mail: wakaba@chem.kindai.ac.jp

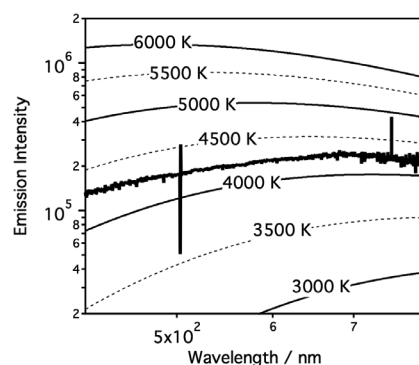


Fig. 1. Spectrum of blackbody radiation of laser ablated carbon particles in hexane (~ 4100 K).

The effect of DNA adsorption on optical transitions in single-walled carbon nanotube depending on base sequence

○Masahiro Ito, Yusuke Ito, Hiroki Kato, Kazuo Umemura, Yoshikazu Homma

Department of Physics, Tokyo University of Science, Tokyo 152-8601, Japan

DNA-SWNT hybrids emit photoluminescence (PL) not only in solution [1], but also on a substrate under the dry condition [2]. PL spectra can be used to analyze the adsorption state of DNA on SWNT. However, it is difficult to evaluate purely the effect of DNA adsorption from DNA-SWNTs in solution or their ensembles on a substrate. In this study, we prepared low density DNA-SWNTs on the SiO₂ substrate to detect a mono-dispersed DNA-SWNT in the laser spot. Single-stranded DNA (ssDNA): (dT)₃₀, (dA)₃₀, (dC)₃₀ and (dG)₃₀ were used and their effect on PL was investigated.

In the case of DNA-SWNT in solution, the difference in PL spectra did not appear specifically, although PL spectra from (dT)₃₀-SWNT showed blue-shifts relative to other ssDNA. In contrast, PL from mono-dispersed DNA-SWNT exhibited different peaks depended on the base sequence of DNA, as shown in Fig. 1 for (9,4) SWNT. The dependence of the energy shift on the DNA type is almost the same for different chiralities. PL emission peaks from each type of ssDNA-SWNT are listed in Table 1. The PL energy of mono-dispersed DNA-SWNT shifted in the order (dT)₃₀, (dA)₃₀, (dC)₃₀ and (dG)₃₀.

PL shifts cannot be explained only by the difference in the number of π - π stacking. If we take into account the number of n- π stacking, the tendency of red shift should be T < A < C < G. PL spectra reflect the interaction between SWNT and DNA base.

[1] M. Zheng et al. Nature, **2**, 338 (2003)

[2] M. Ito et al. Appl. Phys. Lett. **104**, 043102 (2014)

Corresponding Author: M. Ito

Tel: +81-3260-4271-, Fax: +81-3-5261-1023,

E-mail: m-ito@rs.tus.ac.jp

Table 1. PL emission peaks from each type of DNA-SWNT under the dry condition.

chirality	Emission wavelength (nm)			
	(dT) ₃₀	(dA) ₃₀	(dC) ₃₀	(dG) ₃₀
(10,2)	1067	1072	1078	1083
(9,4)	1119	1123	1124	1131
(8,6)	1185	1186	1202	1202
(8,7)	1278	1282	1290	1303

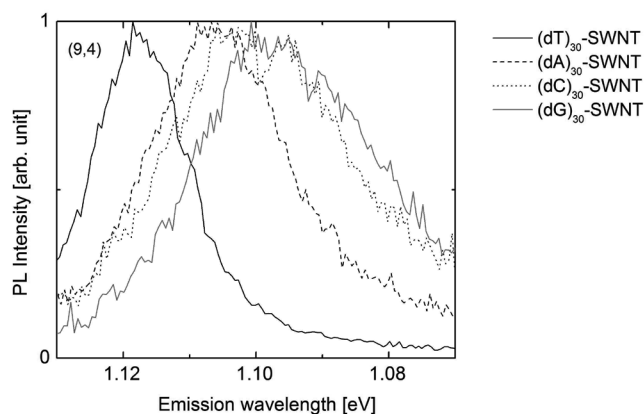


Fig 1. PL peaks from various mono-dispersed DNA-SWNTs.

Electronic properties and polarities of atomic-layer materials: Doped graphene, hexagonal BN layers, and carbon nanotubes

○Susumu Saito^{1,3,4}, Takashi Koretsune², and Yoshitaka Fujimoto¹

¹ *Department of Physics, Tokyo Institute of Technology, Tokyo 152-8551, Japan*

² *RIKEN Center for Emergent Matter Science, Saitama 351-0198, Japan*

³ *International Research Center for Nanoscience and Quantum Physics,
Tokyo Institute of Technology, Tokyo 152-8551, Japan*

⁴ *Materials Research center for Element Strategy, Tokyo Institute of Technology,
Kanagawa 226-8503, Japan*

For more than a decade, we have theoretically studied the electronic properties of a variety of doped and structurally modified atomic-layer materials including graphene, hexagonal BN layers, and carbon nanotubes using the predictive density-functional methods [1-10]. It has been demonstrated that the doping as well as the structural modification can give rise to the defect states which should govern the polarity and the electronic transport properties of the system. In addition, it has been also shown that the adsorption of hydrogen atoms around the impurity site can further modify the electronic properties. In the low-dimensional atomic-layer materials the adsorption of hydrogen and other molecules around the impurity site should take place more easily than in the ordinary bulk materials and therefore the effects of their adsorption on the electronic properties are to be of high importance in the future device applications of the atomic-layer materials.

In this presentation we first review the above-mentioned interesting and important modifications of electronic properties in atomic-layer materials including monolayer graphene, bilayer graphene, monolayer and bilayer hexagonal BN, and carbon nanotubes. Next we propose a rather simple theory to predict the electronic polarities of the doped atomic-layer materials.

- [1] T. Matsumoto and S. Saito, J. Phys. Soc. Japan **71**, 2765 (2002).
- [2] T. Koretsune and S. Saito, Physical Review B **77**, 165417 (2008).
- [3] N. Murata, J. Haruyama, J. Reppert, A.M. Rao, T. Koretsune, S. Saito, M. Matsudaira and Y. Yagi, Phys. Rev. Lett. **101**, 027002 (2008).
- [4] T. Koretsune and S. Saito, Sci. Technol. Adv. Mater. **9** 044203 (2008).
- [5] Y. Fujimoto and S. Saito, Physica E **43**, 677-680 (2011).
- [6] Y. Fujimoto, and S. Saito, J. Phys: Conf. Ser. **302**, 012006 (2011).
- [7] Y. Fujimoto and S. Saito, Phys. Rev. B **84**, 245446 (2011).
- [8] Y. Fujimoto and S. Saito, J. Appl. Phys. **115**, 153701 (2014).
- [9] Y. Fujimoto and S. Saito, JPS Conf. Proc. **1**, 012066 (2014).
- [10] Y. Fujimoto and S. Saito, Surface Science (in press).

Corresponding Author: Susumu Saito

E-mail: saito@stat.phys.titech.ac.jp

Electronic States of Flattened Carbon Nanotubes: Effects of tube chirality and displacement

○ Takeshi Nakanishi¹, and Tsuneya Ando²

¹*Nanosystem Research Institute, AIST, Japan*

²*Department of Physics, Tokyo Institute of Technology, Japan*

We theoretically study effects of inter-wall interaction in flattened carbon nanotubes, first directly calculating effective inter-wall interaction within an effective-mass scheme and second regarding flattened tubes as ribbons of bilayer graphene with closed edges described by boundary conditions explicitly derived.

Within the effective-mass scheme, effects of inter-wall interactions are shown to be important in non-chiral nanotubes such as zigzag and armchair. In fact, with the increase in the width of the flattened region, the band structure approaches that of a bilayer ribbon in which the electron motion in the ribbon-width direction is discretized. In chiral nanotubes, inter-wall interaction can essentially be neglected except in the vicinity of non-chiral tubes. Inter-wall interactions diminish rapidly when chiral angle deviates from zigzag or armchair, although the decay is slower in the vicinity of the armchair tube. When the flattened region has the structure of AA and AB stacked bilayer graphene, the same results can be derived by calculating boundary conditions corresponding to the closed-edge structure in which the top and bottom layers are smoothly connected through a monolayer graphene.

Coherent and squeezed phonons in single wall carbon nanotubes

○ Ahmad R.T. Nugraha, Eddwi H. Hasdeo, Riichiro Saito
Department of Physics, Tohoku University, Sendai 980-8578, Japan

Ultrashort laser pulses with duration less than a typical phonon period given to a single wall carbon nanotube (SWNT) sample may generate lattice oscillations coherently, or called as the coherent phonons. Quantum mechanically, these oscillations can be treated using the concept of coherent states, in which the amplitude-phase uncertainty reach its minimum value [1-3]. In general, we may increase the uncertainty in the amplitude and at the same time decrease the uncertainty in the phase, or vice versa, while still holding the minimum uncertainty principle. These states are referred to as the squeezed states. The squeezed phonons in solid state systems have been previously reported to exist in some materials having strong electron-phonon coupling, such as CdZnTe and ZnTe [4]. Recently, there is also a possibility to generate squeezed phonons in SWNTs via ultrafast spectroscopy using less than 10-fs pulses, in which the coherent oscillations of G' bands involving second-order (two-phonon) process may be relevant as a particular example [5-6].

In this work, we calculate the squeezed phonon amplitude of G' band for a given SWNT and compare it with the coherent phonon amplitude of G band. The squeezed phonon amplitude for the G' band is defined by taking an average of the coherent states of the two phonons generated in the second order process with nonzero wavevectors. By using these phonon amplitudes, we find that the ratio between the G' band and G band intensity ($I_{G'}/I_G$) in ultrafast spectroscopy can be adjusted depending on some parameters such as the laser energy, laser pulse width, and SWNT chirality (electron-phonon coupling). This result might be useful for understanding the coherent control of phonon excitations, i.e. we may be able to selectively excite a certain phonon mode by adjusting some physical parameters. It is also very interesting to see that the coherent states and squeezed states of phonons can be excited simultaneously in an individual SWNT.

[1] J.-H. Kim et al., *Chem. Phys.* **413**, 55-80 (2013).

[2] A. R. T. Nugraha et al., *Phys. Rev. B* **84**, 174302 (2011).

[3] A. R. T. Nugraha et al., *Phys. Rev. B* **88**, 075440 (2013).

[4] Y.-S. Lim et al., *Phys. Rev. B* **68**, 153308 (2003).

[5] Y.-S. Lim et al., *Nano Lett.* **14**, 1426-1432 (2014).

[6] K. Sato et al., *Conference on Lasers and Electro-Optics, QELS JTh 2A* (2013).

Corresponding Author: A.R.T. Nugraha

TEL: +81-22-795-6442, FAX: +81-22-795-6447, E-mail: nugraha@flex.phys.tohoku.ac.jp

Stark effect of excitons in individual air-suspended carbon nanotubes

○M. Yoshida, Y. Kumamoto, A. Ishii, A. Yokoyama, Y. K. Kato

Institute of Engineering Innovation, The University of Tokyo, Tokyo 113-8656, Japan

We investigate electric-field induced redshifts of photoluminescence from individual single-walled carbon nanotubes [1]. Photoluminescence spectra of air-suspended nanotubes within field-effect transistor structures are collected under an application of symmetric bias voltages on source and drain contacts [2]. We find that redshifts scale quadratically with field, while measurements with different excitation powers and energies show that effects from heating and relaxation pathways are small. We attribute the shifts to the Stark effect, and characterize nanotubes with different chiralities. By taking into account exciton binding energies for air-suspended tubes, we find that theoretical predictions are in quantitative agreement.

Work supported by KAKENHI, the Canon Foundation, Asahi Glass Foundation, and KDDI Foundation, as well as the Photon Frontier Network Program of MEXT, Japan. M.Y. is supported by ALPS, and A.I. is supported by MERIT and JSPS Research Fellowship.

- [1] M. Yoshida, Y. Kumamoto, A. Ishii, A. Yokoyama, and Y. K. Kato, *Appl. Phys. Lett.* **105**, 161104 (2014).
- [2] Y. Kumamoto, M. Yoshida, A. Ishii, A. Yokoyama, T. Shimada, and Y. K. Kato, *Phys. Rev. Lett.* **112**, 117401 (2014).

Corresponding Author: Y. K. Kato
Tel: +81-3-5841-7702, Fax: +81-3-5841-7772
E-mail: ykato@sogo.t.u-tokyo.ac.jp

Exciton diffusion, end quenching, and exciton-exciton annihilation in individual air-suspended carbon nanotubes

○A. Ishii, M. Yoshida, and Y. K. Kato

Institute of Engineering Innovation, The University of Tokyo, Tokyo 113-8656, Japan

Luminescence properties of carbon nanotubes are strongly affected by exciton diffusion, which plays an important role in various nonradiative decay processes [1]. Here we perform photoluminescence microscopy on hundreds of individual air-suspended carbon nanotubes to elucidate the interplay between exciton diffusion, end quenching, and exciton-exciton annihilation processes [2]. A model derived from random-walk theory as well as Monte Carlo simulations are utilized to analyze nanotube length dependence and excitation power dependence of emission intensity. We have obtained the values of exciton diffusion length and absorption cross section for different chiralities, and diameter-dependent photoluminescence quantum yield have been observed. The simulations have also revealed the nature of a one-dimensional coalescence process, and an analytical expression for the power dependence of emission intensity is given.

Work supported by KAKENHI (23104704, 24340066, 24654084, 26610080), The Canon Foundation, Asahi Glass Foundation, KDDI Foundation, and the Photon Frontier Network Program of MEXT, Japan. The samples were fabricated at the Center for Nano Lithography & Analysis at The University of Tokyo. A.I. is supported by MERIT and JSPS Research Fellowship, and M.Y. is supported by ALPS.

- [1] S. Moritsubo, T. Murai, T. Shimada, Y. Murakami, S. Chiashi, S. Maruyama, and Y. K. Kato, *Phys. Rev. Lett.* **104**, 247402 (2010).
- [2] A. Ishii, M. Yoshida, and Y. K. Kato, arXiv:1412.7622 (2014).

Corresponding Author: Y. K. Kato

Tel: +81-3-5841-7702, Fax: +81-3-5841-7772,

E-mail: ykato@sogo.t.u-tokyo.ac.jp

Bandgap opening in bilayer graphene at metal contacts

○Ryo Nouchi¹

¹ *Nanoscience and Nanotechnology Research Center, Osaka Prefecture University, Sakai, Osaka 599-8570, Japan*

Bilayer graphene (BLG) possesses a finite bandgap when a potential difference is introduced between the two constituent graphene layers. The potential difference can be generated by applying a perpendicular electric field [1] and by introducing a difference in the carrier concentration between the two graphene layers by means of surface charge transfer from the adsorbed layers [2]. As a possible source for the latter mechanism, in addition to foreign molecules/atoms unintentionally adsorbed on the surface of the BLG, the metal contacts must be taken into account. Finite charges are transferred through the contacts due to the Fermi level alignment between the metallic electrodes and the BLG. Thus, it is expected that a finite bandgap exists at the metal contacts. In this presentation, an experimental signature of the bandgap opening in BLG at the metal contacts will be discussed [3].

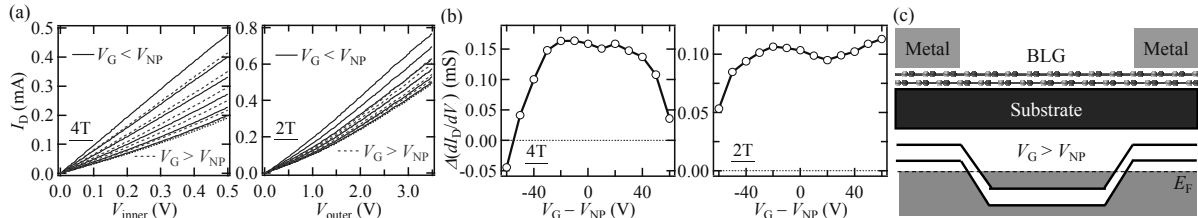


Fig.1 (a) Current-voltage characteristics measured with 4T and 2T configurations. The maximum voltage was chosen to equalize the electric field strength. (b) Gate-voltage dependence of the degree of the nonlinearity extracted from (a). (c) Expected band diagram for the positively-gated region.

BLG flakes were formed on a Si/SiO₂ substrate by mechanical exfoliation from a graphite crystal. The source/drain electrodes made of Cr/Au were formed on the flakes by electron-beam lithography processes. A 300-nm-thick SiO₂ layer acted as the gate insulator.

Figure 1a shows high-field transport characteristics of the fabricated BLG field-effect transistor measured with four- (4T) and two-terminal (2T) configurations. A difference in the first-order derivative of I_D at the maximum voltage and 0 V, $\Delta(dI_D/dV)$, is employed as an indicator of nonlinearity of the current-voltage characteristics, which becomes positive (negative) for superlinear (sublinear) curves. Figure 1b shows the gate-voltage dependence of the indicator of the nonlinearity. The positive values around the charge neutrality point, V_{NP} , in the 4T plot can be understood by multiple carrier tunneling processes through the bandgap induced by charge puddles. The increase in the indicator in the positively-gated region of the 2T plots and its absence in the 4T data coincides with the carrier tunneling through the bandgap at the two pn junctions formed in the BLG channel (Fig. 1c). The opening of a bandgap at the metal-BLG contacts is an additional source of electrode-contact resistance.

[1] Y. Zhang *et al.* Nature **459**, 820 (2009).

[2] T. Ohta, A. Bostwick, T. Seyller, K. Horn, and E. Rotenberg, Science **313**, 951 (2006).

[3] R. Nouchi, Appl. Phys. Lett. **105**, 223106 (2014).

Corresponding Author: R. Nouchi

Tel: +81-72-254-8394, Fax: +81-72-254-8394,

E-mail: r-nouchi@21c.osakafu-u.ac.jp

Band-like transport in reduced graphene oxide films

○R. Negishi¹, M. Akabori², S. Yamada², T. Ito³, Y. Watanabe⁴, Y. Kobayashi¹

¹Department of Applied Physics, Osaka University, Suita 565-0871, Japan

²Center for Nano Materials and Technology, JAIST, Nomi 923-1292, Japan

³Synchrotron Radiation Research Center, Nagoya University, Nagoya 464-8603, Japan

⁴Aichi Synchrotron Research Center, Seto, 489-0965, Japan

Utilizing carrier transport that reflects intrinsic graphene band structure is essential for the excellent electrical performance of the graphene-based transistors. The reduced graphene oxide (rGO) film is one of promising materials for large area synthesis of graphene. However electrical performance of the rGO is insufficient, since electrical transport properties of rGO are described by the 2-dimensional variable range hopping (VRH) model through the localization states [1-3] because of many defects still remaining in the rGO. In this study, we found that the high temperature process above 1100 °C in ethanol environment (hereafter “ethanol treatment”) enables us to overcome this issue from the analysis of X-ray absorption fine structure (XAFS) spectra and conductivity of the rGO films.

The ethanol treatment of the GO films was carried out using the chemical vapor deposition apparatus with a furnace. The unoccupied π^* and σ^* states of the rGO are evaluated from XAFS spectra using synchrotron radiation. The conductivity of the rGO films were measured by Hall-effect measurements using van der Pauw method.

Figure 1 shows XAFS spectra observed from the rGO films after ethanol treatment at 900, 1000, and 1130 °C, thermal annealing in H₂/Ar at 1130 °C and highly oriented pyrolytic graphite (HOPG). The unoccupied π^* and σ^* states are clearly observed at photon energy of 285.4 and 292 eV. The π^* peak intensity as shown by double head arrow becomes stronger for ethanol treatment at 1130 °C compared to the other treatments. This means that high temperature above 1100 °C in ethanol treatment leads to significant expansion of conjugated π -electron system in the rGO films. The expansion of π system is also confirmed by prominent emergence of 2D bands in Raman spectra observed from the rGO samples. Temperature dependences of conductivity in the rGO films after ethanol treatment are shown in Fig. 2. The conductivity can be fitted by only the VRH for 900 °C, and by the sum of VRH and thermally activated (TA) conduction ($\sigma_{TA} \propto \exp(-E_a/2k_B T)$) for 1100 °C as indicated by dots and solid lines. The activation energy (E_a) of 13 meV estimated from fitting analysis is smaller than thermal energy at room temperature. This means that the carrier transport around room temperature for the rGO films after ethanol treatment of 1100 °C shows band-like transport due to decreasing barrier height energy between localization states by expansion of conjugated π -electron system. This result indicates that high temperature process above 1100 °C in ethanol environment is indispensable to derive intrinsic electrical properties of graphene from GO.

[1] A. B. Kaiser *et al.* Nano Lett. **9**, 1787 (2009). [2] G. Eda, *et al.*, Adv. Mater. **22**, 505 (2009). [3] R. Negishi and Y. Kobayashi, Appl. Phys. Lett., **105** 253502 (2014). Corresponding Author: R. Negishi, E-mail: negishi@ap.eng.osaka-u.ac.jp

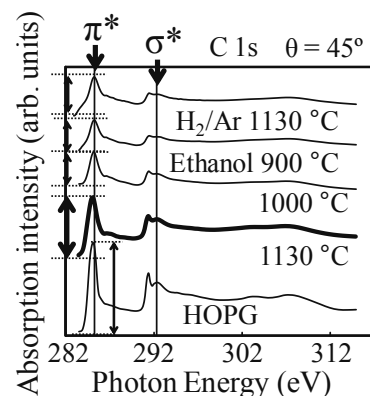


Fig. 1 XAFS spectra observed from the rGO.

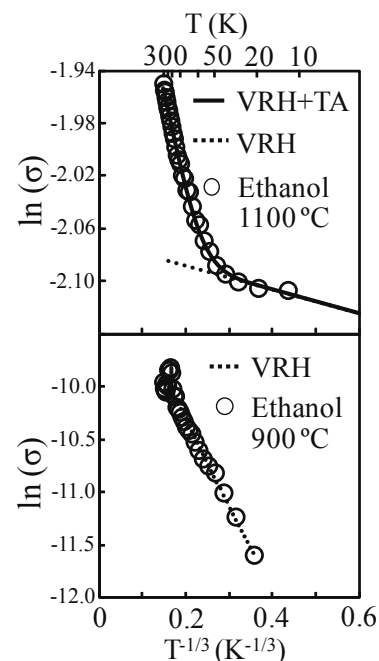


Fig. 2 Temperature dependence of conductivity in rGO samples.

Circularly polarized luminescence from lateral TMD $p-i-n$ junctions

○Yijin Zhang¹, Masaru Onga¹, Yoshihiro Iwasa¹

¹ *Department of Applied Physics, The University of Tokyo, Tokyo 113-8656, Japan*

Transition-metal dichalcogenides (TMDs), ones of the most popular layered materials, are recently attracting growing interests over the world both for device application and for novel peculiar optical physics. Semiconducting members has been proved to be a good transistor channel materials possessing ambipolar high ON/OFF ratio [1], transparency and flexibility [2], possibility of miniaturization[3]. Novel optical properties of TMDs, on the other hand, originate from their unique multi valley band structure in which Fermi pockets exist at the edge (K and $-K$ points) of the Brillouin zone. The innate lack of inversion symmetry in monolayer limit (Fig. 1) lead to inherent valley circular dichroism: optical interband transitions at K and $-K$ are only allowed with σ_+ and σ_- circularly polarized light, respectively [4]. Such a valley dichroic optical selection rule exalts TMDs to potential materials for opto-valleytronics.

In order to merge these two distinct research directions, optoelectronic devices with electrical controllability of valley degree of freedom have been sought. Simple optoelectronic devices can be easily realised by forming lateral (in-plane) $p-i-n$ junction inside TMD channel using ambipolar nature of TMD transistors [5]. We observed electroluminescence from lateral $p-i-n$ junction embedded in WSe₂, a member of TMDs. Interestingly, the luminescence was circularly polarized without valley polarization [6]. Additionally, the degree of polarization changes its sign when the current direction is flipped, indicating the realisation of electrically switchable circularly polarized light source.

The electrical control of circularly polarized light is likely mediated by the band dispersion. In addition to the inversion asymmetry, three-fold rotational symmetry also inheres in monolayer TMDs, which gives rise to anisotropic band dispersion; trigonal warping. The warping is much effective for valence band, while the conduction band is less affected [7]. Therefore, luminescence intensity from a single valley under finite electric field depends on the field direction. Particularly, the intensity differs under rotating field direction by 180° due to the three-fold rotational symmetry.

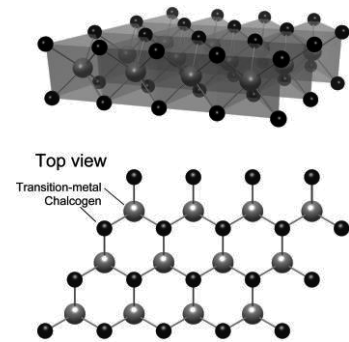


Fig.1 Crystal structure of TMDs

- [1] V. Podzorov *et al.* Appl. Phys. Lett. **95**, 3301 (2004).
- [2] J. Pu *et al.* Appl. Phys. Lett. **103**, 023505 (2013).
- [3] B. Radisavljević *et al.* Nat. Nanotechnol. **6**, 147 (2011).
- [4] D. Xiao *et al.* Phys. Rev. Lett. **108**, 196802 (2012).
- [5] Y. J. Zhang *et al.* Nano Lett. **13**, 3023 (2013).
- [6] Y. J. Zhang *et al.* Science **344**, 725 (2014).
- [7] A. Kormányos *et al.* Phys. Rev. B **8**, 045416 (2013).

Corresponding Author: Y. J. Zhang

Tel&Fax: +81-3-5841-6822,

E-mail: yzhang@mp.t.u-tokyo.ac.jp

Mechanical exfoliation and van der Waals assembly of layered ferromagnetic dichalcogenide Fe_xTaS_2

○Miho Arai¹, Rai Moriya¹, Naoto Yabuki¹, Satoru Masubuchi^{1,3}, Keiji Ueno²,
and Tomoki Machida^{1,3}

¹ *Institute of Industrial Science, University of Tokyo, Tokyo 153-8505, Japan*

² *Department of Chemistry, Saitama University, Saitama 338-8507, Japan*

³ *Institute for Nano Quantum Information Electronics, University of Tokyo, Tokyo 153-8505, Japan*

Recently, two-dimensional (2D) materials and their van der Waals (vdW) heterostructures are received considerable attention for fundamental physics and electronics applications. Previously discovered 2D materials exhibited variety of electronic properties such as metal, semiconductor, insulator, and superconductor. However, ferromagnetic 2D material and its vdW heterostructure are still a missing piece in this field and these are strongly demanded for the purpose of spintronics with 2D materials and vdW heterostructures.

Here we report the mechanical exfoliation and vdW assembly of ferromagnetic layered dichalcogenide Fe_xTaS_2 . The Fe_xTaS_2 has a unique crystal structure; all the Fe atoms intercalate the vdW gap of layered TaS_2 and form ordered structure as illustrated Fig. 1(a) [1]. This material is known to show giant perpendicular magnetic anisotropy below its T_c of 160 K in its bulk form. By using Scotch tape method, we demonstrated the mechanical exfoliation of few tens of nm-thick $\text{Fe}_{0.25}\text{TaS}_2$ flake on SiO_2/Si substrate [Fig. 1(b)]. Magnetic field dependence of Hall and sheet resistance was measured at 2 K and results are shown in Fig. 1 (c). Clear anomalous Hall effect and anisotropic magnetoresistance were observed. The results indicate that the magnetic property of the single crystal $\text{Fe}_{0.25}\text{TaS}_2$ is still conserved in the exfoliated flakes. In addition, we demonstrated vdW assembly of two different $\text{Fe}_{0.25}\text{TaS}_2$ flakes by using dry transfer technique to make it perform as spin valve device [Fig. 2]. Fabricated vdW junction exhibited tunnel magnetoresistance effect.

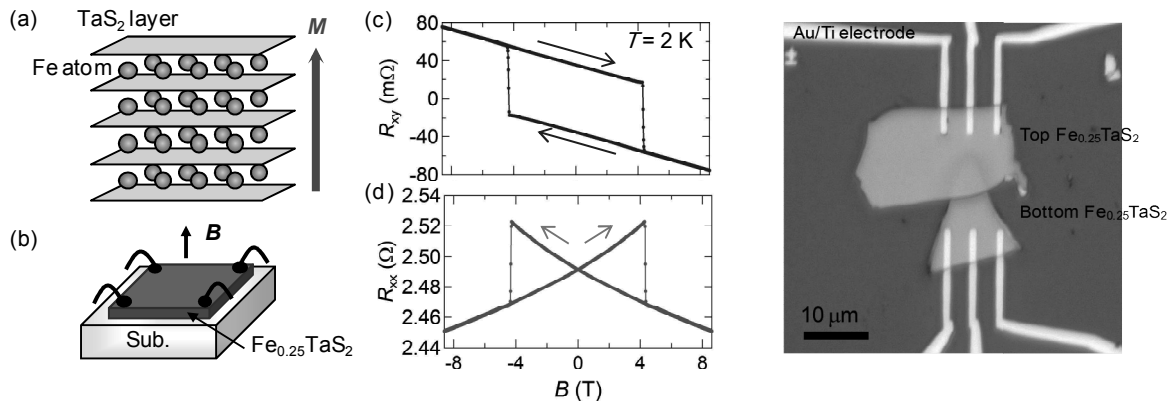


Fig.1 (a) The crystal structure of Fe_xTaS_2 . (b) Illustration of fabricated $\text{Fe}_{0.25}\text{TaS}_2$ devices. (c,d) Magnetic dependence of (c) Hall resistance (R_{xy}) and (d) Sheet resistance (R_{xx}).

Fig.2 Photograph of $\text{Fe}_{0.25}\text{TaS}_2/\text{Fe}_{0.25}\text{TaS}_2$ vdW junction.

[1] J. Checkelsky *et al.*, Phys. Rev. B **77**, 014433 (2008).

Corresponding Author: M. Arai

Tel: +81-3-5452-6158, Fax: +81-3-5452-6157

E-mail: marai@iis.u-tokyo.ac.jp

Optical properties of a few layers black phosphorus, “Phosphorene”

○Takashi Nakamura, Daichi Kozawa, Shinichiro Mouri, Yuhei Miyauchi,
and Kazunari Matsuda

Institute of Advanced Energy, Kyoto University, Kyoto, Japan

Recently atomically thin layered two-dimensional (2D) materials, graphene, and MoS₂, have attracted much interest from the viewpoints of fundamental physics and applications. The black phosphorus is also capable of being mechanically exfoliated to single or several atomic layers, which are called as “phosphorene”. Although the phosphorene is spotlighted as the new material for 2D semiconductor [1], the detail electronic and optical properties have not been fully understood. Thus, we studied single- and multi-layer black phosphorene by using optical spectroscopy, Raman, photoluminescence (PL), and differential reflectivity to understand their characteristic optical and electronic properties.

The inset of Figure 2 shows optical image of a few layers black phosphorene on SiO₂/Si substrate, where the layer number of black phosphorene is confirmed from the optical contrast and Raman spectra [2]. Figure 1 shows the linearly polarized differential reflectivity spectra corresponding to absorption spectrum of black phosphorene on quartz substrate with different thickness. The differential reflectivity spectrum of thick phosphorene (7layers) shows the peak at 0.37 eV, which is almost consistent with the previously reported value of bulk phosphorus [3]. In contrast, the differential reflectivity spectrum of 4layers thin phosphorene shows a peak at 0.42 eV. The observed peak of a few layers black phosphorene at 0.42 eV is assigned as the exciton absorption peak. Moreover, the linearly polarized differential reflectivity spectrum in Fig. 2 shows the strong anisotropic features in the absorption spectrum, which suggest the anisotropic electronic structures of black phosphorene. We will discuss the detail optical and electronic properties of a few layers black phosphorene based on the experimental results of Raman and PL spectroscopy.

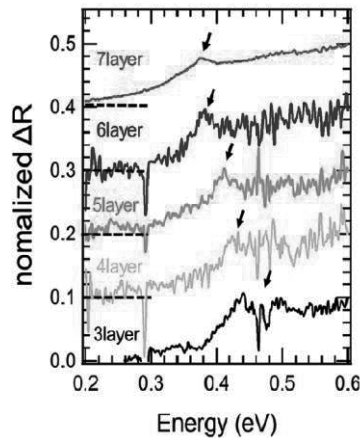


Fig. 1: Differential reflectivity spectrum of phosphorene

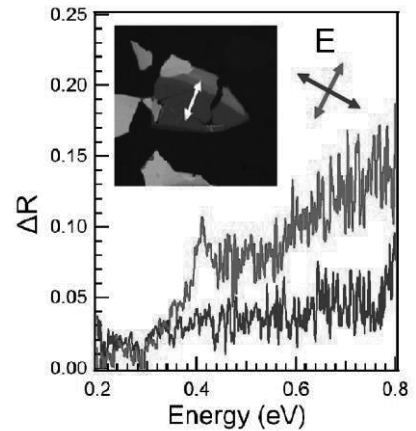


Fig. 2: Polarized differential reflectivity spectrum

[1] Likai Li *et al.*, *Nature Nanotech.* **9**, 372–377 (2014)..

[2] Wanglin Lu *et al.*, *Nano Research* **7**, 853-859 (2014).

[3] Han Liu *et al.*, *ACS Nano* **8**, 4033–4041 (2014).

Corresponding Author: Takashi Nakamura

Tel: +81-774-38-3463,

Fax: +81-774-38-4567,

E-mail: nakamura.takashi.23z@st.kyoto-u.ac.jp

Relaxation of Valley Polarization in Transition Metal Dichalcogenides

○Satoru Konabe and Susumu Okada

Graduate School of Pure and Applied Sciences, University of Tsukuba, Tsukuba, Ibaraki 305-8571, Japan

Monolayer transition metal dichalcogenides (TMDCs) such as MoS₂, MoSe₂, WS₂ and WSe₂ have recently attracted much attention because of their remarkable electronic and optoelectronic properties [1]. The lack of inversion symmetry with a strong spin-orbit interaction gives rise to nontrivial valley-spin coupled physics [2], which enables us to control the valley degrees of freedom using the polarized light [3]. For valleytronics application, it is crucial to keep a specific valley state as long as possible by suppressing a valley relaxation [4]. To achieve this, we have to identify the microscopic mechanism of the valley relaxation. However, despite intensive theoretical and experimental works, it is still unclear [5].

In this study, we theoretically investigate the valley relaxation mechanism in monolayer TMDCs by solving the Bloch equation of a valley pseudo spin associated with an exciton. We find that the exchange interaction between an electron and a hole is essential for determining the valley relaxation time. We also find that the relaxation process exhibits a crossover from the collisional-broadening region at low temperature to the thermal-broadening region at high temperature; the crossover occurs at around the temperature corresponding to the homogeneous broadening that is related to the exciton momentum-relaxation time (Fig. 1). Furthermore, we elucidate the screening effect due to doping on the relaxation process, which drastically changes the temperature dependence of the valley relaxation both qualitatively and quantitatively compared with the non doped case.

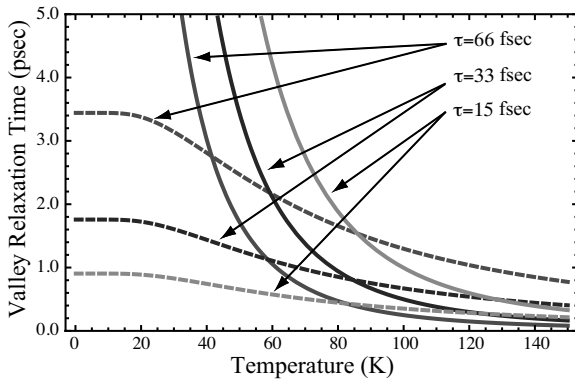


Fig. 1 Temperature dependence of the valley relaxation time for WSe₂ with the carrier density of 10^{12} cm⁻². τ is the exciton momentum relaxation time. The dashed lines indicate the relaxation time where the collisional broadening is dominant for the exciton distribution.

References:

- [1] A. Splendiani *et al.* Nano Lett. **10**, 1271 (2010), K. F. Mak *et al.* Phys. Rev. Lett. **105**, 136805 (2010), Q. H. Wang *et al.* Nat. Nanotechnol. **7**, 699 (2012), M. Chhowalla *et al.*, Nature Chem. **5**, 263 (2013).
- [2] D. Xiao *et al.*, Phys. Rev. Lett. **108**, 196802 (2012).
- [3] H. Zeng *et al.*, Nature Nanotech. **7**, 490 (2012), K. F. Mak, *et al.* Nature Nanotech. **7**, 494 (2012).
- [4] X. Xu *et al.*, Nature Physics **10**, 343 (2014), K. F. Mak *et al.*, Science **344**, 1489 (2014).
- [5] T. Cao *et al.*, Nature Commun. **3**, 887(2012), D. Lagarde *et al.*, Phys. Rev. Lett. **112**, 047401(2014).

Corresponding Author: Satoru Konabe

E-mail: konabe@comas.frsc.tsukuba.ac.jp

Tel: +81-2-9853-5600 ext.8233

Exciton spectroscopy in 3R-MoS₂

○Suzuki Ryuji¹, Sandor Bordacs², Ryosuke Akashi³, Masayuki Ochi⁴, Ryotaro Arita⁴,
Yoshinori Tokura^{1,4}, Yoshihiro Iwasa^{1,4}

¹Quantum-phase electronic centre and Department of Applied Physics, Faculty of Engineering, The University of Tokyo, Tokyo 113-8656, Japan

²Budapest University of Technology and Economics, H-1521 Budapest, Hungary

³Department of Physics, School of science, The University of Tokyo, Tokyo 113-0033, Japan

⁴Center for Emergent Matter Science, RIKEN, Saitama 351-0198, Japan

Transition-metal dichalcogenides (TMDs) are attracting a great deal of interest as beyond graphene materials because of their rich physical properties[1-3]. The key of the monolayer TMDs in contrast to the bulk is the broken inversion symmetry (Fig. 1), which results in novel valley properties, coupled with spins through their strong spin-orbit interaction [4]. On the other hand, 3R-MoS₂ is known to keep the broken inversion symmetry and thus strong valley polarization in PL spectra even in multilayers, providing new opportunities to investigate properties of monolayers with use of bulk materials and the stacking dependent properties between the 2H (centrosymmetric) and 3R (non-centrosymmetric) [5].

In this presentation, we report comparative studies of 2H- and 3R-MoS₂ on dimensionality of the excitons, with reflectivity measurement (Fig. 2). We found energy differences of 3R-MoS₂ between A exciton (appeared as the sharp peaks around 1.9 eV) and that excited states (indicated by arrow) is much larger than 2H-MoS₂. This indicates that the exciton binding energies of both polytype are different from each other, and that dimensionality of excitons depends on its way of stacking. The present result reveals that the dimension engineering can be realized just by manipulating stacking, a new technique to control the novel properties of 2D materials.

[1] B. Radisavljevic *et al.*, Nature Nanotech. **6**, 147 (2011). [2] K. F. Mak *et al.*, Nature Nanotech. **7**, 494 (2012). [3] J. T. Ye *et al.*, Science **338**, 1193 (2012). [4] D. Xiao *et al.*, Phys. Rev. Lett. **108**, 196802 (2012). [5] R. Suzuki, M. Sakano *et al.*, Nature Nanotech. **9**, 611 (2014).

Corresponding Author: R. Suzuki

Tel: +81-3-5841-6822, Fax: +81-3-5841-6822,

E-mail: ryujisuzuki@mp.t.u-tokyo.ac.jp

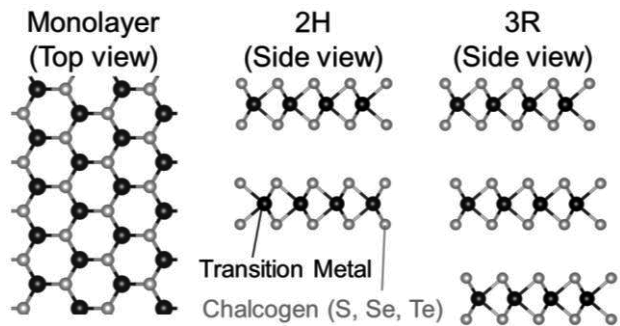


Fig. 1: Crystal structures of monolayer, 2H- and 3R-polytypes of MoS₂

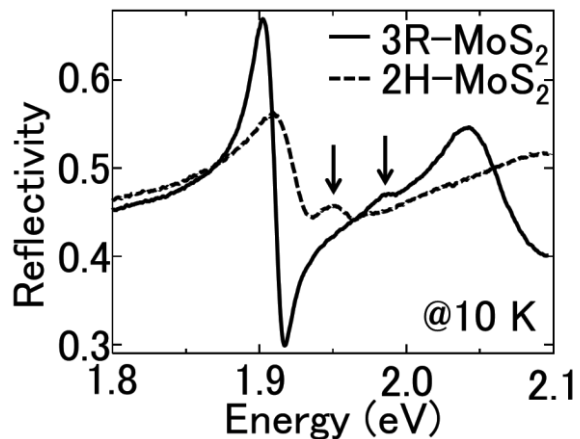


Fig. 2: Reflectivity spectra of 2H- and 3R-MoS₂

CVD synthesis of single-crystal single-layer graphene and bi-layer graphene from ethanol

○Xiao Chen, Kohei Tsushima, Masaki Sota, Rong Xiang, Shohei Chiashi, Shigeo Maruyama

Department of Mechanical Engineering, The University of Tokyo, Tokyo 113-8656, Japan

Graphene synthesis using chemical vapor deposition (CVD) on metal substrates has been intensively investigated in the past few years. Recently, the growth of single-crystal graphene has drawn most attention for that graphene films without grain boundaries show superior electrical and mechanical properties. Several strategies toward such purpose were developed, including inducing surface oxygen on Cu foils, using single-crystal substrates, etc.

We've shown that both self-limited growth of single-layer graphene and self-limited growth bi-layer graphene can be realized using ethanol as the carbon source [1, 2]. Here, we show that by tuning the CVD conditions, graphene single crystals as large as 5 mm can be synthesized on poly-crystal Cu substrates (Fig. 1-a). Cu foils were oxidized on a hot plate at 250 °C in air prior to the CVD reaction, and an extremely low flow rate of ethanol vapor (0.03 sccm) was employed during the growth. The single-crystal nature of the resultant large graphene flakes was confirmed by selected area electron diffraction. Furthermore, by controlling the CVD parameters, after the full coverage of single-layer graphene, large single-crystal bi-layer graphene can be synthesized (Fig. 1-b). Raman spectroscopy confirmed that more than 90% of the bi-layer regions were AB-staked. These results demonstrate great potential of ethanol as a carbon source for the synthesis of high-quality graphene. Especially, the large-grain AB-stacked bi-layer graphene could be very important for applications such as field effect transistors.

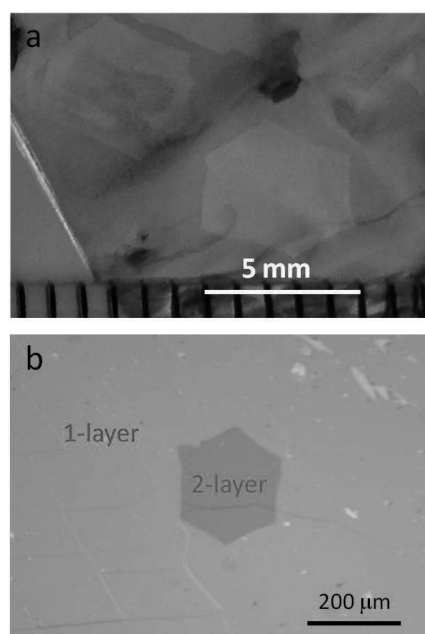


Fig.1 a. Graphene single crystals on a Cu foil. b. Image of single-layer graphene and bi-layer graphene transferred to a Si/SiO₂ substrate.

[1] P. Zhao, *et al.* J. Phys. Chem. C. **117**, 10755(2013).

[2] P. Zhao, *et al.* ACS. Nano. **8**, 11631(2014)

Corresponding Author: S. Maruyama

Tel: +81-3-5841-6408, Fax: +81-3-5841-6408,

E-mail: maruyama@photon.t.u-tokyo.ac.jp

Magnetic Ordering of Two-dimensional Networks of Fused C₃₆ Polyhedra under an Electric Field

○Mina Maruyama and Susumu Okada

Graduate School of Pure and Applied Sciences, University of Tsukuba, 1-1-1 Tennodai, Tsukuba, Ibaraki 305-8571, Japan

Electronic structures of layered materials with internal atomic structures are known to depend on the external electric field. It has been reported that bilayer graphene exhibits the metal-insulator-metal transition under the perpendicular electric field. In our previous work, we theoretically designed two-dimensional networks consisting of fused C₃₆ polyhedra as a possible semiconducting layered materials with nanometer thickness. In this work, we study electronic structures of the 2D networks of C₃₆ polyhedron under the perpendicular electric field using the density functional theory (DFT) with combining the effective screening medium (ESM) method to investigate the possibility of magnetic ordering on all carbon materials. To express the exchange-correlation potential among the interacting electrons, we use the local spin density approximation (LSDA). We adopt the ultrasoft pseudopotential for describing electron-ion interactions. The valence wave function is expanded in terms of plane wave basis set with cutoff energy of 25 Ry.

Our DFT-ESM calculations show that the C₃₆ network exhibit the magnetic ordering under hole doping by the perpendicular electric field, in which the polarized electron spin is primarily localized on the hexagonal ring situated at the top of the C₃₆ covalent network and is ferromagnetically aligned throughout the sheet [Figs 1(a) and 1(b)]. Calculated magnetic moments are 1.74 and 2.22 μ_B/nm^2 for the cases of dual gate and single gate, respectively. In addition, in the case of the dual gate, we also find that the nearly free electron (NFE) state shifts downward and crosses the Fermi level with spin polarized electrons. Therefore, by applying the perpendicular field on the C₃₆ sheet, we indicate the possibility of peculiar spin systems in which the polarized spins coexist on the atomic network and at the vacuum region, being expected to exhibit unusual spin properties.

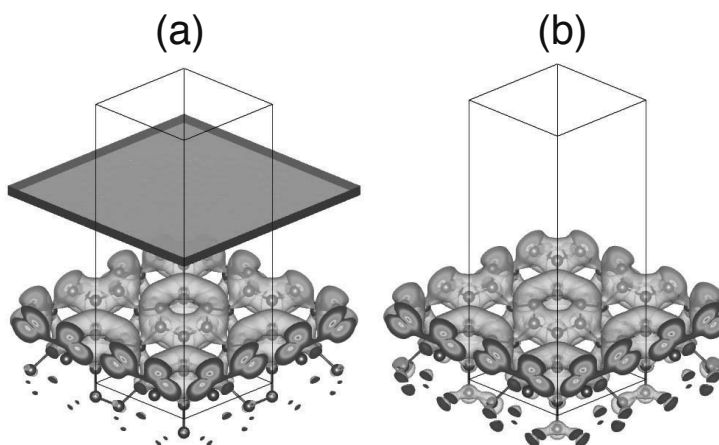


Fig.1: Isosurfaces of spin densities of C₃₆ sheet under the electric field by (a) the dual gate electrodes and (b) by the single gate electrode.

Corresponding Author: Mina Maruyama

E-mail: mmaruyama@comas.frsc.tsukuba.ac.jp

Tel: +81-29-853-5600(ext: 8233)

Effects of electrodeposition conditions on the states of Pt-Ru nanoparticles on carbon materials and their electrocatalytic properties toward methanol oxidation

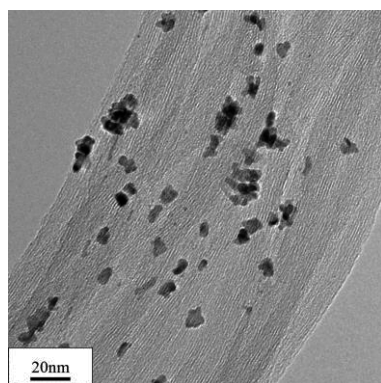
○¹ Haruhiko Yoshitake, ¹ Shohei Hayase, ² Wang Zhipeng and ^{1,3} Hironori Ogata

¹ Graduate School of Science and Engineering, Hosei University Koganei 184-8584, Japan

² Institute of Carbon Science and Technology, Shinshu University, Nagano 380-8553, Japan

³ Research Center for Micro-Nano Technology, Hosei University, Koganei 184-0003, Japan

Direct methanol fuel cells (DMFCs) are one of the most promising transportable power sources which can be used in mobiles, laptops, and small power generation. The basic operation principle of DMFCs involves methanol oxidation and oxygen reduction on the precious metal catalysts, which are loaded on the support surfaces. As is well-known, the dispersion of Pt-based alloys on carbon supports as well as catalyst particle size and shape plays a dominant role in the electrochemical performance for fuel cells. We have explored the electrocatalytic properties of Pt-based nanoparticles supported on the carbon materials by one-step electrodeposition. In this study, we investigated the effects of electrodeposition conditions on the shape and dispersion state and electrocatalytic properties of Pt-based nanoparticles supported on the carbon materials, Single walled Carbon Nanotubes (SWNTs) or highly ordered pyrolytic graphite (HOPG). Figure 1 shows the TEM image of Pt-Ru nanoparticles deposited on SWNTs at constant voltage of -1.36V for 5 sec. and table.1 summarizes their electrochemical characteristics of methanol oxidation. The detailed results on the relationship between the deposition conditions, the shape and dispersion state of Pt-Ru nanoparticles and their electrocatalytic performance for methanol oxidation will be presented.



Supported Carbon	Active area of S_{Pt} [cm^2]	J_f [mA/cm^2]	I_f/I_b	V_f [V]
SWMTs	9.58×10^2	4.49	1.69	0.64

Figure 1. TEM image of Pt-Ru particles deposited on SWNTs at -1.36V for 5s.

Table 1. Electrochemical characteristics of methanol oxidation.

References:

- (1) J.M. Sieben *et al.*, *J. Appl. Electrochem.* **38**(2008)483-490.
- (2) Zhipeng Wang, Mao Shoji and Hironori Ogata, *Appl. Surf. Sci.* **259**(2012)219-224.
- (3) M. Tsai *et al.*, *ElectroChemistry. Communication* **8**(2006)1445-1452.
- (4) S.H. Ahn *et al.*, *Chem. Eng. J.*, (2012) **181-182**, 276-280.

Corresponding Author: Hironori Ogata,

Tel: +81-42-387-6229, Fax: +81-42-387-6229, E-mail: hogata@hosei.ac.jp

Hexahydroxytriphenylene and its derivatives for graphene exfoliation in aqueous and organic media

○Gang Liu, Takahide Kimura, Naoki Komatsu

Department of Chemistry, Shiga University of Medical Science, Seta, Otsu, 520-2192, Japan

Liquid-phase exfoliation of graphite to graphene has received extensive interest because of a facile and inexpensive way for preparation of a large quantity of graphene [1]. The graphene dispersion prepared by this method can be easily processed by drop-casting, filtration, or spin-coating, and the techniques have been widely used in thin film electronic device [2]. Therefore, this method has been considered as one of the most promising routes in mass production of graphene. Herein, we report a simple and scalable preparation of graphene dispersion through direct exfoliation of graphite in the presence of triphenylene derivative (**1**, **2** or **3** in Fig. 1). The advantages of the exfoliation process reported here are; 1) commercially available exfoliants are employed; 2) highly concentrated and high-quality graphene dispersion is obtained in a facile way; 3) THF can be used as low boiling point medium in addition to water as green medium; 4) the dried graphene solid can be easily redispersed as highly concentrated and stable dispersion; and 5) exfoliants are removed in a facile way without causing any damage to the structure of graphene [3].

The graphene dispersion was prepared by bath-sonication of the suspension of graphite powder and triphenylene in water or THF, followed by centrifugation at 1029g. Scanning transmission electron microscope (STEM, Fig. 2) images indicate that almost all the materials observed are the plates with high transparency, implying thin graphene sheets. The exfoliation was further confirmed by the Raman, XRD (Fig. 3), and AFM. Through heat treatment at 440 °C for 3 min under air, the exfoliants are thoroughly removed without disturbing the structure of graphene.

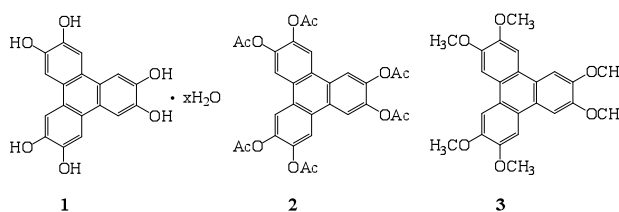


Fig. 1 Chemical structures of hexahydroxytriphenylene (**1**) and its derivatives (**2** and **3**)

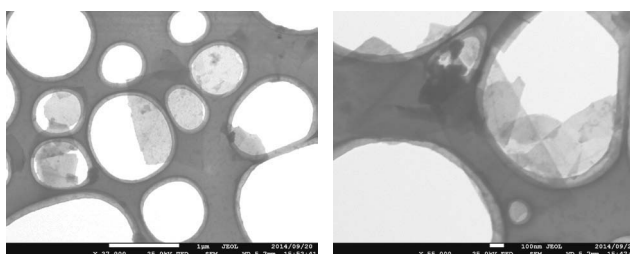


Fig. 2 Typical STEM images of the exfoliated graphene

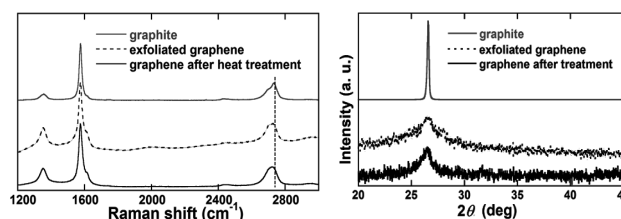


Fig. 3 Raman spectra (left) and XRD patterns (right) of graphite and exfoliated graphene before and after treatment at 440 °C for 3 min under air

[1] A. Ciesielski, P. Samori, *Chem. Soc. Rev.* **43**, 381 (2014).

[2] D. W. Chang, H.-J. Choi, A. Filer, J.-B. Baek, *J. Mater. Chem. A*, **2**, 12136 (2014).

[3] G. Liu, T. Kimura, N. Komatsu, to be submitted.

Corresponding Author: G. Liu

Tel: +81-77-548-2102, Fax: +81-77-548-2405, E-mail: gliu@belle.shiga-med.ac.jp

ポスター発表
Poster Preview

1P-1 ~ 1P-44

2P-1 ~ 2P-44

3P-1 ~ 3P-43

Charge analyses on particles by Ion Mobility Measurement

○Toshiki Sugai, Yasuhiro Hiroshiba, Hironobu Matsubayashi, Kazuki Mimuro,
and Ryota Jinnouchi

Department of Chemistry, Toho University, Miyama 2-2-1 Funabashi, 274-8510, Japan

Ion mobility measurements have revealed varieties of novel information on nano materials. Structures of metallofullerenes show significant dependence on the number of metal atoms and the cage size and their novel structures have been also clarified[1]. Our newly developed ion trap mobility measurement system can hold the ionized particles for more than 2 hours realizing observations on long term transitions with high accuracy. However those measurements mainly performed on a single particle to study relative structural changes. To apply these measurements to larger nano systems and to have statistical information, charge state should be analyzed because the mobility depends not only on the structures but also on the amount of charge. Here we present the analyses on the charge state measured by the ion mobility.

The system consists of a laser ionization source for polystyrene particles and an electrospray ionization source for salt solution, and electrodes for the trap. The produced ionized particles were trapped and moved in air for several minutes. The movement of every particle was observed and recorded by a microscope to evaluate its mobility. The amount of charge was analyzed from the obtained mobility.

Figure 1 shows the observed dependence of the amount of charges on the particles on their diameters. In both particles, the amount of charge increases as the diameter and the amount and dependence are quite similar despite of the totally different ionization methods. The difference between the polystyrene and salt solution, the amount of charge of polystyrene particles more rapidly decreases as the diameter decreases.

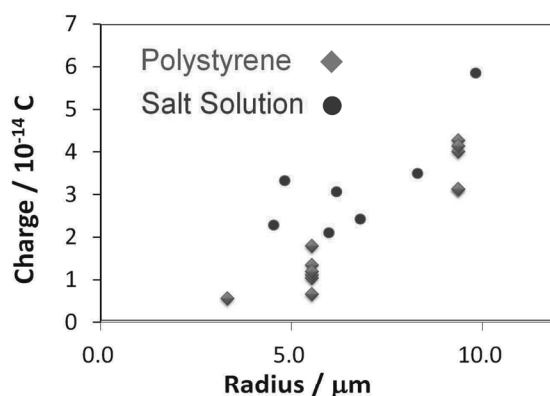


Fig. 1 Charge analyses on particles.

[1] T. Sugai *et al.*, *J. Am. Chem. Soc.* **123**, 6427 (2001).

TEL: +81-47-472-4406, E-mail: sugai@chem.sci.toho-u.ac.jp

Exciton-photon interaction in tip enhanced Raman spectroscopy of single wall carbon nanotubes

○ T.R. Czank, P. Ayria, R. Saito

Department of Physics, Tohoku University, Sendai 980-8578, Japan

Raman spectroscopy is based on the inelastic scattering of light which can be extensively used to analyze nanomaterials. However, when the wavelengths used to probe samples have reached the diffraction limit for given sample size, it is not possible to get higher resolution than those of the probing wavelength. To overcome this limitation, tip enhanced Raman spectroscopy (TERS) is often used by putting an additional metallic tip above the sample to utilize the near field effect, enhancing the Raman intensity. Using this technique, for example, the spatial resolution for a single wall carbon nanotube (SWNT) sample can be increased from the order of μm to nm [1]. Understanding the mechanism behind TERS is thus very important to further improve development of this spectroscopy technique.

In this work, we propose that the interaction between excitons generated in the SWNT sample and near field generated by the metallic tip, is the origin of the intensity enhancement in TERS. To justify this hypothesis, we calculate the exciton-photon interaction in armchair SWNTs in the presence of metallic tip. Within this approach, the near field factor can not be considered as constant as previously considered in the conventional Raman spectroscopy, because the amplitude of the near field factor is already comparable to the exciton wavefunctions [2]. The calculated matrix elements for the armchair SWNTs reveals that, the intensity is enhanced near the K points. Nevertheless, the symmetry breaks [3] because of the near field factor, which gives rise to the chirality-dependence of the exciton photon matrix element with the presence of the metallic tip.

[1] L G Cançado, et al, Phys. Rev. Lett. **103**, 186101 (2009)

[2] P. Tapsanit, *Near field enhancement of optical transitions carbon nanotubes*, Tohoku University, (2012)

[3] H. Ajiki, et al, Nat. Phot. **7**, 550-554 (2013)

Author: Czank T. R., TEL: +81-080-3339-8149, E-mail: thomas@flex.phys.tohoku.ac.jp

Ab Initio Study on Oxidation of (5,4), (6,4), (6,5), and (8,6) Carbon Nanotubes

○Mari Ohfuchi¹

¹ Fujitsu Laboratories Ltd., Atsugi 243-0197, Japan

Oxidation of single-wall carbon nanotubes (SWCNTs) has attracted attention because of their greater luminescence quantum yield than that of pristine CNTs [1]. Oxygen-doped CNTs are prepared by exposure of SWCNTs to ozone and light, whereas the luminescence originating from oxygen doping of SWCNTs has also been observed for thin CNTs separated into single chirality without a particular oxidation treatment [2]. Density functional theory (DFT) has been used to study the adsorption of oxygen molecules (O₂) onto SWCNTs, however the calculations have been limited to zigzag or armchair CNTs with comparatively small unit cells. In this study, we performed DFT calculations of the adsorption of O₂ on to realistic (5,4), (6,4), (6,5), and (8,6) nanotubes.

The O₂ molecules approaching SWCNTs physisorb onto the surface at a distance of approximately 0.31 nm. As shown in Fig. 1, the adsorption energies for the physisorption are small negative values and do not appear to depend either on the adsorption sites or on the chirality of the SWCNTs. When the O₂ molecules move closer to the SWCNTs, the first chemisorption occurs at an O–C distance of approximately 0.15 nm. Although the adsorption energy appears to be affected by the chiral angle of the SWCNTs, in general it increases as the SWCNTs become thicker. We found that the reaction barrier between the physisorption and the chemisorption corresponds approximately to the energy difference between them. The energy difference and the corresponding reaction rate are summarized in Table 1. This is consistent with the experimental results related to chirality-separated CNTs.

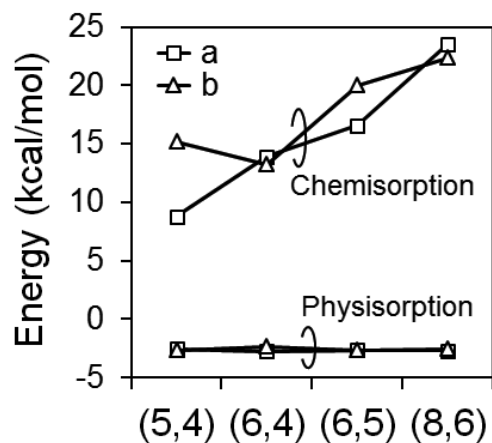


Fig. 1. Adsorption energies of oxygen molecules on carbon nanotubes. The adsorption sites a and b are on the bonds nearly perpendicular and parallel to the nanotube axis, respectively.

Table 1. Energy difference E and reaction rate R .

Chirality	Site	E (kcal/mol)	R (s ⁻¹)*
(5,4)	a	11.31	6.5×10^4
	b	17.81	1.3
(6,4)	a	16.68	8.4
	b	15.60	51
(6,5)	a	19.22	0.12
	b	22.65	4.0×10^{-4}
(8,6)	a	26.23	1.0×10^{-6}
	b	24.87	1.0×10^{-5}

*The prefactor was assumed to be a standard value of 10^{13} s⁻¹.

[1] Y. Miyauchi *et al.* Nature Photon. **7**, 715 (2013).

[2] H. Liu *et al.* Nat. Commun. **2**, 309 (2011).

Corresponding Author: M. Ohfuchi

Tel: +81-46-250-8194, Fax: +81-46-250-8274, E-mail: mari.ohfuti@jp.fujitsu.com

Bias-voltage induced absorption peaks in individual suspended carbon nanotubes

T. Uda, M. Yoshida, A. Ishii, Y. K. Kato

Institute of Engineering Innovation, The University of Tokyo, Tokyo 113-8656, Japan

We investigate longitudinal electric-field effects on photocurrent and photoluminescence excitation spectra of individual air-suspended carbon nanotubes. To apply electric fields on nanotubes, we have fabricated field effect transistors with carbon nanotubes [1-3]. We have also constructed a system which can perform simultaneous photocurrent and photoluminescence spectroscopy [1,2]. A wavelength-tunable continuous wave Ti:sapphire laser is used to excite the nanotubes, and a lock-in amplifier and an InGaAs photodiode array are used to detect photocurrent and photoluminescence, respectively. We find new peaks in the spectra when a bias voltage is applied.

Work supported by KAKENHI (24340066, 24654084, 26610080), the Canon Foundation, Asahi Glass Foundation, and KDDI Foundation, as well as the Photon Frontier Network Program of MEXT, Japan. The devices were fabricated at the Center for Nano Lithography & Analysis at The University of Tokyo. A.I. is supported by MERIT and JSPS Research Fellowship, and M.Y. is supported by ALPS.

- [1] Y. Kumamoto, M. Yoshida, A. Ishii, A. Yokoyama, T. Shimada, and Y. K. Kato, Phys. Rev. Lett. **112**, 117401 (2014).
- [2] M. Yoshida, Y. Kumamoto, A. Ishii, A. Yokoyama, and Y. K. Kato, Appl. Phys. Lett. **105**, 161104 (2014).
- [3] S. Yasukochi, T. Murai, S. Moritsubo, T. Shimada, S. Chiashi, S. Maruyama, and Y. K. Kato, Phys. Rev. B **84**, 121409(R) (2011).

Corresponding Author: Y. K. Kato

Tel: +81-3-5841-7702, Fax: +81-3-5841-7772

E-mail: ykato@sogo.t.u-tokyo.ac.jp

Photoluminescence studies on individual small-diameter carbon nanotubes

○Shun Aota¹, Naoto Akizuki¹, Shinichiro Mouri¹, Xiaojun Wei², Takeshi Tanaka²,
Hiromichi Kataura², Kazunari Matsuda¹, and Yuhei Miyauchi¹

¹*Institute of Advanced Energy, Kyoto University, Uji, Kyoto 611-0011, Japan*

²*Nanosystem Research Institute, AIST, Tsukuba, Ibaraki 305-8562, Japan*

Single-walled carbon nanotubes (SWNTs) show distinctive physical properties originating from their one-dimensional (1D) nature. In addition, zero-dimension (0D)-like local states in SWNTs have recently attracted increasing attention because of their potential usefulness in optoelectronics, bioimaging and quantum information fields [1,2]. In this context, we have been exploring optical properties of localized exciton states prepared by means of chemical treatments. The previous studies have revealed that SWNTs with chemically-derived local states can be viewed as unique 0D-1D hybrid low-dimensional systems that show novel exciton photophysics such as brightening of excitons [1] and enhanced photoluminescence (PL) nonlinearity [2]

In this study, we performed optical measurements on individual small-diameter (5,4) SWNTs that exhibit a low energy PL feature attributable to localized exciton states. The high purity (5,4) SWNTs were prepared using the multicolumn gel chromatography method [3]. The isolated SWNTs were dispersed in an agarose gel matrix to immobilize them. The measurements were performed in the ambient air.

Figure 1 shows a PL image observed with an excitation photon energy of 1.49 eV that corresponds to the E_{11} resonance of (5,4) SWNTs. Each bright spot in Fig. 1 corresponds to PL from an individual (5,4) SWNT. The inset of Fig. 1 shows a PL spectrum taken for one of the bright spot observed in the PL image. A characteristic low energy PL feature was observed at ~ 1.26 eV, indicating the existence of localized states in the SWNTs. Detailed photophysics of the localized states in the separated individual (5,4) SWNTs will be discussed in the conference.

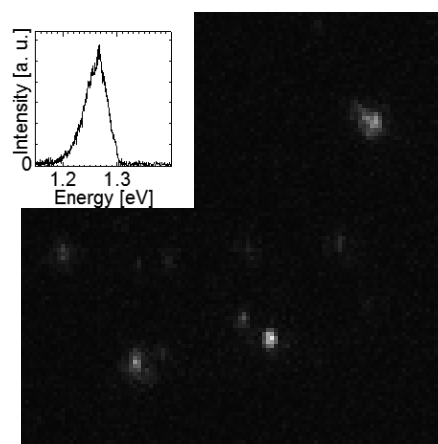


Fig. 1. PL image of separated (5,4) SWNTs dispersed in agarose gel matrix. The excitation photon energy of 1.49 eV was used. Inset shows a PL spectrum taken for one of the bright spots.

[1] Y. Miyauchi *et al.*, Nat. Photonics **6**, 715 (2013)

[2] M. Iwamura *et al.*, ACS Nano **8**, 11254 (2014)

[3] H. Liu *et al.*, Nat. Commun. **2**, 309 (2011)

Corresponding Author: S. Aota

Tel: +81-774-38-3465,

E-mail: aota.shun.23z@st.kyoto-u.ac.jp

Assigning (n,m) of Random Single-Walled Carbon Nanotubes on Silicon Substrates by Resonant Raman Spectroscopy

○Daqi Zhang, Feng Yang, Juan Yang, Yan Li

College of Chemistry and Molecular Engineering, Peking University, Beijing 100871, China

The application of single-walled carbon nanotube (SWNT) based devices requires an experimental method to assign the (n,m) of SWNTs on standard silicon substrates. Various spectroscopic methods have been developed to assign (n,m) , including resonant Raman, absorption, photoluminescence, and Rayleigh scattering [1]. For as-grown SWNTs on silicon substrate, resonant Raman is the most widely used and accepted way to obtain (n,m) [2], while other spectroscopic methods are limited due to the substrate.

In this work, we use resonant Raman spectroscopy with two excitation lasers (i.e., 532 nm and 633 nm) to assign (n,m) for our random SWNTs on silicon substrates catalyzed by Ni, Co, and Fe. Based on 28 different chiralities assigned in the diameter range of 1.2-2.1 nm, we propose an equation of $\omega_{\text{RBM}}=235.9/d_t+5.5$ as the best fit for our random SWNT samples on silicon substrates (Fig. 1). No significant catalyst-specified effects on the $\omega_{\text{RBM}}-d_t$ relation is observed. The assignments are further verified by electron diffraction pattern and some structure-dependent Raman features (e.g., G band shape [3] and the intermediate frequency mode features [4]). This method is further applied to assign our chirality-specific SWNT samples [5].

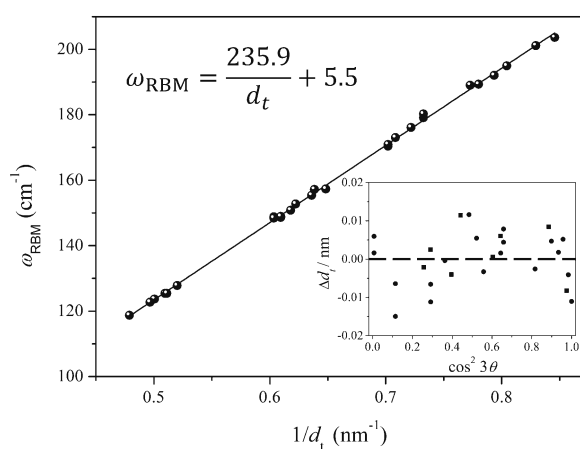


Fig. 1 Linear fit of ω_{RBM} with respect to $1/d_t$. The fitting line gives $\omega_{\text{RBM}}=235.9/d_t+5.5$.

Inset: difference between calculated d_t and the actual d_t with respect to $\cos^2 3\theta$ for both S- (dots) and M-SWNTs (squares).

- [1] D. Zhang, J. Yang, Y. Li, *Small* **9**, 1284 (2013).
- [2] A. Jorio, *et al.*, *Phys. Rev. Lett.* **86**, 1118 (2001).
- [3] T. Michel, *et al.*, *Phys. Rev. B* **80**, 245416 (2009).
- [4] J. Wang, Y. Li, *et al.*, *J. Phys. Chem. C* **116**, 23826 (2012).
- [5] F. Yang, Y. Li, *et al.*, *Nature*, **510**, 522 (2014).

Corresponding Author: Y. Li

Tel: +86-10-62756773 Fax: +86-10-62756773

E-mail: yanli@pku.edu.cn

Trions in individual air-suspended carbon nanotubes

○A. Popert, M. Yoshida, Y. K. Kato

Institute of Engineering Innovation, The University of Tokyo, Tokyo 113-8656, Japan

We perform photoluminescence measurements on individual air-suspended single-walled carbon nanotubes at room temperature and under high vacuum, using field-effect transistor structures [1,2]. Upon application of gate voltage, the bright exciton peak quenches [3], and a new redshifted peak appears. The diameter dependent energy separation from the bright exciton peak shows that the gate-induced peak originates from trions. We perform statistical analysis of the trion binding energies for a diameter range of 0.9 to 1.3 nm, and they are found to be 20-40 meV higher than previous values reported for solution-based carbon nanotubes. We attribute the difference to the absence of dielectric screening when using air-suspended carbon nanotubes. We further observe blueshifts in the trion emission at high gate electric fields.

Work supported by KAKENHI (24340066, 24654084, 26610080), the Canon Foundation, Asahi Glass Foundation, and KDDI Foundation, as well as the Photon Frontier Network Program of MEXT, Japan. The devices were fabricated at the Center for Nano Lithography & Analysis at The University of Tokyo. M.Y. is supported by ALPS and A.P. is supported by JASSO.

- [1] M. Yoshida, Y. Kumamoto, A. Ishii, A. Yokoyama, and Y. K. Kato, *Appl. Phys. Lett.* 105, 161104 (2014).
- [2] Y. Kumamoto, M. Yoshida, A. Ishii, A. Yokoyama, T. Shimada, and Y. K. Kato, *Phys. Rev. Lett.* 112, 117401 (2014).
- [3] S. Yasukochi, T. Murai, S. Moritsubo, T. Shimada, S. Chiashi, S. Maruyama, and Y. K. Kato, *Phys. Rev. B* 84, 121409(R) (2011).

Corresponding Author: Y. K. Kato
Tel: +81-3-5841-7702, Fax: +81-3-5841-7772
E-mail: ykato@sogo.t.u-tokyo.ac.jp

Electronic properties of CNT thin films under an electric field

○U Ishiyama and Susumu Okada

*Graduate School of Pure and Applied Sciences, University of Tsukuba, Tennodai, Tsukuba
305-8577, Japan*

Carbon nanotubes (CNTs) are attracting much attention because of its unique geometric and electronic structures that allow them to be an emerging material for semiconductor electronic devices in the next generation. It has been shown experimentally that CNTs work as a conducting channel of field-effect transistors (FETs), in which the CNTs form a mat structure with nano-scale interfaces among these CNTs. However, the fundamental properties of these CNT-CNT interfaces under an electric field are not fully understood. In this work, we aim to elucidate the electronic properties of the CNT thin films, which consist of the double layer of CNTs, under the external electric field which injects electrons/holes into these CNT thin films.

All calculations are performed by using the density functional theory with local density approximation. To express the exchange correlation potential among interacting electrons, we apply the local density approximation. We use an ultrasoft pseudopotential to describe the interaction between valence electrons and ions. The effective screening medium (ESM) method is applied to investigate electronic properties of CNT with carriers under the electric field in the framework of the first-principles calculations. Here, we consider thin films of CNTs consisting of (11,0), (12,0), (13,0), (14,0), and (15,0) CNTs forming CNT double layers. To simulate the CNT-FET device, we consider the model system shown in Fig. 1.

Figure 2 shows the electrostatic potential of a CNT thin film consisting of (12,0) and (11,0) CNTs without electric field. As shown in Fig. 2, intrinsic electric field occurs in the interface between these CNTs because of their different workfunctions. According to the electric field, carrier accumulations depend on the mutual arrangement of CNTs with respect to the electrode.

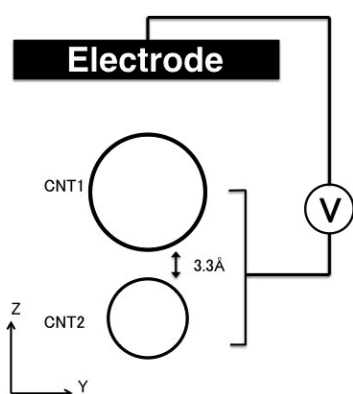


Fig. 1 A structural model of CNT thin films

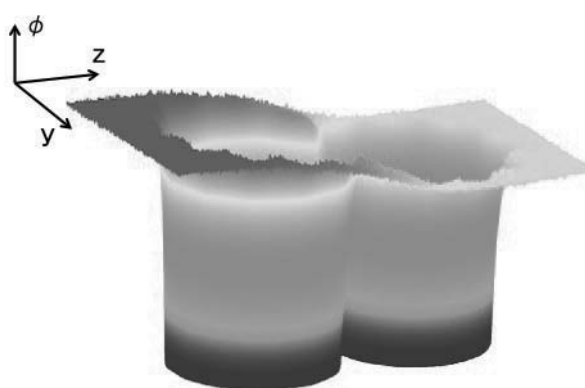


Fig. 2 Electrostatic potential of a CNT thin film without external field.

Corresponding Author: U Ishiyama

Tel: +81-29-853-5600 (ext. 8233), Fax: +81-29-853-5924,

E-mail: yishiyama@comas.frsc.tsukuba.ac.jp

Electrical contact of parallel adjacent CNTs estimated from in-plane conductivity of dense CNT forest on silicon carbide

○Masafumi Inaba¹, Chih-Yu Lee¹, Kazuma Suzuki¹, Yu Hirano¹, Megumi Shibuya¹,
Miho Myodo¹, Wataru Norimatsu², Michiko Kusunoki², Hiroshi Kawarada¹
¹ Graduate School of Advanced Science and Engineering, Waseda University, Tokyo
169-8555, Japan

² Eco Topia Science Institute, Nagoya University, Aichi 464-8603, Japan

We have reported the in-plane conductivity of dense carbon nanotube forest on silicon carbide substrate (CNT forest on SiC).^[1] Here we additionally discuss the contact conductivity estimation of parallel adjacent CNTs yielded from the in-plane conductivity.

The experimental setup is the same as the previous report.^[1] On-axis C-face (000-1) of semi-insulating SiC substrates ($< 10^{-8}$ S/cm) were annealed at 1600 °C in vacuum ($\sim 10^{-2}$ Pa). The in-plane conductivity was measured by van der Pauw method. Fig.1 shows (a) the schematic image of sheet conductivity measurement and (b) its equivalent circuit. By changing the CNT length or CNT film thickness, there were constant part and CNT length dependent part as shown in Fig. 2. As a result, the contributive in-plane conduction parts were CNT top region and CNT bulk region.

In CNT bulk region, where in-plane conductivity was 50 S/cm, CNT should be parallel adjacent to each other. We assumed three approximations to conduct the contact resistivity. First, CNTs have the same diameter and are densely packed with the hexagonal pattern. Second, CNT/CNT contact conductivity is the same for CNTs with the same diameter. Third, CNT conductivity is much higher than the CNT/CNT contact conductivity. With these approximations, CNT forest is described as the net-like circuit in Fig.3, where each wire corresponds to the CNT/CNT contact conductive path and each node corresponds to CNT. With brief calculations, the contact conductivity normalized by CNT contact length was written as $\sigma_{C,CNT/CNT} = \sigma_S / \sqrt{3}t$. $\sigma_S t$ is the slope of Fig. 2. Thus the CNT/CNT contact conductivity is yielded as ~ 30 S/cm (contact resistivity: $\sim 3 \times 10^{-2} \Omega\text{cm}$).

Only a few groups reported the CNT-CNT junction electrical properties in dispersed CNT network. Znidarsic et al.^[2] reports the CNT/CNT contact resistance range of 200 k Ω for X-type connection and 60 k Ω for Y-type connection. In X-type contact, the CNTs are point-contacted with each other and in Y-type case CNTs are parallel-contacted with each other in a part. In CNT forest on SiC case, CNTs should be considered as metallic due to their large diameters. Even though the chirality is semiconducting, the bandgap should be even smaller for larger diameter CNTs. The contact resistivity of semiconducting/semiconducting or semiconducting/metallic contact should be higher than that of metallic/metallic. The Y-type contact resistance of 60 k Ω corresponds to the contact length of 5 nm in case the contact type is metallic/metallic, which is calculated as the method of Lan et al.^[3] We will discuss the detail in this presentation.

This study was supported by JSPS (No. 26630136)

[1] Inaba et al., The 47th Fullerenes-Nanotubes-Graphene General Symposium, 2P-7

[2] A. Znidarsic et al., J. Phys. Chem. C 117, 25 (2013).

[3] C. Lan et al., Nanotechnology 19, 12 (2008).

Corresponding Author: M. Inaba

Tel&Fax: +81-3-5286-3391

E-mail: inaba-ma@ruri.waseda.jp

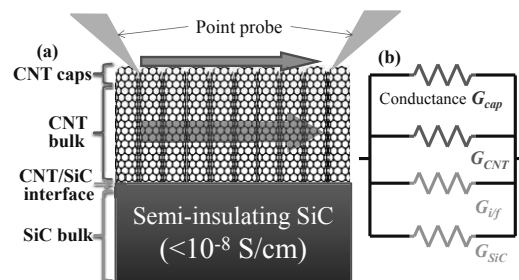


Fig. 1 (a) Schematic image of sheet conductivity measurement and (b) its equivalent circuit

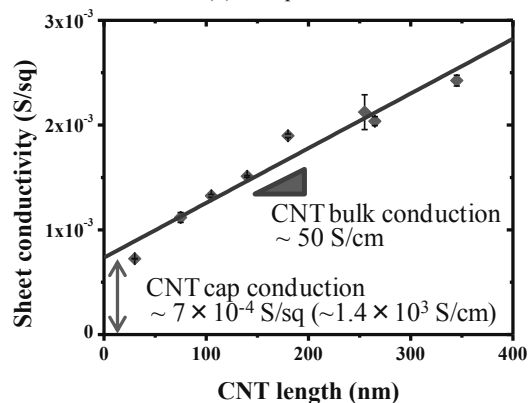


Fig. 2 Relationship between CNT sheet conductivity and CNT length

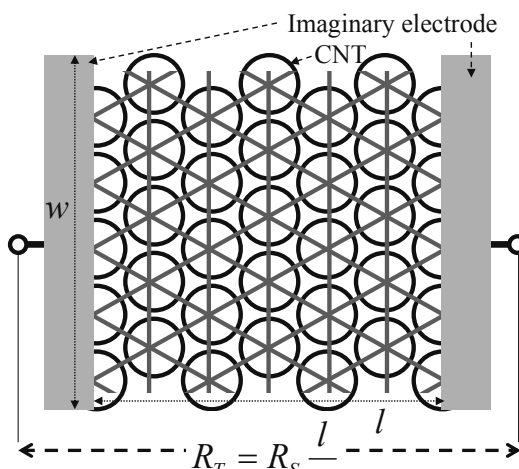


Fig. 3 Upside view of approximated electrical circuit of dense carbon nanotube forest.

Overcoming the Quality-Quantity Trade-Off in Printing Carbon Nanotubes by Repetitive Dispersion-Extraction Process

○Hiroyuki Shirae¹, Dong Young Kim¹, Kei Hasegawa¹, Taishi Takenobu², Yutaka Ohno³, and Suguru Noda^{1,*}

¹ Department of Applied Chemistry, Waseda University, Tokyo 169-8555, Japan

² Department of Applied Physics, Waseda University, Tokyo 169-8555, Japan

³ Department of Quantum Engineering, Nagoya University, Nagoya 464-8603 Japan

Carbon nanotubes (CNTs) are an attractive candidate material for electrodes and wirings in flexible electronic devices owing to their fair electric conductivity, excellent stability in ambient, flexibility, and compatibility with printing processes. Their uniform films with excellent conductivities have been realized through mild dispersion followed by centrifugation and printing, however a significant fraction of expensive CNTs are wasted during centrifugation. Moreover, in the fabrication of patterned electrodes/wirings, photo- or electron-beam lithography is often applied to the uniform films, which causes additional loss of CNTs. Toward the practical application of CNTs to flexible electronics, simple and loss-free printing of conductive CNT films is highly demanded.

In this work, we propose and examine a repetitive dispersion-centrifugation process, which minimize the damage to CNTs via mild dispersion and the material loss of CNTs via reuse of undispersed CNTs. We also propose and examine a filtration process using a metal mask with a membrane filter, which yields patterned CNT films with minimal material loss.

We used as-produced CNTs synthesized via floating-catalyst CVD, the so-called eDIPS method [1] (MEIJO eDIPS, EC grade; Meijo Nano Carbon Co., Ltd.). CNTs were added at 0.01 wt% to the 0.5 wt% aqueous solution of sodium dodecylbenzenesulfonate (SDBS). The solution was sonicated at 30 W, 45 kHz for a set time, and then centrifuged at 3500 rpm for 20-30 min. The supernatant (3/4 of the solution) was taken out and used for printing while the sediment was used for next cycle of dispersion with adding SDBS aq. at the same amount (Fig. 1). The amount of dispersed CNTs was determined by UV-Vis absorption spectroscopy for each cycle. CNTs lines were formed by vacuum filtration through a membrane filter with a metal mask (slit widths of 88–215 μm), washed with hot water, and then transferred to PET films (Fig. 2). These processes were repeated until the CNTs were mostly dispersed ($\geq 90\%$).

90% of the CNT aggregates were converted into conductive CNTs films within 13 cycles (39 min), demonstrating the improved conductivity and reduced energy/time requirements for ultrasonication. CNTs lines with a high conductivity of 1400–2300 S cm^{-1} were obtained without doping. Lengths and crystallinities of dispersed CNTs will be discussed.

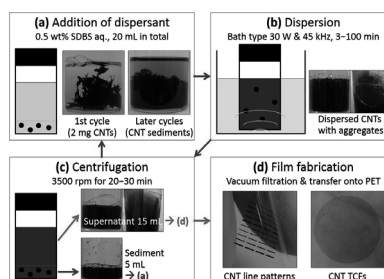


Fig. 1 The repetitive dispersion-extraction process

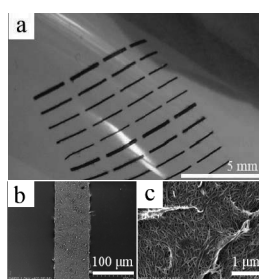


Fig. 2 The CNT lines on PET

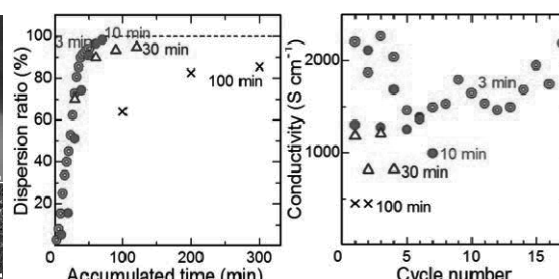


Fig. 3 Dispersion ratio and conductivity of the CNT lines prepared at different cycles.

[1] T. Saito *et al.* J. Phys. Chem. **B** 110, 5849 (2006).

Corresponding Author: S. Noda, Tel&Fax: +81-3-5286-2769, E-mail: noda@waseda.jp

Controlled formation of nanogaps of single-walled carbon nanotubes on substrates and field emission from the nanogaps

○Keigo Otsuka, Yuuki Shimomura, Taiki Inoue, Shohei Chiashi, Shigeo Maruyama
Department of Mechanical Engineering, The University of Tokyo, Tokyo 113-8656, Japan

Nanogaps of single-walled carbon nanotubes (SWNTs) formed by electrical breakdown are useful as true nanoscale electrodes contacting with nanocrystals, phase-change materials [1], and so on. Controlling the nanogap size for the electrode applications is necessary for reliable and efficient device performance. Although the gap size can be somehow decreased by using Ar gas flow or short SWNTs [1], the mechanisms which determine the gap size remain unclear. Here, we report that field emission occurs at the nanogaps of SWNTs lying on substrates and plays an important role in the formation/growth of the nanogaps during/after the breakdown.

Horizontally aligned SWNT arrays were grown on r-cut crystal quartz and transferred onto silicon substrates with 100-nm-thick oxide and photolithographically-patterned electrodes. After plasma etching of unwanted SWNTs, nanogaps were fabricated by electrical breakdown. Typical I - V curves for single nanogap devices with two gap sizes taken in vacuum and corresponding Fowler-Nordheim (FN) plots are shown in Fig. 1, indicating the occurrence of field emission. Field enhancement factors are estimated to be 6×10^7 and $2 \times 10^7 \text{ m}^{-1}$ for the 30 and 300 nm gaps, respectively, from the slope of the FN plots, which agrees with a previous report [2] despite the difference of device configurations. We also extended the nanogaps in air by applying various voltages on SWNT array devices after nanogap formation. The nanogap sizes after the process showed linear increase with the applied voltage as shown in Fig. 2. Interestingly, only anodic SWNTs were gradually etched by increasing voltage as shown in Fig. 3, probably due to electron-stimulated oxidation.

This field emission-induced gap growth explains the nanogap size dependence on original SWNT length by electrical breakdown [1]; since the voltage needed to initiate SWNT breakdown is proportional to the SWNT length [3], the gap size just after the breakdown depends on the SWNT length.

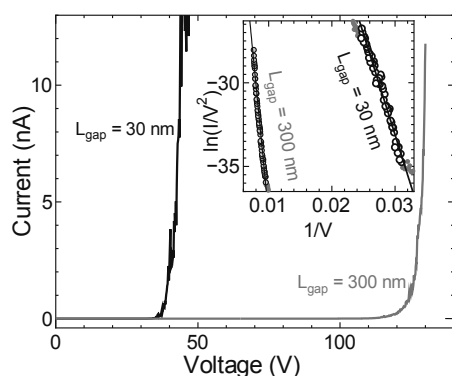


Fig. 1 I - V curves for single nanogap devices. FN plots are given in the inset. Measurements were conducted in vacuum.

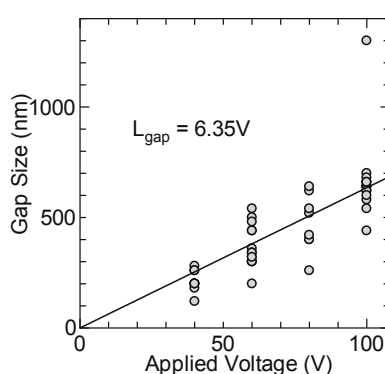


Fig. 2 Extended gap sizes vs applied voltage. Experiments were performed in air.

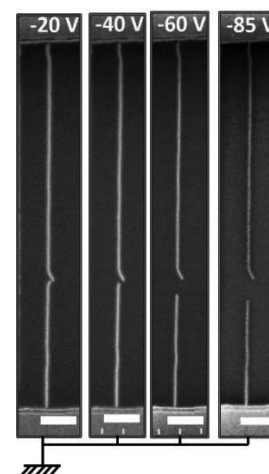


Fig. 3 SEM images of the gap growth for an identical SWNT after various voltages were applied. Scale bars are 500 nm.

[1] F. Xiong *et al.*, *Science* **332**, 568 (2011).

[2] J.-M. Bonard *et al.*, *Phys. Rev. Lett.* **89**, 197602 (2002).

[3] E. Pop, *Nanotechnology* **19**, 295202 (2008).

Corresponding Author: S. Maruyama

Tel: +81-3-5841-6421 Fax: +81-3-5800-6983,

E-mail: maruyama@photon.t.u-tokyo.ac.jp

Surface modification of carbon nanotubes utilizing photo-induced radical formation from benzyl derivatives

○Tomoya Takada¹, Shigeaki Abe²

¹ Department of Bio- and Material Photonics, Chitose Institute of Science and Technology, Chitose 066-8655, Japan

² Graduate School of Dental Medicine, Hokkaido University, Sapporo 060-8586, Japan

Surface modification of carbon nanotubes (CNTs) is an essential subject for their industrial application, since homogeneous dispersion of CNTs in solvents are effectively enhanced by appropriate surface modification. In addition, functional groups introduced by surface modification of CNTs act as reaction sites for subsequent bond formation with, for example, other organic molecules and polymers. Many methods for the surface modification have been reported previously. However, modification methods employing photochemical reactions have been scarcely studied. In this work, a simple method for the surface modification of CNTs with radicals formed by photo-irradiation was developed. We reported the surface modification of CNTs with photochemically generated benzyl radical derivatives last year. Here, some additional results on the mechanism of the photo-induced surface modification are shown.

As a radical source, 4-(bromomethyl)benzoic acid (4-BMBA, Wako Pure Chemicals, Co. Ltd.) was used in this work. BMBA and multi-walled carbon nanotubes (MWCNTs, diameter 10-30 nm, Wako Pure Chemicals, Co. Ltd.) were added into dimethylformamide (DMF) and then dispersed by sonication. Light from an Xe lamp (wavelength $\geq 300\text{nm}$) was irradiated to the mixture at 30 °C for 24 hours. During the irradiation, oxygen in the mixture solution was purged with Ar gas. MWCNTs after the irradiation were filtered, washed and dried in the air. Amount of the 4-carboxybenzyl radicals introduced on the MWCNTs surface was determined by conventional acid-base back titration; carboxyl groups attached on MWCNTs were neutralized with sodium hydrogen carbonate (NaHCO_3) aqueous solution, and the amount of residual NaHCO_3 was then measured by titration with hydrochloric acid (HCl). In addition, dark control experiment (i.e. the similar procedure without the light irradiation) was also carried out.

On the basis of the back titration results, partial neutralization of NaHCO_3 aqueous solution caused by carboxybenzyl groups introduced on MWCNTs was confirmed. In addition, dispersibility in water of the MWCNTs modified with light irradiation was drastically improved compared to those of pristine MWCNTs and dark control sample. These results indicate that carboxybenzyl groups generated by photo-induced C-Br bond cleavages are successfully attached to the MWCNTs surface through chemical bonds. This work has been supported by JSPS KAKENHI (Grant-in-Aid for Scientific Research (C)) No. 25420814.

Corresponding Author: T. Takada

Tel/Fax: +81-123-27-6056, E-mail: t-takada@photon.chitose.ac.jp

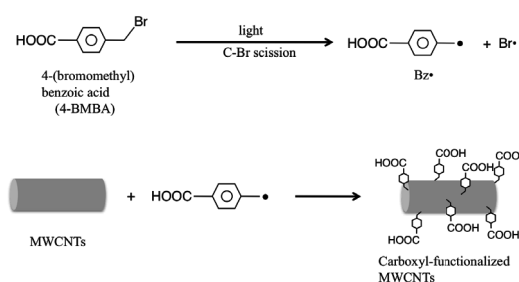


Fig. 1 Scheme of the surface modification in this work.

The new method for CNT and VGCF dispersion by Nano Premixer

○Taro Ikuta, Takayuki Takatsuka,

Thinky Corporation, 3-21-5 Kandasakuma-cho Chiyoda-ku, Tokyo 101-0025, Japan

In this study, multi-wall carbon nanotube (Elicarb) and vapor grown carbon fiber (VGCF-H) were dispersed by dual ultrasonic with rotation mixer; Nano Premixer, ultrasonic bath and homogenizer (Fig.1). To be compared with conventional type of ultrasonic instruments, nano premixer has superior in dispersion, uniformity, and usability. The surface resistivity was measured by low resistivity meter. After mixing MWNT by nano premixer, the surface resistivity of it (5wt%) was lower than ultrasonic bath (Fig.2). Dispersion state of MWNT and VGCF-H were evaluated by TEM, SEM. Nano Premixer can disperse MWNT and VGCF-H well without cutting them. These results shows that it can loosen aggregated MWNT by ultrasonic and mix them uniformly by rotate motion.



Fig.1 Nano Premixer

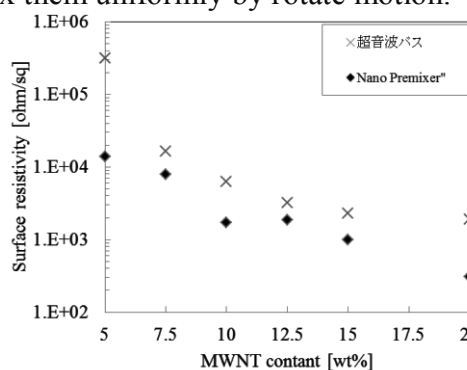


Fig.2 Surface resistivity of multi-wall nanotube

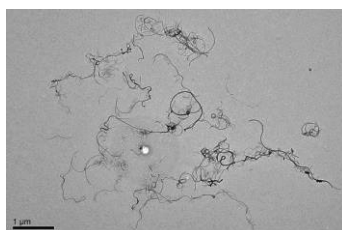
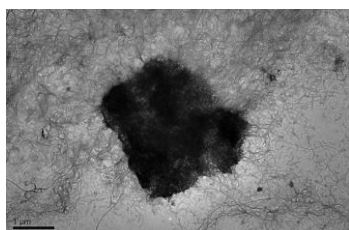


Fig.3 TEM micrographs of dispersed multi-wall nanotube (Left: ultrasonic bath, Right: Nano Premixer)

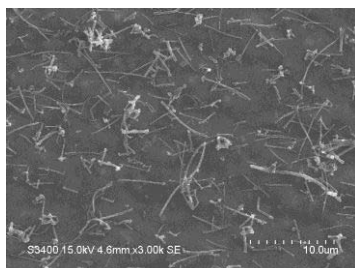
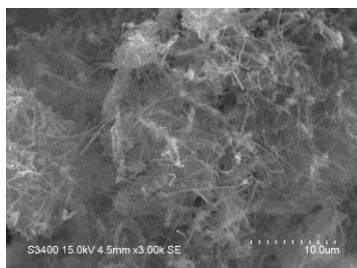


Fig.4 SEM micrographs of vapor grown carbon fiber VGCF-H (Left: Original Bulk, Right: Nano Premixer)

Corresponding Author: T.Takatsuka

Tel: +81-3-5821-7401, Fax: +81-3-5821-7422,

E-mail: takatsuka@thinky.co.jp

Optical Properties of Optical Isomer of Single-Chirality SWCNTs

○Xiaojun Wei, Mayumi Tsuzuki, Takuya Hirakawa, Yohei Yomogida, Atsushi Hirano, Shunjiro Fujii, Takeshi Tanaka and Hiromichi Kataura

Nanosystem Research Institute, National Institute of Advanced Industrial Science and Technology (AIST), Tsukuba, Ibaraki 305-8562, Japan

Single-wall carbon nanotubes (SWCNTs) show narrow optical absorption peaks corresponding to $E_{i,i}$ transitions between i -th one-dimensional van Hove singularities for parallel polarization of electric field to nanotube axis. From a selection rule, we expect optical absorption of $E_{i,i+1}$ transitions for the cross polarization, but a strong local field effect smears out such absorptions. This makes difficult to analyze energy band structure of SWCNTs by optical absorption. Recently, however, Castillo and Noguez theoretically demonstrated that circular dichroism (CD) spectrum clearly shows both $E_{i,i}$ and $E_{i,i+1}$ transitions equally [1]. This means that CD spectrum of single-chirality optical isomer SWCNT enables detailed analysis of band structure.

Very recently, we developed a new separation method by combining the overloading and stepwise elution chromatography [2]. This method can sort out single-chirality and optical isomers simultaneously. In this work, we prepared high-purity optical isomers of nine distinct (n, m) species and measured CD spectra. Figure 1 shows CD (up) and absorption spectra (down) of M- and P- (6, 5) SWCNT isomers. Here, CD intensity was normalized by $E_{2,2}$ absorption intensity. Twice large intensity of CD signal compared with the previous work [3] suggests extremely high-purity optical isomer separation. Furthermore, in the CD spectra, in addition to $E_{i,i}$ transitions, some other peaks are also observed. These additional peaks can be assigned to $E_{i,i+1}$ transitions. For example, CD peaks at 640, 441 and 272 nm are assigned to $E_{1,2}$, $E_{2,3}$ and $E_{4,5}$ transitions, respectively. Detailed analysis will be given in the presentation.

This work was supported by KAKENHI No. 25220602.

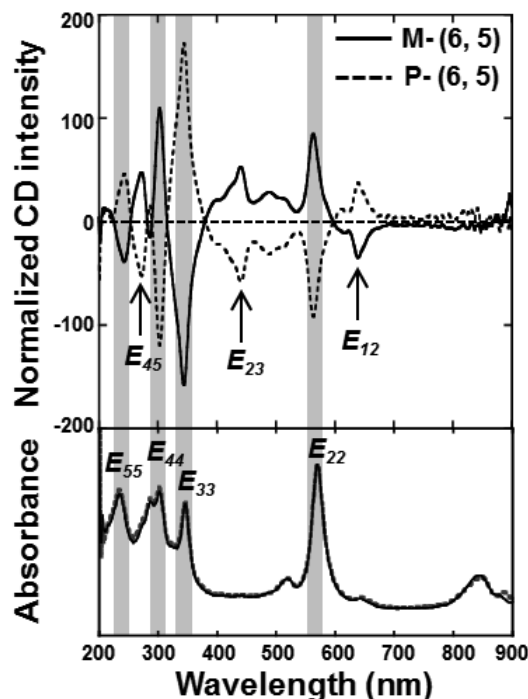


Figure 1. The normalized CD spectra (up) and absorption spectra of separated M- and P- (6, 5) isomers.

[1] A. Sánchez-Castillo and C. Noguez, *J. Phys. Chem. C* **114**, 9640-9644 (2010).

[2] X. Wei et al. 47th FNTG **2P-5**, p.92 (2014).

[3] S. Ghosh et al. *Nat. Nanotechnol.* **5**, 443-450 (2010).

Corresponding Author: H. Kataura

Tel: +81-29-861-2551, Fax: +81-29-861-2786, E-mail: h-kataura@aist.go.jp

Synthesis of Submillimeter-Long Carbon Nanotubes on Small Ceramic Powders by Fluidized Bed

○Kosuke Kawabata, Zhongming Chen, Kei Hasegawa, Toshio Osawa and Suguru Noda*

Department of Applied Chemistry, Waseda University, Tokyo 169-8555, Japan

Fluidized bed chemical vapor deposition (FBCVD) has realized mass production of carbon nanotubes (CNTs) [1]. The resulting CNTs are, however, aggregated with porous catalyst-support particles and less conductive. We previously realized sub-millimeter-long CNTs growing vertically from large Al_2O_3 beads (0.5 mm) with smooth surface by FBCVD [2,3]. Such CNTs can be easily separated from the beads by gas-flow, yielding highly pure CNTs (C content ≥ 99.6 wt% [3]) with fair conductivity. Moreover, semi-continuous production was realized by switching the gas; catalyst deposition from metal-organic vapors, CNT growth from C_2H_2 , and separation and collection of CNTs by carrier gas, in a single reactor at a fixed temperature. Highly reactive C_2H_2 enables its efficient conversion to CNTs at a yield $\sim 70\%$ in a residence time ~ 0.3 s [2], however needs be fed at a low concentration ~ 1 vol% with a large amount of carrier gas to avoid catalyst deactivation by carbonization [4].

In this work, we use less reactive C_2H_4 as a carbon source, which can be fed at much higher concentration with much less carrier gas. We need a different design principle; converting C_2H_4 to CNTs in a longer residence time but with a retained volumetric productivity due to its high feed concentration. Smaller gas feed rate enables the use of small catalyst support particles, which provide larger surface and promote the reaction of C_2H_4 . Small particles with smooth surface will still yield sub-millimeter-long CNTs in vertically aligned arrays, possibly enabling the collection of particles with CNTs by gas-flow. The particles and CNTs will be separated from each other outside the FBCVD reactor and the particles will be fed again to the FBCVD reactor. Aiming at this (semi-)continuous process, we studied the catalyst deposition and CNT growth processes separately using two reactors and inexpensive small Al_2O_3 abrasive powder (~ 0.2 mm) as catalyst supports.

Al_2O_3 powder was washed with ~ 7 wt% HCl aq, filtrated, and dried at 150 °C for 2 h to remove the impurities on the surface. Treated abrasives were set in the catalyst deposition reactor, heated in a N_2 flow to and calcined in 4 vol% O_2/N_2 for 10 min at 800 °C. AlO_x support layer and Fe catalyst were successively deposited by CVD from aluminum isopropoxide and ferrocene, respectively. The catalyst-supported powders were then filled in the CVD reactor, heated to and kept for 10 min at 800 °C in 10 vol% H_2/N_2 . CVD was then carried out by switching the gas to 0.7 vol% $\text{C}_2\text{H}_2/1.5$ vol% $\text{CO}_2/10$ vol% H_2/N_2 for 20 min. By this process, VA-CNTs grew on Al_2O_3 powder with a length ~ 150 μm (Fig. 1). CNT growth from C_2H_4 will also be discussed.

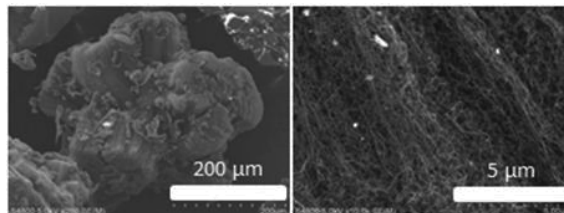


Fig. 1 CNTs on Al_2O_3 abrasive powder.

[1] Q. Zhang, et al., *ChemSusChem* **4**, 864 (2011).

[2] D.Y. Kim, et al., *Carbon* **49**, 1972 (2011).

[3] Z. Chen, et al., *Carbon* **80**, 339 (2014).

[4] K. Hasegawa, et al., *Carbon* **49**, 4497 (2011)

Corresponding Author: S. Noda, Tel&Fax: +81-3-5286-2769, E-mail: noda@waseda.jp

Controlled Growth of Single-Walled Carbon Nanotubes Using W-Co Catalyst at Different Temperatures and Carbon Feedings

oFeng Yang, Xiao Wang, Daqi Zhang, Juan Yang, Yan Li

Beijing National Laboratory for Molecular Science, Key Laboratory for the Physics and Chemistry of Nanodevices, State Key Laboratory of Rare Earth Materials Chemistry and Applications, College of Chemistry and Molecular Engineering, Peking University, Beijing 100871, China

The structure-controlled synthesis of single-walled carbon nanotubes (SWNTs) is a crucial issue for their advanced applications in nanoelectronics. The catalysts play an essential role in controlling the structure of the SWNTs [1,2]. Recently, employing tungsten-based alloy catalyst with high melting points and consequently are able to maintain their specific crystal structure during the chemical vapor deposition (CVD) process, which regulates the chirality of the grown SWNTs [3]. Here we further systematic study the effects of CVD conditions (e.g., temperature and carbon feeding) on the selective growth of the chiral SWNTs.

Using the specific structure of the W_6Co_7 alloy, we are able to grow the high abundance of the (12,6) and (14,4) SWNTs, respectively, at different growth temperatures by altering the carbon feedings (Fig. 1). We find that CVD conditions during the growth process play key role in controlled growth of the single chiral SWNTs.

- [1] L. Yan *et al.* *Adv. Mater.* **22**, 1508 (2010).
 [2] Y. Chen *et al.* *Carbon* **81**, 1 (2015)
 [3] F. Yang, X. Wang, D. Zhang, L. Yan *et al.* *Nature*. **510**, 522 (2014).

Corresponding Author: Yan Li

Tel: +86-010-62756773, Fax: +86-010-62756773,
 E-mail: yanli@pku.edu.cn

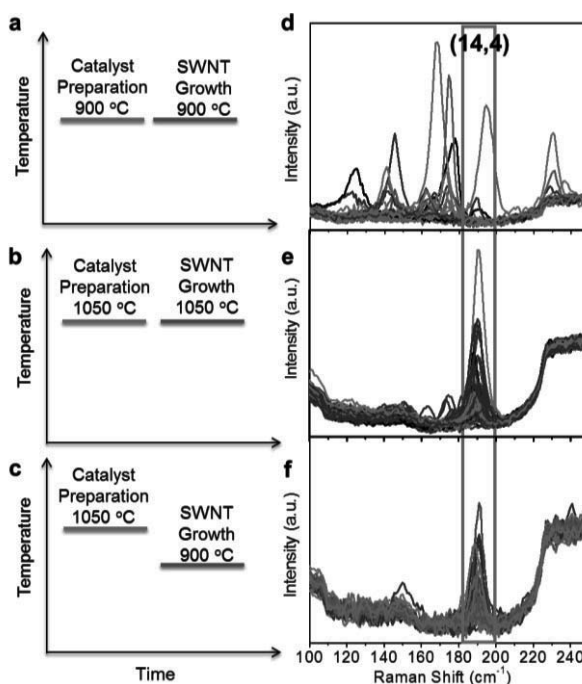


Fig. 1 The Raman spectra of SWNTs grown at different processes. **a-c**, Schemes showing the different growth processes. **d-f**, The Raman spectra of the corresponding SWNTs samples. Regions in which (14,4) tubes are located are indicated with frame (excitation wavelength, 532 nm).

Growing carbon nanotubes on acetylene black particles to form their hybrid and controlling the reaction on a few second time scale

○Masaaki Kuriya¹, Kei Hasegawa¹, Yusaku Harada², Suguru Noda¹

¹ Department of Applied Chemistry, Waseda University, Tokyo 169-8555, Japan

² Denki Kagaku Kogyo Kabushiki Kaisha, Tokyo 103-8338, Japan

Acetylene black (AB) and carbon nanotubes (CNTs) are representative conductive fillers for Li ion batteries and resin compounds. Their hybrid was developed by growing CNTs on AB particles by fixed-bed chemical vapor deposition (CVD), which effectively enhanced the conductivity of resin compounds due to their easy dispersability [1]. Aiming at higher productivity, higher crystallinity, and smaller CNT diameters, we propose the production of such hybrid in the AB production furnace. AB is currently produced at ~ 2000 °C and several second time scale. If ferrocene is fed, Fe particles will form on AB and CNTs will grow as the gas cools down to 1000–1400 °C at the downstream. Such short process time will minimize the aggregation of Fe particles on AB and yield small Fe particles and small-diameter CNTs. As a first step, we fixed AB particles on Si substrates and applied the “pulse current heating method [2]” to basically understand such high-temperature, short-time process.

Fig. 1a shows the experimental apparatus. AB was supported on Ti/SiO₂/Si and the substrate was set in a reaction tube and connected to electrodes. The substrate was resistively heated to a target temperature with the gas flow being changed; ferrocene vapor/2 vol% CO₂/17 vol% H₂/Ar for supporting catalyst, 3 vol% CO₂/27 vol% H₂/ Ar for annealing, and 0.5 vol% C₂H₂/3 vol% CO₂/26 vol% H₂/Ar for CVD.

First, we examined the reactions at a fixed temperature of 1100 °C; 1 s for catalyst deposition from ferrocene, 9 s for annealing, and 10 s for CVD. Multiple Fe particles formed on each primary AB particle (Fig. 1b) and grew CNTs but with a rather large diameter of ~ 20 nm (Fig. 1c) and wavy morphology (Fig. 1d).

Next we applied the different temperature history mimicking the target process; 1400 °C for 1 s for decomposition of ferrocene into Fe vapor, 1100°C for 1 s for deposition of Fe particle from Fe vapor, and 1100 °C for 5 s for CVD. CNTs grew much densely, much longer, and much more straightly (Fig. 1e). High temperature process actually forms Fe particles and CNTs on AB in a few seconds.

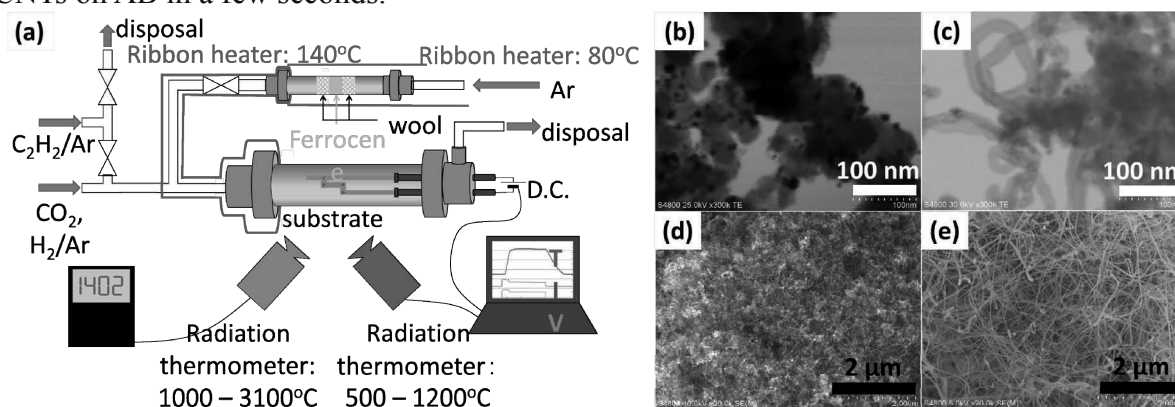


Fig.1 (a) Schematic diagram of the apparatus. STEM image before CVD (b) and STEM (c) and SEM (d) images after CVD for the fixed 1100 °C process. (e) SEM images for the cooling process from 1400 to 1100 °C.

[1] Y. Harada *et al.* the Carbon Society of Japan, 3A04 (2012). [2] K. Sekiguchi *et al.* Carbon, **50**, 2110 (2012).

Corresponding Author: S. Noda, Tel&Fax: +81-3-5286-2769, E-mail: noda@waseda.jp

FT-ICR study of chemical reaction of ethanol and acetonitrile molecules on transition metal clusters

○Kazuki Ogasawara¹, Yuta Tobari², Yoshinori Sato¹, Makoto Saito¹, Shohei Chiashi¹,
Toshiki Sugai², and Shigeo Maruyama¹

¹ *Department of Mechanical Engineering, The University of Tokyo, Tokyo 113-8656, Japan*

² *Department of Chemistry, Toho University, Funabashi 274-8510, Japan*

Chemical vapor deposition (CVD) method is one of the most common techniques for production of single walled carbon nanotubes (SWNTs). During the CVD process, SWNTs grow with carbon atoms decomposed from molecules such as CO, CH₄ or ethanol on catalytic metal particles at high temperature. Even though the surface chemical reaction on metal particles is critically important, little is known due to the complexity in properties of these nanoparticles. Moreover, Thurakitseree et al. [1] reported that changing the carbon feedstock from pure ethanol to a few % mixture of acetonitrile (CH₃CN) in ethanol during CVD drastically reduces the average diameter of the SWNTs, and this diameter-modification is reversible and repeatable. It is suggested that the nitrogen atoms in acetonitrile molecules temporarily impeded the formation of larger diameter SWNTs on the surface of catalytic particles. However, the detailed mechanism of this reaction is still not clear.

In this study, the chemical reactions of transition metal (Fe, Ni, and Co) cluster cations with ethanol and acetonitrile was observed by Fourier transform ion cyclotron resonance (FT-ICR) mass spectrometer with direct injection laser vaporization cluster beam source [2]. Metal clusters were trapped within the FT-ICR cell, subsequently the reactant molecules was introduced. Figure 1 shows the typical mass spectrum of the reaction products from Co₁₃⁺ clusters. We can observe the dehydrogenated chemisorption such as +HCCN or +(CCN)₂. Figure 2 shows the schematic diagram of the reaction products. These reactions drastically depended on cluster size and the species of metals or reactant molecules in respect to the change of simple / dehydrogenate chemisorption ratio and reaction rate constants.

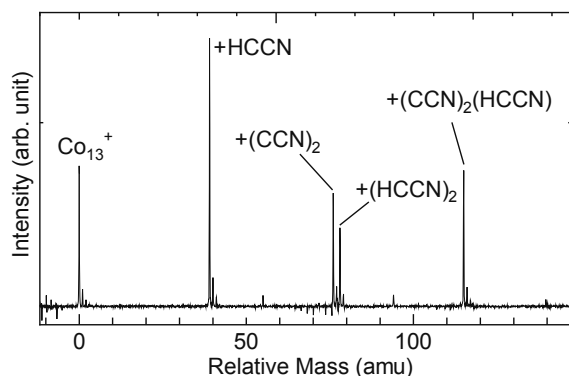


Fig.1 Mass spectra of isolated Co₁₃⁺ clusters after reaction with CH₃CN.

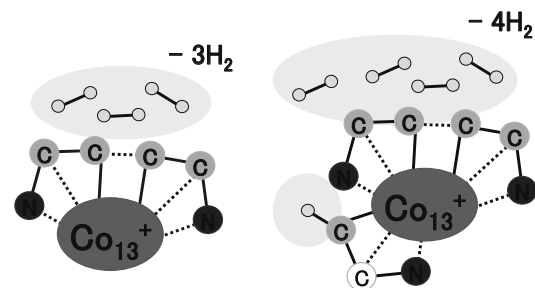


Fig.2 Schematic diagram of [Co₁₃(CCN)₂]⁺ and [Co₁₃(CCN)₂(HCCN)]⁺ clusters.

[1] T. Thurakitseree *et al.*, ACS Nano, **7** (2013) 2205.

[2] S. Maruyama *et al.*, Rev. Sci. Instrum., **61** (1990) 3686.

Corresponding Author: S. Maruyama

Tel: +81-3-5841-6421, Fax: +81-3-5841-6983,

E-mail: maruyama@photon.t.u-tokyo.ac.jp

Flame Synthesis of Single-Wall Carbon Nanotubes and Control over the Temperature Field and Reactions

○Mai Yamaguchi, Kei Hasegawa, Toshio Osawa, Suguru Noda

Department of Applied Chemistry, Waseda University, Tokyo 169-8555, Japan

Floating catalyst chemical vapor deposition (FCCVD) has realized mass-production of multi-wall carbon nanotubes (MWCNTs) at ~ 100 tons annually per plant. It also enabled continuous production of high-quality single-wall CNTs (SWCNTs), however at much smaller scales. Because single SWCNT of 1 nm in diameter weighs only 1/10,000 of single MWCNT of 100 nm in diameter at the same length, small catalyst particles need to be fed at much higher density. Such particles, however, quickly aggregate in the reactor at second time-scale of FCCVD. We previously proposed to use a flame as a solution; ferrocene decomposes and yields Fe vapor in the premixed flame at ~ 3000 K, Fe vapor mixes with CVD gas, cools down and forms Fe nanoparticles. All processes can occur in millisecond time-scales, possibly yielding Fe nanoparticles at high density. Using a small burner (1 mm in diameter), highly crystalline SWCNTs were produced, but at a small amount [1].

This time, we aim to enhance the productivity of SWCNTs via more careful control over the temperature field. Mixing of hot flame gas with cold CVD gas enabled rapid cooling of Fe vapor and formation of small catalyst particles, while the mixed gas continued to cool down, resulting in a short CVD time [1]. Thus we applied a furnace to keep the temperature suitable for CVD at second time scale, the internal preheater for the CVD gas, and additional Ar gas line for cooling the flame gas and nucleating Fe nanoparticles (Fig. 1).

We introduce three parameters for temperatures; T_{flame} at the premixed flame, T_{cat} at the mixing point of the flame gas with Ar cooling gas, and T_{CVD} at the furnace. We calculate T_{flame} and T_{cat} values by dividing the heat by the heat capacity of the gas, but actual temperature is lower due to the decomposition of gas molecules and heat loss.

Fig. 2 shows the SWCNTs produced under the current optimum condition. $\text{C}_2\text{H}_4/\text{O}_2/\text{Ar}$ with ferrocene and sulfur vapors is fed to the inner tube and ferrocene is decomposed quickly in the premixed flame at $T_{\text{flame}} = 3700$ °C. The flame gas is mixed with Ar and cooled down to $T_{\text{cat}} = 1100$ °C to nucleate Fe nanoparticles. CH_4 is preheated and fed radially to mix and start CVD at $T_{\text{CVD}} = 900$ °C. Products were collected by a membrane filter and analyzed by scanning electron microscopy (SEM) and Raman spectroscopy. SWCNTs with 1 nm diameter was obtained but still at a small amount.

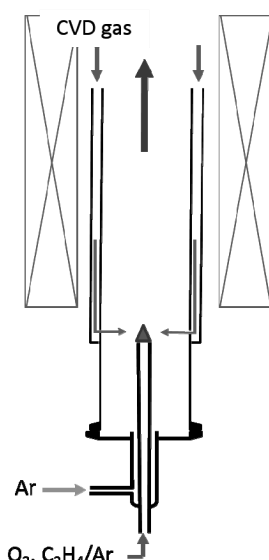


Fig.1 Experimental apparatus

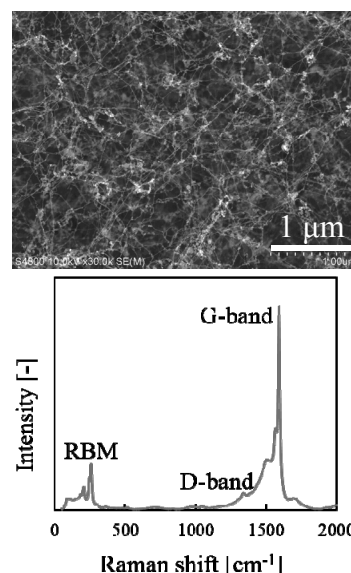


Fig.2 SEM image and Raman spectrum

[1] J. Oshima *et al.* 42nd FNTG Symposium, 1P-11 (2012).

Corresponding Author: S. Noda, Tel&Fax: +81-3-5286-2769, Email: noda@waseda.jp

An Effective Method for the Production of Single Walled Carbon Nanotubes by the Bipolar Pulsed Arc Discharge Method

¹Kazi Hanium Maria, ¹Tetsu Mieno

¹Graduate School of Science and Technology, Shizuoka University, Shizuoka, 422-8529, Japan

Single-walled carbon nanotubes (SWNTs) are synthesized by an innovative low-frequency bipolar pulsed arc discharge method using a newly developed bipolar pulsed current circuit with constant current and constant pulse duration. In this set-up, the arc is produced between two graphite electrodes containing a metal catalyst (Ni+Y), and both electrodes will sublime carbon alternately roughly at a same rate as shown in Fig.1. In this case, all the sublimated carbon becomes soot containing single-walled nanotubes [1, 2] and there is no deposition on the electrodes. The carbon sublimation rate and the deposition rate of the bipolar pulsed arc discharge method are compared with those of the DC, and the AC arc discharge methods, as listed in Table 1. TEM micrograph reveals that the bipolar pulsed arc discharge has a tendency to produce thicker bundles of SWNTs as shown in Fig.2. The average numbers of SWNTs in a bundle are 3 to 4 and the tube diameters are approximately 1.0-1.5 nm. This diameters result is in good agreement with the results obtained from the Raman experiment. The intensity ratio I_D/I_G in the Raman measurement varies from 0.021 to 0.026 with the frequency which indicates the good quality of SWNTs.

Table 1. Comparison between the different arc discharge methods

Type	Current (A)	Frequency (Hz)	Sublimation Rate (mg/min)	Deposition Rate (mg/min)
DC	55	0	25.40	8.92
AC	50(effective current)	60	4.19	no deposit
Bipolar	55	2	18.08	no deposit

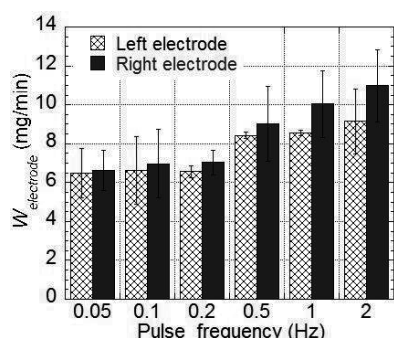


Fig.1 Variation of sublimation rates, $W_{electrode}$, from the two electrodes.

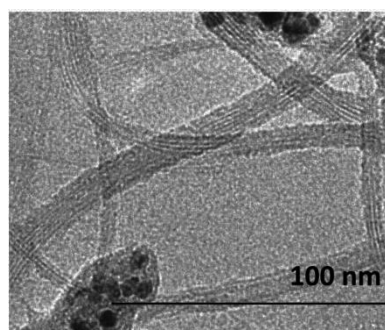


Fig.2 TEM image ($\times 100000$) of the soot synthesized by the bipolar pulsed arc discharges of frequency $f = 0.05$ Hz.

[1] M. J. Rahman, T. Mieno. Jpn. J Appl. Phys. **52**, 056201 (2013).

[2] K. H. Maria, T. Mieno. Vacuum. **112**, In Press, (2015).

Corresponding Author: T. Mieno

Tel & Fax: +81-54-238-4750, E-mail: sptmien@ipc.shizuoka.ac.jp

Selective precipitation of few/multi-layer graphene on/around h-BN on SiO₂ from metal-carbon films

○Kohtaro Yamaguchi, Kei Hasegawa, and Suguru Noda*

Department of Applied Chemistry, Waseda University, Tokyo 169-8555, Japan

Direct synthesis of graphene on dielectric/insulator substrates is important for simple fabrication of graphene-based devices. Some studies have reported such growth [1,2], however there are still many issues to be solved for practical fabrication of graphene. Graphene on h-BN is gathering great interests due to the enhanced mobility in graphene [3]. In this work, we target at direct growth of graphene on h-BN.

We used metal-carbon (M-C) mixed/bilayer films as a starting material for graphene. Upon heating, carbon precipitates to form graphene if the carbon concentration is higher than the solubility at the heating temperature. For M-C films with a free surface, graphene selectively precipitates not at the film/substrate interface but at the free surface to minimize the free energy of the system. Thus we used a cap layer to make the cap/M-C film interface more stable than the M-C film/substrate interface to precipitate graphene at the substrate side.

First we worked on precipitating graphene on SiO₂ using SiO₂ (500 nm)/Ni (300 nm)/a-C (30 nm) multilayer sputter-deposited on a quartz glass substrate. The sample was annealed in a tubular furnace for 10 min at 1000 °C under Ar atmosphere to precipitate graphene. SiO₂ and metal layers were then removed using hydrofluoric acid and iron (III) chloride aqueous solutions, respectively. With a SiO₂ cap-layer, many graphite islands precipitated at the interface between quartz glass substrate and Ni film. Without a cap layer, on the other hand, precipitation occurred only at the Ni surface.

We then studied graphene precipitation on h-BN (Fig. 1a). First, h-BN flakes were prepared on a quartz glass substrate by mechanical exfoliation using Kapton® tapes. Cu is used as a cap layer on Fe-C films because of the minimal solubilities of C and Fe in it. Cu (500 nm)/Fe-C (300 nm) was sputter-deposited on the substrate. The sample was annealed and metals were then removed as mentioned above. Fig. 1b shows the optical and Raman mapping images of the two typical h-BN flakes after removing the metal layers. Few/multi-layer graphene precipitated on the h-BN surface and/or at the edge. Factors contributing to various precipitation modes will be discussed.

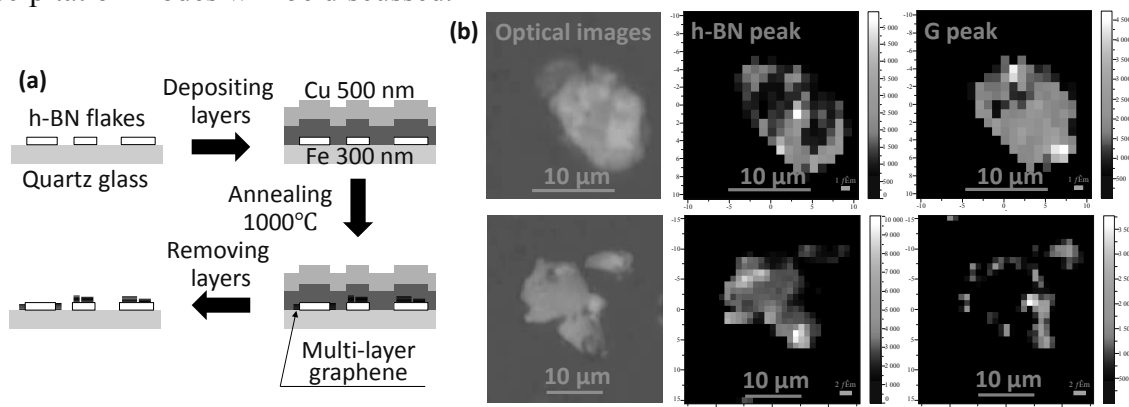


Fig. 1(a) Process flow diagram. (b) Optical and Raman mapping images of h-BN and G peaks on h-BN flakes.

[1] K. Hirano *et al.* *Nanoscale* **4**, 7791 (2012). [2] M. Kosaka *et al.* *Carbon* **82**, 254 (2015). [3] C. R. Dean *et al.* *Nat. Nanotechnol.* **5**, 722 (2010).

Corresponding Author: S. Noda, Tel&Fax: +81-3-5286-2769, E-mail: noda@waseda.jp

Two-step growth and characterization of WS₂/MoS₂ heterostructures

Shohei Mori¹, Yutaka Maniwa¹, Yasumitsu Miyata^{1,2}

¹*Department of Physics, Tokyo Metropolitan University, Hachioji, 192-0397, Japan*

²*JST, PRESTO, Kawaguchi, 332-0012, Japan*

The heterostructures of two-dimensional semiconductors have attracted much attention for their potential applications in electronics and optoelectronic. Recently, several groups have reported the vapor-phase growth of lateral and stacked heterostructures based on typical semiconductor transition metal dichalcogenides (TMDCs) such as MoS₂, MoSe₂, and WS₂ [1-3]. These studies basically use the continuous feeding of two precursors for the growth of two different TMDCs without changing reaction chambers. This process often leads to the alloying of heterojunction interfaces and/or secondary-grown materials because of the contamination of the remaining first precursors in the chambers. To avoid the contamination, it is highly desired to develop a two-step growth technique of the heterostructures with clean reaction chambers.

Here, we report the two-step growth of WS₂/MoS₂ heterostructures by using such clean environment. First, WS₂ monolayers were formed on a SiO₂/Si substrate by the sulfurization of WO₃ thin films. Then, the samples were put on another quartz tube to avoid the contamination of WO₃ during MoS₂ growth. The MoS₂ atomic layers were grown from sulfur and MoO₃ by chemical vapor deposition. This process leads to the formation of triangle-shaped MoS₂ grains on the WS₂ as shown in the AFM image and Raman spectra (Fig. 1). In the poster, the details of sample preparation and characterization will be presented.

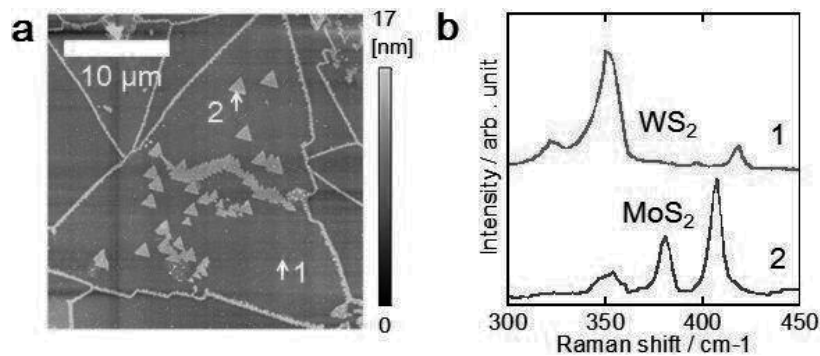


Fig.1 (a) AFM image and (b) Raman spectra of the WS₂/MoS₂ heterostructures.

[1] Y. Gong, *et al.* Nat. Mater. 13, 1135 (2014)., [2] X. Duan, *et al.* Nat. Nanotechnol, 9, 1024 (2014).,

[3] C. Huang, *et al.* Nat. Mater. 13, 1096 (2014).

Corresponding Author: Yasumitsu Miyata, TEL:+81-42- 677-2508, E-mail: ymiyata@tmu.ac.jp

Production of graphene quantum dots with molecule-like fluorescence

○Misaki Takahashi, Toshiki Sugai

Department of Chemistry, Toho University, Miyama 2-2-1 Chiba, 274-8510, Japan

Graphene quantum dots (GQDs) are nanometer-size graphene fragments. They are promising materials because of their unique electronic and optical properties originating in quantum size and edge effects. In particular, their fluorescence should be constant like fluorescent molecules even if the excitation wavelength is changed for the applications such as biomarkers. However, the emission wavelength of GQDs, especially derived from bulk carbon such as carbon fibers, depend on excitation wavelength, which may come from their defects [1]. Although there have been a few reports on the GQDs with molecule-like fluorescence [2,3], emission wavelength cannot be controlled by changing the size of GQDs with keeping molecule-like fluorescence properties. Here we present production and size control of GQDs with molecule-like fluorescence by chemical oxidation of single-walled carbon nanotubes (SWNTs) in various conditions without any post-processing.

GQDs were prepared from CoMoCAT-SWNTs (Sigma-Aldrich) by oxidation in a mixture of concentrated H_2SO_4 and HNO_3 . The solution was sonicated for 24 hours and/or sonicated for two hours and refluxed for 24 hours at temperatures from 70 to 150 °C. The oxidized mixture was diluted with deionized water followed by centrifugation at 10000 rpm for 20 min to separate GQDs and residue SWNTs. The produced GQDs were characterized by TEM, absorption, and photoluminescence (PL) observations.

Fig.1 shows PL spectra of the GQDs prepared at temperature of 100°C. The emission wavelength of 520 nm, which have been reported as one of the major emission wavelengths, does not depend on the excitation wavelength without further purification and separation such as dialysis and size exclusion chromatography. The results show that the starting material is crucial to the emission properties. Furthermore, the emission wavelength and the size of GQDs were controlled by the reaction conditions with keeping the properties of molecular-like fluorescence.

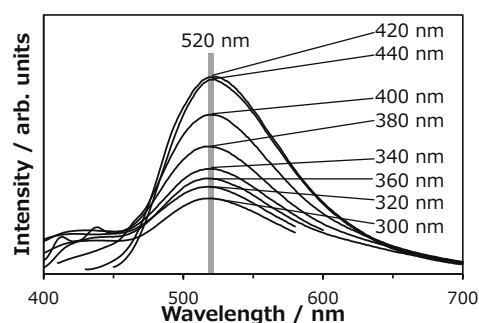


Fig.1 PL spectra of the GQDs prepared reaction temperature at 100°C

[1] J. Peng *et al.* *Nano Lett.* **12**, 844 (2012). [2] M. Zhang *et al.* *J. Mater. Chem.* **22**, 7461 (2012).

[3] Y. Dong *et al.* *Carbon.* **64**, 245 (2013).

Corresponding Author: T. Sugai

Tel: 047-472-4406 E-mail: sugai@chem.sci.toho-u.ac.jp

Growth of bilayer graphene and its electric property

○Ryo Hoshino, Ryoya Kimura, Kentaro Imai, Yutaro Hayashi, Tomoko Nagata,
Nobuyuki Iwata, Hiroshi Yamamoto

*College of Science & Technology, Nihon University, 7-24-1 Narashinodai, Funabashi-shi,
Chiba 2748501*

In order to realize superconductivity at room temperature, we fabricate metal intercalated bilayer graphene. The electron-exciton coupling is expected to generate high temperature superconductivity [1]. In this study, we report the growth of bilayer graphene and its electric property.

The bilayer graphene was fabricated by stacking two single-layered graphene sheets. The single layered graphene was prepared by chemical vapor deposition (CVD) method on Cu foil and transferred on SiO₂/Si substrate. For the transport, poly methyl methacrylate (PMMA) was used as a tentative protection film. Cu foil and PMMA film were removed after the transport using soaking the specimen in an Fe(NO)₃ aqueous solution and acetic acid solution. The removal conditions were optimized to obtain high purity graphene.

Figure 1 shows the Raman spectrum of graphene on SiO₂/Si substrate prepared using optimized removal conditions. The G- and G'- peaks were observed at 1591.5 cm⁻¹ and 2689.2 cm⁻¹, respectively. The ratio of G/G' peak intensity and shift of the G'-peak indicate the growth of single-layered graphene sheet.

The electric properties of bilayer graphene fabricated by stacking this single-layered graphene sheets and details for removal conditions will be discussed.

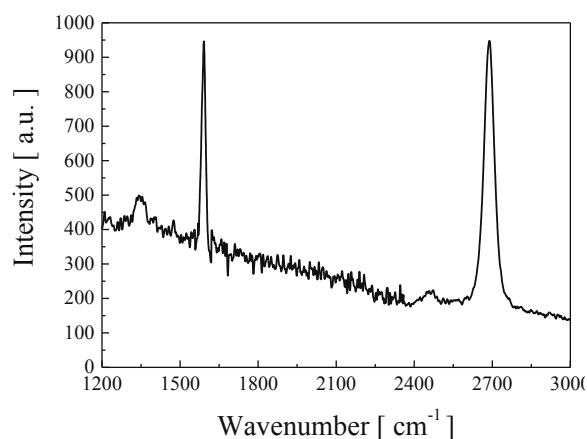


Fig.1 Raman spectrum of graphene

[1] Akimitsu. Parity. MARUZEN. **05**, 6-12 (2008).

Corresponding Author: Nobuyuki Iwata

Tel: +81-47-469-5457

E-mail: iwata.nobuyuki@nihon-u.ac.jp

Growth and characterization of W-doped NbS₂ atomic layers

○Shogo Sasaki¹, Yutaka Maniwa¹, Yasumitsu Miyata^{1,2}

¹ *Department of Physics, Tokyo Metropolitan University, Hachioji 192-0397, Japan*

² *JST, PRESTO, Kawaguchi 332-0012, Japan*

Atomic-layer transition metal dichalcogenides (TMDCs) are attractive two-dimensional materials because of their tunable electronic properties and unique spin-valley physics. To date, there have been many reports on the growth of semiconducting monolayer TMDCs such as MoS₂ and WS₂ [1]. In contrast, very few synthesis studies have been reported for metallic TMDCs such as NbS₂ nanosheets [2]. It is, therefore, still highly desired to prepare high quality, large area metallic TMDC atomic layers for unraveling their unique electronic phases including charge-density wave and superconductivity in the two-dimensional limit.

In this presentation, we report the growth and characterization of metallic W-doped NbS₂ atomic layers. For the crystal growth, stacked WO₃ and Nb films were prepared on various substrates including sapphire and graphite by electron beam deposition. These films were sulfurized by annealing at 1200°C under hydrogen/sulfur/argon atmosphere. We found that the addition of W atoms effectively prompts the growth of Nb-based TMDC crystals. Figure 1a shows atomic force microscope (AFM) image of a typical hexagonal-shaped crystal of W-doped NbS₂. The thickness of such crystals ranges from 4.2 to 70 nm. High-resolution AFM and FFT images reveal the honeycomb lattice of samples with lattice constant of 3.2 Å (Fig. 1b). These crystals have two characteristic Raman peaks at 360 cm⁻¹ and 392 cm⁻¹, which can be assigned to WS₂ E_{2g} and NbS₂ A₁ modes, respectively (Fig. 1c). The resistivity of samples is around 10⁻⁵ Ω·m, which is comparable to that of bulk NbS₂ (~10⁻⁶ Ω·m). These results strongly suggest that the present approach provides atomic layer W-doped NbS₂ crystals with metallic properties.

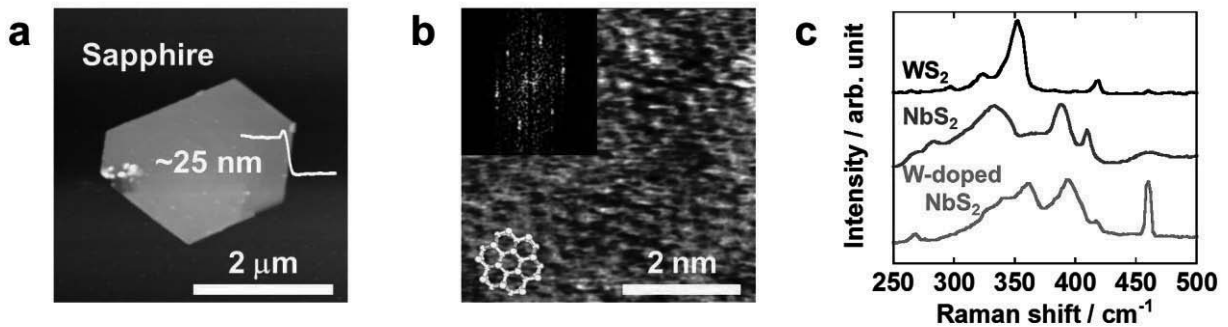


Fig 1 (a) AFM image of a typical W-doped NbS₂ crystal. (b) High-resolution AFM and FFT images of the crystal surface. (c) Raman spectra of monolayer WS₂, bulk NbS₂ and W-doped NbS₂.

[1] M. Chhowalla, *et al.* Nat. Chem. 5 (2013) 263.

[2] W. Ge, *et al.* Nanoscale, 5 (2013) 5773.

Corresponding Author: Yasumitsu Miyata

TEL:+81-42- 677-2508, FAX:+81- 42-677-2483

E-mail: ymiyata@tmu.ac.jp

π -Conjugated Polymer Microspheres Covered by Graphene Oxide

○Yusuke Aikyo¹, Kenichi Tabata², Soh Kushida², Daniel Braam³, Junpei Kuwabara², Takaki Kanbara², Takahiro Kondo², Junji Nakamura², Dao Duy Thang⁴, Satoshi Ishii⁴, Tadaaki Nagao⁴, Axel Lorke³, Yohei Yamamoto²

¹College of Science Engineering, University of Tsukuba, Ibaraki 305-8573, Japan

²Graduate School of Pure and Applied Sciences and TIMS, University of Tsukuba, Ibaraki 305-8573, Japan

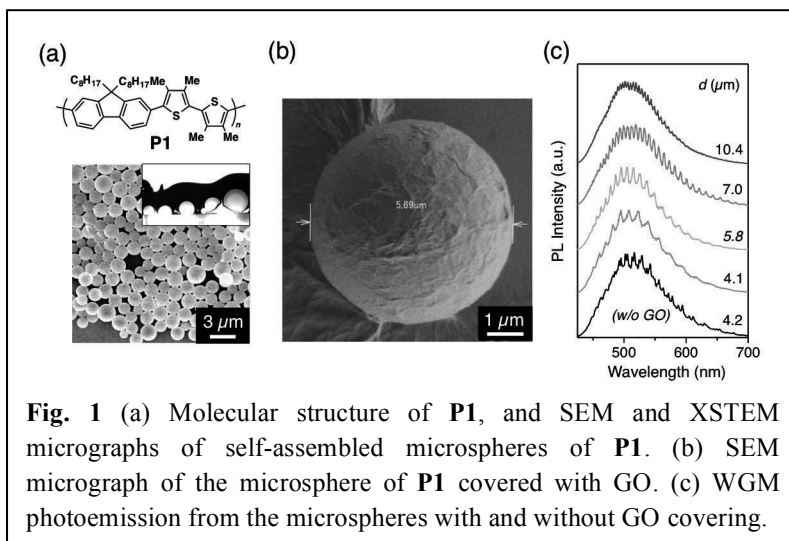
³Department of Physics, University of Duisburg-Essen, Duisburg D47048, Germany

⁴National Institute for Materials Science (NIMS), Ibaraki 305-0044, Japan

Carbon materials are studied for application in electronic and optoelectronic devices. Recently, we reported that π -conjugated polymers self-assemble to form microspheres^[1,2], which exhibited whispering gallery mode (WGM) photoemission upon laser irradiation to single spheres.^[3] Here, we attempt covering the polymer microspheres with 2D carbon materials such as graphene and graphene oxide (GO).

π -Conjugated polymer spheres were prepared by vapor diffusion of MeOH into a CHCl_3 solution of **P1** (**Fig. 1a**). The resultant suspension of the polymer microspheres was then dropped into

an aqueous solution of GO. **Figure 1b** shows a SEM micrograph of the obtained precipitate, where the surface of the polymer microsphere was covered by GO. μ -PL measurements of the single sphere showed clear WGM photoemission with periodic and sharp lines (**Fig. 1c**).



[1] T. Adachi *et al.* *J. Am. Chem. Soc.* **2013**, *135*, 870–876.

[2] L. Tong *et al.* *Polym. Chem.* **2014**, *5*, 3583–3587.

[3] K. Tabata *et al.* *Sci. Rep.* **2014**, *4*, 5902/1–5.

Corresponding Author: Y. Yamamoto

Tel: +81-29-853-5030, Fax: +81-29-853-4490. e-mail: yamamoto@ims.tsukuba.ac.jp

Direct and real-time TEM observation of aqueous solution sandwiched by graphene layers

○Yuki Sasaki, Ryo Kitaura and Hisanori Shinohara

Department of Chemistry and Institute for Advanced Research, Nagoya University, Nagoya 464-8602, Japan

High-resolution transmission electron microscopy (HRTEM) observations provide real-time atomic-level structural information on nanomaterials^{[1]-[3]}. If we can apply HRTEM for observation of liquids and solutions, that will be a great impact on physical chemistry of liquids and solutions. One of the biggest problems of HRTEM observations of liquids is that liquid samples have to be placed under a high vacuum condition, the liquid samples being lost spontaneously by vaporization. To overcome this problem, we have here focused on development of a new method for HRTEM observations of liquids by using graphene-sandwiched-type environmental cell. The environmental cell has been successfully applied to observe water at various temperature and dynamics of aqueous solution of iron nitrate.

Figure 1 and figure 2 shows a typical HRTEM image of Fe nitrate aqueous solution and a corresponding electron energy loss spectrum, respectively. EELS peaks arising from oxygen and iron have been clearly observed which respectively originates from oxygen in water molecules and iron in iron nitrate. A contrast marked by the circle in Fig. 1 probably corresponds to precipitated iron nitrate, which moves rapidly and blinks during the observation. In this poster, details of sample preparation and detailed results of TEM observations are addressed.

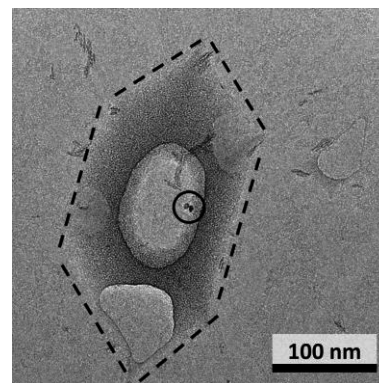


Fig.1 Typical HRTEM image of the graphene pocket, shown by dashed line.

Black circle shows iron nitrate.

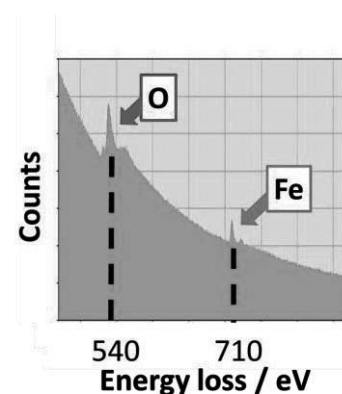


Fig.2 Electron energy-loss spectrum of $\text{Fe}(\text{NO}_3)_3$ aqueous solution encapsulated inside graphene pockets.

K-edge peak of oxygen and iron were observed.

- [1] J. C. Meyer, *et al.* Nature **454**, 319 (2008).
 [2] R. Kitaura, *et al.* Nano. Lett. **8**, 693 (2008).
 [3] R. Kitaura, *et al.* Angew. Chem., Int. Ed. **48**, 8298 (2009).
 Corresponding Author: Ryo Kitaura and Hisanori Shinohara
 Tel: +81-52-789-2482, Fax: +81-52-747-6442,
 E-mail: r.kitaura@nagoya-u.jp and noris@nagoya-u.ac.jp

Influence of the surface structure of substrate for proximity effect on Graphene

Akinori Izumiyama¹, ○Kazuyuki Takai^{1,2}

¹*Department of Chemical Science and Technology, Hosei University, Tokyo 184-8584, Japan*

²*Research Center for Micro-Nano Technology, Hosei University, Tokyo 184-0003, Japan*

Atomic membrane system like graphene is intrinsically sensitive to chemical environment, where all atoms possess surface. Indeed we have demonstrated a proximity effect on the electronic properties of graphene on SiO₂ substrate on which surface a large polarization is introduced by modification with self-assemble monolayer (SAM) of polar molecules [1, 2]. However, the observed shift of the Fermi energy E_F by the SAM-induced proximity effect is almost half of that estimated by a simple band calculation [1]. This is attributed to the less polarization caused by poor packing of SAM on the SiO₂ substrate. In this study, the surface of SiO₂ is chemically treated for improvement of the structure of over-layer SAM, which is evaluated by XPS and the contact angle measurement. The SiO₂ / Si substrate was treated by a piranha solution to make more hydrophilic surface by introduce of the hydroxyl functional groups. SAM fabrication was performed by dipping substrates into the solution of SAM molecule ($\text{CF}_3(\text{CF}_2)_5(\text{CH}_2)_2\text{Si}(\text{OCH}_3)_3$) with hexane solvent. XPS measurement was carried out by using Al K α excitation beam. Fig. 1 shows XPS C1s spectra for SAM on SiO₂ substrate with / without hydrophilic treatment. SAM without hydrophilic treatment exhibits the peak for C-O in addition to the large contribution of the peak for C-C, indicating the presence of the large amount of SAM molecules without any chemical bonding to the substrate. On the other hand, the peaks for C-C and C-O significantly reduced in the hydrophilic substrate, suggesting the well formation of the silane-coupling between the SAM molecules and hydroxyl functional groups on the substrate. The contact angle measurement also supports the well hydrophilic nature of the substrate treated by piranha solution.

[1] Y. Yokota, K. Takai, and T. Enoki, *Nano. Lett.* **11**, 3669-3675 (2011)

[2] K. Yokota, K. Takai, Y. Kudo, Y. Sato and T. Enoki, *Phys. Chem. Chem. Phys.* **16**, 4313-4319 (2014)

Corresponding Author: Kazuyuki Takai,
Tel: +81-42-387-6138, Fax: +81-42-387-7002,
E-mail: takai@hosei.ac.jp

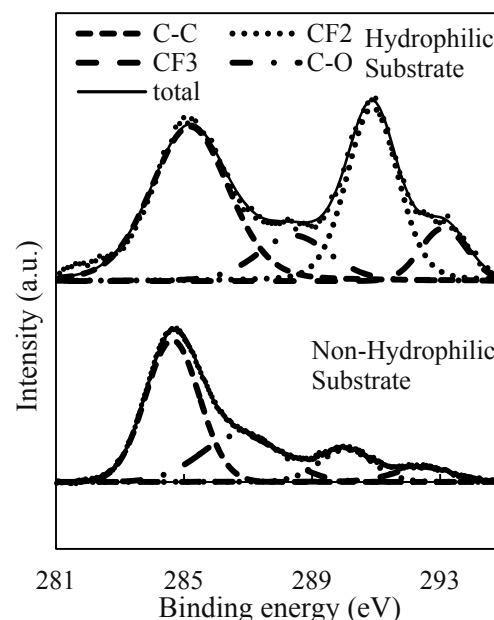


Fig. 1 XPS C1s spectra for SAM on SiO₂ substrate with / without hydrophilic treatment

Photoluminescence Properties of Van der Waals Hetero Structure

Composed of Monolayer Transition Metal Dichalcogenides

○Shinichiro Mouri¹, Daichi Kozawa¹, Goki Eda², Yuhei Miyauchi¹
and Kazunari Matsuda¹

¹*Institute of Advanced Energy, Kyoto University, Uji, Kyoto 611-0011, Japan*

²*Department of Physics, National University of Singapore, Singapore*

Monolayer transition metal dichalcogenides (1L-TMDs) have attracted much attention as a novel two-dimensional semiconductor, and also are promising candidate for the future optoelectric devices [1,2]. Van der Waals hetero-structures composed of 1L-TMDs can be suitable platform to realize functional semiconductor devices such as high performance solar cell [3]. In this study, we studied photoluminescence (PL) properties of Van der Waals hetero-structures building from three 1L-TMDs.

Bold black line in Fig.1 shows the PL spectrum of 1L-WSe₂/1L-MoSe₂/1L-MoS₂ hetero-structure. Gray lines in Fig. 1 show the PL spectra of 1L-WSe₂ (Peak X: 1.66 eV), 1L-MoS₂ (Peak Y: 1.83 eV) and 1L-MoSe₂ (Peak Z: 1.56 eV). In the PL spectrum of the hetero-structure, these peaks were quenched and new PL peak (Peak W: 1.58 eV) was appeared. In the Van der Waals hetero-structures building from two 1L-TMDs (1L-WSe₂/1L-MoS₂), the photo-generated carriers are spatially separated and formed interlayer excitons [4,5]. The PL peak energy of 1L-WSe₂/1L-MoSe₂/1L-MoS₂ hetero-structure is almost same as that of interlayer excitons in 1L-WSe₂/1L-MoS₂ hetero-structure (1.5 eV ~ 1.65 eV [4,5]). This result suggests that photo-generated carriers in 1L-WSe₂/1L-MoSe₂/1L-MoS₂ hetero-structure might be separated spatially as shown in the inset of Fig. 1 and form interlayer excitons. The detailed PL properties including valley polarization effects and many-body effects will be discussed in the presentation.

[1] K. F. Mak *et al. Phys. Rev. Lett.* **105**, 136805 (2012).

[2] S. Mouri *et al. Nano Lett.* **14**, 5944 (2013).

[3] A. K. Geim *et al. Nature* **499**, 419 (2013).

[4] H. Fang *et al. PNAS* **111**, 6198 (2014).

[5] M. H. Chiu *et al. ACS Nano* **8**, 9649 (2014).

Corresponding Author: S. Mouri

Tel: +81-774-38-3463,

Fax: +81-774-38-4567,

E-mail: iguchan@iae.kyoto-u.ac.jp

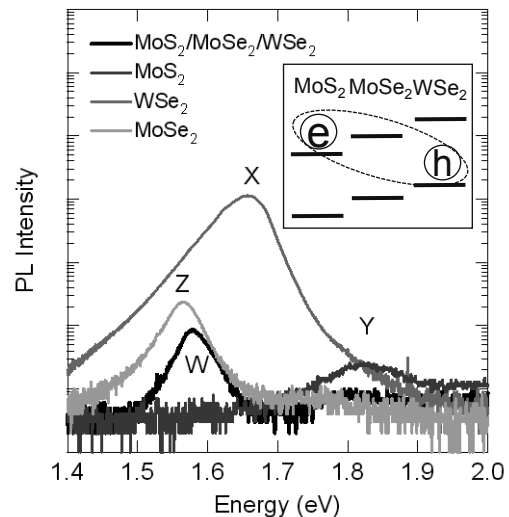


Figure 1 PL spectra of 1L-MoS₂, 1L-MoSe₂, 1L-WSe₂ and their Van der Waals hetero-structure.

Crossover between Localization and Delocalization in Edge-Disordered Graphene Nanoribbons

○Kengo Takashima¹ and Takahiro Yamamoto^{1,2}

¹ *Department of Electrical Engineering, Tokyo University of Science, Tokyo 162-8601, Japan*

² *Department of Liberal Arts, Tokyo University of Science, Tokyo 162-8601, Japan*

Graphene is expected to be a channel material of field effect transistors (FETs) because of its high carrier mobility. However no band gap of the graphene is a serious problem for its FET application. One possible way to overcome the gap-opening problem is to process it in the form of a nanometer width ribbon, referred as graphene nanoribbons (GNRs). They have been successfully applied to FETs with high on-off ratio. A recent experiment reported that the resistance of GNRs increases exponentially with their length even at the room temperature [1]. This non-Ohmic behavior is due to the edge vacancy of GNRs. The effects of edge vacancy become more remarkable when the ribbon width becomes narrower in the future. However the electronic transport properties of such narrow GNRs have not been clarified yet.

In this study, we have investigated the coherent electronic transport in edge-disordered armchair GNRs (ED-AGNRs) using the nonequilibrium Green's function method combined with a tight-binding model. In our simulation model, the edge vacancy is modeled by adding or removing pairs of carbon atoms at the armchair-type edges. We calculated electrical conductances of various ED-AGNRs by changing the amount of edge vacancies from 4% to 50% and the ribbon-width from 0.74nm to 2.95nm. We confirmed that the electrical conductances G of ED-AGNRs decrease exponentially with their lengths L , *i.e.*, $G \propto \exp(-L/\xi)$, where ξ is the localization length [2]. Moreover, we numerically determined (i) the vacancy-concentration dependence of ξ and (ii) the ribbon-width dependence of ξ . In addition, we gave a physical interpretation of (i) and (ii) through theoretical analysis based on the perturbation theory. This result provides a guideline for developing GNR-based FETs.

References:

[1] G. Xu *et al.*, Nano Lett. **11**, 1082 (2011).

[2] K. Takashima and T. Yamamoto., Appl. Phys. Lett., **104**, 093105 (2014).

Corresponding Author: Takahiro Yamamoto

Tel: +81-3-5876-1486, Fax: +81-3-5876-1486,

E-mail: takahiro@rs.tus.ac.jp

G* band Raman spectra of single layer graphene revisited

○ S. Siregar¹, E.H. Hasdeo¹, A.R.T. Nugraha¹, H.-L. Liu², and R. Saito¹

Department of Physics, Tohoku University, Sendai 980-8578, Japan

Department of Physics, National Taiwan Normal University, Taipei 11677, Taiwan

Weak Raman band existing around 2400 cm^{-1} in graphene, called as the G* band, is studied theoretically for several laser excitation energies (E_L), from infrared to long-frequency visible light region, such as 355 nm, 532 nm, and 785 nm wavelengths. This study is especially stimulated by a recent observation of G* band in single layer graphene by Liu *et al.*, in which the peak position of G* band is found to be sensitive to the E_L [1]. An early attempt to explain the G* band by Shimada *et al* [2] assigned three possibilities for the G* band based on the double resonance Raman process: (1) $q = 0$, LO overtone phonon mode, (2) $q = 0$ LO and iTA combination phonon mode, and (3) $q = 2k$, iTO and LA combination phonon mode, where q is the phonon wavevector and k is the electron measured from the K point.

However, by calculating the Raman intensity directly in this work, we propose that the G* band might corresponds to the $q = 2k$, iTO and LA combination (iTOLA) phonon mode [3]. The combination phonon mode means that the excited electron emits the phonon twice, firstly by emitting an iTO phonon and secondly by emitting an LA phonon, as can be seen in Fig. 1. In the calculation of the Raman spectra, we use the phonon dispersion obtained from the force constant model considering up to twentieth nearest neighbor [4] and the electron-photon together with electron-phonon matrix elements obtained within the extended tight binding model [5]. Our calculated Raman spectra of the G* band for the different laser excitation energies are in good agreement with the experimental results by Liu *et al.* when we consider the $q = 2k$ iTOLA phonon mode and thus ruling out the other possible assignments. This might be because of the much stronger electron-phonon interaction for the iTOLA compared to the other modes. It is expected that the G* band of single layer graphene could also be a unique signature of the single layer graphene and thus enrich the possibility to characterize different graphene-related materials.

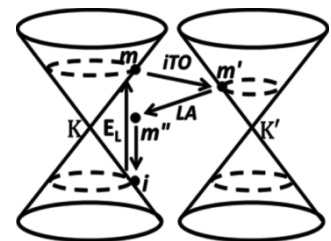


Figure 1: G* band schematic double-resonance process

[1] H.-L. Liu, S. Siregar *et al.*, Carbon **81**, 807-813 (2015).

[2] T. Shimada *et al.*, Carbon **43**, 1049-1054 (2005).

[3] R. Saito *et al.*, Solid State Communications **175-176**, 18-34 (2013)

[4] R. Saito *et al.*, J. Phys.:Condens. Matter **22**, 334203 (2010).

[5] K. Sato *et al.*, Chem. Phys. Lett. **427**, 117 (2006).

Corresponding Author: Syahril Siregar

TEL: +81-22-795-5719, FAX: +81-22-795-6447

E-mail: siregar@flex.phys.tohoku.ac.jp

Geometric and Electronic Structures of Corannulene Polymers

○Kohei Narita and Susumu Okada

*Graduate School of Pure and Applied Sciences, University of Tsukuba
1-1-1 Tennodai, Tsukuba, Ibaraki 305-8571, Japan*

Graphene nanoribbons (GNR) has unique electronic properties depending on their edge shape and width. It has been pointed out that the GNRs with armchair edges are metals or semiconductors because of the discretization condition imposed on the two-dimensional hexagonal Brilluin zone of graphene where the conduction and valence bands touch each other with linear dispersion at K point. In this work, we focus on one-dimensional sp^2 networks with curvatures, since the curvature in sp^2 networks occasionally induces the peculiar electronic structure near the Fermi level. We study the geometric and electronic structures of one-dimensionally polymerized corannulene which possesses the corrugated structure arising from the dish-like shape of the constituent molecule based on the density functional theory with local density approximation.

We investigate two possible chain structures of polymerized corannulene molecules, a 55-polymer and a 46-polymer: Corannulene is connected with its adjacent ones by forming five-membered rings (the 55-polymer) while it is connected via four- and six-membered rings (46-polymer) (Fig. 1). The total energy of the 46-polymer is found to be higher by 867 meV than that of the 55-polymer because of the four-membered ring possessing large strain around the atoms connecting the molecules. Electronic structures of these polymers are semiconductor with direct energy gaps of 0.97 and 0.51 eV for 55- and 46-polymers, respectively, with the relatively small dispersion bands near the fundamental gap (Fig. 2). Detailed analysis on the energetics of the dimerized corannulene molecules unravels the relative stability of the corannulene polymers.

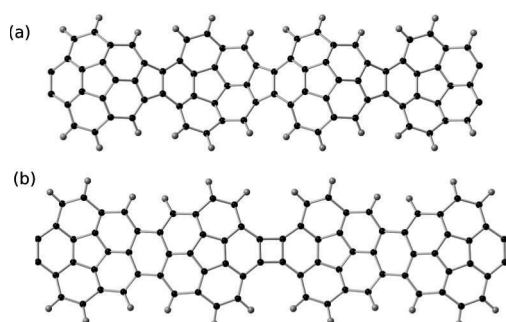


Fig. 1 Geometric structures of (a) the 55-polymer and (b) 46-polymer.

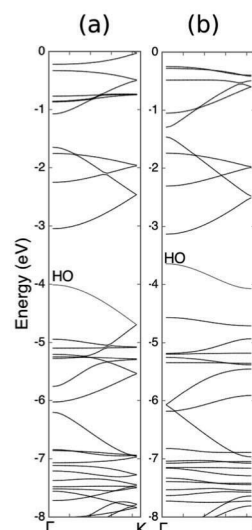


Fig. 2 Electronic structures of (a) 55-polymer and (b) 46-polymer. HO denote the HOMO band.

Corresponding Author: K. Narita
Tel: +81-29-853-5921, Fax: +81-29-853-5924,
E-mail: sokada@comas.frsc.tsukuba.ac.jp

Electron-wave dephasing suppressed by spin–orbit interaction in slightly hydrogenated graphene within a topological insulating regime

J. Kamijyo, °Y. Katagiri, T. Kato, T. Nakamura¹, S. Katsumoto¹, M. Ezawa², B. Ozyilmaz³,
J. Haruyama

*Faculty of Science and Engineering, Aoyama Gakuin University, 5-10-1 Fuchinobe,
Sagamihara, Kanagawa252-5258, Japan*

¹*Institute for Solid State Physics, The University of Tokyo, 5-1-5 Kashiwanoha, Kashiwa,
Chiba277-8581, Japan*

²*Department of Applied Physics, The University of Tokyo, Tokyo 113-8656, Japan*

³*Graphene Research Center, National University of Singapore, Singapore 119077*

The small mass of carbon atoms has prevented the experimental introduction of intrinsic spin–orbit interaction (SOI) into graphene, which produces various interesting phenomena such as topological insulating states and the spin Hall effect (SHE) [1]. However, it was recently reported that the controlled addition of small amounts of covalently bonded hydrogen atoms (e.g., $N_H < 0.1\%$) can introduce a colossal enhancement of the SOI as a result of out-of-plane symmetry breaking (i.e., Rashba-type SOI) [2].

Oh the other hand, phase interference of electron spin waves in two-dimensional (2D) materials is one of the attractive quantum effects within a diffusive carrier transport regime, and is highly valuable for spintronics. In conventional 2D materials, SOI causes spin flipping and transforms weak localization (WL; a constructive phase interference) to anti-localization (AL; a destructive phase interference) through a π phase shift^{9,10}. Phenomena arising from phase interference have also been reported in SOI-absent graphene containing a large amount of adatoms (foreign atoms or defects) and ripples in the substrate [3]. For instance, a large magnitude of WL has been reported.

However, none has experimentally revealed how SOI affects phase interference in graphene except for few theories [4], because the realization of the coexistence of SOI with phase interference in graphene is difficult. Precise control and optimization of a small amount of N_H is crucial to produce the crossover N_H regime between the SOI and phase interference regimes.

Here, we report that Rashba-type SOI, which was introduced by precise slight-hydrogenation ($N_H < 0.1\%$) of graphene using specified EB resist (i.e., HSQ resist) and EB irradiation, can strongly suppress dephasing in interference phenomena (e.g., causing no spin flipping and no transformation of WL to AL) in graphene with out-of-plane symmetrical SOI, in contradiction to that in other 2D materials [5]. This implies that the SOI-suppressed dephasing in topological insulating graphene are highly useful for future spintronic devices because spin coherence can be maintained much more effectively, despite the presence of SOI and one can control spin through the SOI by applying electric fields. This opens the door to novel carbon spintronics manifested by spin interference with SOI as a topological insulator.

[1] S. Murakami, N. Nagaosa, and S. C. Zhang *Science* **301**, 1348 (2003).

[2] A. H. Castro Neto, B. Özyilmaz et al., *Nature Physics* **9**, 284 (2013).

[3] M. B. Lundeberg, R. Yang, J. Renard, and J. A. Folk, *Phys. Rev. Lett.* **110**, 156601 (2013)

[4] E. McCann and V. I. Fal'ko, *Phys. Rev. Lett.* **108**, 166606 (2012).

[5] J. Kamijyo, T. Nakamura, J. Haruyama et al., *Science In-depth-review*(<http://www.ee.aoyama.ac.jp/haru-lab/>)

Corresponding Author: J. Haruyama

Tel: +81-42-759-6256, E-mail: J-haru@ee.aoyama.ac.jp

Anomalous electronic properties of mono(few)-atomic layers of black phosphorous

Y. Katagiri, T. Makino, °C. Ohata, T. Nakamura¹, S. Katsumoto¹, M. Ezawa², H. Shinohara³,
J. Haruyama ,

*Faculty of Science and Engineering, Aoyama Gakuin University, 5-10-1 Fuchinobe,
Sagamihara, Kanagawa252-5258, Japan*

¹*Institute for Solid State Physics, The University of Tokyo, 5-1-5 Kashiwanoha, Kashiwa,
Chiba277-8581, Japan*

²*Department of Applied Physics, The University of Tokyo, Tokyo 113-8656, Japan*

³*Department of Chemistry, Nagoya University, Nagoya, 464-8602, Japan*

Physics and applications of two-dimensional atomic layers of various materials are attracting significant attention (e.g., graphene, h-BN, MoS₂, WSe₂). Among those, mono-atomic layer and few layers of black phosphorus are highly important and interesting from the following theoretical reasons [1-4]; e.g., (1) They provide energy band gaps (i.e., E_g of 0.4 ~ 1 eV) existing at the position between E_g of graphene and chalcogenide compounds (e.g., MoS₂), depending on layer number. (2) They also have an in-plane anisotropic atomic and physical structure. Individual layers are buckled, with two in-plane, mutually perpendicular directions having armchair and zigzag edges. For example, it leads to the anisotropic electron effective mass, which is several times lighter in the armchair direction than in the zigzag direction. Thus, it is crucial to reveal such physical properties, experimentally.

Here, we report on observation of various unique electronic behaviors of mono(few)-layers of black phosphorus. The samples were fabricated by mechanical exfoliation of bulk black phosphorous and the thickness was confirmed by optical micro scope, Raman spectroscopy, and AFM observation. Anomalous quantum Hall effect linearly depending on $B^{2/3}$, hole doping by oxidation, and PN junction spontaneously formed by partial oxidation etc. will be shown. Details will be presented at poster.

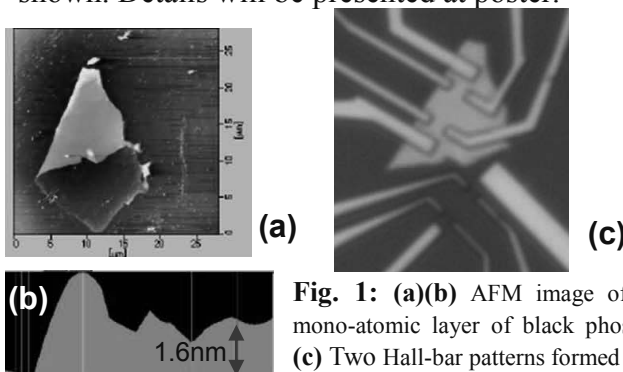


Fig. 1: (a)(b) AFM image of folded mono-atomic layer of black phosphorus. (c) Two Hall-bar patterns formed on (a).

- [1] L. Li et al., *Nature Nanotech.* **9**, 372 (2014)
- [2] P.-J. Herrero et al., *Nature Nanotech.* **9**, 330 (2014)
- [3] S. Kenig, A Neto et al., *Appl. Phys. Lett.* **104**, 103106 (2014)
- [4] A. -C. Gomez et al., *2D Materials* **1**, 25001 (2014)

Corresponding Author: J. Haruyama

Tel: +81-42-759-6256, E-mail: J-haru@ee.aoyama.ac.jp

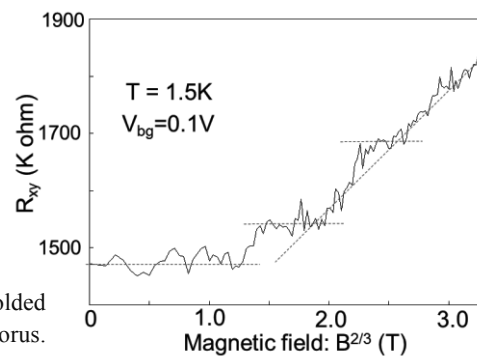


Fig. 2: R_{xy} as a function of perpendicular magnetic field $B^{2/3}$ in Hall effect measurement of few-layer black phosphorus. Three plateaus are observed as shown by three horizontal dotted lines. The trend of R_{xy} back ground exhibits a linear relationship on $B^{2/3}$. This originates from in-plane anisotropic electronic structures (i.e., Dirac and conventional Fermion) unique to atomic-layered black phosphorous.

Magnetism arising from edges of nanomesh of mono(few)-atomic layered black phosphorous

○Y. Nakanishi, C. Ohata, R. Iwaki, k. Nomura¹, M. Ezawa¹, H. Shinohara², J. Haruyama

Faculty of Science and Engineering, Aoyama Gakuin University, 5-10-1 Fuchinobe, Sagami-hara, Kanagawa 252-5258, Japan

¹*Department of Applied Physics, The University of Tokyo, Tokyo 113-8656, Japan*

²*Department of Chemistry, Nagoya University, Nagoya, 464-8602, Japan*

Physics and applications of mono(few) atomic layers of various materials are attracting large attention (e.g., graphene, h-BN, MoS₂, WSe₂). Among those, mono(few)-atomic layer of black phosphorus (BP) are highly important and interesting because (1) they provide energy band gaps (i.e., E_g of 0.4 ~ 1 eV) existing at the position between E_g of graphene and chalcogenide compounds (e.g., MoS₂) and (2) they also have an in-plane anisotropic atomic structure, resulting in anisotropic physical behaviors [1, 2]. With respect to magnetism driven from edge states [4, 5], the latter is very important.

In the case of graphene, flat band ferromagnetism arising from edge state of zigzag atomic-structure edges were theoretically well known and we experimentally observed it in hydrogenated graphene nanomesh, which has honeycomb like array of hexagonal nanopores with zigzag pore edges [3]. In mono-atomic layers of BP, individual layers are buckled, with two in-plane, mutually perpendicular directions having armchair and zigzag edges. Thus, this induces possibility of formation of zigzag pore edges when one forms the abovementioned nanomesh consisting of hexagonal nanopores on the BP.

Following the method employed to graphene nanomesh [3], we formed similar nanomesh on few-layer BP, which was fabricated by mechanical exfoliation of bulk BP. As shown in Fig. 1, indeed, we can observe ferromagnetism approximately 10 – 100 times greater ($\sim 10^{-4}$ emu/100 μm^2) than those in graphene nanomesh, in the BP nanomesh. Various dependence (e.g., on temperature, strong oxidation, hydrogen termination, degradation) will be presented at poster.

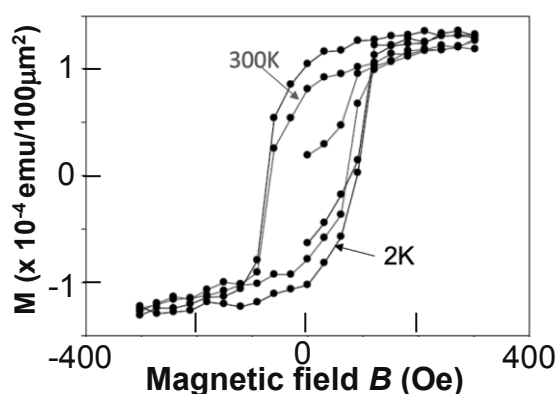


Fig. 1: Magnetization curve of oxidized nanomesh formed on few-layer black phosphorus for different temperatures. The magnetization values are ~ 100 times greater than those in hydrogenated graphene nanomesh. This is attributed to in-plane anisotropic edge atomic structure unique to few-layered BP.

[1] L. Li et al., *Nature Nanotech.* **9**, 372 (2014)

[2] P.-J. Herrero et al., *Nature Nanotech.* **9**, 330 (2014)

[3] J. Haruyama et al., *Appl. Phys. Lett.* **104**, 252410 and **105**, 183111 (2014)

[4] X. Peng et al., *Appl. Phys. Lett.* **116**, 144301 (2014)

[5] Z. Zhu et al., *Appl. Phys. Lett.* **105**, 113105 (2014)

Corresponding Author: J. Haruyama

Tel: +81-42-759-6256, E-mail: J-haru@ee.aoyama.ac.jp

Electronic properties of thin films of all-metallic carbon nanotubes with ionic gel-gate

T. Honma, R. Kikuchi, S. Yamada, C. Ohata, M. Koyata, J. Haruyama, A. Rao¹

Faculty of Science and Engineering, Aoyama Gakuin University, 5-10-1 Fuchinobe, Sagami-hara, Kanagawa252-5258, Japan

¹Nanomaterials Center, Clemson University, 81 Technology Drive, Suite 200 Anderson, SC 29625, USA

High-transition temperature (T_c) superconductivity (SC) of carbon nanotubes (CNTs) is eagerly expected for next breakthrough for physics and applications of CNTs [1]. Although previously some groups reported on it, the T_c was below 12K with poor reproducibility. Our group also reported on SC with $T_c = 12K$ in the following two-different type CNTs; (1) Array of entirely end-bonded multi-walled CNTs [2] and (2) Thin films consisting of slightly boron-doped single-walled CNTs (SWNTs) [3]. The former was attributed to elimination of Tomonaga-Luttinger liquid, while the latter originated from alignment of Fermi level to van Hove singularity. However, they had problems similar to others. Thus, other method should be employed to realize high- T_c and highly reproducible SC in CNTs.

Recently, SC realized by using ionic liquid(gel) gate is attracting considerable attention. Bias voltages applied to the gate collects extremely high two-dimensional electronic density of states on the sample surface by field effect, resulting in appearance of SC in various materials. In the present experiment, we formed $LiClO_4$ and $KClO_4$ as ionic gel on thin film consisting of SWNTs with only metallic behaviors (Fig. 1) and explored SC by changing gel and SWNT-film conditions.

Figure 2(a) shows typical relationships of drain current (I_d) vs. $LiClO_4$ -ionic-gel gate voltage (V_{ig}) and two drain voltages (V_d) of Fig.1-sample. Leakage current (i.e., at $V_d = 0$) is reduced, while I_d shows no significant increase on V_{ig} increase. Figure 2(b) shows two-probe measurement result of resistance as a function of temperature. Resistance drop due to SC cannot be confirmed. To date, SC has not been observed in this type samples.

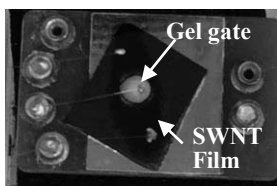


Fig. 1: Top-view photomicroscope image of an ionic-gel gate FET consisting of $LiClO_4$ gel gate on a metallic SWNT thin film.

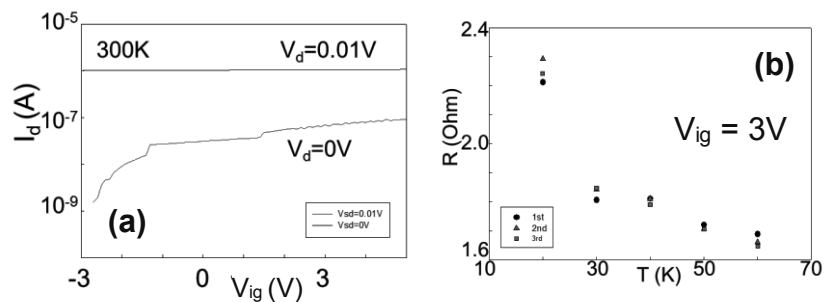


Fig. 2: (a) I_d as a function of V_{ig} and V_d of Fig. 1-sample. (b) Resistance as a function of temperature at $V_{ig} = 3V$ in (a). Measurement was carried out three times at each temperature.

[1] J. Haruyama, Book of Carbon-based Superconductors: Towards High- T_c Superconductivity, ISBN 9814303305 (Pan Stanford Publishing 2014)

[2] I. Takesue, J. Haruyama et al., *Phys.Rev.Lett.* **96**, 057001 (2006)

[3] N. Murata, J. Haruyama et al., *Phys.Rev.Lett.* **101**, 027002 (2008)

Corresponding Author: J. Haruyama

Tel: +81-42-759-6256, E-mail: J-haru@ee.aoyama.ac.jp

Photo-reduction of graphene oxide for improvement of the purity of carbon nanopot

○Hiroyuki Yokoi^{1,2}, Kazuto Hatakeyama^{1,2}, Shogo Matsumoto³, Mako Ueda³,
Takaaki Taniguchi^{1,2}, Michio Koinuma^{1,2}, Yasumichi Matsumoto^{1,2}

¹ Graduate School of Science and Technology, Kumamoto University, Kumamoto 860-8555, Japan

² JST, CREST, K's Gobancho 6F, 7 Gobancho, Chiyoda-ku, Tokyo, 102-0076, Japan

³ Faculty of Engineering, Kumamoto University, Kumamoto 860-8555, Japan

In the previous symposium, we reported on the creation of novel nanocarbon named ‘carbon nanopot’[1]. Carbon nanopot is a pot-like shaped material composed with multi-layered graphene sheets and is produced in series to form fibers (nanopot fibers). Its typical size is 20-40 in diameter and 100-200 nm in length. The length-to-diameter ratio of carbon nanopot is much larger than that of conventional nanoball, which suggests higher potential of carbon nanopot for the application to drug delivery vehicles[2]. In addition, carbon nanopot consists of fanwise hollow pourer, multi-walled-nanotube like hollow neck, tapering hollow belly, and thick multi-walled dead-end bottom. This complex structure could allow one to classify carbon nanopot into higher-ordered nanomaterial.

In the formation of the complex structure, the wettability between catalyst metal and graphene oxide (GO) utilized as catalyst support could be one of the key factors. In order to clarify the contribution of the wettability of GO, we have investigated the effect of photo-reduction of GO on the production of carbon nanopot. We have aimed at modifying wettability of GO through controlling the oxidation degree of GO.

In the experiments, we used mixture of iron acetate and cobalt acetate as catalyst, and prepared aqueous suspension of GO following modified Hummers method. The metal acetates are mixed with the GO suspension to obtain GO supported catalyst. The catalyst was dropped and dried on silicon substrates. Some substrates were used as prepared in the synthesis and the others were photo-reduced in the atmosphere of oxygen for three hours. In the synthesis, the in-liquid chemical vapor deposition method was employed. 2-Propanol was used as the carbon source. The temperature and time of synthesis were 1100-1110 K and 10 minutes, respectively.

After the synthesis, deposited materials were investigated with FE-SEM. As shown in Fig. 1, some nanoball-type nanofibers were observed among nanopot fibers in the deposit for non-photoreduced catalysts, whereas almost all fibers were nanopot fibers for photoreduced ones. Though the above difference seems small, the tendency supports our hypothesis that the wettability between catalyst metal and GO is one of key factors to select productions from nanopot and nanoball.

[1] H. Yokoi et al., in Abstracts of the 47th FNTG General Symposium (Sept. 2014), p.96.

[2] Y. Zhao et al., ACS Nano, 6, 6912 (2012).

Corresponding Author: H. Yokoi

Tel: +81-96-342-3727, Fax: +81-96-342-3710,

E-mail: yokoihr@kumamoto-u.ac.jp

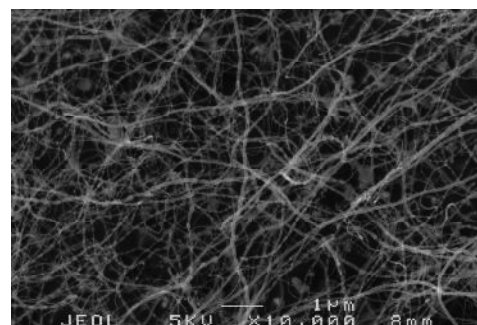


Fig.1: Carbon nanofibers deposited for non-photoreduced catalyst.

Structure and electronic properties of nanodiamond and its fluorination effect

○Kenta Kogane¹ · Hidekazu Touhara² · Yoshiyuki Hattori² · Kazuyuki Takai^{1,3,4}

¹Graduate School of Science and Engineering, Hosei University, Tokyo 184-8584, Japan

²Faculty of Textile Science and Technology, Shinshu University,
Nagano 386-8567, Japan

³Faculty of Bioscience and Applied Chemistry, Hosei University, Tokyo 184-8584, Japan

⁴Hosei University, Research Center for Micro-nano Technology, Tokyo 184-0003, Japan

Nanodiamond (ND) is featured with the large surface area as well as many excellent properties of bulk diamond, although it has a problem of aggregation [1]. Fluorination of ND is expected not only to stabilize the surface structure for disaggregation, but also to introduce functional groups on the surface, the conduction carriers, and so on [2]. In this study, we evaluate the structure and magnetic properties of ND and fluorinated nanodiamond (FND) in order to consider the change in the electronic state and the surface structure by fluorination by using X-ray diffractometer (; XRD, Mo K α), X-ray photoelectron spectroscopy (; XPS, Al K α), and electron spin resonance (; ESR, X-band).

FND was synthesized by the direct reaction between detonation nanodiamond and 1 atm of fluorine gas at the temperature of 623 K, 773 K and 873 K for 3 days. For the sample reacted at 873 K, re-fluorination at 873 K was carried out for 7 days after annealing under vacuum. Hereafter, each sample is labeled as FND623K, FND733K, and FND873K according to the maximum temperature during synthesis, while Non-fluorinated one is referred to as ND.

Sharp peaks observed in XRD for ND and FND623K was associated with the diamond lattice constant ($a = 3.567 \text{ \AA}$ [3]). Also, average crystalline sizes of both ND and FND623K are estimated from FWHM of their peaks by using the Scherrer equation as 3 ~ 4 nm. These suggest that fluorination modifies only the surface structure without affecting the crystal structure of the core of ND. The F1s peaks of XPS for FNDs does not appear at the position for physisorbed fluorine, and additional shoulder peak appears at the higher energy side of the C1s peak, suggesting the presence of the some chemical bonding between C and F in FND. ESR linewidth for FNDs indicates the increasing in the spin relaxation in comparison with ND (Fig. 1). However, the spin relaxation was enhanced also in ND heat-treated under the same condition as FND873K. Therefore, effects of fluorination of ND on the magnetism should be examined taking the influence of the structural relaxation by heat-treatment into consideration [4].

[1] Eiji Osawa, *Journal of the surface science society of japan*, **30**, 258-266 (2009).

[2] Hidekazu Touhara, Akiko Yonemoto, *Nanocarbon Handbook*, part3, chapter 4 (2007).

[3] S.V. Kidalov, *Diamond & Related Materials*, **19**, 976-980 (2010).

[4] J.W. Park, *Current Applied Physics*, **6**, 188-193 (2006).

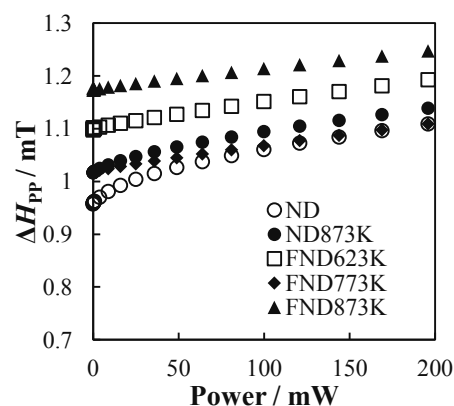


Fig. 1 Power dependence of ESR linewidth

Corresponding Author: Kazuyuki Takai

Tel: +81-42-387-6138, Fax: +81-42-387-7002, E-mail: takai@hosei.ac.jp

Spheroidization of microdiamond by self-ablation: preliminary results

○Ryoko Yamanoi and Eiji Ōsawa

NanoCarbon Research Institute, AREC, Faculty of Fiber Science and Technology, Shinshu University, Ueda, Nagano 386-8567, Japan

Natural diamonds show remarkably rich polymorphism¹, which can be adequately interpreted as the results of etching apexes and edges surface asperities like truncation and dual operations². Final products of such surface metamorphosis are novel spherical diamonds, and they are indeed found in nature on rare occasions³. Recently Moseler⁴ proposed atomistic mechanism of the metamorphosis in diamond by using MD simulation as amorphization by self-ablation among diamond followed by the formation of graphitic fragments under pressure, which will finally drop off to effect wear.

We attempt here to bring diamond spheroidization into reality by combining three essential feature of the Moseler mechanism into one set-up: rolling, self-ablation of diamond crystals, under pressure. We used commercial microdiamond as the starting material and modified electric Chinese ink-stick grinder to the self-ablation of microdiamond *under pressure and rolling* (SAUPR) (**Photo. 1**)

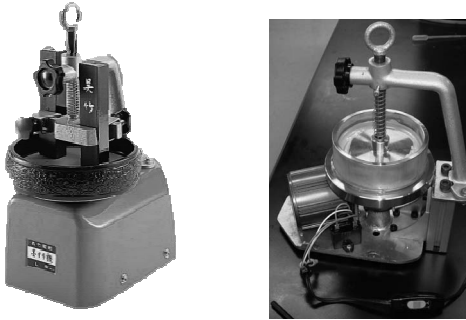


Photo 1. Left: original, Right: modified

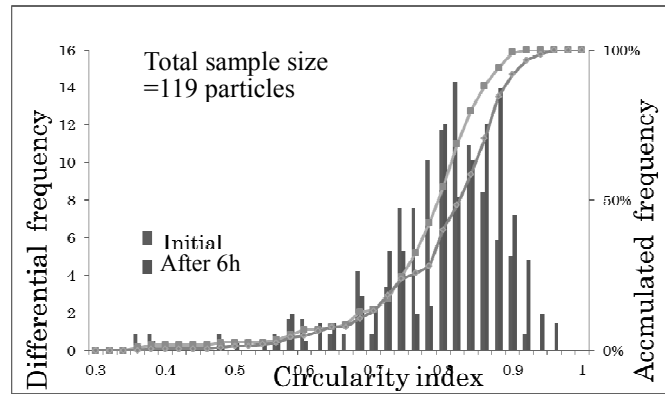


Fig. 1. Circularity distribution before and after treatments

Distribution of circularity among randomly selected 119 crystals increased (**Fig 1**), and that of diameter decreased. F-test on the both data-sets indicated equal variance. Subsequent t-test confirmed significant increase in circularity by 4% as well as significant decrease in diameter by 8.3% (**Tab 1**). We are now improving the SAUPR machine for more precise control of operation conditions. The surfaces in contact with microdiamond layers will be lined with CVD diamond films.

Tab. 1. Application of F- and t-test statistical methods

		<i>Circularity index (std dev), %</i>	<i>Heywood diameter (std dev), μm</i>
Initial		78(10)	29.15(5.65)
After 6 hours		82(9)	26.73(5.67)
t-test p<0.05 (both sides)	Variance	equal	equal
	t(freedom)	3.316(236)	3.286(236)
	p	0.001	0.001
	Judgement	Significant	Significant

[1] V. M. Goldschmidt, “*Atlas der Krystallformen*”, Band III, Diamant, Tafeln 27-48, Fig. 1-364, Carl Winters Universitätsbuchhandlung, Heidelberg, 1916. [2] E. Ōsawa, A. Barnard, manuscript in preparation. [3] E. A. Skalwold, *Gems & Gemology*, Summer issue, 128 (2012). [4] L. Pastewka et al. *Nature Mater.* 10, 34 (2011).

Corresponding Author: E. Ōsawa

Tel: +81-268-75-8381 Fax: +81-268-75-8551 E-mail: Osawa@nano-carbon.jp

The Topological Structure of Starfish Nanocarbon

○Natsuki Namba, Yukihiro Takada and Kyoko Nakada

*College of Science and Engineering, Aoyama Gakuin University,
5-10-1, Fuchinobe, Chuo-ku Sagamihara 252-5258, Japan*

We proposed new structures named “starfish nanocarbon” (SFNC, Fig.1) and analyzed the relationships between their structures and electronic states. The structures and electronic states of 12 SFNCs are determined by the configuration of four 7-membered rings per arm.

We now report two findings on the structure of SFNCs.

- (1) The following formula is attested by a topological consideration for all SFNCs with N arms:(Fig.2).
(the total number of 7-membered rings) = $N \times 6$.
- (2) Two or more different SFNCs are able to combine and make chimera.12 SFNCs are divided into 2 groups depending on whether the structure has 7-membered rings at the sites B (GroupB7) or not (GroupB6). Both groups have 6 different structures as whole SFNCs, and 4 different tube types as the arms. SFCNs in the same group are able to be combined and make chimera. We can decide freely configuration of tubes and the resultant chimera has many different types of structures. We show 3 examples (Fig.3). The number of kind of chimera1/2, chimera1/3, chimera1/6 is 60, 80, 240, respectively. SFNC is therefore a potential junction that connects different types of NTs.

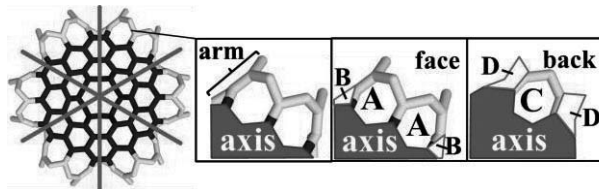


Fig. 1 : Name of the parts of SFNC.

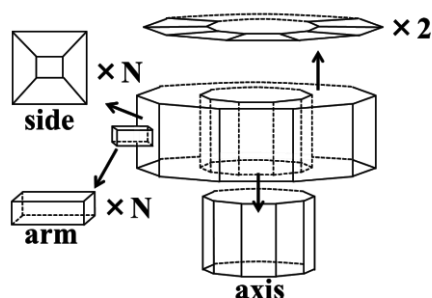


Fig. 2 : Topological structure of SFNC.

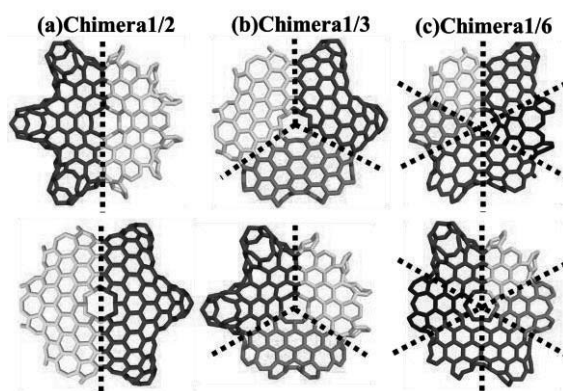


Fig. 3 : 3types of chimera.

Corresponding Author: K. Nakada

Tel: +81-42-759-6219 Fax: +81-42-759-6493 E-mail: nakada@chem.aoyama.ac.jp

Double resonance Raman modes in mono- and few-layer MoTe₂

Huaihong Guo¹, Teng Yang², Mahito Yamamoto³, Lin Zhou⁴, Ryo Ishikawa⁵, Keiji Ueno⁶, Kazuhito Tsukagoshi³, Zhidong Zhang², M. S. Dresselhaus⁴, and R. Saito¹

Department of Physics, Tohoku University, Sendai, Miyagi 980-8578, Japan,

Institute of Metal Research, CAS, Shenyang 110016, China

International Center for Materials Nanoarchitectonics (WPI-MANA), National Institute for Materials Science (NIMS), Tsukuba, Ibaraki 305-0044, Japan

Department of Electrical Engineering and Computer Science, Massachusetts Institute of Technology, Cambridge, Massachusetts 02139-4037, USA,

Department of Physics, Massachusetts Institute of Technology, Cambridge, Massachusetts 02139-4307, USA

Department of Functional Materials Science, Graduate School of Science and Engineering, Saitama University, Saitama 338-8570, Japan

Department of Chemistry, Graduate School of Science and Engineering, Saitama University, Saitama 338-8570, Japan

We study the second-order Raman process of mono- and few-layer MoTe₂, by combining ab initio density functional perturbation calculations with experimental Raman spectroscopy at 1.58 eV, 1.96 eV and 2.33 eV laser excitation energies. The calculated electronic band structure and the density of states show that the electron-photon resonance process occurs at the high-symmetry M point in the Brillouin zone, where a strong optical absorption occurs by a logarithmic Van-Hove singularity. Double resonance Raman scattering with inter-valley electron-phonon coupling connects two of the three inequivalent M points in the Brillouin zone, giving rise to second-order Raman peaks due to the M point phonons. The predicted frequencies of the second-order Raman peaks agree with the observed peak positions that cannot be assigned in terms of a first-order process. Our study attempts to supply a basic understanding of the second-order Raman process occurring in transition metal di-chalcogenides (TMDs) and may provide additional information both on the lattice dynamics and optical processes especially for TMDs with small energy band gaps such as MoTe₂ or at high laser excitation energy.

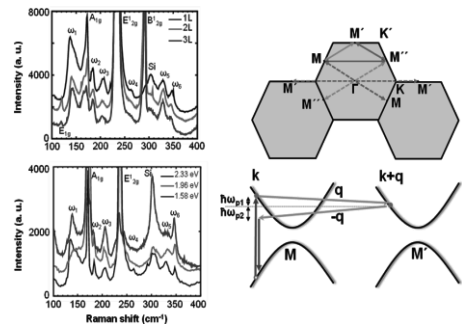


Fig.1 Raman spectrum of MoTe₂.

Corresponding Author: Huaihong Guo

Tel: +81-22-795-5717, Fax: +81-22-795-6447

E-mail: hhguo@flex.phys.tohoku.ac.jp

Improving the property of electric double layer capacitor by using activated carbon nanoballoon

○A. Mizutani¹, Y. Suda¹, H. Takikawa¹, H. Ue², K. Shimizu³, Y. Umeda⁴

¹ Department of Electrical and Electronic Information Engineering, Toyohashi University of Technology, Toyohashi, Aichi 441-8580, Japan

² Fuji Research Laboratory, Tokai Carbon Co., Ltd., Oyama, Sizuoka 410-1431, Japan

³ Development Department, Shonan Plastic Mfg. Co., Ltd., Hiratsuka, Kanagawa 254-0807, Japan

⁴ Toho Gas Co., Ltd., Nagoya, Aichi 456-8511, Japan

1. Introduction

Electric double layer capacitor (EDLC) is an energy device. When EDLC charges and discharges, ions in electrolyte respectively adsorb and desorb on the electrode surface. EDLC has advantages that provide higher charge/discharge rate capability and perform longer cycle life than rechargeable batteries, because chemical reaction such as redox reaction does not occur during the charge and discharge. In this study, the performance of the EDLC using carbon nanoballoon was evaluated.

2. Experimental

According to our previous research, carbon nanoballoon (CNB) was synthesized by heat treatment of arc black at 2600 °C in Ar gas [1]. The particle shape of CNB is hollow. CNB is graphitic and has high conductivity. In this study, we prepared CNB from carbon black. It is hereinafter referred to as CNB-CB. In addition, activated CNB-CB (ACNB-CB) was prepared through the potassium hydroxide (KOH) activation. We prepared the electrode of EDLC using ACNB-CB. The specific capacitance of EDLC was measured from the electrochemical measurement. The electrodes were compared to the activated carbon (AC) electrode.

3. Results

Fig. 1 shows the specific capacitance obtained from the galvanostatic charge/discharge curves. The AC electrode showed the highest specific capacitance at current densities between 0.1 and 0.5 A/g. But, the CNB electrodes showed higher specific capacitance than the AC electrode at a current density of 1.0 A/g and more. In addition, the CNB-CB electrode showed higher specific capacitance than the CNB electrode, and the ACNB-CB electrode showed highest specific capacitance. So the specific capacitance of EDLC was increased by ACNB-CB when using at a high charge/discharge rate.

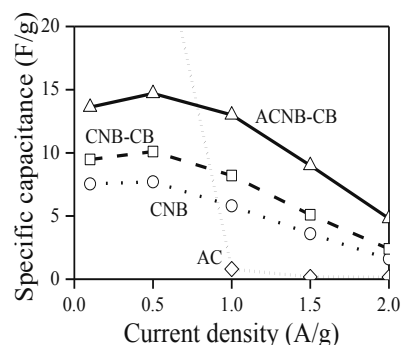


Fig.1. Specific capacitance of EDLCs at different current densities.

This work has been partly supported by the EIIRIS Project from Toyohashi University of Technology (TUT); JSPS KAKENHI Grant Number 24360108 and 25630110.

[1] Y. Okabe *et al.* *Electrochim. Acta.* **131**, 207 (2014).

Corresponding Author: A. Mizutani

Tel: +81-532-44-1228,

E-mail: mizutani.akitaka@pes.ee.tut.ac.jp

Spontaneous antiferromagnetism in the α -graphyne single layer

Teng Yang¹, Baojuan Dong¹, Huaihong Guo², R. Saito², and Zhidong Zhang¹

*Shenyang National Laboratory for Materials Science, Institute of Metal Research,
Chinese Academy of Sciences, Shenyang 110016, China*

Department of Physics, Tohoku University, Sendai, Miyagi 980-8578, Japan,

We study the electronic structure of α -graphyne based on Density functional calculations using hybrid functionals of GGA and Hartree Fock (so-called HSE). This new type of carbon structure can be derived from graphene by inserting one carbon pair between each two nearest carbon atoms in graphene. Interestingly, we found that a spontaneous antiferromagnetic (AFM) order forms in α -graphyne with magnetization of $0.1 \mu_B$ on each site, which is concurrent with a band gap of approximately 0.5 eV. A tensile biaxial strain tends to increase both band gap and magnetization, while the compressive strain has an opposite effect and even gives rise to a K-point Dirac cone once the band gap is closed. This spontaneous AFM ordering and non-zero band gap at zero strain can be understood based on the Hubbard model. The effective hopping parameter, which can be derived from a renormalization method, is found to be much smaller than that in graphene. Value of U/t (U : Coulomb interaction, t : hopping integral) in α -graphyne is therefore larger than the critical one required for the Mott-Hubbard transition, giving rise to a spontaneous AFM semiconductor of carbon planar structure.

Corresponding Author: Teng Yang

Tel: +86-24-23971136, +86-24-23891320 (FAX)

E-mail: yangteng@imr.ac.cn

Characteristic of spectral sensitivity for the composite film of Zn doped iron oxide nanotubes and organometal halide perovskite

○ Yuta Kosugi¹, Hiroyuki Kusuda¹, Ayano Saiki¹, Shunji Bandow²

*Department of Materials Science & Engineering¹ and of Applied Chemistry²,
Meijo University, Nagoya 468-8502, Japan*

The nanotube (NT) synthesis involves the polycondensation of iron nitric nonahydrate and zinc nitric hexahydrate in 1-propanol including surfactant of a Pluronic F-127 at 45°C. After 5 days reaction, a gel obtained is heated up to 120°C at a rate of 1°C/min in order to scroll up gel to form tubular structure. Detail of the nanotube preparation is in the reference [1]. Regarding the sample preparation, stoichiometric ratio of Zn/Fe is easily controllable by changing the amount of zinc nitrate hexahydrate (0~10 wt%). According to the analyses of TEM, XRD, XPS and optical absorption spectra, we find the nanotube (outer diameter of 4-10 nm and inner one of 2-6 nm, and the length of ~50 nm) is represented by $Zn_xFe_{3-x}O_4$ and the band gap is decreased upon low level Zn doping. Fig. 1 is the Zn/Fe atomic ratio dependence of the band gap evaluated by the Tauc plot method [2-4]. From this figure, we can see that non doped Fe_3O_4 NTs have a band gap of ~2.4 eV and the band gap indicates a minimum of ~2.0 eV for $Zn_{0.27}Fe_{2.73}O_4$ NTs. Hence, we selected this sample and non-doped one for the evaluation of spectral sensitivity.

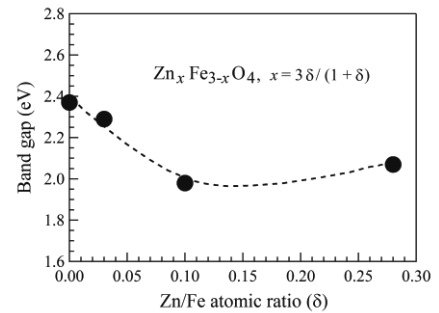


Fig. 1. Zn/Fe atomic ratio dependence of the band gap.

Cell for the spectral sensitivity measurement was assembled by coating the dense layer of iron oxide on FTO and then the NT sample was stacked as a porous layer. Next the organometal halide perovskite of $CH_3NH_3PbI_3$ was spin coated, and finally the Au electrode was vacuum deposited. Optical power monitored band pass filtered light from a Xe arc lamp was irradiated on the cell and the photo induced current was measured. Results are in Fig. 2. IPCE (incident photon to current conversion efficiency) of NT based samples have higher efficiency than that of NP (nanopowder) at long wavelength region. In addition Zn doped NTs have better IPCE than non-doped one at short wavelength region.

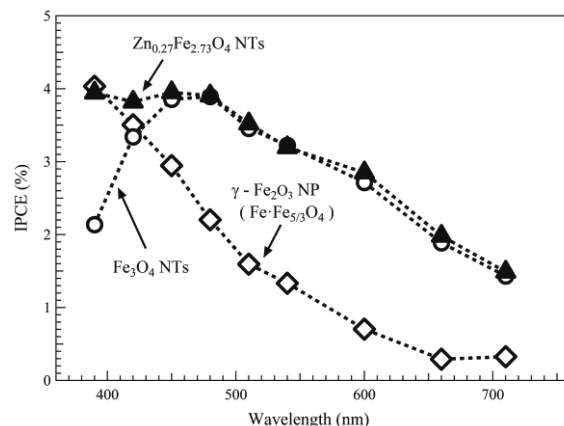


Fig. 2. IPCE of iron oxide based NTs and nanopowder (NP, $d < \sim 50$ nm).

[1] Y. Kosugi, S. Bandow, J. Inorg. Organomet. Polym. **24**, 933 (2014). [2] K. Wongsaprom et al., Appl. Phys. A **114**, 373 (2014). [3] S.S. Kumar *et al.*, Inter. Nano Lett. **3**, 30 (2013). [4] V. Džimbeg-Malčić *et al.*, Technical Gazette **18**, 117 (2011).

Corresponding Author: S. Bandow, Tel: +81-52-838-2404, E-mail: bandow@meijo-u.ac.jp

Isolation and Characterization for Each Isomer of (5,6)- and (6,6)-[Li⁺@C₆₁Ph₂]NTf₂⁻

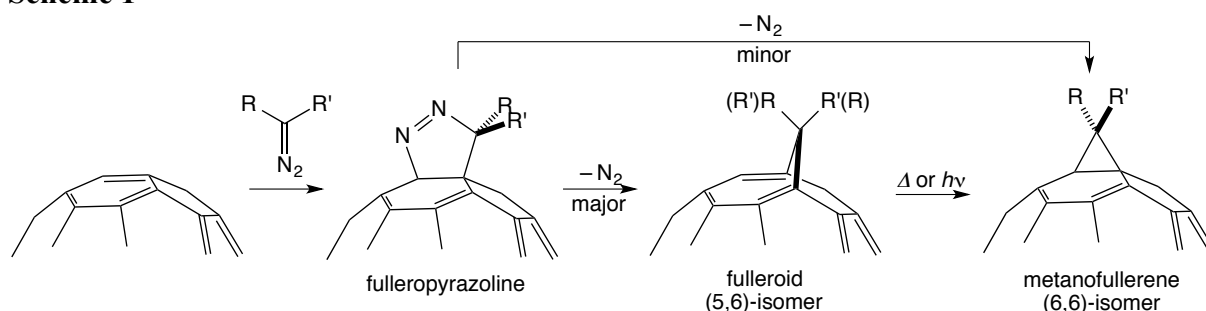
○Hiroshi Okada,¹ Hiroki Kawakami,¹ Shinobu Aoyagi,² Yutaka Matsuo¹

¹*Department of Chemistry, School of Science, The University of Tokyo,
Tokyo, 113-0033, Japan*

²*Department of Information and Biological Sciences, Nagoya City University,
Nagoya 467-8501, Japan*

The reaction of fullerene and diazoalkane is representative methodology for synthesizing various methanofullerene derivatives.[1] 1,3-Dipole cycloaddition on (6,6)-bond of C₆₀, followed by elimination of nitrogen molecule, affords fulleroid as a major product, which is thermally or photochemically converted to methanofullerene (Scheme 1). In the reaction obtaining fulleroid, methanofullerene is also generated as a minor product.

Scheme 1



Recently, we reported synthesis of lithium-ion-encapsulated diphenylmethanofullerene, [Li⁺@C₆₁Ph₂]NTf₂⁻, by the reaction of [Li⁺@C₆₀]NTf₂⁻ and dipenyldiazomethane.[2] In the previous report, we obtained a mixture of (5,6)-fulleroid and (6,6)-methanofullerene isomers, and isolated pure (6,6)-isomer by thermolysis of this mixture.

Herein, we report the isolation of (5,6)-isomer. Separation from the mixture was performed with HPLC using ion-exchange column (Inertsil CX, GLscience). Analytical HPLC and ⁷Li NMR confirmed absence of (6,6)-isomer. We will also present properties of both isomers as well as structural analysis. The crystal structure of (6,6)-isomer revealed by SR-XRD single crystal structure analysis at SPring-8 is shown in Figure 1. The Ph₂C= moiety bounded on (6,6)-bond with inside Li⁺ was clearly shown with this study

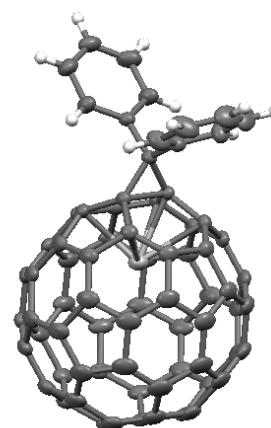


Figure 1. Crystal structure of (6,6)-[Li⁺@C₆₁Ph₂]NTf₂⁻(ODCB). Counter anion and crystal solvent are omitted for clarity.

[1] M. Yamada *et al.*, *Chem. Rev.* **2013**, 113, 7209–7264.

[2] H. Okada *et al.* 47th Fullerene Nanotubes-Graphene General Symposium, 3P-35.

Corresponding Author: H. Okada and Y. Matsuo

Tel: +81-3-5841-1476, Fax: +81-3-5841-1476

E-mail: h_okada@chem.s.u-tokyo.ac.jp; matsuo@chem.s.u-tokyo.ac.jp

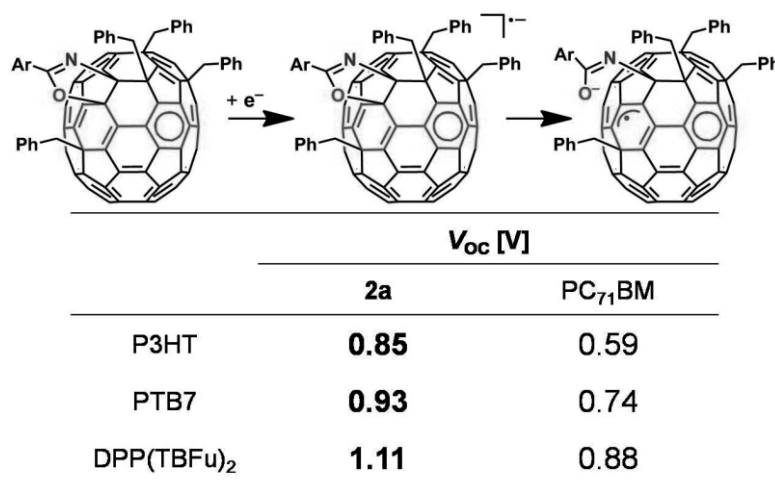
Approach to High Open-circuit Voltage in Organic Solar Cells Utilizing Structural Change of Oxazolino-C₇₀ Derivative

○Yutaka Matsuo¹, Shu-Hui Li,² Zong-Jun Li,² Takafumi Nakagawa,¹ James W. Ryan,¹ and Xiang Gao²

¹ Department of Chemistry, School of Science, The University of Tokyo, 7-3-1 Hongo, Bunkyo-ku, Tokyo 113-0033, Japan

² State Key Laboratory of Electroanalytical Chemistry, Changchun Institute of Applied Chemistry, University of Chinese Academy of Sciences, Chinese Academy of Sciences, 5625 Renmin Street Changchun, Jilin 130022, China

Reaction of 2,5-Bn₂C₇₀ (Bn = CH₂Ph) with hydroxide and ArCN (Ar = Ph, *m*-ClPh) followed by reaction with I₂ and BnBr afforded dibenzylated (**1a,b**) and tetrabenzylated oxazolino[70]fullerenes (**2a,b**), respectively. The latter has a novel structural configuration, where the addends are positioned from the polar to the transequatorial region. A key structural feature of this compound was the oxygen atom of the oxazoline ring is bound to the equatorial belt region of C₇₀, giving structural change in its reduced state. This enables stabilization of the reduced state, suppresses charge recombination dynamics in organic solar cells to give high open-circuit voltage (0.85, 0.93, and 1.11 V in devices using P3HT, PTB7, and DPP(TBFu)₂, respectively).



[1] S.-H. Li, Z.-J. Li, T. Nakagawa, J. W. Ryan, Y. Matsuo, X. Gao, *Chem. Eur. J.*, in press. [DOI: 10.1002/chem.201405890]

Corresponding Author: Y. Matsuo and X. Gao

Tel: +81-3-5841-1476, Fax: +81-3-5841-1476

E-mail: matsuo@chem.s.u-tokyo.ac.jp

Effects of water molecules on the proton dynamics in fullereneol solids investigated by solid-state ^1H NMR

○Yoshiaki Sano¹ and Hironori Ogata^{1,2}

¹Graduate School of Engineering, Hosei University, Koganei, Tokyo 184-8584, Japan

²Research Center for Micro-Nano Technology, Hosei University, Koganei, Tokyo, 184-0003, Japan

Fullerenols (Polyhydroxylated Fullerenes : $\text{C}_{60}(\text{OH})_x$) have structures with addition of hydroxyl groups on fullerene (C_{60}) cage and their solids possess 3-dimensional hydrogen-bonding networks. It has been thought to have potential applications in proton conductive materials. It has been reported that $\text{C}_{60}(\text{OH})_{12}$ solids have proton conductivity in a dry atmosphere and that On the other hands, $\text{C}_{60}(\text{OH})_{24}$ solids did not show ionic conductivity at all^[1]. However, detailed proton conduction mechanism of fullereneol solids have not been fully elucidated. We previously reported proton dynamics in fullereneols solids by solid-state ^1H NMR^[2-3]. In this study, we investigated effects of water molecules on their proton dynamics in fullereneol solids by using ^1H -NMR spectroscopy. We synthesized the methods reported by Chiang et al.[4] and prepared two types of $\text{C}_{60}(\text{OH})_{12}$ samples: one was dried in air after synthesis(dried sample), the other was dried using a vacuum pump after dehydration with acetonitrile(thoroughly dried sample).Figure 1(a) and (b) shows the NMR spectrum of the dried and thoroughly dried $\text{C}_{60}(\text{OH})_{12}$ solids at room temperature, respectively. Detailed results on the relationship between the composition of fullereneol-based composites and the properties of proton motions will be presented.

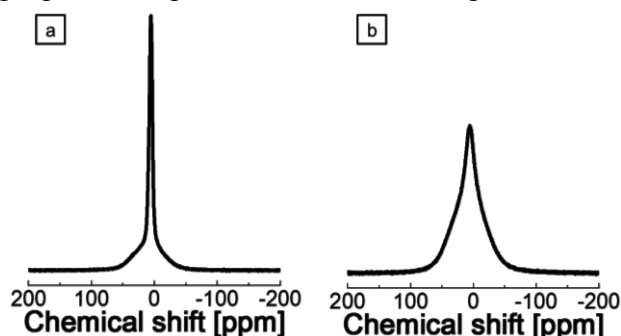


Figure 1 ^1H NMR spectra (a) as *synthesis* (b) *dry* fullereneol solids (r.t.)

References:

- [1] K. Hinokuma *et al.*, *Chem. Phys. Lett.*, 341, 442 (2001)
- [2] K. Baba *et al.*, Proc.of the 44th Fullerene-Nanotubes-Graphene General Symposium (1-5)
- [3] Y. Sano *et al.*, Proc.of the 46th Fullerene-Nanotubes-Graphene General Symposium (2P-1)
- [4] L. Y. Chiang *et al.*, *Org. Chem.* **59**, 3960 (1994)

Corresponding Author: H. Ogata

Tel: +81-42-387-6229, Fax: +81-42-387-6229, E-mail: hogata@hosei.ac.jp

Photoinduced Electron Transfer from Anionic Phthalocyanines to $\text{Li}^+@C_{60}$ and Light-Energy Conversion

○Yuki Kawashima¹, Kei Ohkubo¹, Vicente Manuel Blas-Ferrando², Hayato Sakai³, Enrique Font-Sanchis², Javier Ortíz², Fernando Fernández-Lázaro², Taku Hasobe³, Ángela Sastre-Santos², Shunichi Fukuzumi¹

¹ Department of Material and Life Science, Graduate School of Engineering, Osaka University, ALCA, Japan Science and Technology Agency, Osaka 565-0871, Japan

² División de Química Orgánica, Instituto de Bioingeniería, Universidad Miguel Hernández, Edificio Vinalopó, Avda. Universidad s/n, Elche, E-03202, Spain

³ Department of Chemistry, Faculty of Science and Technology, Keio University, Yokohama, 223-8522, Japan

Supramolecular complexes composed of fullerenes and porphyrinoids have been widely synthesized because they are suitable electron donor and acceptor for the formation of long-lived charge separated (CS) state.[1] When a nonpolar solvent is used to form a supramolecular complex with strong binding, photoinduced electron transfer does not occur efficiently due to the higher energy of the CS state than the triplet excited energies of fullerene and porphyrinoid. In contrast, a polar solvent can afford the long-lived CS state, however the supramolecular binding between the donor and acceptor moieties is normally weak due to the solvent polarization. We report herein formation of strong supramolecular complexes of cationic lithium-ion encapsulated C_{60} ($\text{Li}^+@C_{60}$)[2] with anionic phthalocyanines (Figure 1) and photoinduced charge separation in a polar mixed solvent.

Two phthalocyanines possessing carboxylate groups ($\text{H}_2\text{Pc}\cdot\mathbf{1}^{4-}$ and $\text{H}_2\text{Pc}\cdot\mathbf{2}^{4-}$) form 1:2 supramolecular complexes with $\text{Li}^+@C_{60}$ [$\text{H}_2\text{Pc}\cdot\mathbf{1}^{4-}/(\text{Li}^+@C_{60})_2$ and $\text{H}_2\text{Pc}\cdot\mathbf{2}^{4-}/(\text{Li}^+@C_{60})_2$] in a polar mixed solvent. From the UV-Vis spectral changes, the binding constants (K) were estimated as *ca.* 10^{12} M^{-2} . Upon the photoexcitation of constructed supramolecular complexes, photoinduced electron transfer occurred to form the CS state. The lifetime of the CS state was determined to be 1.2 ms for $\text{H}_2\text{Pc}\cdot\mathbf{2}^{4-}/(\text{Li}^+@C_{60})_2$, which is the longest CS lifetime among the porphyrinoid/fullerene supramolecular complexes. $\text{H}_2\text{Pc}\cdot\mathbf{1}^{4-}/(\text{Li}^+@C_{60})_2$ also afforded the long-lived CS state of 1.0 ms. The reorganization energy (λ) and the electronic coupling term were determined to be $\lambda = 1.70 \text{ eV}$, $V = 0.15 \text{ cm}^{-1}$. Supramolecular complex of zinc anionic phthalocyanine with $\text{Li}^+@C_{60}$ was also prepared and investigated. The $\text{ZnPc}\cdot\mathbf{4}^{4-}/\text{Li}^+@C_{60}$ supramolecular nanoclusters were assembled on the optically transparent electrode of nanostructured SnO_2 (OTE/ SnO_2) to construct the dye-sensitized solar cell. The IPCE (incident photon-to-photocurrent efficiency) values of OTE/ $\text{SnO}_2/(\text{ZnPc}\cdot\mathbf{4}^{4-}/\text{Li}^+@C_{60})_n$ were much higher than the sum of the two IPCE values of the individual systems OTE/ $\text{SnO}_2/(\text{Li}^+@C_{60})_n$ and OTE/ $\text{SnO}_2/(\text{ZnPc}\cdot\mathbf{4}^{4-})_n$, covering the near-infrared region.

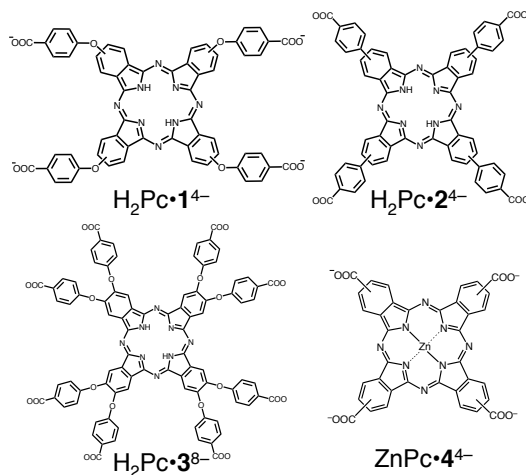


Figure 1. Chemical structure of phthalocyanines.

[1] Fukuzumi, S.; Ohkubo, K.; Suenobu, T. *Acc. Chem. Res.* **2014**, *47*, 1455-1464.

[2] Kawashima, Y.; Ohkubo, K.; Fukuzumi, S. *Chem. Asian J.* **2015**, *10*, 44-54.

Corresponding Author: S. Fukuzumi, Tel: +81-6-6879-7369, E-mail: fukuzumi@chem.eng.osaka-u.ac.jp

Addition Reactions of Trimetallic Nitride Template Endohedral Metallofullerenes with Disilirane and Digermirane

○Kyosuke Miyabe¹, Masahiro Kako^{*1}, Kumiko Sato², Mitsuaki Suzuki³, Naomi Mizorogi², Yutaka Maeda³, Marilyn M. Olmstead⁴, Alan L. Balch⁴, Wei-Wei Wang⁵, Shigeru Nagase⁵, Takeshi Akasaka^{2,3,6}

¹Department of Engineering Science, The University of Electro-Communications, Chofu, Tokyo 182-8585, Japan

²Life Science Center of Tsukuba Advanced Research Alliance, University of Tsukuba, Tsukuba, Ibaraki 305-8577, Japan

³Department of Chemistry, Tokyo Gakugei University, Tokyo 184-8501, Japan

⁴Department of Chemistry, University of California, Davis, California 95616, United States

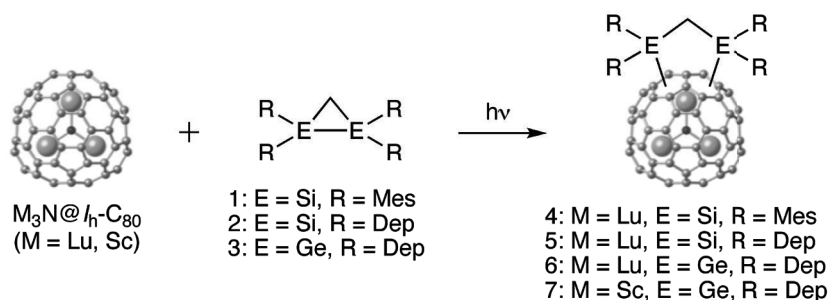
⁵Fukui Institute for Fundamental Chemistry, Kyoto University, Kyoto 606-8103, Japan

⁶Foundation for Advancement of International Science, Ibaraki 305-0821, Japan

Endohedral metallofullerenes (EMFs) have been of great interest because of their unique electronic properties due to the efficient electron-transfer from the encapsulated metal atoms to the fullerene cages. To date, a number of studies have been carried out to develop exohedral functionalization of EMFs, which will open up various applications such as organic photovoltaics and biological diagnostic agents. It has been demonstrated that functionalization of EMFs with electron-donating silyl groups alters the electronic characteristics of EMFs significantly. Such exohedral silylation also affects the positions and dynamic behaviors of the metal atoms encapsulated in EMF cages, which is a potential strategy for preparation of electronically functional materials. However, the examples of heteroatoms introduced onto the cages of EMFs have been hitherto limited to those of oxygen, nitrogen, silicon, germanium, and some transition elements [1]. To expand the fields of potential applications of EMFs, it is important to develop efficient methods to derivatize EMFs with heteroatom functional groups.

Previously, we reported the bis-germylation of trimetallic nitride template endohedral metallofullerenes (TNT EMFs) using digermirane [2]. Preliminary results show that introduction of germyl groups alter the oxidation potentials more cathodically than silyl groups do while the reduction potentials did not differ between **5** and **6**. Meanwhile, the photoreaction of digermirane **3** proceeded more efficiently than disilirane **2** probably due to the structural and electronic advantages of **3**. Herein we report the details of investigation of structural and electronic properties of bis-silylated and bis-germylated TNT EMFs, as well as the relative reactivities of disiliranes and digermirane toward TNT EMFs.

Scheme 1.



[1] L. Dunsch *et al.* *Chem. Rev.* **134**, 5989–6113 (2013).

[2] M. Kako *et al.* *The 47th Fullerenes-Nanotubes-Graphene General Symposium*, 3P-38 (2014).

Corresponding Author: Masahiro Kako Tel: +81-42-442-5570 E-mail: kako@e-one.uec.ac.jp

Energetics of the Nano-Saturn

○Shota Kigure¹, Haruka Omachi², Hisanori Shinohara², and Susumu Okada¹

¹*Graduate School of Pure and Applied Science, University of Tsukuba,
1-1-1 Tennodai, Tsukuba, Ibaraki 305-8571, Japan*

²*Department of Chemistry, Graduate School of Science, Nagoya University, Furo,
Chikusa, Nagoya 464-8602, Japan*

Structural hierarchy of nanocarbon materials allows us to design and synthesize new inclusion complexes which exhibit unusual geometric and electronic structures. For example, C₆₀ encapsulated into oligoarene molecules with a nanohoop structure, such as cycloparaphenylene (CPP) and cyclochrysenylene, leading to the carbon inclusion complexes with a unique geometric structure. In the present work, we study the energetics and dynamical properties of C₆₀ included into cyclohexabiphenylene (nano-Saturn) based on the density functional theory (DFT) with local density approximation.

Our calculations showed that the nano-Saturn is energetically stable compared with the other known inclusion compounds consisting of C₆₀ and CPP. Furthermore, the inclusion reaction of C₆₀ is exothermic without any energy barriers during the reaction. Furthermore, C₆₀ oscillates with the frequency of about 1 THz around its equilibrium position while hardly rotates inside the cyclohexabiphenylene ring due to the large energy barrier of 0.1 eV.

Corresponding author:

S. Kigure and S. Okada

Email:

skigure@comas.frsc.tsukuba.ac.jp

sokada@comas.frsc.tsukuba.ac.jp

TEL/FAX:

029-853-5600(8233)/029-853-5924

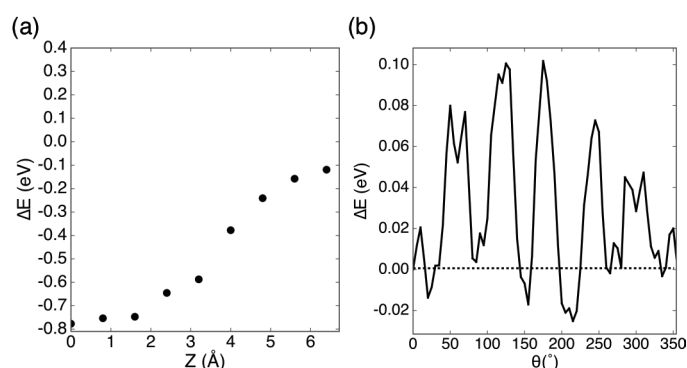


Figure. 1 (a) An energy potential surface during the reaction coordinate of inclusion process of C₆₀ into cyclohexabiphenylene. (b) Relative total energy of the nano-Saturn as a function of the mutual arrange of C₆₀.

Enegetics of H₂O encapsulated in fullerenes under an electric field

○Jun-ya Sorimachi, Susumu Okada

Graduate school of Pure and Applied Sciences, University of Tsukuba, Tsukuba 305-8571, Japan

Fullerenes can encapsulate atoms or molecules inside their C-C networks because of their hollow-cage structures with nanometer diameters. Recently, single H₂O molecule has been encapsulated into inner space of C₆₀ by using the molecular surgery technique. Because of the moderate reactivity of the other higher fullerenes, similar complexes are expected to be synthesized using the same experimental technique. According to the dipole moment of H₂O inside the fullerene cages, the water-encapsulated fullerenes under the external electric field exhibit unusual properties depending on the cage size, cage geometry, and the mutual arrangement of H₂O. In this work, we investigate the energetics of H₂O molecule encapsulated into fullerenes, C₆₀~C₈₀, with respect to the mutual direction of its dipole moment against the external electric field, in which the dipole has parallel, antiparallel, and perpendicular directions to the field, to elucidate the screening effect of the fullerene cage. To investigate the electronic structures and energetics of H₂O inside the fullerene cages under an electric field, we use the density functional theory (DFT) with the effective screening medium method (ESM).

Our DFT-ESM calculations show that the screening effect of the fullerene cages on the dipole moment of water strongly depends on the size, symmetry, and mutual arrangement of fullerene cages. We also find that a particular dipole direction is energetically favored (Fig. 1(a)) because of double cusps of the electrostatic potential inside some fullerene cages (Fig. 1(b)). In the case of the C₇₄, the relative energies of dipole with parallel and antiparallel to the field exhibit asymmetric nature that is unusual for the bare dipole under the electric field. Those facts indicates that the π electrons on fullerene cages strongly affect the screening against the external electric field being expected to lead unusual conformations of encapsulated molecules with dipole moments.

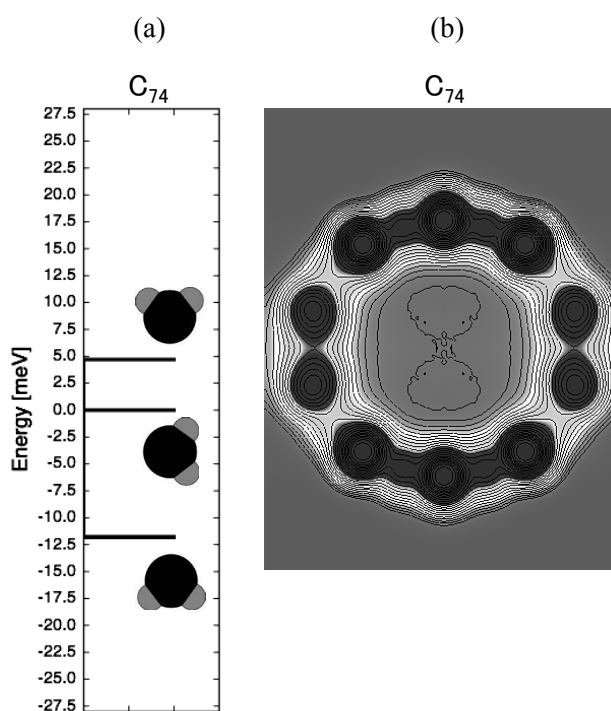


Fig. 1;
(a) Dipole energy of H₂O inside C₇₄ with respect to the dipole direction. (b) A contour plot of electrostatic potential of the empty C₇₄.

Corresponding Author: J. Sorimachi
Tel: +81-29-853-5600(ext.; 8233)
E-mail: jsorimachi@comas.frsc.tsukuba.ac.jp

Absolute yield of fullerene formed by graphite laser ablation at room temperature

○Hitomi Endo,¹ Yuki Taguchi,¹ Jun Matsumoto,¹ Tomonari Wakabayashi,²
Takeshi Kodama,¹ Yohji Achiba,¹ and Haruo Shiromaru¹

¹ Department of Chemistry, Tokyo Metropolitan University, Tokyo, 192-0397, Japan

² Department of Chemistry, Kindai University, Osaka, 577-8502, Japan

Since the appearance of epoch making mass spectra (MS) of C₆₀ in 1985 [1], many attempts to obtain a macroscopic amount of C₆₀ by laser vaporization (ablation) had all failed, until it was come to know that a high temperature condition was indispensable to C₆₀ formation [2]. The striking MS [1] undoubtedly opened up a new field of nanocarbon science, but a simple question still remains, “how many C₆₀ molecules were really formed by laser ablation without heating devices in 1985?” At the FNTG46, we reported that the laser ablation (300 mJ/pulse, 10 Hz, 30 min) without heating devices yields perceptible amount of C₆₀ [3]. It is likely to be due to higher local temperature of the graphite surface irradiated by laser. In the present study, we repeated the laser ablation under the same conditions and measured the absolute yield of C₆₀, to examine whether the yield is consistent with a tacit consensus that it might be very few but high enough to be detected by MS.

The temperature of the graphite surface under laser irradiation was measured to be about 200 °C, by a thermocouple pasted on the surface and a pyrometer. The soluble ablation products, which were carried by Ar gas flow, were analyzed by HPLC and UV absorption, and the amount of C₆₀ was evaluated to be 6×10^{-10} mol (4×10^{-4} mg), namely 2×10^{10} molecules per laser shot. The C₆₀ attached to the wall were about 1×10^{-3} mg. Therefore, although typical laser vaporization cluster source yields much smaller ablation products, MS-detectable amount of C₆₀ should be included in the cluster beam.

Total amount of the vaporized carbon was evaluated to be about 10 mg from a SEM image (Fig. 1). The C₆₀ yield, the ratio (wt%) of C₆₀ (gas-carried + wall-attached ones) to the total, is shown in Fig. 2 together with those previously obtained by the laser ablation in a heated cell so-called “laser-furnace experiment” [4]. The fullerene yield is not significantly deviate from the extrapolation of the high-temperature values. Such a low yield suggests that the signal of synthesized C₆₀ may be easily hidden by artificial enhancement of C₆₀⁺ due to dissociative ionization of larger clusters, especially if multiphoton ionization is employed.

[1] H. W. Kroto *et al.*, *Nature*, **318** 162 (1985). [2] R. E. Haufler *et al.*, *Proc. Mat. Res. Soc. Symp.*, **206**, 627 (1991). [3] Y. Abe *et al.*, FNTG46, 141 (2014). [4] D. Kasuya *et al.*, *Eur. Phys. J. D*, **9** 355 (1999).

Corresponding Author: H. Endo, Tel: +81-42-677-1111, Fax: +81-42-677-2525, E-mail: endo-hitomi@ed.tmu.ac.jp

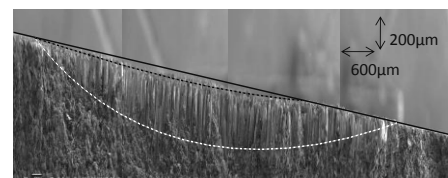


Fig. 1 The cross-section SEM image around the ablation area. The solid line indicates the surface position, which is interpolated from the intact surface. The carbons in the area surrounded by the solid line and black dashed line are lost by ablation. The area above the white dashed line is filled by cone-shaped pillars, where the space occupancy rate is roughly assumed to be 0.5.

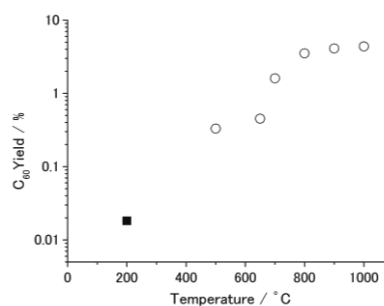


Fig. 2 C₆₀ yield vs. temperature graph.
○: “Laser-furnace” [4] ■: present study

Fabrication and characterization of SWCNT-TFTs using chirality separated DNA-wrapped SWCNTs

○Yuki Kuwahara^{1,2}, Fumiyuki Nihey^{2,3}, Shigekazu Ohmori², Takeshi Saito^{1,2}

¹ Nanotube Research Center, National Institute of Advanced Industrial Science and Technology (AIST), Tsukuba 305-8565, Japan

² Technology Research Association for Single Wall Carbon Nanotubes (TASC), Tsukuba 305-8565, Japan

³ NEC Corporation, Tsukuba, Ibaraki 305-8501, Japan

The thin film transistors (TFTs) using SWCNTs as a semiconducting material have been studied. Recently, progresses in various techniques for the separation of SWCNTs by their electric structures enable us to produce highly purified semiconducting SWCNTs, which have improved the device performance of SWCNT-TFTs extremely. Using such highly purified semiconducting SWCNTs can increase the density of SWCNT networks in TFT channel preserving the better device performances in both on/off ratio and carrier mobility. Therefore highly purified semiconducting SWCNTs are crucial for fabricating the SWCNT-TFTs of high performances with their uniformity.

Previously, we reported the effective way to fabricate SWCNT-TFTs by preparing homogeneous network of DNA wrapped SWCNTs (DNA-SWCNTs) [1]. However, the electronic structure of SWCNTs was still uncontrolled, which resulted in the low device performance of SWCNT-TFTs due to the presence of metallic SWCNTs pathway in the channel. Here in this study, we have separated DNA-SWCNTs by their electronic structures using ion exchange chromatography (IEX) method reported by Tu *et al.* [2], and fabricated SWCNT-TFTs with the enriched fraction of semiconducting DNA-SWCNTs.

Figure 1 plots the device performances of SWCNT-TFTs using DNA-SWCNTs before and after IEX. Comparing their on/off ratios at the same mobility, SWCNT-TFTs after IEX possess higher values (10^4 - 10^7) than that before IEX. This result indicates that IEX method sufficiently improves the performance of SWCNT-TFTs, probably due to the reduction of metallic SWCNTs pathway. SWCNT-TFTs with the on/off ratio of around 10^6 was successfully obtained by IEX processed DNA-SWCNTs.

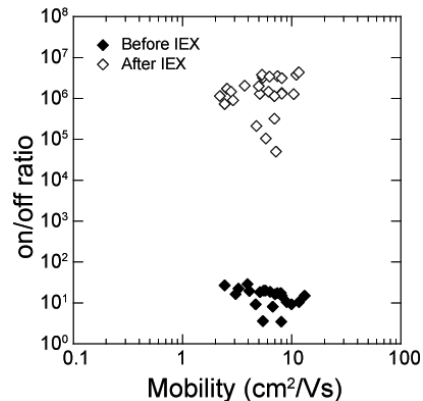


Fig.1 On/off ratio as a function of carrier mobility ($L_{ch} = 40 \mu\text{m}$) measured from transfer characteristics ($V_{DS} = -1 \text{ V}$).

Acknowledgment: This work was supported by Iketani Science and Technology Foundation. A part of this work was conducted at the Nano-Processing Facility, supported by IBEC Innovation Platform, AIST and "Nanotechnology Network Japan" of the Ministry of Education, Culture, Sports, Science and Technology (MEXT), Japan.

References: [1] Y. Asada *et al.*, Adv. Mater. 23, 4631 (2011). [2] X. Tu *et al.*, Nature. 460, 250 (2009).

Corresponding Author: T. Saito, Tel: +81-29-861-4863, Fax: +81-29-861-4413, E-mail: takeshi-saito@aito.go.jp

Energetics and electronic structures of deformed carbon nanotubes

○Jumpei Nishikawa, Susumu Saito

Department of Physics, Tokyo Institute of Technology, Meguro-ku, Tokyo 152-8551, Japan

Because of its unique properties, carbon nanotube (CNT) has been intensively studied in various fields since its discovery by S. Iijima in 1991 [1]. Cylindrical structure is known as a stable structure of CNTs, but it is also found experimentally that flatly deformed CNTs are stable in the case of large diameter CNTs [2]. Moreover, electronic-structure change with this deformation is theoretically reported [3].

To discuss the energetics of deformed CNTs, we calculate the total energy using the tight-binding model which can deal with interlayer interactions between sp^2 layers [4]. To discuss the electronic structure of these CNTs, we use Hamada-Sawada tight-binding model which can reproduce the first-principles electronic structure of CNTs very well [5]. We also use the first-principles density functional calculation. In this study, we report the change of stability and electronic structure of cylindrical and deformed CNTs.

As a result, we find the critical diameters where deformed structure appears as one of stable structures and those where the deformed geometry becomes more stable than a cylindrical structure. As for the electronic structure, we discuss the energy-gap change with the deformation, and we also discuss the differences with prior works [6,7].

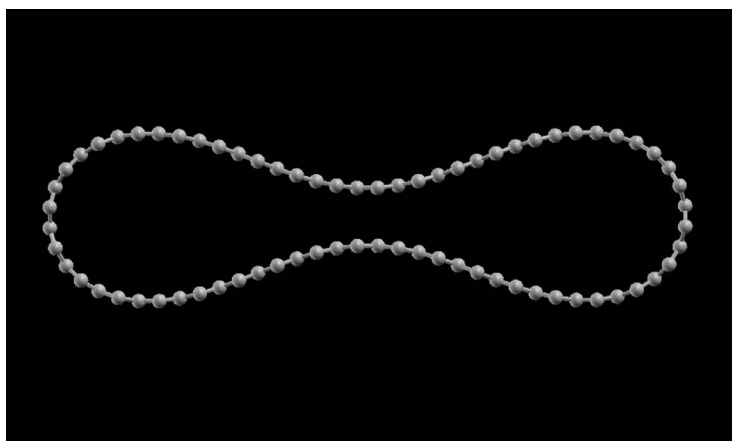


Fig.1 Fully optimized deformed (36,0) CNT.

- [1] S. Iijima. *Nature*. **354**,56 (1991).
- [2] Y. Miyata, M. Suzuki, M. Fujihara, Y. Asada, R. Kitaura and H. Shinohara. *ACS nano* **4**,5807 (2010).
- [3] K. Nishidate and M. Hasegawa. *Phys. Rev. B*. **81**,125414(2010).
- [4] Y. Omata, Y. Yamagami, K. Tadano, T. Miyake and S. Saito. *Physica.E* **29**,454 (2005).
- [5] N. Hamada, S. Sawada and A. Oshiyama: *Phys. Rev. Lett.* **68**, 1579 (1992).
- [6] S. Zhang *et al.* *Phys. Rev. B* **73**, 075423 (2006).
- [7] G. Gao *et al.* *Nanotechnology*. **9**, 184 (1998).

Corresponding Author: Jumpei Nishikawa
E-mail: nishikawa.j.aa@m.titech.ac.jp

Effect of Chemical Doping on the Electronic States of Single-Walled Carbon Nanotubes (1) : Experiment

Tomonari Shiraishi¹, Naoto Akizuki², Yuhei Miyauchi², Kazunari Matsuda², Naotoshi Nakashima^{1,4,5}

¹Department of Applied Chemistry, Kyushu University, Fukuoka 819-0395, Japan

²Institute of Advanced Energy, Kyoto University, Uji, Kyoto 611-0011, Japan

³WPI-I2CNER, Kyushu University, 744 Motoooka, Fukuoka 819-0395, Japan

⁴JST-CREST, Japan Science and Technology Agency, 5 Sanbancho, Chiyoda-ku, Tokyo 102-0075, Japan

Local luminescent states in single-walled carbon nanotubes (SWNTs) have been of great interest due to the bright photoluminescence (PL) from such states promising for their applications in optoelectronics and bioimaging. Recently, Miyauchi *et al.* [1] and Piao *et al.* [2] have reported the extraordinary exciton brightening in such local states generated by chemical doping and clarified the mechanism of the PL enhancement induced by dimensionality modification of excitons. However, detailed electronic structure of the local states has been still unclear. To investigate the origin of the local states, it is important to evaluate the electron potentials in conduction and valence bands of the chemical doped SWNTs. We have reported that electronic potentials of (n,m) SWNTs can be determined based on *in situ* PL spectroelectrochemistry [3]. Here, we used this method to determine the electronic potentials of the chemical doped SWNTs dispersed in a carboxymethylcellulose (CMC) film.

Chemical doped SWNTs in a sodium dodecyl benzene sulfonate (SDBS) solution were prepared according to the previous paper [1] and [2], and the SDBS molecules were replaced with CMC. A CMC film containing the chemical doped SWNTs was formed on an ITO plate and used for the PL spectroelectrochemical measurements in an aqueous solution.

Fig. 1 shows a 2D-PL map obtained from the chemical doped SWNTs in the CMC film. The clear spot at around 1000 nm is the PL from the (6,5)SWNTs. We clearly observe a new spot at around 1150-1200 nm is the new band generated by the chemical doping that is attributed to the chemical doped (6,5)SWNTs. The PL intensities of the new band were found to change by applying the electrochemical potentials to the ITO electrode; thus the oxidation and reduction potentials of the local states in the chemical doped SWNTs were determined. We will provide detailed results on the electronic states of the chemical doped SWNTs at the meeting.

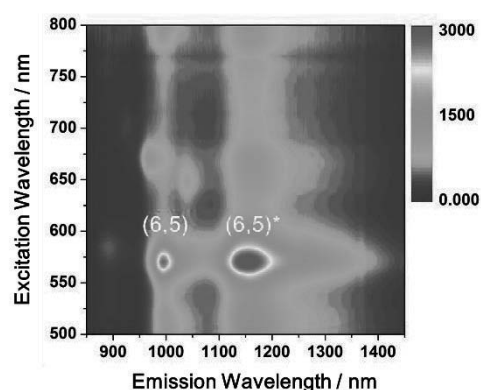


Fig. 1. 2D-PL mapping of a film of the chemical doped SWNTs on an ITO electrode.

[1] Y. Miyauchi *et al. Nat. Photonics*, **7**, 715 (2013).

[2] Y. Piao *et al. Nat. Chem*, **5**, 840 (2013).

[3] N. Nakashima *et al. Angew. Chem. Int. Ed.* **48**, 7655 (2009);
N. Nakashima *et al. Sci. Rep.*, **3**, art no. 2959 (2013).

Corresponding Author: Naotoshi Nakashima

E-mail: nakashima-tcm@mail.cstm.kyushu-u.ac.jp

Effect of Chemical Doping on the Electronic States of Single-Walled Carbon Nanotubes: Theory

○Gergely Juhász,¹ Tomonari Shiraishi,¹ Naotoshi Nakashima¹

¹Department of Applied Chemistry, Kyushu University, Fukuoka 81-0395, Japan

Covalent doping of single-walled carbon nanotubes (SWCNTs) can potentially control and tune the band structure of the nanotubes. This control allow tuning electrochemical and optical properties, therefore it has a major importance. Such covalent modifications are often quenches the photoluminescence in semi-conducting the SWCNTs. A very important counter example was reported by Piao *et al.* [1]: sp^3 doping with a controlled number aryl groups can produce a new photoluminescence peak, substantially brighter than that of the pristine tubes.

To explain the optical effect a better understanding of electronic structure in sp^3 doped nanotubes is needed. We performed DFTB and TD-DFTB-based calculations on short models of semiconducting (6,5) SWNT. We focused on single and double dopant scenarios, using H and aryl groups as dopants. The analysis of the orbital structure revealed a significant radical character in tubes with single doping sites. A double radical character was also observed in tubes with two doping sites, when the dopant positions were distant. Moreover the calculated orbital energies, and therefore the energy of the optical transitions are very sensitive to the position of the dopants (see Fig. 1). On the other hand no experimental evidence of unpaired electrons have been reported so far. The relatively large experimental bandgap and the observed sharp photoluminescence transitions also exclude the possibility of such electronic structures.

Such contradiction can be explained if the doping reaction is selective and leads to geometries with weak radical character. The analysis of frontier orbitals and large stability difference between different doping configurations suggest that indeed such selectivity can be an important factor during the doping reaction. If so, the mild reaction conditions can actually support such a selectivity, and experimental photoluminescence spectrum is dominated by a handful of doping products.

[1] Piao *et al.* *Nature Chem.* **5**,840 (2013).

Corresponding Author: N. Nakashima

Tel: +81-92-802-2840, Fax: +81-92-802-2840,

E-mail: nakashima-tcm@mail.cstm.kyushu-u.ac.jp

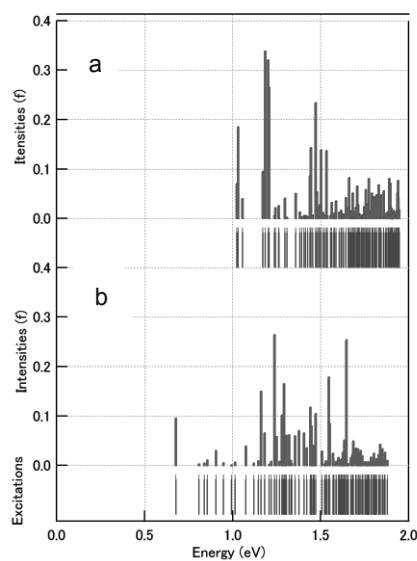
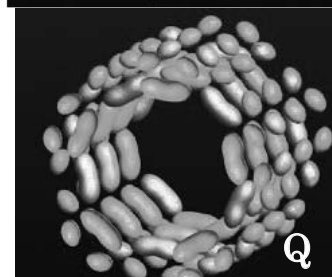
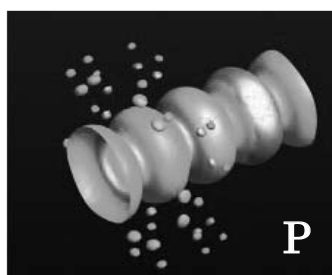
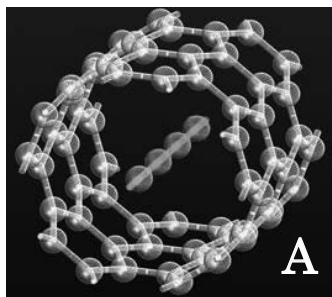


Fig.1 Calculated intensity of optical transitions and excitation energies (*below*) for tubes two doping configurations: close (*a*) and distant doping sites (*b*).

Ab initio calculation for electronic bands of CNT in which the chain of sulphur is inserted

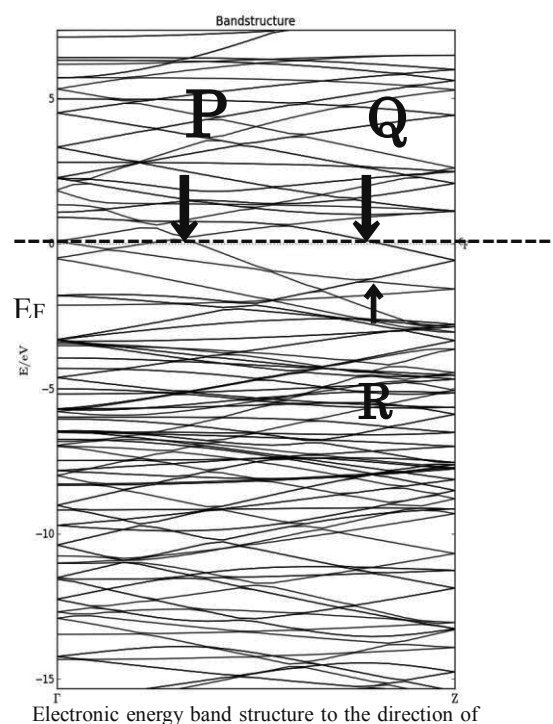
○Yuhei Natsume¹

¹ Chiba University, chiba 263-8522, Japan



We discuss electronic band structures in the linear chain of sulphur encapsulated by single-walled CNT. The calculation is made on the basis of DFT method [1]. Experimental work has been reported by research group of Shinshu University[2]. They emphasize the stabilization of one-dimensional system of sulphur in CNT in relation with conducting characters. ■ In the present work, sulphur atoms are set at the center axis of CNT in which chiral number (n,m) is (5,5), as shown in Fig.A. The three unit cells of pure CNT are contained in the unit cell, which is constructed by four atoms of sulphur. The distance between atoms of sulphur in the chain is 1.845 Å. In calculation, the optimization is made in consideration of properties of CNT systems [3] under this condition of periodicity. The obtained result is represented in right figure, where bands in corresponding BZ for above-mentioned unit cell are expressed.

Here, the dotted line indicates Fermi level. We can find several crossings of bands at Fermi surface (line). As for these bands, Bolch states are illustrated in Figs. P,Q,R. Though the overall electron density suggests that the chain and CNT are coupled by week van der Waals interaction, significant mixing between the chain and CNT is found only for Fermi level.



the axis for CNT.

■[1]Atomistix ToolKit version 13.8, QuantumWise A/S (www.quantumwise.com). M. Brandbyge, J.-L. Mozos, P. Ordejo'n, J. Taylor, and K. Stokbro, Phys. Rev. **B 65**, 165401 (2002). <<http://dx.doi.org/10.1103/PhysRevB.65.165401>>

■[2]T.Fujimori, A.Morelos-Gomez, Z.Zhu, H.Muramatsu, R.Futamura, K.Urita, M.Terrones, T.Hayashi, M.Endo, S.Y.Hong, Y.C.Choi, D.Tomanek & K. Kaneko, "Conducting linear chains of sulphur inside carbon nanotubes", Nature Commun. 4:2162 (2013) doi 10.1038/ncomms 3162. <<http://www.nature.com/ncomms/index.html>>

■[3]Y.Natsume, "Numerical study of electronic states in double-walled carbon nanotubes---Formation of metallic bands by covalent bridge between tubes---" 3P-11, The 46th Fullerenes Nanotubes Graphene General Symposium, 3-5 Mar. 2014, Tokyo University, Hongo.

Fabrication of Thermoelectric Device using P- and N-Type Controlled Single Wall Carbon Nanotubes by Electric Double Layer Carrier Injections

○Yuki Oshima, Yoshimasa Kitamura, Shouhei Kanda, Hideki Kawai, Yusuke Nakai,
Yutaka Maniwa, Kazuhiro Yanagi

Department of Physics, Tokyo Metropolitan University, Minami-Osawa 192-0397, Japan

Development of high performance thermoelectric devices is of great importance for efficiently converting waste heat into electric power. To understand the physical background, it is very important to clarify the relationships between the Seebeck coefficients and the Fermi level. We have controlled various physical properties of Single Wall Carbon Nanotube (SWCNTs) by tuning the Fermi level through carrier injections caused by electric double layers using an ionic liquid.^{[1],[2]} Recently, we have revealed that the semiconducting SWCNT networks show very large Seebeck coefficient.^[3] Furthermore, we have controlled the Seebeck coefficient of semiconducting SWCNT networks by electric double layer transistor (EDLT) setups.^[4]

In this study, we fabricated thermoelectric device using P and N-type controlled SWCNTs. The semiconducting SWCNTs with diameter of 1.4nm were prepared by using density gradient centrifugations. The ionic liquid (TPMA-TFSI) was used to form electric double layers. The schematic device structure is shown in the inset of Figure 1. The channel voltage was applied to one of the semiconducting SWCNT thin film, and another thin film was kept p-type, which was initial state. After the channel voltage was applied, we fixed the doped state by freezing the ionic liquid for the precise data collection. Then, the thermoelectric voltages were measured as a function of applied channel voltage.

Figure 1 shows the thermoelectric power of the device as a function of channel voltage. As shown here, the thermoelectric powers, and even polarities, were changed by the shift of channel voltage, and the values of the thermoelectric power were controlled. Thus, we could fabricate the tunable thermoelectric device by EDLT setups using an ionic liquid. Our results suggest that the EDLT techniques are quite useful to develop the high performance thermoelectric devices.

[1] K.Yanagi *et al. Adv. Mater* **23**, 2811 (2011).

[2] K.Yanagi *et al. Phys. Rev. Lett.* **110**, 086801 (2013).

[3] Y.Nakai *et al. Appl. Phys. Express* **7**, 025103 (2014).

[4] K.Yanagi *et al. Nano Lett.* **14**, 6437 (2014).

Corresponding Author: K.Yanagi

Tel: +81-42-677-2494,

Fax: +81-42-677-2483,

E-mail: yanagi-kazuhiro@tmu.ac.jp

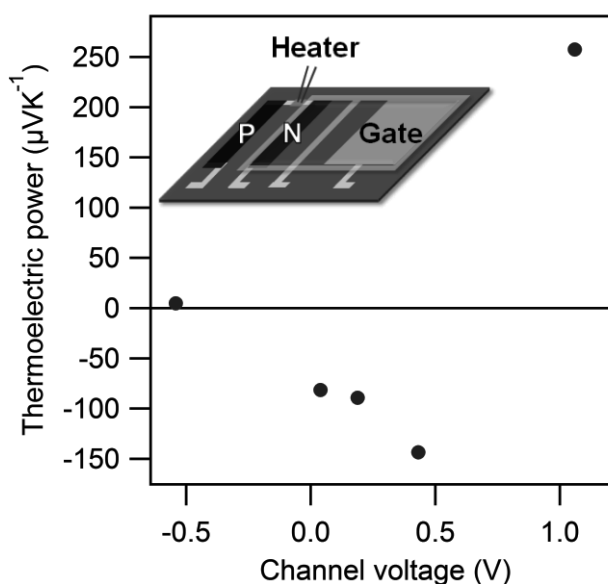


Fig.1: Thermoelectric power of the device as a function of Channel voltage (Inset: Schematic device structure)

Polyglycerol-functionalized SWNTs: size separation, toxicological study and biomedical application

○Keisuke Nakamura^{1,2}, Li Zhao¹, Hongmei Qin¹, Shuji Aonuma², Takahide Kimura¹, Naoki Komatsu¹

¹ Department of Chemistry, Shiga University of Medical Science, Otsu, 520-2192, Japan

² Department of Materials Chemistry, Osaka Electro-Communication University, Osaka, 572-8530, Japan

For biomedical in vivo applications of nanocarbons as an imaging probe and a drug carrier, they have to be solubilized in a physiological environment. Recently, we have found that surface functionalization with polyglycerol (PG) affords very good hydrophilicity to various nanocarbons (nanodiamond [1] and graphene [2]) as well as metal oxides (ZnO [3] and Fe₃O₄ [4]). In this paper, we will report solubilization, chromatographic separation, toxicological study and biomedical application of PG-functionalized SWNTs. After cutting SWNTs (*c*-SWNTs) under ultrasonic irradiation in mixed acid for 48 h, *c*-SWNTs were functionalized with PG through ring opening polymerization of glycidol [1]. The solubility of the resulting PG-functionalized SWNTs (*c*-SWNT-PG) was >10 mg/mL in pure water and >8.5 mg/mL in phosphate buffer. Since these solutions were very stable without any precipitation for more than one month, they were subjected to size separation by size-exclusion chromatography [1] and evaluation of cytotoxicity. After incubating HeLa cells in the presence of *c*-SWNTs with

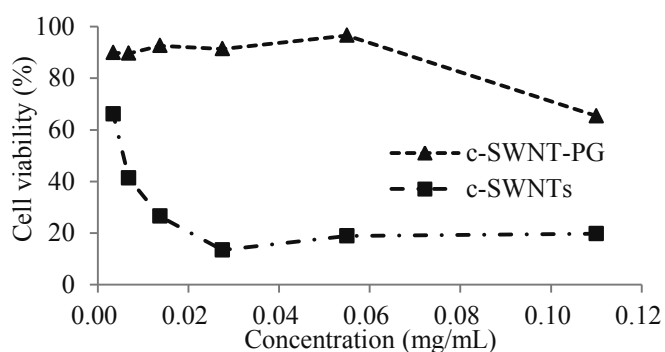


Fig.1 Cytotoxicity of *c*-SWNT-PG and *c*-SWNTs

or without PG for 24 h, cell viability was measured by use of cell counting kit-8. The result shown in Fig. 1 indicates that PG coating efficiently reduce the cytotoxicity of *c*-SWNTs probably because of stealth effect of PG [5]. Application of *c*-SWNT-PG to photodynamic therapy is now in progress.

[1] L. Zhao, N. Komatsu, et al. *Angew. Chem. Int. Ed.*, **50**, 1388 (2011)

[2] T. Yasuda, N. Komatsu, et al. The 43rd Fullerenes-Nanotubes-Graphene General Symposium, 1-14

[3] L. Zhao, N. Komatsu, et al. *J. Indian Chem. Soc.*, **88**, December, 1787 (2011)

[4] L. Zhao, N. Komatsu, et al. *Adv. Funct. Mater.*, **22**, 5107 (2012).

[5] L. Zhao, N. Komatsu, et al. *Adv. Funct. Mater.*, **24**, 5348 (2014).

Corresponding Author: Naoki Komatsu

Tel: +81-77-548-2102, Fax: +81-77-548-2405, E-mail: nkomatsu@shiga-med.ac.jp

Gate-controlled generation of optical pulse trains using individual carbon nanotubes

M. Jiang, Y. Kumamoto, ○A. Ishii, M. Yoshida, T. Shimada, and Y. K. Kato

Institute of Engineering Innovation, The University of Tokyo, Tokyo 113-8656, Japan

We report on optical pulse-train generation from individual air-suspended carbon nanotubes under an application of square-wave gate voltages [1]. Electrostatically-induced carrier accumulation quenches photoluminescence [2], while a voltage sign reversal purges those carriers, resetting the nanotubes to become luminescent temporarily. Frequency domain measurements reveal photoluminescence recovery with characteristic frequencies that increase with excitation laser power, showing that photoexcited carriers quench the emission in a self-limiting manner. Time-resolved measurements directly confirm the presence of an optical pulse train synchronized to the gate voltage signal, and flexible control over pulse timing and duration is demonstrated.

Work supported by KAKENHI (24340066, 24654084, 26610080, 26870167), SCOPE, Canon Foundation, Asahi Glass Foundation, and KDDI Foundation, as well as the Nanotechnology Platform and Photon Frontier Network Program of MEXT, Japan. A.I. is supported by MERIT and JSPS Research Fellowship, and M.Y. is supported by ALPS.

- [1] M. Jiang, Y. Kumamoto, A. Ishii, M. Yoshida, T. Shimada, and Y. K. Kato, arXiv:1407.7086 (2014).
- [2] S. Yasukochi, T. Murai, S. Moritsubo, T. Shimada, S. Chiashi, S. Maruyama, and Y. K. Kato, Phys. Rev. B **84**, 121409(R) (2011).

Corresponding Author: Y. K. Kato
Tel: +81-3-5841-7702, Fax: +81-3-5841-7772,
E-mail: ykato@sogo.t.u-tokyo.ac.jp

Electroluminescence from individual air-suspended carbon nanotubes within split-gate structures

○N. Higashide, M. Jiang, T. Uda, M. Yoshida, A. Ishii and Y. K. Kato

Institute of Engineering Innovation, The University of Tokyo, Tokyo 113-8656, Japan

Electrically induced light emission from chirality-identified single-walled carbon nanotubes are investigated by utilizing split-gate field-effect devices fabricated on silicon-on-insulator substrates. We begin by etching trenches through the top silicon layer into the buried oxide, and the silicon layer is thermally oxidized for use as local gates [1]. We partially remove the oxide and form gate electrodes, then we attach electrodes on both sides of the trench for contacting nanotubes. Catalyst particles are placed on the electrodes, and nanotubes are grown over the trench by chemical vapor deposition. We use photoluminescence microscopy to locate the nanotubes and perform excitation spectroscopy to identify their chirality [2]. By applying opposite polarity voltages on the split-gates, p-n junctions can be formed along the length of the nanotubes. Electroluminescence is observed under forward bias, whose spectral shape is similar to that of photoluminescence. We find that the dependence of electroluminescence intensity on the two gate voltages is consistent with emission from a split-gate p-n diode.

Work supported by KAKENHI, The Canon Foundation, and The Asahi Glass Foundation, as well as the Nanotechnology Platform and Photon Frontier Network Program of MEXT, Japan.

[1] M. Jiang, Y. Kumamoto, A. Ishii, M. Yoshida, T. Shimada, Y. K. Kato, arXiv 1407.7086 (2014)

[2] S. Moritsubo, T. Murai, T. Shimada, Y. Murakami, S. Chiashi, S. Maruyama, and Y. K. Kato, Phys. Rev. Lett. 104, 247402 (2010).

Corresponding Author: Y. K. Kato

Tel: +81-3-5841-7702, Fax: +81-3-5841-7772,

E-mail: ykato@sogo.t.u-tokyo.ac.jp

Redox-dependent separation of single-wall carbon nanotubes in hydrogels

○Atsushi Hirano, Takeshi Tanaka, Hiromichi Kataura

Nanosystem Research Institute, National Institute of Advanced Industrial Science and Technology (AIST), Tsukuba, Ibaraki 305-8562, Japan

It has been reported that single-wall carbon nanotubes (SWCNTs) dispersed in sodium dodecyl sulfate (SDS) solutions are separated into metallic and semiconducting species by hydrogel columns such as agarose [1] and Sephacryl columns. Our previous study suggested that the separations are accounted for by the oxidation of SWCNTs with an O_2/H_2O redox couple; specifically, metallic SWCNTs that are readily oxidized flow through the columns, whereas semiconducting ones are retained in the columns [2]. In this study, various oxidants for the SWCNTs were used for the separation to support the above suggestion.

K_2IrCl_6 and NaClO have been reported to oxidize SWCNTs [3,4]. Such oxidation was also observed in the present study. Figure 1 shows the absorption spectra of the SWCNTs dispersed in SDS solutions, which correspond to their S_{11} bands. The absorbances decreased with increasing concentration of the oxidants. The oxidation effects were more pronounced for K_2IrCl_6 than NaClO. After the injection of the SWCNTs into Sephacryl columns in the absence of the oxidants, the retained semiconducting SWCNTs in the columns were eluted using these oxidants. Figure 2 shows the amount of eluted semiconducting SWCNTs from the columns. It was found that the semiconducting SWCNTs were effectively eluted in the presence of the oxidants at 1 mM; the elution effect was more pronounced for K_2IrCl_6 than NaClO. Importantly, K_3IrCl_6 had less effect on the elution. Similar results were obtained with one of the SDS analogs, sodium 1-undecanesulfonate. Oxidation of SWCNTs is thus demonstrated to be a contributory factor in the interaction of the SWCNTs with the hydrogels.

Oxidized SWCNTs are positively charged, which enhances electrostatic attraction between the SWCNT and the negatively charged surfactants. Condensation of the surfactants on the SWCNTs through the attractive interaction should lead to the enhanced elution of the SWCNTs from the columns.

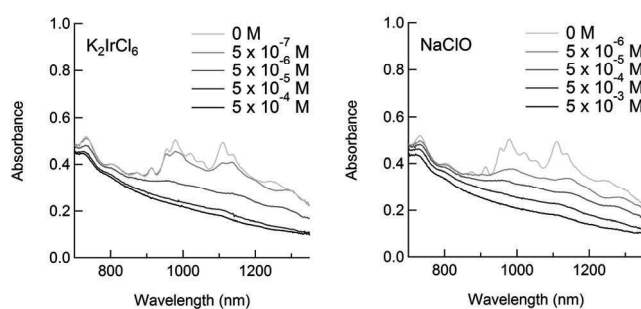


Fig.1 Absorption spectra of the SWCNTs dispersed SDS in the presence of K_2IrCl_6 or NaClO at different concentrations.

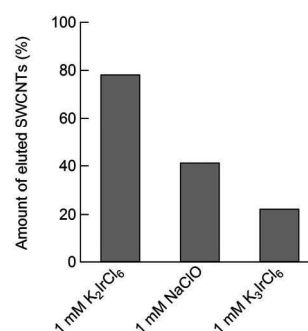


Fig.2 Amount of eluted semiconducting SWCNTs from the hydrogel in the presence of three oxidants at 1 mM.

- [1] T. Tanaka *et al.* Appl. Phys. Express **2**, 125002 (2009)
 [2] A. Hirano *et al.* ACS Nano **7**, 10285 (2013)
 [3] F. J. Knorr *et al.* Langmuir **25**, 10417 (2009)
 [4] M. Zheng *et al.* J Am Chem Soc **126**, 15490 (2004)

Corresponding Author: T. Tanaka

Tel: +81-29-861-2903, Fax: +81-29-861-2786,

E-mail: tanaka-t@aist.go.jp

Optimization of the synthesis parameters of Carbon Nanotube (CNT) forest using the Taguchi Method

○Adam PANDER¹, Hiroshi FURUTA^{1,2}, Akimitsu HATTA^{1,2}
Kochi Univ. Technol. ¹, Research Inst., Kochi Univ. Technol. ²

E-mail: 186001x@gs.kochi-tech.ac.jp, furuta.hiroshi@kochi-tech.ac.jp

Carbon Nanotubes (CNT), since their discovery by Iijima in 1991¹, has attracted much attention for various applications due to their extraordinary electrical, thermal and physical properties. A CNT forest with high density and alignment may provide uniform CNTs with desirable length, diameter and structure. It is known, that physical properties of CNTs influence directly their thermal, electrical and mechanical properties². Currently many various methods of CNTs synthesis are available, among which Chemical Vapor Deposition (CVD) is the most popular due to low cost, high production yield and ease in modifications³.

The growth of CNT forest may cause many difficulties related to the large number of parameters influencing the growth during synthesis process. Choosing the proper parameters of the growth can be long lasting process, and even that may not give the optimal growth values. One of the possible solutions to decrease the number of the experiments is to apply optimization methods to the design the experiment parameter matrix⁴.

In this work, optimization of the parameters of the Carbon Nanotubes synthesis process was studied using Taguchi Method. This method was applied for development of the plan of the experiments and elaboration of obtained experimental results. The aim of Taguchi Method is to minimize the changes of the product properties in dependence on noise factor (N – noise) and maximize the changes in dependence on signal factors (S – signal). In Taguchi method statistic coefficient called signal-to-noise (S/N) ratio is used. S/N ratio allows to evaluate the influence of process parameters on the properties of the product. Taguchi Method provides data that consist statistically significant factors of the process and allow to find optimum level of the parameters, using S/N ratio analysis and experimental data analysis^{5,6}. The Taguchi Method utilize 3 main optimization problems: the smaller the better; the bigger the better and nominal value.

In this paper the growth parameters were: (a) thickness of iron catalyst, (b) hydrogen flow during annealing, (c) annealing time, (d) process temperature and (e) acetylene flow during growth stage. For each parameter, four values were tested. Fig. 1. shows the table of the CNTs growth experiments. The results of the optimization were verified by the diameter, height and density of CNTs forest. Fig. 2. shows S/N ratios of diameter of CNTs for optimized parameters. As shown, according to Taguchi statistical analysis, the biggest influence on the diameter of CNTs has annealing time, where parameter 3 (5 min) is the most optimal value.

In future, Taguchi Method would provide optimal route from catalysts to growth of CNTs with desirable properties (like diameter, length, waviness and etc.) through the Taguchi growth parameters with minimum trials among huge number of possible growth condition matrix.

Taguchi, L16					
Exp. No.	a	b	c	d	e
1.	0.5	0	3	700	10
2.	0.5	25	5	730	15
3.	0.5	50	7	760	20
4.	0.5	75	9	790	25
5.	1.0	0	5	760	25
6.	1.0	25	3	790	20
7.	1.0	50	9	700	15
8.	1.0	75	7	730	10
9.	1.5	0	7	790	15
10.	1.5	25	9	760	10
11.	1.5	50	3	730	25
12.	1.5	75	5	700	20
13.	2.0	0	9	730	20
14.	2.0	25	7	700	25
15.	2.0	50	5	790	10
16.	2.0	75	3	760	15

Fig 1. Plan of the experiments according to Taguchi's orthogonal table L16

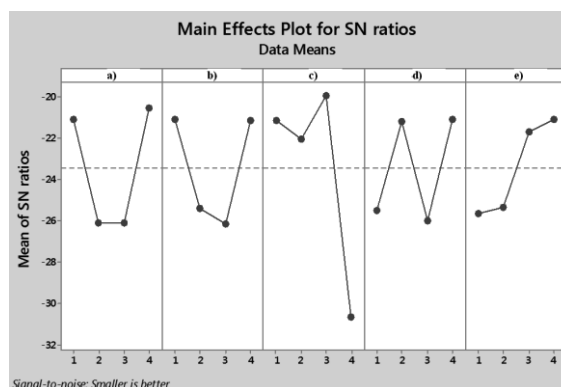


Fig 2. The influence of selected process parameters used in the experiments on CNTs diameter. (a) thickness of iron catalyst, (b) hydrogen flow during annealing, (c) annealing time, (d) process temperature and (e) acetylene flow during growth stage.

[1] S. Iijima, *Nature* 354, 56 (1991), [2] H. Furuta et al. *App. Phys. Exp.* 3 (2010), [3] M. Kumar, *J. Nano. Sci. Tech.* 10 (2010), [4] S. Porro, et al., *Phys. E* 37 (2007), [5] M. Pancielejko, A. Pander, et al., *Arch. Mat. Sci. Eng.* 54 (2012), [6] J. Walkowicz, et al., *J. Mat. Sci. Perf.* 22(2) (2013)

Synthesis of single-walled carbon nanotubes from woody bioethanol

○Takuma Araki¹, Atsushi Honda¹, Yuhei Yabushita², Toshiya Murakami¹, Kenji Kisoda², Masanori Yamaguchi², and Chihiro Itoh¹

¹Department of Materials Science and Chemistry, Wakayama University, Wakayama 640-8510, Japan

²Faculty of Education, Wakayama University, Wakayama 640-8510, Japan

While properties of single-walled carbon nanotubes (SWNTs), the synthesis of SWNT involves consumption of fossil fuels and emission of large amount of carbon dioxide. This is one of the reasons of high cost of SWNTs. One of the ideas to resolve these problems is use of bioethanol as a carbon source. In this report, we have demonstrated the synthesis of SWNT from woody bioethanol and characterized the woody SWNTs by Raman scattering spectroscopy.

The woody bioethanol was produced by hydrolysis of wood chips using sulfuric acid, and subsequent fermentation of glucose.[1] The bioethanol thus obtained had an ethanol concentration of 5 vol%. Chemical vapor deposition (CVD) of SWNT was carried out using the as-synthesized bioethanol as the carbon source with Co/a-SiO₂ catalysts. We also synthesized SWNT by typical CVD using high-grade ethanol and 5 vol%-ethanol aqueous solution for comparison. The samples were characterized by Raman measurement with a probe laser of 532 nm.

In Fig. 1, we show the Raman spectra of the SWNT obtained from woody bioethanol, together with the spectra of SWNTs obtained from high-grade ethanol and its 5% aqueous solution. The spectrum of the woody bioethanol clearly shows G band and Radial breathing mode (RBM), indicating that SWNTs were grown by woody bioethanol. The low S/N spectrum indicates SWNT yield was low. The relative intensity of G band to D band, which is a measure of the quality of SWNT, was ~15. Based on the analysis of RBM frequency, we showed that most of the woody SWNTs obtained in the present study had the diameter of 0.9 nm. This characteristic is similar to the tubes grown with 5%-ethanol solution, in contrast to the SWNT obtained by CVD with high-grade ethanol where the dominant tube had the diameter of 1.1 nm. The diameter reduction of the SWNT is conceivably attributed to water vapor etching of tubes during the CVD process. In detail, the distribution of RBM of the woody SWNT is different from SWNTs obtained from 5%-ethanol solution. This difference may be ascribed to the effects by impurities in refined woody bioethanol. The impurity originated from wood has a possibility of changing SWNT properties, so further detail analyses are required.

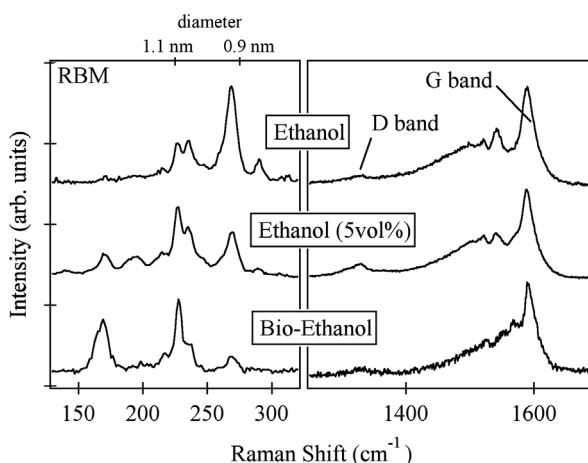


Fig.1 Raman spectra of grown samples

[1] M.Yamaguchi, et. al., Society of Japan Science Teaching, Kinki branch (Kyoto), P-2, 2010.

Corresponding Author: T. Araki, Tel: +81-73-457-8532, E-mail: s143001@center.wakayama-u.ac.jp

Nitrogen doping of single-walled carbon nanotubes prepared from fluorinated SWCNTs using ammonia gas

○Koji Yokoyama¹, Yoshinori Sato², Kazutaka Hirano², Kenichi Motomiya¹, Kazuyuki Tohji¹, Yoshinori Sato^{1,3,*}

¹ Graduate School of Environmental Studies, Tohoku University, Sendai 980-8579, Japan

² Stella Chemifa Co., Osaka 595-0075, Japan

³ Institute for Biomedical Sciences, Interdisciplinary Cluster for Cutting Edge Research, Shinshu University, Matsumoto 390-8621, Japan

Nitrogen doping of single-walled carbon nanotubes (SWCNTs) plays a significant role as a means to control their electronic density of states and carrier transport properties. The methods of nitrogen doping are classified into two categories: “direct-synthesis doping” and “post-synthesis doping”. Although a number of direct-synthesis nitrogen doping methods for SWCNTs have hitherto been studied, it is difficult to control the number of nitrogen atoms and retain the crystallinity of nanotube framework. In contrast, little post-synthesis doping has been reported until now. In addition, these methods require high temperature (>1000 K), and the nitrogen contents of the resulting samples were low (<1.0 at.%). These are considered to be due to the low reactivity of SWCNT surface. Here, we report a new facile method for synthesizing nitrogen doped SWCNTs by the reaction of fluorinated SWCNTs (F-SWCNTs) with ammonia gas.

We prepared F-SWCNTs by fluorination of highly crystalline SWCNTs (hc-SWCNTs) synthesized by a direct current arc discharge, using a mixture of F₂ (20%) and N₂ (80%). 10 mg of F-SWCNTs placed into a reactor tube reacted with flowing a mixture of NH₃ (1%) and N₂ (99%) at the temperature range of 298-873 K for 30 min. The resulting samples were characterized using X-ray photoelectron spectroscopy (XPS), high-resolution transmission electron microscopy (HRTEM), and Raman scattering spectroscopy.

The XPS survey spectra of the samples after ammonia gas reaction revealed that nitrogen atoms were introduced into the SWCNTs at all reaction temperatures, and the maximum nitrogen content was estimated to be 3.0 at.% at 673 K (Fig. 1). The XPS spectra of N_{1s} region showed the SWCNTs had pyridinic, pyrrolic, and graphitic nitrogen atoms. We will report the detailed characterization in this presentation.

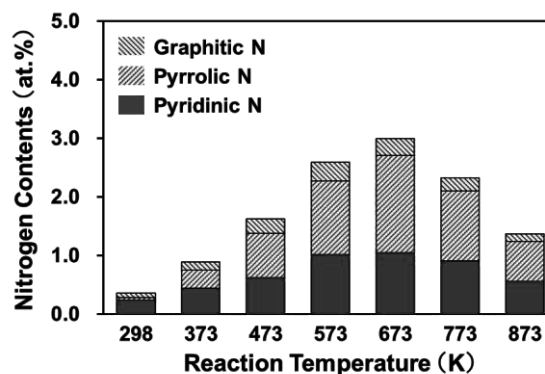


Fig. 1 Nitrogen contents and composition of the samples reacted at various reaction temperatures measured by XPS.

*Corresponding Author: Yoshinori Sato
Tel: +81-22-795-3215, Fax: +81-22-795-3215,
E-mail: hige@ncsimd.kankyotohoku.ac.jp

Molecular Dynamic Simulation of Defect Free Growth of Single-Walled Carbon Nanotube

○Ryo Yoshikawa, Yukai Takagi, Shohei Chiashi and Shigeo Maruyama

Department of Mechanical Engineering, The University of Tokyo, Tokyo 113-8656, Japan

Good atomic scale simulation is anticipated for understanding the growth mechanism of single-walled carbon nanotubes (SWNTs). Often molecular dynamics (MD) simulations are employed [1]. However, it has been difficult to simulate the growth of SWNTs whose chirality can be clearly assigned. The high-quality (defect-free) SWNTs in MD simulation are desired for analyzing the relation between detailed SWNT structures and simulation conditions (temperature, gas carbon density, and catalyst metal species).

We prepared cobalt cluster with 40-60 atoms in a periodic cell ($10 \times 10 \times 10 \text{ nm}^3$, 1300-1600 K), and carbon atoms were supplied to the cell keeping one free carbon atom which are not connected to other carbon atoms or metal atoms. The interaction between carbon and metal atoms is expressed by our home-made Tersoff-type potentials [2].

After carefully adjusting growth parameters, defect-free SWNT was successfully obtained. Figure 1(a) shows image of a defect-free SWNT, whose chirality is assigned to (14, 1). In order to investigate the growth process in detail, we made unwrapped projection view of the grown SWNT (Fig. 1(b)). The pentagonal and heptagonal rings appeared just only on the cap part, and the atomic structure of the side wall part is fully composed of hexagonal rings. Whole edge part of the SWNT connecting with the catalyst was found to be zigzag structure except for a one kink. There are several carbon chains connected to zigzag tops. The carbon chains formed hexagonal rings and then the SWNT grew up. In addition to the growth mechanism based on the time evolution of hexagonal ring generation, cap formation mechanism in the earlier stage will be discussed.

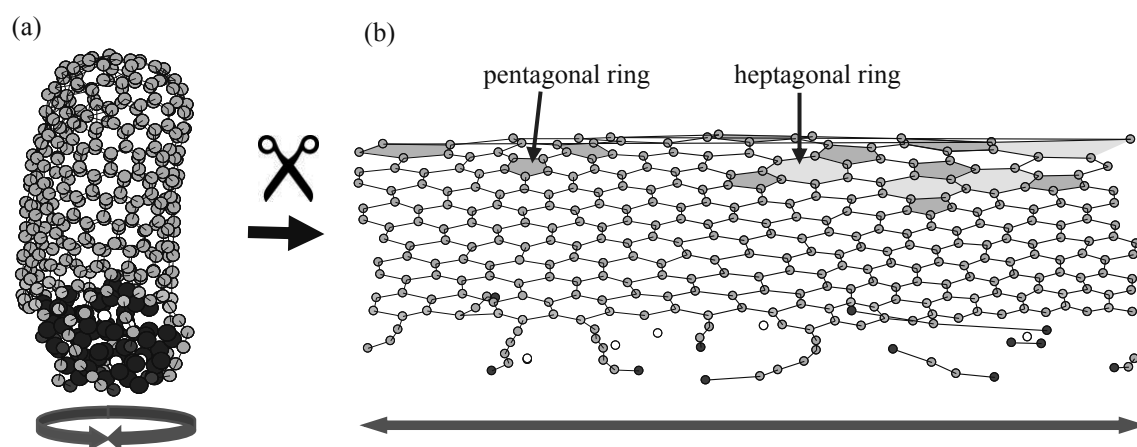


Fig. 1(a) Structure of SWNT grown from Co_{60} catalyst, which has (14, 1) chirality.
(b) Developed diagram view of the (14, 1) SWNT.

[1] Y. Shibuta and S. Maruyama, *Chem. Phys. Lett.*, **382** (2003) 381.

[2] T. Matsuo et al., to be submitted.

Corresponding Author: Shigeo Maruyama

Tel: +81-3-5841-6421, Fax: +81-3-5800-6983,

E-mail: maruyama@photon.t.u-tokyo.ac.jp

Automatic Gradient Elution Gel Filtration for Separation of Metal and Semiconducting Single-Wall Carbon Nanotubes

○Boanerges Thendie¹, Haruka Omachi¹, Ryo Kitaura¹, Yasumitsu Miyata^{2,3},
and Hisanori Shinohara¹

¹Department of Chemistry and Institute of Advanced Research, Nagoya University, Nagoya, 464-8602, Japan

²Department of Physics, Tokyo Metropolitan University, Tokyo, 192-0397, Japan

³JST, PRESTO, Tokyo, 102-0075, Japan

Semiconducting single wall carbon nanotubes (s-SWCNTs) are attractive materials for electronic devices. However, conventional as-grown carbon nanotubes contain mixture of metallic (m-SWCNTs) and s-SWCNTs. Hence, separation is required to attain high purity s-SWCNTs. In the past 5 years, our group have developed recycling gel filtration to obtain high-purity s-SWCNTs [1]. We have also demonstrated that simultaneous electronic-type and length-based separation of s-SWCNTs can be attained by a simple fractionation method [2].

In the present work, we introduce “automatic gradient elution” (AGE) of gel filtration. In AGE system, two different solution of surfactant: sodium dodecyl sulfate (SDS) and sodium cholate (SC) are mixed to obtain different elution composition over time. Gradual change of the elution composition allows remaining m- and s-SWCNTs to be eluted separately, increasing the purity of s-SWCNTs. We also observed diameter-based separation by using AGE system.

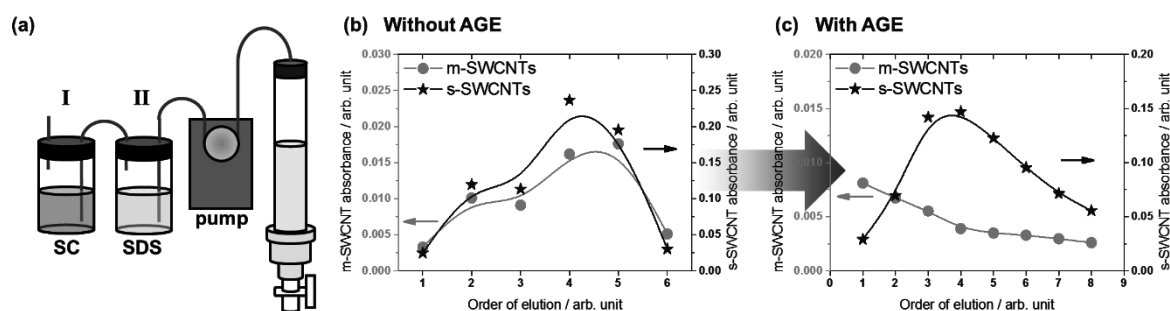


Fig. 1 (a) schematic of the AGE system: SC and SDS are mixed in chamber II before entering column. Absorbance of m- and s-SWCNTs vs elution order for gel filtration (b) without AGE and (c) with AGE. Without AGE, remaining m- and s-SWCNTs eluted concurrently while in the AGE system, m- and s-SWCNTs eluted separately.

[1] Y. Miyata *et al.* Nano Res. **4**, 963 (2011)

[2] B. Thendie *et al.* Appl. Phys. Express **6**, 065101 (2013)

Corresponding author: Hisanori Shinohara

Tel: (+81) 52-789-2482, **Fax:** (+81) 52-747-6442, **E-mail:** noris@nagoya-u.jp

Facile sorting and release of semiconducting single-walled carbon nanotubes based on dynamic formation of supramolecular polymers

Fumiyuki Toshimitsu¹, Naotoshi Nakashima^{1, 2, 3}

¹ Department of Applied Chemistry, Kyushu University, Fukuoka 819-0395, Japan

² WPI-F²CNER, Kyushu University, Fukuoka 819-0395, Japan

³ JST-CREST, Chiyoda-ku, Tokyo 102-0075, Japan

Highly purified single-walled carbon nanotubes (SWNTs) are essential for fundamental studies and applications, however, they are produced as mixtures of semiconducting- and metallic-SWNTs. Full utilization of the unique optical and electrical properties of semiconducting-SWNTs (sem-SWNTs) would be exhibited only when they are separated from poisoning metallic-tubes. One of the key techniques for SWNT-chirality sorting is wrapping method by conjugated polymers such as polyfluorenes.^[1, 2] Selective extraction of the sem-SWNTs using such polymers is simple and powerful, however, removal of them from the extracted sem-SWNT surfaces is difficult due to the strong multi-point interactions between the polymers and the SWNTs. In addition, the preparation of these synthetic polymers is usually complicated.

In order to address these problems simultaneously, we have developed detachable solubilizer systems based on a supramolecular approach. We have previously reported that coordination polymers of phenanthroline-capped fluorene (Fig. 1, **1**) and various metal ions extracted sem-SWNTs selectively.^[1] We here report that the alternative non-covalent bond formation, hydrogen-bond polymerization using various conjugated monomers (Fig. 1, **2-6**) are examined for the solubilization/separation of sem-SWNTs. All the used compounds are confirmed to form one-dimensional polymers just by mixing with each complementary, which was confirmed using NMR technique. Solubilization of SWNTs by using these polymers were screened by atomic force microscopy, photoluminescence, and Vis-NIR absorption and Raman spectroscopic analysis, and was found that only the polymers of **2** and **3** acted as sem-SWNT solubilizers, in which both components possess fluorene moiety. Molecular-mechanics calculations was employed to visualize the difference of interactions between these supramolecular polymers and sem-SWNTs. Furthermore, the reversible bond formation and depolymerization by an outer stimulus, such as an addition of acid, change in pH or temperature was examined to remove the polymers from sem-SWNTs, resulting the finding that even a simple washing with solvents worked.

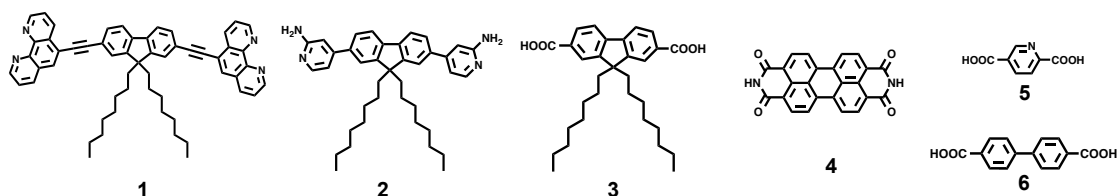


Fig. 1. Chemical structures of supramolecular polymer components.

[1] F. Chen, et al., *Nano Lett.* **2007**, 7, 3013. [2] A. Nish, et al., *Nat. Nanotech.* **2007**, 2, 640.

[3] F. Toshimitsu, N. Nakashima, *Nat. Commun.* **2014**, 5, 5041.

Corresponding Author: N. Nakashima

Tel: +81-92-802-2845, Fax: +81-92-802-2845;

E-mail: nakashima-tcm@mail.cstm.kyushu-u.ac.jp

Structural transformation of tellurium encapsulated in the inner space of carbon nanotubes depending on tube diameter

○Keita Kobayashi¹, Hidehiro Yasuda^{1,2}

¹ *Research Center for Ultra-High Voltage Electron Microscopy, Osaka University, Ibaraki, Osaka 567-0047, Japan*

² *Division of Materials and Manufacturing Science, Graduate School of Engineering, Osaka University, Suita, Osaka 565-0871, Japan*

Some materials encapsulated in the confined inner space of carbon nanotubes (CNTs) show anomalous structures compared with their bulk phases. For example, some chalcogens (sulfur and selenium) encapsulated in CNTs with a diameter of ~ 1 nm show linear, zigzag, and helical structures [1, 2]. Moreover, the anomalous structures tend to depend on the inner diameter of the CNTs. Because anomalous structures can produce novel physical properties, determining the relationship between the size of the confined nanospace and structure of the material is important for developing novel nano devices.

In this study, we aimed to clarify the relation between CNT diameter and the structure of encapsulated chalcogens by analyzing tellurium encapsulated in CNTs of various inner diameters.

Transmission electron microscopy showed that tellurium adopts a double helix structure in CNTs of less than ~ 2 nm in diameter (Fig. 1). The tellurium structure was also confirmed by electron diffractometry of a bundle of CNTs and by Raman spectroscopy. In contrast, the tellurium in CNTs with a diameter greater than ~ 2 nm had an ordinary crystal structure.

According to previous theoretical studies [3], guest materials encapsulated in CNTs tend to be located off center near the CNT wall because of the interaction between the guest material and CNT wall [3]. The interaction decreases as the inner diameter of CNTs increases; therefore, the guest materials encapsulated in larger diameter CNTs tend to aggregate in the center of the inner space.

Based on our experimental results and previous theoretical studies, we conclude that the structure of tellurium encapsulated in CNTs is determined by competition between the interaction and lattice energy of tellurium aggregated in the center. Although the details of the formation mechanism for the double helix structure remains unclear, our hypothesis well explains the diameter dependency of the structure of tellurium encapsulated in CNTs.

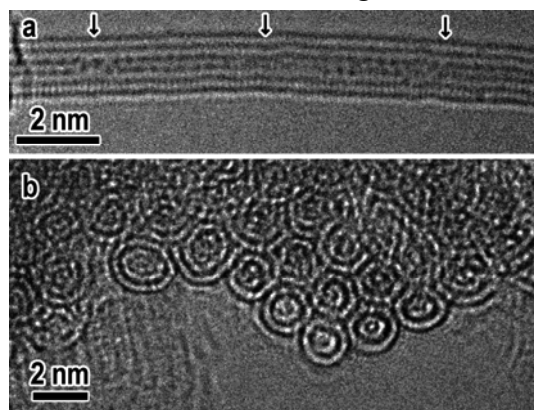


Fig.1 (a) Typical TEM images of Te encapsulated in double-wall (DW) CNTs. Arrow heads indicate crossing section of Te chain attributed to double-helix structure. (b) Cross section TEM image of Te encapsulated in DWCNTs.

[1] T. Fujimori *et al.*, *Nature Commun.* **4**, 2162 (2013).

[2] T. Fujimori *et al.*, *ACS Nano* **7**, 5607 (2013).

[3] M. Wilson, *Chem. Phys. Lett.* **366**, 504 (2002).

Corresponding Author: K. Kobayashi

Tel: +81-6-6879-7941, Fax: +81-6-6879-7942, E-mail: kobayashi-z@uhvem.osaka-u.ac.jp

Synthesis of Diamantane Chains inside Carbon Nanotubes from Bridgehead-halogenated Diamantane

○Yusuke Nakanishi,¹ Haruka Omachi,¹ Natalie A. Fokina,² Ryo Kitaura,¹ Peter R. Schreiner,² Jeremy E. P. Dahl,³ Robert M. K. Carlson,³ and Hisanori Shinohara¹

¹Department of Chemistry, Nagoya University, Nagoya 464-8602, Japan.

²Institute of Organic Chemistry, Justus-Liebig University, Heinrich-Buff-Ring 58, 35392 Giessen, Germany.

³Institute for Materials and Energy Science, Stanford University, Stanford, California 94305, United State.

Over the past decade, we have developed a synthetic methodology for one-dimensional (1D) nanomaterials utilizing the cavities of carbon nanotubes (CNTs), in which encapsulated species are molded into 1D nanostructure *via* thermal annealing. To date, various kinds of 1D nanomaterials have been synthesized, including metal atomic wires,¹ ultrathin boron-nitride nanotubes,² and well-defined CNTs,³ which exhibit different properties from those of their bulk counterparts. As part of our exploring for novel 1D nanomaterials, we have studied the synthesis of 1D diamond-shaped materials from diamondoids, the molecules in the diamond configuration.^{4,5}

Here we report the synthesis of diamondoid chains from bridgehead-halogenated diamantane (a kind of diamondoids) within the inner spaces of CNTs. The sublimed precursors undergo dehalogenation to form the diamantane radicals, which subsequently link up to produce the polymer chains. Using experimental and theoretical techniques, we revealed that the diamantane skeletons were linked with each other inside CNTs. Our synthesis of this new class of diamond nanomaterials might offer a new direction for the nano-diamond research as well as a new strategy for the design and synthesis of 1D nanomaterials.

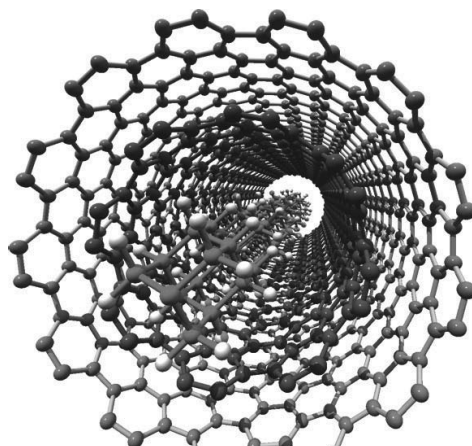


Fig.1 Structural model of a diamantane chain formed inside double-walled CNTs.

- [1] R. Kitaura *et al. Nano Lett.*, 8, 693, (2008).
 [2] R. Nakanishi *et al. Sci. Rep.*, 3, 1385, (2013).
 [3] H. E. Lim *et al. Nat. Commun.*, 4, 2548, (2013).
 [4] J. Zhang *et al. ACS Nano*, 6, 8674, (2012).
 [5] J. Zhang *et al. Angew. Chem. Int. Ed.*, 125, 3805, (2013).

Corresponding Author: H. Shinohara

Tel: +81-52-789-2482, Fax: +81-52-747-6442,

E-mail: noris@nagoya-u.ac.jp

A Computational Study on Properties of Multimeric π Conjugated Oligomers inside Carbon Nanotubes

○Takashi Yumura¹, Hiroki Yamashita¹

¹ Department of Chemistry and Materials Technology, Kyoto Institute of Technology, Matsugasaki, Sakyo-ku, Kyoto, 606-8585, Japan

We have investigated the arrangements of π conjugated oligomers inside a nanotube by using density functional theory (DFT) including dispersion corrections (B97D functional). Previously, we discussed methyl-terminated ter-thiophene oligomers inside a nanotube, and found that nanotube confinement has a strong impact on determining arrangements of the inner ter-thiophene chains [1]. Recently, oligofurans with various chain lengths have been successfully synthesized [2]. However, the oligofurans readily degrade when they are exposed to a combination of light and dioxygen. If oligofurans can be encapsulated into a nanotube, similar to the thiophene oligomer cases [3], inner oligomers would be stable due to preventing dioxygen from attacking them. Along our expectation, we extended our DFT studies to focus on multimeric oligofuran chains inside a nanotube. The current study aims at obtaining electronic properties of multimeric oligofuran inside a nanotube whose diameter ranges from 10.9 to 13.7 Å, and then we compared the results with the thiophene cases. DFT calculations indicated a variety of arrangements of multimeric ter-furan chains, depending on host-tube diameters and the number of chains. In terms of stacking fashions, we found a difference between the inner furan and thiophene oligomers as shown in Figure 1 displaying π conjugated dimer inside a nanotube with a diameter of 10.9 Å. In fact, the inner oligofurans slide significantly along the long chain axis as well as along the short chain axis, whereas the inner oligothiophenes slightly slide along the long chain axis. Because of the different inner arrangements, the oligomer chains interact differently. The interchain interactions, which split frontier orbitals of the multimeric chains, are responsible for changing electronic properties of inner π conjugated oligomers. Therefore, our DFT calculations found that nanotubes have power to modulate the electronic properties of inner π conjugated oligomers, depending on types of oligomer.

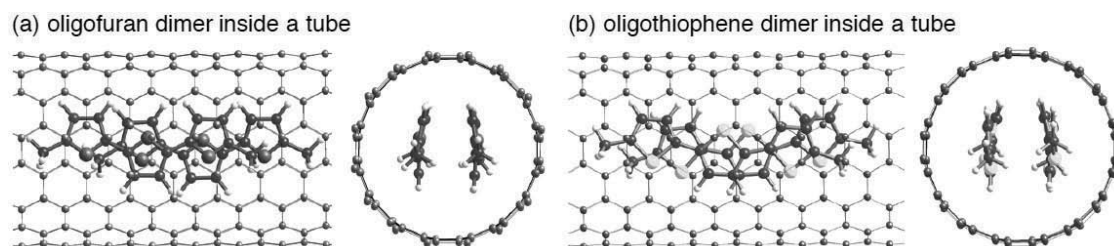


Fig. 1 B97D-optimized structures for tubes containing (a) oligofuran dimer and (b) oligothiophene

[1] (a) H. Yamashita *et al.*, J. Phys. Chem. C **116**, 9681 (2012). (b) T. Yumura *et al.*, J. Phys. Chem. C **118**, 5510 (2014).

[2] (a) O. Gidron *et al.*, J. Am. Chem. Soc. **132**, 2148 (2010). (b) O. Gidron *et al.*, Angew. Chem. Int. Ed. **53**, 2546 (2014).

[3] (a) M. A. Loi *et al.*, Adv. Mater. **22**, 1635 (2010). (b) L. Alvarez *et al.*, J. Phys. Chem. C **115**, 11898 (2011).

Corresponding Author: Takashi Yumura

Tel: +81-75-724-7571, Fax: +81-75-724-7571, E-mail: yumura@kit.ac.jp

Growth Dynamics of Single-Layer Graphene on Epitaxial Cu Surfaces

○Y. Ohta,¹ S. Mizuno,¹ H. Hibino,³ K. Kawahara,¹ R. Takizawa,¹ M. Tsuji,^{1,2} and H. Ago^{1,2,4}

¹Graduate School of Engineering Sciences, Kyushu University, Fukuoka 816-8580, Japan

²Institute for Materials Chemistry and Engineering, Kyushu University, Fukuoka 816-8580, Japan

³NTT Basic Research Laboratory, NTT Corporation, Kanagawa 243-0198, Japan

⁴PRESTO, Japan Science and Technology Agency, Saitama 332-0012, Japan

Graphene has attracted a great deal of interest because of its unique properties, which promise applications in electronics and related fields. Recently, chemical vapor deposition (CVD) using Cu catalyst is widely used to grow large-area, single-layer graphene (SLG) due to self-limiting mechanism [1]. Considering relatively low melting temperature of Cu (1083 °C), it is interesting to investigate the growth dynamics of graphene at typical CVD temperatures, 1000-1075 °C [2-5], which are close to the Cu melting temperature. As the large single-crystalline graphene domains are grown at high temperatures, it also helps us to develop a method to grow giant graphene domains on Cu surface.

In this work, we report a systematic study on the domain structure and the orientation of SLG grown on epitaxial Cu(111) surface. We obtained hexagonal graphene domains with the lateral size of 10-100 μm, which increases with increasing the CVD temperature ($E_a \approx 4.5$ eV), while the domain density decreased with the temperature. These results suggest that higher CVD temperature enhances surface diffusion of carbon intermediate on the Cu(111) surface and also promotes the catalytic decomposition of CH₄ feedstock. The orientations of graphene sheets were studied by low-energy electron diffraction (LEED). When SLG was synthesized at 900~1020 °C, six sharp diffraction spots were observed, as shown in Fig. 1a, consistent with our previous work [2-4]. However, when we increased the temperature to 1050 °C, the diffraction spots were rotated by 2-3° from the original spots (Fig. 1b). Higher CVD temperature (1070 °C) resulted in a ring-like streak pattern together with six diffraction spots (Fig. 1c), indicating mis-orientation of graphene domain due to thermal fluctuation of the surface Cu(111) lattice. Such effect was more clearly observed for the epitaxial Cu(100) film. We will also present transport properties of the SLG sheets having different domain sizes and orientations grown on Cu(111) and Cu(100) films.

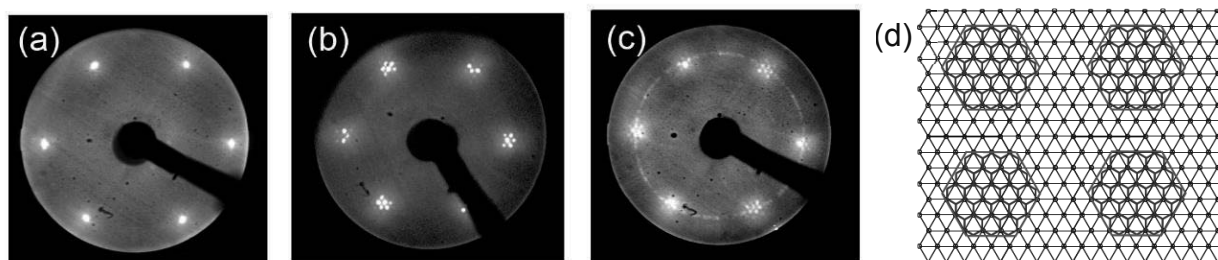


Figure 1 LEED patterns of SLG/Cu(111) at 1000 (a), 1050 (b), and 1070 °C (c). (d): Atomic model of hexagonal graphene domains grown on the Cu(111) surface at 1000 °C.

References: [1] X. Li *et al.*, *Science*, **324**, 1312 (2009). [2] H. Hu *et al.*, *Carbon*, **50**, 57 (2012). [3] C. M. Orofeo *et al.*, *Carbon* **50**, 2189 (2012). [4] Y. Ogawa *et al.*, *J. Phys. Chem. Lett.*, **3**, 219 (2012). [5] H. Ago *et al.*, *Appl. Phys. Exp.*, **6**, 75101 (2013).

Corresponding Author: Hiroki Ago (Tel & Fax: +81-92-583-7817, E-mail: ago@cm.kyushu-u.ac.jp)

Preparation of Small-Sized Nano-Graphene Oxide for Biological Application

○Minfang Zhang¹, Toshiya Okazaki¹, Yoko Iizumi¹, Eijiro Miyako¹, Sumio Iijima^{1,2}, Masako Yudasaka¹

¹*Nanotube Research Center, National Institute of Advanced Science and Technology (AIST),*

²*Faculty of Science & Technology, Meijo University*

Because of their interesting electronic, thermal, mechanical and optical properties, graphene and graphene oxide (GO) have been considered to be useful in various fields, such as advanced electronics, membranes engineering, and medicines, for example, drug delivery system and cellular imaging [1]. Recently, the small sized graphene-sheets (GS) with polyethylene glycol coating showed ultrahigh *in vivo* tumor uptake and high efficiency of photo-thermal therapy [2]. However, GS and GO samples obtained so far are typically microns or larger in size which limited their developments in biological applications. Although the small-sized GS or GO can be obtained by size-separation using density gradient centrifugation [1-2], preparation of the small-sized GS or GO with large quantity is still a challenge.

To get small-sized GO, we used carbon nanohorns (CNHs) as start materials, and prepared GO (CNH-GO) by an oxidation exfoliation method similar to the Hummers method [3] in which graphite is commonly used. The obtained CNH-GO had unique characteristics comparing with those so far obtained. They had uniformly small sizes of about 10 nm, high solubility in aqueous solutions and in most of the organic solvents, and strong fluorescence. They had abundant oxygenated functional groups on the surface, therefore easily modified. It should be especially emphasized that CNH-GO could be prepared in a large quantity without using any surfactant for separation. All these superior characteristics suggest that CNH-GO is a promising material for biological and medicine applications. As an example, we have used CNH-GO to conjugate with immunoglobulin G (IgG) antibodies for an immunoassay. The results showed that CNH-GO conjugated IgG was successfully immunoprecipitated with protein G-attached magnetic beads. The CNH-GO conjugates eluted from beads also had strong fluorescence, indicating their potential as fluorescence labels in immunoassay.

[1]. X. Sun, Z. Liu, K. Welsher, J. Robinson, A. Goodwin, S. Zaric, H. Dai. *Nano Res.* **1**, 203(2008).

[2]. K. Yang, S. Zhang, G. Zhang, X. Sun, S. Lee, Z. Liu. *Nano Lett.* **10**, 3318 (2010).

[3]. W. S. Hummers, R. E. Offeman. *J. Am. Chem. Sci.* **80**, 1339 (1958)

Corresponding Authors: M. Zhang, M. Yudasaka

E-mail: m-zhang@aist.go.jp, m-yudasaka@aist.go.jp

Direct transfer of CVD graphene to insulating substrates by metal melting

○Ryosuke Inoue¹, Yutaka Maniwa¹, Yasumitsu Miyata^{1,2}

¹Department of Physics, Tokyo Metropolitan University, Hachioji, 192-0397, Japan

²JST, PRESTO, Kawaguchi, 332-0012, Japan

Chemical vapor deposition (CVD) has been a widely used technique for the growth of large-area, uniform monolayer graphene films. Generally, CVD graphene is grown on metal substrates such as Cu and Ni foil, and thus requires a post-growth transfer process of graphene films from metal substrates to insulating substrates for electronics applications [1]. Conventional transfer process includes polymer coating to support graphene films during etching Cu foil, and polymer washing by organic solvent. In this process, however, there are several issues such as remaining polymer and time-consuming multiple processes. Therefore, the development of polymer-free, direct transfer process is still highly desired for improving the processes and properties of CVD graphene.

Here, we report a facile, direct transfer process of CVD graphene using metal melting. First, Cu foil was put on insulating substrates such as SiO₂ and sapphire, and then graphene was grown by atmospheric CVD with methane at 1075 °C. After the growth, the furnace temperature was increased to 1150 °C to melt Cu foil on the substrates. During the melting, graphene films were directly transferred to the substrates. Optical microscopy image and Raman spectrum clearly show the presence of hexagonal-shaped graphene with negligible D-band intensity on the substrate (Figs. 1a,b). Moreover, typical ambipolar behaviors are observed in a graphene-based electrical double-layer transistors (EDLT) (Fig. 1c). In the poster, the details of the direct transfer process and properties of graphene will be presented.

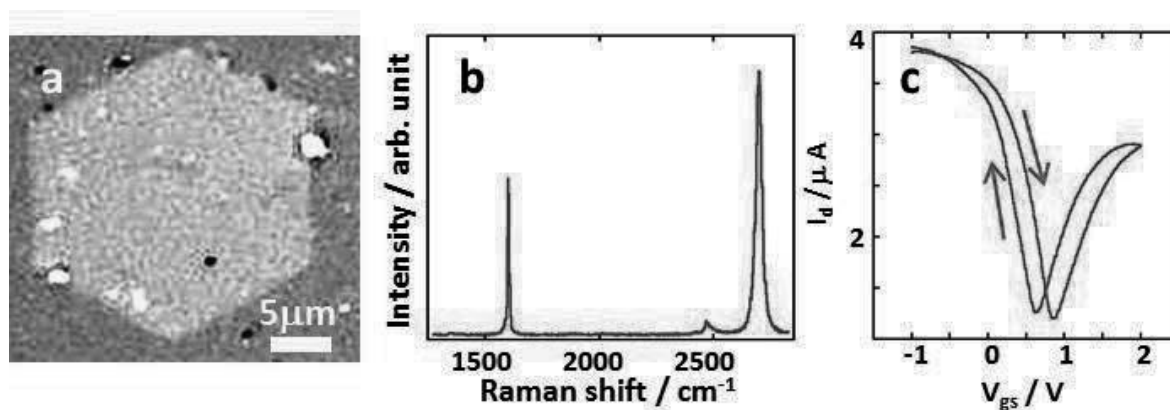


Fig.1 (a) Optical microscope image and (b) Raman spectrum of a hexagonal-shaped graphene single crystal on a quartz substrate. (c) I_d - V_{gs} curve of a graphene-based EDLT.

[1] X. Li, *et al.*, Science **324**, 1312 (2009).

Corresponding Author: Yasumitsu Miyata

TEL:+81-42-677-2508,FAX:+81-42-677-2483,

E-mail: ymiyata@tmu.ac.jp

Vibronic Coupling Density as a Reactivity Index: Applications for Diels-Alder Reactions of Graphene Fragments

Naoki Haruta¹, ○ Tohru Sato^{1,2}, Kazuyoshi Tanaka¹

¹*Department of Molecular Engineering, Graduate School of Engineering, Kyoto University, Kyoto, 615-8510, Japan*

²*Unit of Elements Strategy Initiative for Catalysts & Batteries, Kyoto University, Nishikyo-ku, Kyoto 615-8510, Japan*

Graphene fragments with different structures have been extensively studied because of their applications in the field of material chemistry [1,2]. To develop novel graphene fragments, theoretical prediction of the reactivities would be helpful. The frontier orbital theory is one of the most successful theories for such a theoretical prediction. However, it sometimes fails to predict the regioselectivities of large molecules because frontier orbitals tend to be delocalized. Recently we have proposed the concept of vibronic coupling density (VCD) as a reactivity index [3,4]. The VCD theory is based on not only electronic states but also molecular deformations. This is in contrast to the frontier orbital theory in which only electronic states are considered. The VCD theory has succeeded in explaining the regioselectivities of fullerenes whose frontier orbitals are delocalized[4-6].

In this study, we investigated the regioselectivities of perylene (C₂₀H₁₂), bisanthene (C₂₈H₁₄), and tribenzoperylene (C₃₀H₁₆) with the VCD theory [7]. According to experimental works by Clar *et al.* [8,9], Diels-Alder reactions of maleic anhydride to perylene, bisanthene, and tribenzoperylene yield larger graphene fragments, coronene (C₂₄H₁₂), ovalene (C₃₂H₁₄), and dibenzocoronene (C₃₂H₁₆). The VCD analysis clearly shows that the reactive sites of perylene and bisanthene, which are the bay regions with arm-chair edges, have butadiene-like VCD distributions. This is consistent with experimental observations that perylene and bisanthene, just like butadiene, react with dienophiles. We will present the VCD analyses for the consecutive cycloadditions to perylene and bisanthene as well. In addition, tribenzoperylene will be also discussed. Since it has four different types of bay regions, its regioselectivity is of interest.

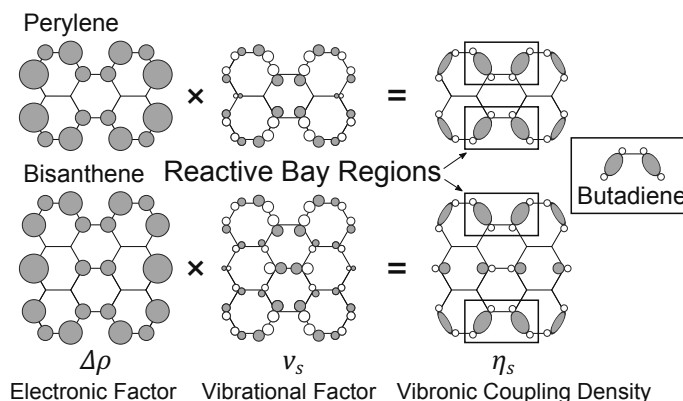


Fig. 1: Vibronic coupling density analyses for perylene (C₂₀H₁₂) and bisanthene (C₂₈H₁₄).

[1] J. Wu *et al.*, Chem. Rev. **107**, 718 (2007). [2] O. V. Yazyev *et al.*, Rep. Prog. Phys. **73**, 056501 (2010). [3] T. Sato *et al.*, J. Phys. Chem. A **112**, 758 (2008). [4] T. Sato *et al.*, Chem. Phys. Lett. **531**, 257 (2012). [5] N. Haruta *et al.*, J. Org. Chem. **77**, 9702 (2012). [6] N. Haruta *et al.*, J. Org. Chem. **80**, 141 (2015). [7] N. Haruta *et al.*, Tetrahedron Lett. **56**, 590 (2015). [8] E. Clar and M. J. Zander, J. Chem. Soc. 4616 (1957). [9] E. Clar, Nature **161**, 238 (1948).

Corresponding Author: T. Sato

Tel: +81-75-383-2803, Fax: +81-75-383-2555

E-mail: tsato@moleng.kyoto-u.ac.jp

Growth of high-quality monolayer WS₂ on graphite

○Yu Kobayashi¹, Shogo Sasaki, Shohei Mori¹, Hibino Hiroki², Kenji Watanabe³,
Takashi Taniguchi³, Yutaka Maniwa¹, and Yasumitsu Miyata^{1,4,*}

¹*Department of Physics, Tokyo Metropolitan University, Hachioji, 192-0397, Japan*

²*NTT Basic Research Laboratories, NTT Corporation, Atsugi, Kanagawa 243-0198, Japan*

³*National Institute for Materials Science, Tsukuba, Ibaraki 305-0044, Japan*

⁴*JST, PRESTO, Kawaguchi, 332-0012, Japan*

Atomic-layer transition metal dichalcogenides (TMDCs) have attracted appreciable interest due to their tunable bandgap, spin-valley physics, and potential device applications. In recent years, many studies have been reported for the growth of high-quality TMDCs, mainly using chemical vapor deposition (CVD) and metal-film sulfurization.[1-3] Monolayer WS₂ grown by CVD on hexagonal boron nitride (hBN) was very recently reported to exhibit a photoluminescence (PL) peak with a relatively narrow full width at half maximum (FWHM) of 26 meV and a weak asymmetric profile.[1] Considering monolayer growth on commonly-used substrates such as SiO₂/Si and sapphire, this clearly indicates that the growth substrate is one of the essential factors for reducing charged impurities and structural defects.

Here, we report on the CVD growth of high-quality, monolayer WS₂ onto exfoliated graphite. Unlike commonly-used substrates such as SiO₂/Si and sapphire, monolayer WS₂ grown on graphite presents a uniform, single excitonic PL peak with a Lorentzian profile and a very small full-width at half maximum (FWHM) of 8 meV, whereas WS₂ grown on SiO₂/Si has a broad FWHM of 48 meV at 79 K (Fig.1).

Furthermore, no additional peaks are observed for charged and/or bound excitons, even at low temperature. These results indicate that the cleaved graphite surface is an ideal substrate for the growth of high-quality, non-doped TMDCs, and such samples will be essential for revealing intrinsic physical properties and for future applications.

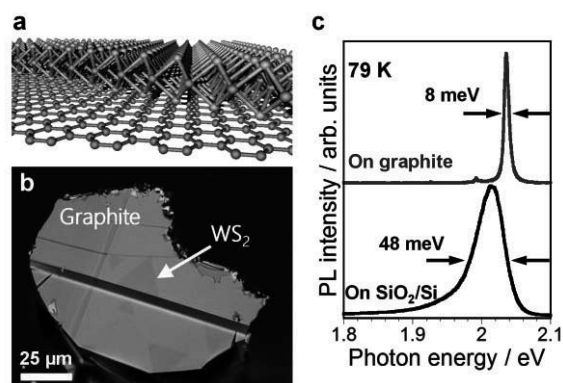


Fig.1 (a) Structure model and (b) optical image of WS₂ grown on graphite. (c) PL spectra of WS₂ on graphite and SiO₂/Si substrates at 79 K.

[1] M. Okada, et al., ACS Nano 8 (2014) 8273.

[2] Y. -H. Lee et al., Adv. Mater., 24 (2012) 2320.

[3] C. M. Orofeo et al., Appl. Phys. Lett., 105 (2014) 083112.

Corresponding Author: Yasumitsu Miyata, Tel: 042-677-2508, E-mail: ymiyata@tmu.ac.jp

Amplitude modulation of optical field by arm-chair graphene nanoribbons: A First-principles Study

○Yoshiyuki Miyamoto¹, Hong Zhang²

¹ *Nanosystem Institute of National Institute of Advanced Industrial Science and Technology (AIST), Central 2, Umezono 1-1-1, Tsukuba 305-8568, Japan*

² *College of Physical Science and Technology, Sichuan University, Chengdu 610065, China*

We present modulation of optical field by graphene nano-ribbon. We have chosen semiconducting arm-chair graphene nano-ribbons as our test-cases. We here present $N=7$, $N=9$ graphene nano-ribbons with the definition of Ref. 1, which have energy gaps of 1.62 eV and 0.78 eV, respectively. Although the band-gap are so different, the optical absorption spectrum of these ribbons become similar when optical polarization vector is perpendicular to the ribbon edge and parallel to the ribbon plane as displayed in Figure 1.

We have performed real-time electron dynamics simulation of graphene nano-ribbons by using the framework of the time-dependent density functional theory[2]. We used a code [3,4] for the real-time propagation of electrons under alternating electric field that mimics optical field. Then we monitored electric field 3.34 Å above the center-line of graphene ribbon, dot-dashed line of Fig. 1. When the frequency of applied field was in UV region corresponding to absorption peak with an E-field polarization shown in Fig.1, a significant enhancement of optical field was observed which modulated in a period of 10 THz, see Fig. 2.

In this presentation, we will discuss the origin of the modulation and possible applications.

[1] Y.-W. Son, M. L. Cohen, and S. G. Louie, Phys. Rev. Lett **97**, 216803 (2006).

[2] E. Runge, and E. K. U. Gross, Phys. Rev. Lett. **52**, 997 (1984).

[3] O. Sugino and Y. Miyamoto, Phys. Rev. **B59**, 2579 (1999)

[4] Y. Miyamoto and H. Zhang, Phys. Rev. **B77**, 165123 (2008)

Corresponding Author: Y. Miyamoto

Tel: +81-29-849-1498, Fax: +81-29-861-3171,

E-mail: yoshi-miyamoto@aist.go.jp

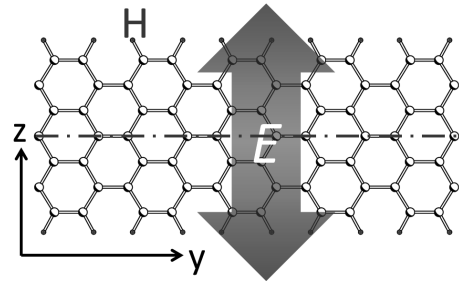


Fig.1 Structure of an arm-chair graphene nano-ribbon ($N=7$) under optical field.

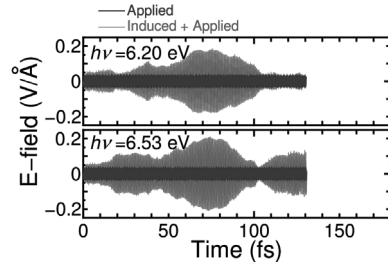


Fig. 2 Computed electric field with several optical frequencies, 3.34 Å above the central line (dot-dashed line in Fig. 1) of graphene nano-ribbon.

Spectroscopic studies of single layer molybdenum ditelluride (MoTe₂)

○Sandhaya Koirala, Daichi Kozawa, Shinichiro Mouri, Yuhei Miyauchi, Kazunari Matsuda
Institute of Advanced Energy, Kyoto University, Kyoto, Japan

Recently, atomically-thin layered materials, transition-metal dichalcogenides (MX₂; M=Mo, W, X=Se, S,) have attracted much interests from the viewpoints of fundamental physics and potential applications. The studies of transition-metal dichalcogenide (TMDs) are mainly focused on the model system of MoS₂. In contrast, molybdenum ditelluride (MoTe₂) is a member of TMDs, which shows emerging research interest due to perspective of novel optical properties. MoTe₂ is a newly studied material with a bandgap energy at 1.09 eV in the spectral range of near-infrared region [1]. However, the detail optical properties of this material have not reported so far.

In this study, we have investigated the optical properties of monolayer molybdenum ditelluride (MoTe₂) by spectroscopic studies of Raman, photoluminescence (PL) and differential reflectivity measurements. We exfoliated the monolayer and multilayers MoTe₂ on Si and quartz substrate. Figure 1(a) shows the Raman spectra of MoTe₂ with various layer thicknesses. The layer number of MoTe₂ was confirmed from Raman spectra. Figure 1(b) shows temperature dependence of PL spectra of monolayer MoTe₂. The PL spectra at room temperature (300 K) show the peak at 1.09 eV. With decreasing temperature, the PL peak is shifted towards higher energy side, shown in Fig. 1(c). Moreover, two clear peaks (1.16 and 1.19 eV) are observed at low temperature (<40 K), which are assigned as the radiative recombination of free-excitons and charged excitons (trion), respectively. We will discuss the detail information of exciton relaxation dynamics and valley-polarization dynamics of MoTe₂ during the presentation. Obtained results provide us important insights of this material.

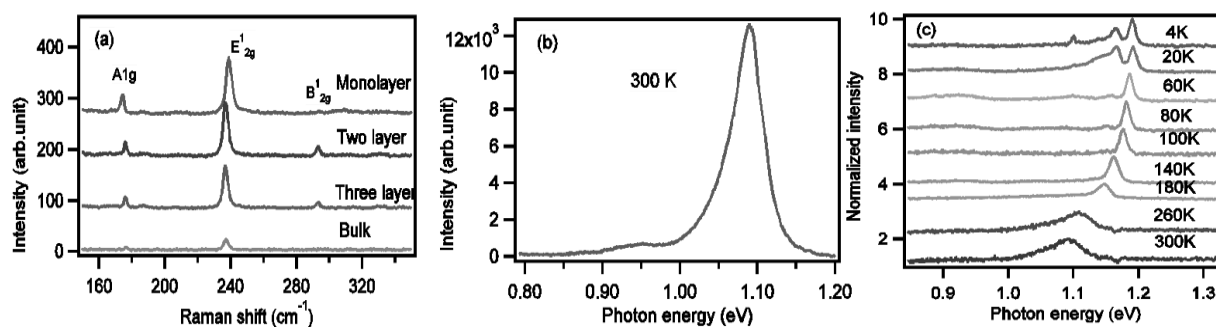


FIG.1 (a) Raman spectra of MoTe₂ with various thicknesses. (b) PL spectrum of monolayer MoTe₂ (c) Temperature dependence of PL spectra of monolayer MoTe₂.

[1] Claudia Ruppert *et al.* Nano. Lett. 14 (2014) 6231-6236.

Corresponding Author: Sandhaya Koirala,
 Tel: +81-774-38-3463,
 Fax: +81-774-38-4567,
 E-mail: sandhaya@iae.kyoto-u.ac.jp

Seebeck effect of monolayer transition metal dichalcogenides

○Kaito Kanahashi¹, Jiang Pu², Nguyen Thanh Cuong³, Lain-Jong Li⁴,
Susumu Okada³, Hiromichi Ohta⁵, Taishi Takenobu^{1,2,6}

¹ Department of Applied Physics, Waseda University, Shinjyuku 169-8555, Japan

² Department of Advanced Science and Engineering, Waseda Univ., Tokyo 169-8555, Japan

³ Graduate School of Pure and Applied Sciences, University of Tsukuba, Japan

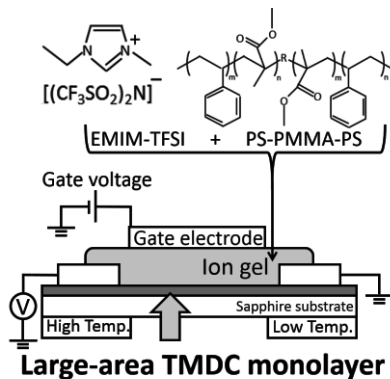
⁴ Physical Sciences and Engineering Division, KAUST, Thuwal 23955-6900, Saudi Arabia

⁵ Research Institute for Electronic Science, Hokkaido University, Sapporo 001-0020, Japan

⁶ Kagami Memorial Laboratory, Waseda University, Tokyo 169-0051, Japan

Transition metal dichalcogenides (TMDC) monolayers, such as MoS₂ and WSe₂, have attracted attention due to their graphene like structure and spin-valley coupled system. Recently, the thermoelectric properties of TMDC monolayers were measured and the extremely huge Seebeck coefficient (> 1 mV/K) was observed in single-crystal samples [1, 2]. Although CVD-grown large-area samples are suitable for future application, the thermoelectric properties of large-area TMDC monolayers have not yet been investigated. In particular, because Seebeck coefficient correlates directly with material conductivity, carrier-density dependence is very important. Therefore, in this paper, we tried to measure the Seebeck coefficient of large-area TMDC monolayers with modulating their carrier density by electric double layer transistors (EDLTs), in which one can accumulate extremely high density carriers ($> 10^{13}/\text{cm}^2$) [3, 4].

Figure 1 shows the device structure of EDLTs. As the gate dielectric, we selected the ion gel, which is the mixture of ionic liquid (EMIM-TFSI) and organic polymer (PS-PMMA-PS). As shown in Fig. 2, we successfully accumulated hole and electron carriers in p-type WSe₂ and n-type MoS₂, respectively. Finally, we measured the Seebeck coefficient of TMDC EDLTs at room temperature. The sign of Seebeck coefficient agrees with the carrier type of each material (positive for p-type WSe₂ and negative for n-type MoS₂) and it reasonably controlled by EDL gating, suggesting the solid success of the thermoelectric measurements.



Large-area TMDC monolayer

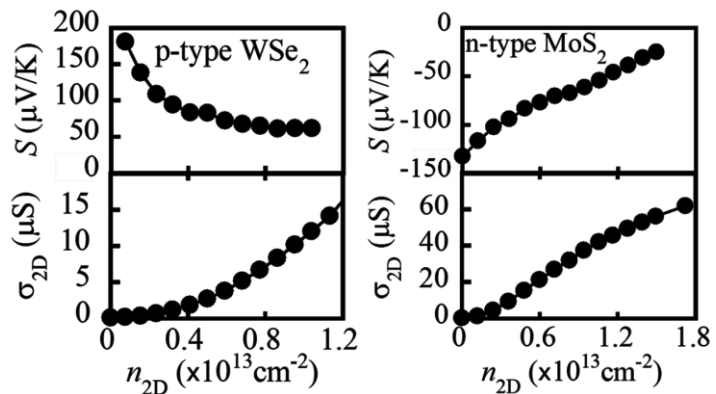


Fig.1. Schematic of Seebeck measurement Fig.2. Seebeck coefficient and sheet conductivity of TMDCs

[1] M. Busceme *et al.*, *Nano Lett.* 13, 358 (2013), [2] J. Wu *et al.*, *Nano Lett.* 14, 2730 (2014)

[3] J. K.Huang, T. Takenobu *et al.*, *ACS Nano.* 8, 923 (2014), [4] J. Pu *et al.*, *Nano Lett.* 12, 4013 (2012)

Corresponding Author: Taishi Takenobu, Tel&Fax: +81-3-5286-2981, E-mail: takenobu@waseda.jp

Electronic transport properties of graphene between metal electrodes

○Hideyuki Jippo^{1,2}, Susumu Okada², Mari Ohfuchi¹

¹ Fujitsu Labs. Ltd., 10-1 Morinosato-wakamiya, Atsugi, Kanagawa 243-0197, Japan

² Univ. of Tsukuba, 1-1-1 Tennodai, Tsukuba, Ibaraki 305-8577, Japan

High contact resistance between graphene and metal electrodes is one of major problems for realizing graphene-based electronic devices. It has been reported that the contact resistance depend on the metal species. In this work, we perform first-principles electronic transport calculations of armchair graphene nanoribbons (AGNRs) bridging between Ti electrodes. The results are compared with our previous data for Au electrodes [1], to discuss the dependence of the transport properties on metal species.

Figure 1 shows a structural model in our transport calculations. Two Ti electrodes are bridged by the AGNRs with a channel length L_{ch} of about 10 nm. The equilibrium spacing between the graphene and metal surface was found to be 0.20 nm (cf. 0.37 nm for Au) indicating that the strong π - d orbital interaction between them. The contact length was fixed to be 0.86 nm. We calculated current densities I at a bias voltage $V_b = (\mu_L - \mu_R)/e = 0.1$ V, where μ_L (μ_R) is the chemical potential of the left (right) lead, using the nonequilibrium Green's function method. Fig. 2 shows I as a function of the channel length L_{ch} . We found that the current densities for Ti are about 10 times as large as those for Au all L_{ch} (i.e. N) studied here. As shown in Fig. 3(a), the transmission occurs at a wide range of the energy eigenvalues E and the wave number along ribbon k_y around those of the AGNR (Fig. 3(b)) arising from the strong π - d coupling that substantially enhances the electron transfer through the Ti-graphene contact. The fact indicates that the contact resistance between graphene and metal electrodes decisively depends on the amount of the hybridization between them.

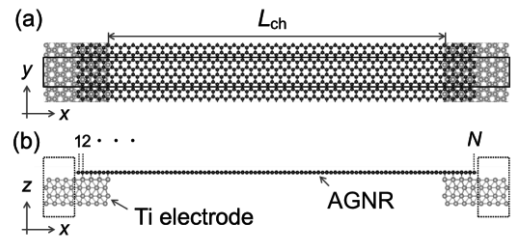


Fig. 1: (a) Top and (b) side views of a structural model. The AGNR with the width $N = 95$ bridges two Ti electrodes. The solid and dotted rectangles indicate the unit cells of the model and leads, respectively.

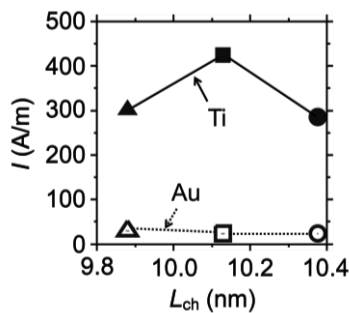


Fig. 2: Current densities I for AGNRs with $N = 95$ (triangle), 97 (square), and 99 (circle).

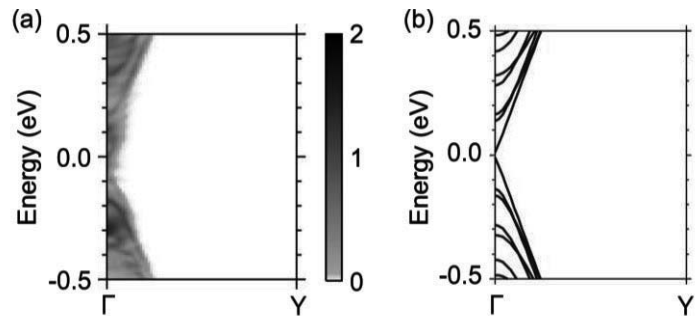


Fig. 3: (a) Transmission spectra $T(k_y, E)$ for the AGNR with $N = 95$ bridging two Ti electrodes. The color bar of the value from 0 to 2 of the transmission is shown. The μ_L is set to 0 eV. (b) Band structure of the isolated AGNR with $N = 95$.

[1] H. Jippo *et al.*, FNTG 47, 1-3 (2014).

Corresponding Author: H. Jippo, Tel: +81-46-250-8843, E-mail: jippo.hideyuki@jp.fujitsu.com

Anharmonicity of Phonons and Thermal Conduction in Graphene

○Masashi Mizuno¹, Riichiro Saito¹

¹*Department of Physics, Tohoku University, Sendai 980-8578, Japan*

Graphene and other low-dimensional carbon materials have a lot of potential for various applications because of their outstanding physical properties [1]. We focused on the thermal conductivity of graphene ($\sim 3,000 - 5,000 \text{ W / m K}$), which is about ten times larger than pure copper [2-4].

In graphene, phonons are the dominant carrier of heat and thermal conductivity is determined by the phonon mean free path (MFP). And the most intrinsic cause of phonon scattering is the anharmonicity (cubic or higher order terms) of lattice potential. The main purpose of our study is to understand how anharmonicity effects on thermal conductivity in graphene. We also studied how thermal conductivity continues from diffusive transport to ballistic transport which occurs when MFP is larger than the sample size of graphene.

Anharmonicity can be calculated by *ab initio* calculation [6] or from empirical inter-atomic potentials [7,8]. However, the former is too complicated to study the basic relationships between anharmonicity and thermal conductivity. Also, we never had very suitable empirical inter-atomic potentials for calculation of anharmonicity. We have therefore integrated simple formed cubic-anharmonic terms into the harmonic force constant model which is well optimized to experimental data [9]. And we optimized the coefficients for anharmonic potential to *ab initio* calculation or measured thermal conductivity.

We have found that anharmonic scatterings involving one in-plane phonon and two out-of-plane phonons have an strong effect on thermal conductivity. This is because, in graphene, ZA phonons and low-frequency TA and LA phonons carry the main part of heat and these scattering processes affects the lifetime of these phonons.

We also found that, at room temperature or lower, MFPs of some phonons are comparable to or larger than typical size of graphene sample ($1 \mu\text{m}$). In this case, ballistic transport of phonons should occur and thermal conductivity depends on the sample size of graphene. We will show the estimation of this dependency in the poster.

[1] R. Saito, *et al.*, *Physical Properties of Carbon Nanotubes*, Imperial College Press, London (1998).

[2] A. A. Balandin, *Nat. Mater.* **10**, 569 (2011).

[3] E. Pop, *et al.*, *MRS Bull.* **37**, 1273 (2012).

[4] S. Chen, *et al.*, *Nat. Mater.* **11**, 203 (2012).

[5] G. P. Srivastava, *The Physics of Phonons*. (CRC Press, UK, 1990).

[6] L. Paulatto, *et al.*, *Phys. Rev. B.* **87**, 214303 (2013).

[7] L. Lindsay, *et al.*, *Phys. Rev. B.* **81**, 205441 (2010).

[8] V. K. Tewary, *et al.*, *Phys. Rev. B.* **79**, 075442 (2009).

[9] M. Furukawa, unpublished (2009).

Corresponding Author: M. Mizuno

E-mail: mizuno@flex.phys.tohoku.ac.jp

Structure and electronic properties of epitaxial graphene and its molecular adsorption effect

Keisuke Nakamoto¹, Takashi Akatsu², Kazuyuki Takai^{1,3,4}

¹Graduate School of Science and Engineering, Hosei University, Tokyo 184-8584, Japan

²Material and structures laboratory, Tokyo Institute of Technology, Tokyo 226-8503, Japan

³Department of Chemical Science and Technology, Hosei University, Tokyo 184-8584, Japan

⁴Research Center for Micro-Nano Technology, Hosei University, Tokyo 184-0003, Japan

Exfoliated graphene has been extensively investigated mainly on the transport study toward the electronics application. Recently graphene research has been extended to studies for spectroscopy and reactivity with other chemical species where large-area and high quality sample is necessary. In this study, we examined the structure and the electronics structure of epitaxial graphene (EG) grown on a SiC substrate as a typical large-area high quality graphene sample, and its effect of the adsorption of guest chemical substance by XPS (Al K α), Raman spectroscopy (wavelength 532nm). EG was grown by annealing SiC at 1750 °C for 5 minutes under Ar atmosphere. Molecular adsorption was performed by immersing EG in hydrazine hydrate (N₂H₂•H₂O) for 12 hours and dried (Hydrazine-EG).

Fig.1 shows XPS spectra for EG and hydrazine-EG. Emerging of N1s peak in hydrazine-EG indicates the successful introduction of hydrazine in EG. However, N1s peak position suggests the presence of C-N bonding. Fig.2 shows Si2p spectra for EG and hydrazine-EG. Peak intensity for the buffer layer (102 eV) decreases after hydrazine introduction, suggesting hydrazine hydrate is intercalated and decouples the buffer layer and the SiC substrate as reported for hydrogen adsorption [1]. In Raman spectroscopy, the G-band position for hydrazine-EG shifts toward a higher energy side as compared with EG. Hydrazine-EG might be electron-doped by the influence of the introduction of hydrazine hydrate.

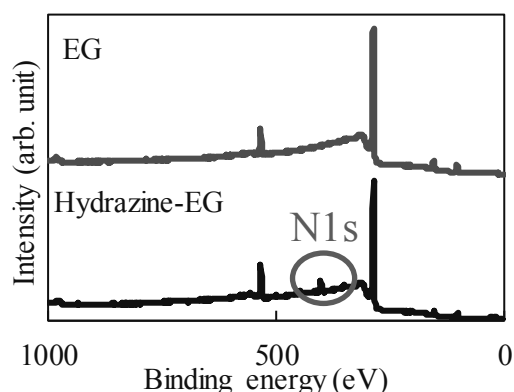


Fig.1 XPS spectra for EG and hydrazine-EG

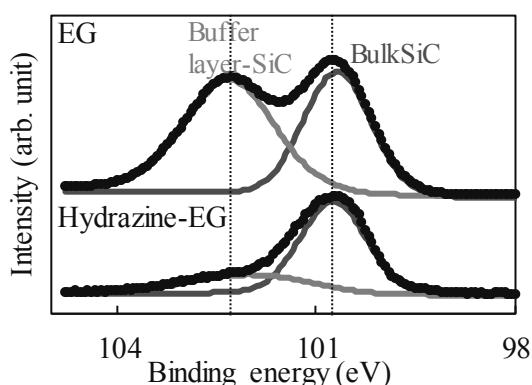


Fig.2 Si2p spectra for EG and hydrazine-EG

[1]C. Riedl, C.Coletti, T. Iwasaki, A.A.Zakharov, and U.starke, *PRL* 103, 246804 (2009)

Corresponding Author : Kazuyuki Takai

Tel: +81-42-387-6138, Fax: +81-42-387-7002, E-mail:takai@hosei.ac.jp

Bandgap Opening in Graphene Adsorbed on Defective Graphene

○Ken Kishimoto and Susumu Okada

Graduate school of Pure and Applied Sciences, University of Tsukuba, Tsukuba 305-8571, Japan

Electronic structures of graphene sensitively depend on imperfections such as atomic defects, topological defects, and edges. It has been demonstrated that graphene with defects is either a metal or a semiconductor depending on the defect structure and arrangement. In addition to the atomic imperfections, the interlayer stacking arrangements of graphene thin films also lead to the interesting variations in their electronic structures because of the substantial interlayer π - π interactions. These facts imply that the electronic structure of pristine graphene is modulated by adsorbing the defective graphene due to the interlayer interaction. In this work, we aim to study the electronic structure of bilayer graphene consisting of pristine and defective graphene layers using the density functional theory (DFT) with the effective screening medium (ESM) method.

Our DFT-ESM calculations show that all bilayer graphene are semiconductors with finite energy gap of about a few hundred meV irrespective of the defect structures and mutual stacking arrangements (Fig. 1). Detailed analysis on the electronic structures unraveled that the defects on one of graphene layers causes inhomogeneous electrostatic potential on pristine graphene layer leading to the finite energy gap between π and π^* states (Fig. 2). The results indicate the possible procedure for realizing semiconducting bilayer graphene by modulating the atomic arrangements of one of two layers.

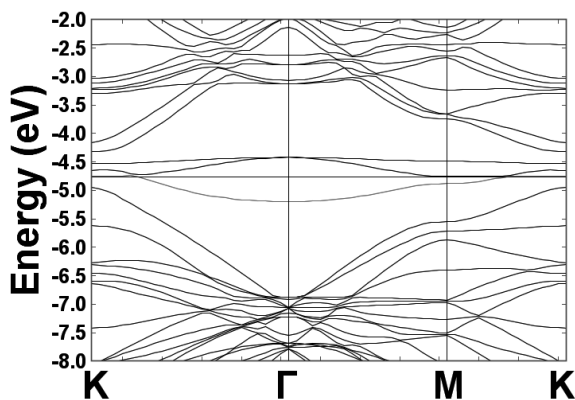


Fig.1, Electronic energy band of bilayer graphene consisting of pristine and defective graphene layers.

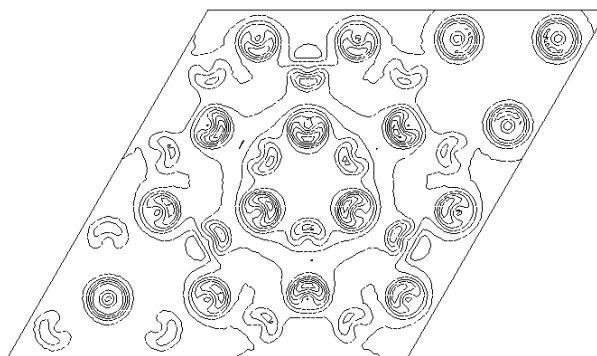


Fig. 2, A contour plot of the electrostatic potential on the pristine layer of bilayer graphene.

Corresponding Author: K. Kishimoto
 Tel: +81-29-853-5600(ext.; 8233)
 E-mail: kkishimoto@comas.frsc.tsukuba.ac.jp

Fabrication and In-situ TEM Characterization of Freestanding Graphene Nanoribbons Devices

○Qing Wang, Ryo Kitaura*, Shoji Suzuki, Hisanori Shinohara*

*Department of Chemistry & Institute for Advanced Research, Nagoya University,
Nagoya 464-8602, Japan*

Size and shape can strongly affect properties of nanomaterials. Graphene nanoribbons (GNRs) have recently attracted intensive interests because electronic structure of GNR, including bandgap and localized edge states, strongly depends on their width and edge structure: width-dependent bandgap and gapless edge states arising from zigzag edges. The combination of precise structural characterization and electronic property measurement is therefore essential to fully understand the intrinsic properties of GNRs. For this purpose, a new experimental technique using freestanding GNR devices has been developed, leading to the simultaneous characterization of electronic properties and atomic structure of GNRs.

High quality graphene was transferred onto a Si substrate with an open slit covered by a SiO₂ layer. To fabricate a freestanding structure, we first made electronic contacts on isolated graphene ribbons by Cr/Au, and then SiO₂ membrane underneath the graphene ribbons was etched away by buffered hydrogen fluoride acid. The so-prepared freestanding graphene device was assembled to a home-made transmission electron microscopy (TEM) holder for in-situ characterization. The freestanding graphene was sculpted by a focused electron beam in TEM, purified and narrowed by Joule heating down to several nanometers width. Structure-dependent electronic properties were investigated in TEM. We have observed significant increase in resistance and found that semiconducting behavior became more dominant with decreasing width of GNR. The details of device preparation and characterization of GNRs devices will be addressed in the presentation.

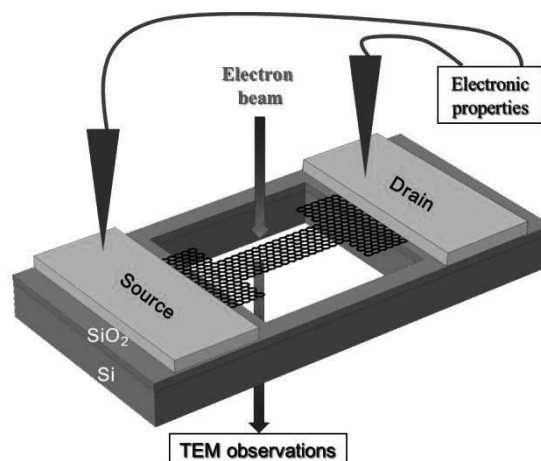


Fig.1 Schematic diagram of the freestanding structure

[1] J. Huang, *et al.* PNAS **106**, 10103, (2009).

[2] Han *et al.* PRL **104**, 056801 (2010)

Corresponding Author: Ryo Kitaura and Hisanori Shinohara

TEL: (+81) 52-789-2482, FAX: (+81) 52-789-6442,

E-mails: r.kitaura@nagoya-u.jp and noris@nagoya-u.jp

Graphite laser ablation products carried by coaxial gas flow

○Yuki Taguchi,¹ Hitomi Endo,¹ Yurika Abe,¹ Jun Matsumoto,¹ Tomonari Wakabayashi,² Takeshi Kodama,¹ Yohji Achiba¹ and Haruo Shiromaru¹

¹ Department of chemistry, Tokyo Metropolitan University, Tokyo 192-0397, Japan

² Department of Chemistry, Kindai University, Osaka 577-8502, Japan

Previously we have shown that hydrogen-terminated polyynes (HC_{2n}H , hereafter merely polyynes) are effectively produced by laser ablation of graphite in argon/propane gas flow, and information on the polyyne-formation reactions would be obtained from the yields as a function of the ratio of propane gas ($R = f_p/(f_a+f_p)$, where f_a and f_p are the flow rates of Ar and propane, respectively) [1]. In that experiment, ablation products were emitted 45 degrees toward the wall and only those successfully carried by the gas flow were detected. Thus, high velocity products were not detected causing a bias in the measured yields. In the present study, laser ablation was conducted in a new apparatus (Fig. 1) to improve the collection efficiency. A graphite disk with small through-holes was set as shown in the inset, so as to make the gas flow (50 mL/min) and ejected carbon clusters to be directed coaxially to the exit. A pulsed Nd: YAG laser with the power of 150 mJ/pulse was irradiated to the graphite for 60 seconds. After laser ablation, the soluble products were analyzed by UV absorption. The yields were commonly several times higher than those by the old setup.

The R -dependence of the yields of the polyynes is shown in Fig. 2, which well reproduces our previous measurements [1]. It follows that the limited collection efficiency does not cause a serious bias. As can be seen in the figure, the yields increase with the increase of the R values. At high R values, the yields of C_6H_2 and C_8H_2 become to be almost a plateau, while those of C_{12}H_2 and C_{14}H_2 still continue to increase. A reasonable explanation for the chain-size dependence of the yield curves is that the precursors, bared carbon clusters of C_6 and C_8 , are nearly exhausted at around $R = 0.5$. On the other hand, such the saturation effect is not observed for the longer polyynes, probably due to the lower reactivity of the longer bared carbon clusters. The enhancement of the longer polyynes at large R indicates that the hydrogen termination occurs after the size distribution of the chain-form carbon clusters is fixed.

[1] Y. Abe *et al.* FNTG 46, 141 (2014).

Corresponding Author: H. Shiromaru, Tel: +81-42-677-1111, Fax: +81-42-677-2525, E-mail: shiromaru-haruo@tmu.ac.jp

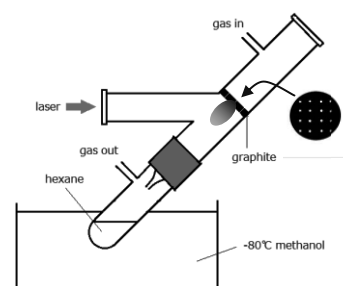


Fig. 1 Schematic drawing of the laser ablation setup.

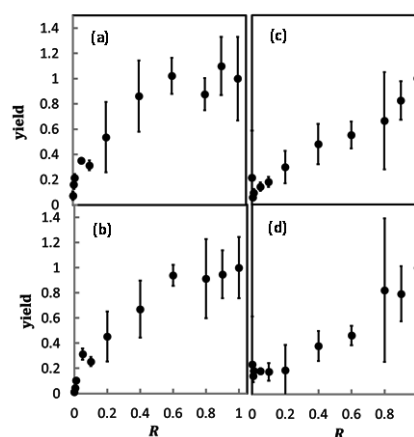


Fig. 2 Plots of relative yields of the polyynes, (a) - (d) for C_6H_2 , C_8H_2 , C_{12}H_2 and C_{14}H_2 , respectively. The yields are normalized at $R = 1$. The error bars are standard deviation of four independent lots.

Controlling and functionalizing phase transitions in two-dimensional crystals

○Masaro Yoshida¹, Yijin Zhang¹, Jianting Ye², Ryuji Suzuki¹, Yasuhiko Imai³,
Shigeru Kimura³, Akihiko Fujiwara³, Yoshihiro Iwasa^{1,4}

¹Quantum-Phase Electronics Center (QPEC) and Department of Applied Physics,
The University of Tokyo, Tokyo, 113-8656, Japan

²Zernike Institute for Advanced Materials (ZIAM), University of Groningen, Nijenborgh 4,
9747 AG, Groningen, the Netherland

³Japan Synchrotron Radiation Research Institute (JASRI), SPring-8, Hyogo 679-5198, Japan

⁴RIKEN, Center for Emergent Matter Science (CEMS), Wako, 351-0198, Japan

Two-dimensional (2D) crystals, including graphene and transition metal dichalcogenides [1], provide an ideal platform for exotic electronic band structures in mono- or multi-layer forms. The thinning to nanoscale may also affect collective phenomena in interacting electron systems and can lead to unconventional states that are dramatically different from those in bulk. Here, we show the systematic control of charge density wave (CDW) transitions by changing thickness and cooling rate in nano-thick crystals of 1T-type tantalum disulfide (1T-TaS₂) [2]. First, we discovered a supercooled nearly commensurate CDW state, which has never been observed in bulk crystals. We also performed quasi *in situ* microbeam X-ray diffraction measurement at SPring-8 and succeeded in the direct observation of systematic change in lattice constant as a function of thickness, which may be the origin of the novel supercooled state. Furthermore, we achieved current-induced switching between various CDW states. The current-voltage characteristic reminds us that of phase-change memory (PCM) or memristor [3]. The glassy behavior and non-linear response, possibly due to the reduced dimensionality, manifest the emergent complex nature and potential functionalities of correlated electrons in 2D crystals with nanometer thickness.

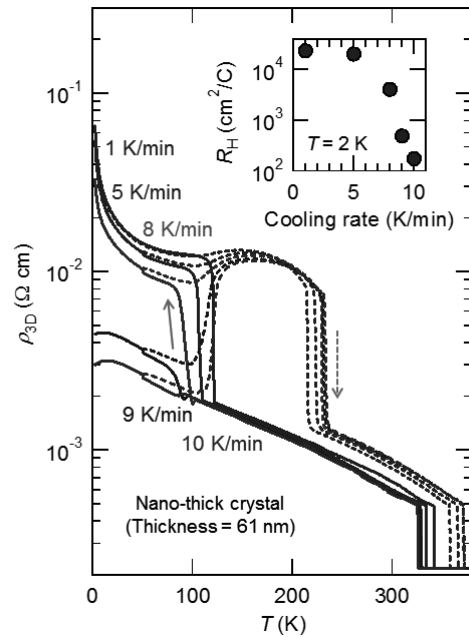


Fig.1 Resistivity-temperature (ρ_{3D} - T) curves of a 1T-TaS₂ nano-thick crystal at different cooling rates, demonstrating that the super-cooled conducting state is realized by rapid cooling. Inset is the cooling rate dependence of Hall coefficient (R_H), showing that a large number of carriers are mobile in the supercooled state.

[1] K. S. Novoselov *et al.* PNAS **102**, 10451 (2005).

[2] M. Yoshida *et al.* Sci. Rep. **4**, 7302 (2014).

[3] M. Yoshida *et al.* in preparation.

Corresponding Author: M. Yoshida

Tel: +81-3-5841-6822, Fax: +81-3-5841-6822,

E-mail: masaro-yoshida@mp.t.u-tokyo.ac.jp

Structure and Spectra of Polyynes-Iodine Complex

○ Dai Nagashima¹, Tohru Sato^{1,2}, Naoya Iwahara¹, Kazuyoshi Tanaka¹, Yoriko Wada³,
Tomonari Wakabayashi³

¹*Department of Molecular Engineering, Graduate School of Engineering, Kyoto University,
Kyoto 615-8510, Japan*

²*Unit of Elements Strategy Initiative for Catalysts and Batteries, Kyoto University,
Kyoto 615-8510, Japan*

³*Department of Chemistry, Graduate School of Science and Engineering, Kinki University,
Osaka 577-8502 Japan*

Polyynes, $C_{2n}H_2$, are highly conjugated linear carbon chains which are synthesized by the laser ablation of graphite and isolated size-selectively[1]. For $C_{2n}H_2$ ($n = 5, \dots, 9$), it has been reported that the mixtures of polyynes and iodine in a non-polar solvent such as hexane drastically changes in the UV/vis absorption spectra by the irradiation of visible light[2]. It was found that the stoichiometries are $C_{2n}H_2I_6$, and they have at least one C_2 symmetry axis[2] from the experimental observations including NMR. However, the molecular structures and formation mechanism of these complexes are still open.

In this study, we assigned the IR, UV/vis and NMR spectra of $C_{10}H_2I_6$ by using the density functional theory (DFT) and time-dependent DFT (TD-DFT) to clarify the molecular structure of the complex. All calculations were performed with the Zeroth-Order Regular Approximation (ZORA) Hamiltonian[3] using the Amsterdam Density Functional (ADF) package. Prior to the calculations, we performed benchmark calculations for $C_{10}H_2$. We employed the PBE/TZP, B3LYP*/TZP, KT2/TZP level of the theory for the IR spectra, UV/vis spectra, and NMR spectra, respectively. We also simulate the observed vibronic progressions in the UV/vis spectrum to obtain the vibronic coupling constant.

As shown in Fig.1, we presumed eight $C_{10}H_2I_6$ isomers with a C_2 symmetry axis. According to the results of the DFT calculations for the ground states, (a.1) isomer is the most stable structure among them as shown in Fig.2. Fig.3 shows the comparison of the calculated IR spectrum of (a.1) with the experimental one[4]. We found that the simulated IR, UV/vis, and NMR spectra for (a.1) reproduce the experimental ones well.

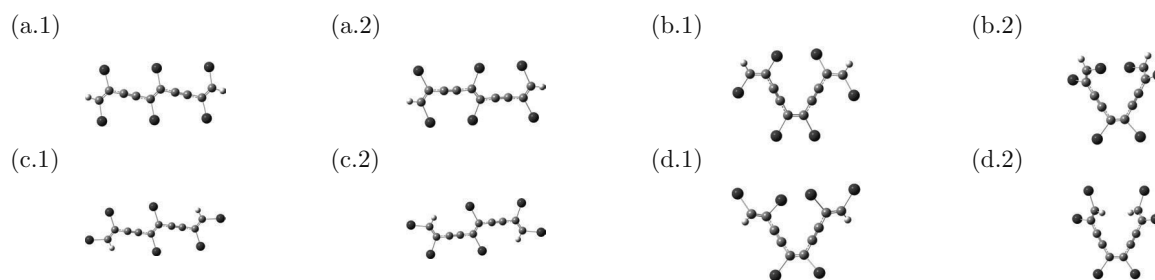


Figure 1: Calculated $C_{10}H_2I_6$ isomers.

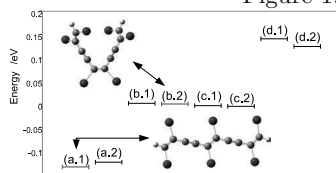


Figure 2: Relative energy of the isomers at the PBE/TZP level of the theory.

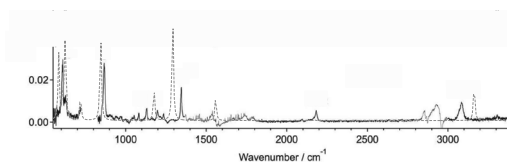


Figure 3: Experimental (solid line) and calculated (dotted line) IR spectra of (a.1) isomer.

- [1] H. Tabata *et al.*, *Carbon* **44**, 3168(2006).
 [2] Y. Wada *et al.*, *J. Phys. Chem. B.* **115**, 8439(2011).
 [3] E. van Lenthe *et al.*, *J. Phys. Chem.* **99**, 4597(1993).
 [4] Y. Wada *et al.*, *Chem. Phys. Lett.* **541**, 54(2012).

Corresponding Author: Tohru Sato

Tel: +81-75-383-2803, Fax: +81-75-383-2555,

E-mail: tsato@moleng.kyoto-u.ac.jp

Ambipolar Transistor and Superconductivity in Transition Metal Dichalcogenides

oWu Shi¹, Jianting Ye^{1,2}, Yijing Zhang¹, Ryuji Suzuki¹, Masaro Yoshida¹,
Naoko Inoue¹, Yu Saito¹, and Yoshihiro Iwasa^{1,3}

¹ *Quantum-Phase Electronics Center and Department of Applied Physics, The University of Tokyo, 7-3-1 Hongo, Bunkyo-ku, Tokyo, 113-8656, Japan*

² *Zernike Institute for Advanced Materials, University of Groningen, The Netherlands*

³ *Center for Emergent Matter Science, RIKEN, Hirosawa 2-1, Wako 351-0198, Japan*

Two-dimensional materials such as transition metal dichalcogenides (TMDs) have attracted substantial interest since the discovery of graphene. By mechanical cleavage, atomically flat and chemically stable thin flakes of TMDs can be readily obtained from bulk crystals and employed as ideal channel materials for field effect transistor (FET) devices. Recently, coupling with novel functioned ionic liquid (IL) dielectrics, TMD thin flakes have exhibited new functionalities such as superconductivity and opto-valleytronics [1, 2] in the form of electrical double layer transistors (EDLTs) due to the extremely large electric field created at the EDL interface. In this work, we report systematic evolution of field effect properties and gate-induced superconductivity in MoX₂ (X = S, Se, and Te) utilizing the EDLT configuration. The ambipolar transistor characteristics of MoX₂ were nicely explained by the interface energy alignment between ionic liquids (ILs) and MoX₂. As a consequence of decreasing efficiency in electron accumulation, gate-induced superconductivity (GIS) was found in MoSe₂ but not in MoTe₂. Further experiments by replacing IL with KClO₄/polyethylene glycol (PEG) electrolyte significantly reduced electron injection barrier and amplified transistor performance, leading to the emergence of superconductivity in MoTe₂. The present result reveals the correlation between transistor operation and superconductivity, providing an important guidance to systematically induce superconductivity using an EDLT technique.

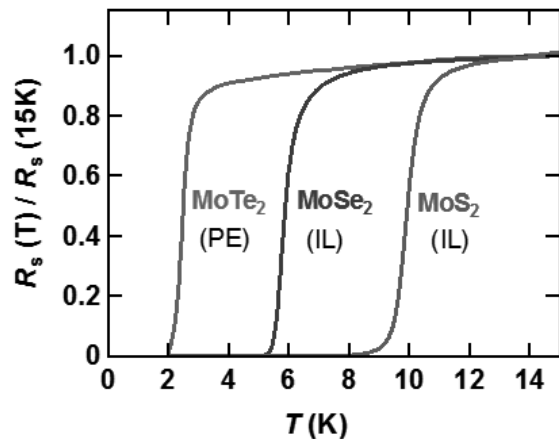


Figure 1. Superconductivity of 2H-type MoS₂, MoSe₂ and MoTe₂ by ionic gating using ionic liquid (IL) and polymer electrolyte (PE), respectively.

[1] J. T. Ye, Y. J. Zhang, R. Akashi, M. S. Bahramy, R. Arita, Y. Iwasa, *Science* **338**, 1193 (2012)

[2] Y. J. Zhang, T. Oka, R. Suzuki, J. T. Ye, Y. Iwasa, *Science* **344**, 725 (2014).

Corresponding Author: W. Shi

Tel: +81-3-5841-6822, Fax: +81-3-5841-6822

E-mail: shiwu@ap.t.u-tokyo.ac.jp

Solid-State NMR Studies on the Aggregated Structures of Organic Bulk Heterojunction Solar Cells with Solvent Additives(II)

○Saki Kawano¹ and Hironori Ogata^{1,2}

¹ Department of Chemical Science and Technology, Hosei University Koganei 184-8584 Japan

³ Research Center for Micro-Nano Technology, Hosei University, Koganei 184-0003, Japan

Bulk heterojunction (BHJ) organic solar cells are an emerging technology that has the potential to provide a low cost photovoltaic devices. It is well known that the nanomorphology of the polymer:fullerene BHJ is a critical factor which affects the solar cell performance. The addition of processing additives such as 1,8-diiodooctane (DIO) is widely used approach to increase power conversion efficiencies for many organic solar cells^[1-2]. Solid-state NMR spectroscopy offers several techniques for the investigation of the morphological, structural, and dynamics properties of BHJ organic solar cells.

We have explored the effects of DIO addition of P3HT/PCBM BHJ films on the local crystallinity and morphology by using solid-state NMR spectroscopy. In this study, we investigated the change in the crystallinity, morphology, and the properties of molecular motions of P3HT/PCBM BHJ film by adding another solvent additives(1,8-Octanedithiol (ODT)) and also effects of annealing by using ¹³C and ¹H solid-state NMR spectroscopy.

Mixed solution of P3HT/PCB of 1:1(w/w) was prepared by mixing P3HT and PCBM into chlorobenzene at a concentration of 1 wt% for 50 hrs in a glove box under argon atmosphere. A 3% by volume of ODT was then dropped into the solution and then stirred for 1 hr. The solution was filtered using 0.45μm filter before making films to remove undissolved materials. P3HT/PCBM BHJ films were prepared by dropping the solution in a glass plate and dried in a glove box under argon atmosphere for 40 hrs and then put in the vacuum for 24hrs. Dried film were removed from the glassplate and sealed into 4 mm zirconia NMR rotor. Figure 1. shows the ¹³C-DD/MAS NMR spectra of P3HT/PCBM BHJ films (a)with and (b)without ODT additive.

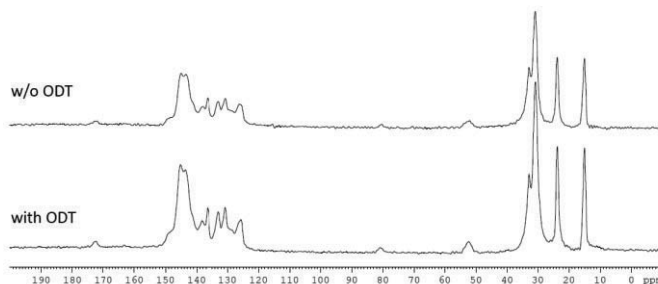


Figure 1. ¹³C DD/MAS NMR spectra of P3HT/PCBM BHJ films with and without ODT additive

The detailed results of the change of the crystallinity and morphology of P3HT/PCBM BHJ film by the addition of ODT and comparison with other additives will be presented

References:

[1] Cuiying Yang *et al.* J.Am.Chem.Soc., vol.128, no.36, pp.12007–12013, 2006.

[2] Jae Kwan Lee *et al.*, J. Am. Chem. Soc., vol.130 no.11, pp.3619–3623, 2008.

[3] S. Kawano, S. Ishikawa and H. Ogata, Abstract of the 47th Fullerenes-Nanotubes-Graphene General Symposium (1P-38)

Corresponding Author: H. Ogata, Tel: +81-42-387-6229, Fax: +81-42-387-6229, E-mail: hogata@hosei.ac.jp

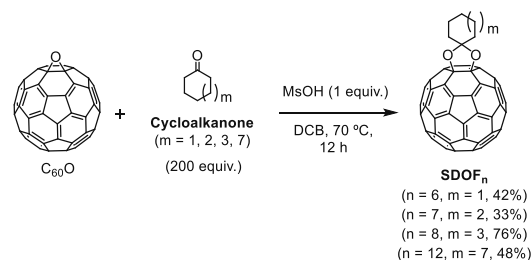
Application of spiro-1, 3-dioxolanofullerenes with low-lying LUMO level to low bandgap polymer based organic photovoltaic cell

○Tsubasa Mikie, Akinori Saeki, Naohiko Ikuma, Ken Kokubo, Shu Seki

Department of Applied Chemistry, Graduate School of Engineering, Osaka University,
2-1 Yamadaoka, Suita, Osaka 565-0871, Japan.

Bulk heterojunction (BHJ) type organic photovoltaic (OPV) cell is one of the promising technologies because of its low-cost scalable solution process on a light-weight flexible substrate. Since low bandgap polymers (LBP) have been developed, the power conversion efficiency (PCE) of single cell LBP:[6,6]-phenyl-C₆₁₍₇₁₎-butyric acid methyl ester (PCBM and PC₇₁BM) reached 9-10% [1]. However, there has been little alternative of PCBM suitable for LBP. A general molecular design of LBP is to narrow the band gap with keeping a deep HOMO level. Therefore, some of LBPs lead to small offset in the LUMO levels between LBP and fullerenes, which might inhibit an efficient charge separation.

Herein, we report spiro-1,3-dioxolano [60]fullerene (**SDOF_n**) bearing six, seven, eight, and twelve-membered rings ($n = 6, 7, 8, 12$) (Scheme 1) [2]. This molecular design is followed by our recent study on spiro-(thio)acetalized [60]fullerenes (**SAF_n** and **STAF_n**, $n = 5-7$), which revealed 4.0% PCE for the poly(3-hexylthiophene), P3HT blend (P3HT:**SAF₇**) comparable to P3HT:PCBM [3]. Unlike **SAF_n** and **STAF_n**, electron-withdrawing spiro-dioxolano unit of **SDOF_n** is directly attached to the fullerene core, so that their LUMO levels become shallower than those of **SAF_n**. The blend film of **SDOF₁₂** and benchmark LBP (PTB7) showed the good PCEs of 4.43 and 5.39% for normal (ITO/PEDOT:PSS/BHJ/Ca/Al) and inverted (ITO/ZnO/BHJ/MoO_x/Ag) devices, respectively (Figure 1), suggesting high potentials of SDOFs as the fullerene alternatives in BHJ-OPV systems.



Scheme 1. Synthesis of **SDOF_n**s.

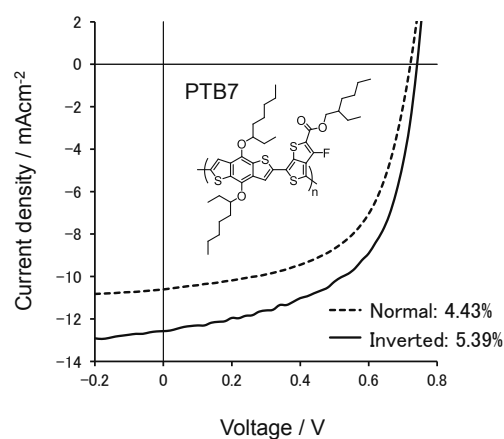


Figure 1. J - V curves of PTB7: **SDOF₁₂** (dashed line: normal cell, solid line: inverted cell) under 100 mWcm⁻² AM1.5G.

[1] J. Kong, I.-W. Hwang, K. Lee, *Adv. Mater.* **2014**, *26*, 6275.

[2] T. Mikie, A. Saeki, N. Ikuma, K. Kokubo, S. Seki, *Chem. Lett.* DOI:10.1246/cl.141008.

[3] T. Mikie, A. Saeki, H. Masuda, N. Ikuma, K. Kokubo, S. Seki, *J. Mater. Chem. A* **2015**, *3*, 1152-1157.

*Corresponding Author: Shu Seki

Tel: +81-6-6879-4586, Fax: +81-6-6879-4586, E-mail: seki@chem.eng.osaka-u.ac.jp

Fabrication of semitransparent tandem organic solar cells using multiple-device stacked structure

○Shunjiro Fujii¹, Takeshi Tanaka¹, and Hiromichi Kataura¹

¹Nanosystem Research Institute, National Institute of Advanced Industrial Science and Technology (AIST), Ibaraki 305-8562, Japan

Organic solar cells (OSCs) are of special interest owing to the advantages of low-cost and solution-processable fabrications. Previously, we reported semitransparent bulk-heterojunction OSCs based on a benzodithiophene polymer of PTB7*^[1] and phenyl-C₇₁-butyric-acid-methyl-ester (PC₇₁BM) utilizing an oxide/metal/oxide transparent anode [2]. However, the photocurrents of the semitransparent OSCs remained low due to the optical loss through the semitransparent electrode. In this work we fabricated stacking structure of two separated OSCs to harvest an increased amount of photons which enhanced the power conversion efficiency (PCE).

The device structure was Glass/ITO/PFN**/PTB7:PC₇₁BM/MoO₃/Au/MoO₃ (Figure 1). Two identical semitransparent OSCs were stacked on top of each other and connected in series or in parallel to form a tandem structure. Figure 2 shows the current density-voltage (J-V) curves for the single and stacked cells connected in series and in parallel, respectively. The PCEs extracted from the J-V curves were 2.7%, 2.6% and 3.3%, respectively. The stacked cells in parallel connection showed improved PCE compared to a single cell. The detailed device characteristics will be discussed.

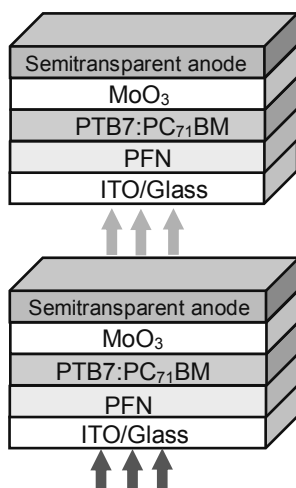


Figure 1 Schematic illustration of the stacked semitransparent solar cells.

- [1] Y. Liang et al., *Adv. Mater.*, 22 (2010) E135
 [2] S. Fujii et al., *The 47th FNTG General symposium 2014*, 1p-35

Corresponding Author: Hiromichi Kataura
E-mail: h-kataura@aist.go.jp

*PTB7; poly[[4,8-bis[(2-ethylhexyl)oxy]benzo [1,2-b:4,5-b']dithiophene-2,6-diyl][3-fluoro-2-[(2-ethylhexyl)carbonyl]thieno[3,4-b]-thiophenediyl]]

**PFN; poly[(9,9-bis(3'-(N,N-dimethylamino) propyl)-2,7-fluorene)-alt-2,7-(9,9-dioctylfluorene)]

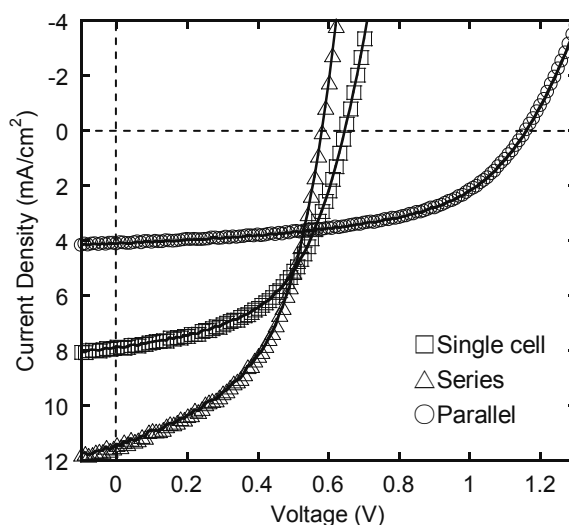


Figure 2 J-V characteristics under AM 1.5G.

Isolation and characterization of [5,6]-pyrrolidino-Sc₃N@I_h-C₈₀ diastereomers

○Yutaka Maeda¹, Masato Kimura,² Chihiro Ueda,¹ Mitsuaki Suzuki,¹ Michio Yamada,¹ Nikolaos Karousis,³ Nikos Tagmatarichis,³ Marilyn M Olmstead,⁴ Alan L Balch,⁴ Wei-Wei Wang,⁵ Shigeru Nagase,⁵ Takeshi Akasaka²

¹*Department of Chemistry, Tokyo Gakugei University, Koganei, Tokyo 184-8501, Japan*

²*Life Science center of Tsukuba Advanced Research Alliance, University of Tsukuba, Tsukuba, Ibaraki 305-8577, Japan*

³*Theoretical and Physical Chemistry Institute, National Hellenic Research Foundation, 48 Vassileos Constantinou Avenue, Athens 11635, Greece*

⁴*Department of Chemistry, University of California at Davis, One Shields Ave, Davis, CA 95616, USA*

⁵*Fukui Institute for Fundamental Chemistry, Kyoto University, Kyoto, 606-8103, Japan*

Recent developments in the chemistry of endohedral metallofullerenes (EMFs) have led to increasing efforts to elucidate how the chemical reactivity and selectivity of empty fullerenes are changed by endohedral metal doping and how the electronic properties of metallofullerenes affect chemical functionalization. The preparation and isolation of trimetallic nitride template endohedral metallofullerenes (TNT-EMFs) in macroscopic quantities have facilitated the study of their structures, properties, and chemical reactivities. For practical application, such as organic photovoltaic cells, it is essential to control its solubility or electronic properties by chemical modification. As practical reagents for the functionalization of TNT-EMFs, we focus on a azirizine, precursor of azomethyne ylide.¹ Since custom-synthesized aziridines, carrying groups with advanced functionality, can be prepared from commercially available reagents in high yields through only a few steps. Herein, we report the synthesis of [5,6]-pyrrolidino-Sc₃N@I_h-C₈₀ from Sc₃N@I_h-C₈₀ and aziridine derivatives. In addition, isolated pyrrolidino-Sc₃N@I_h-C₈₀ diastereomers were characterized by electronic absorption, NMR, and single-crystal X-ray crystallography.²

[1] M. Prato *et al.* J. Am. Chem. Soc. **129**, 14580 (2007).

[2] Y. Maeda *et al.* Chem. Commun. **50**, 12552 (2014).

Corresponding Author: Y. Maeda

Tel: +81-42-329-7512, Fax: +81-42-329-7512, E-mail: ymaeda@u-gakugei.ac.jp

Reactions of Trimetallic Nitride Template Endohedral Metallofullerenes with Silacyclopropanes

○Kazuya Minami¹, Takeshi Sugiura¹, Masahiro Kako^{*,1}, Kumiko Sato²,
Shigeru Nagase³, Takeshi Akasaka^{2,4,5}

¹*Department of Engineering Science, The University of Electro-Communications, Chofu, Tokyo 182-8585, Japan*

²*Life Science Center of Tsukuba Advanced Research Alliance, University of Tsukuba, Tsukuba, Ibaraki 305-8577, Japan*

³*Fukui Institute for Fundamental Chemistry, Kyoto University, Kyoto 606-8103, Japan*

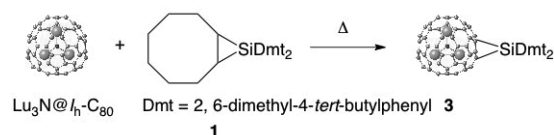
⁴*Department of Chemistry, Tokyo Gakugei University, Tokyo 184-8501, Japan*

⁵*Foundation for Advancement of International Science, Ibaraki 305-0821, Japan*

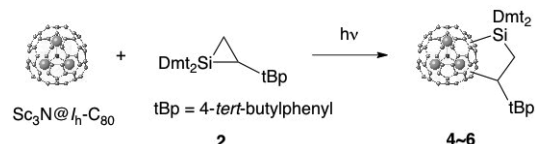
Endohedral metallofullerenes (EMFs) have been the focus of extensive research because of their remarkable structures and properties. During the past decade, exohedral functionalization of EMFs has been exploited intensively as crucial methods to modify the physical and chemical properties of EMFs, which will expand the range of potential applications in molecular electronics, nanomaterials sciences, and biochemistry [1]. As a method for heteroatom functionalization, silylation using reactive silicon compounds has been reported to induce remarkable changes of the characteristics of EMFs. For example, the silylated fullerene derivatives possess more electronegative charge on the cage than parent fullerenes. Moreover, it has been also demonstrated that the movement of the encapsulated metal atom are affected by the introduction of silyl groups on the fullerene cages [2].

As a part of our continuing study of silylation of EMFs, we now report the reactions of silacyclopropanes **1** and **2** with trimetallic nitride template EMFs, $M_3N@I_h-C_{80}$ ($M = Sc, Lu$). The thermal reaction of $Lu_3N@I_h-C_{80}$ with **1** at 150°C afforded an adduct **3** by addition of silylene (Dmt_2Si). On the basis of the NMR and visible-near-infrared (vis-NIR) spectra, the silylene addition was occurred at the [6,6] ring junction of $Lu_3N@I_h-C_{80}$. Meanwhile, when the $Sc_3N@I_h-C_{80}$ was photoirradiated with **2**, three adducts **4**, **5**, and **6** were obtained as carbosilylated $Sc_3N@I_h-C_{80}$. The NMR and vis-NIR spectra indicate that the structures of **4** and **5** are adducts at the [5,6] ring junctions of $Sc_3N@I_h-C_{80}$, while **6** is an isomer derivatized at the [6,6] junction. The structural and electronic properties of these silylated derivatives will be discussed based on electrochemical and theoretical studies.

Scheme 1.



Scheme 2.



[1] M. Yamada, T. Akasaka *Bull. Chem. Soc. Jpn.* **87**, 1289–1314 (2014).

[2] K. Sato *et al. J. Am. Chem. Soc.* **134**, 16033–16039 (2012).

Corresponding Author: Masahiro Kako Tel: +81-42-442-5570

E-mail: kako@e-one.ucc.ac.jp

Ionic Donor-Acceptor Supramolecules: Complexation of Molecular Nanocarbons with Cationic $\text{Li}^+\text{@C}_{60}$

○Hiroshi Ueno^{1,2}, Taishi Nishihara^{1,2}, Katsuma Matsui²,
Yasutomo Segawa^{1,2}, Kenichiro Itami^{1,2,3}

¹ *JST-ERATO, Itami Molecular Nanocarbon Project, Nagoya University,
Nagoya 464-8602, Japan*

² *Graduate school of Science, Nagoya University, Nagoya 464-8602, Japan*

³ *Institute of Transformative Bio-Molecules (WPI-ITbM), Nagoya University,
Nagoya 464-8602, Japan*

It is well known that cycloparaphenylenes (CPPs),^[1] ring-shaped π -conjugated molecules, selectively encapsulate fullerenes. For example, [10]CPP encapsulates C_{60} to form a shortest fullerene peapod.^[2] On the other hand, lithium-ion-encapsulated fullerene ($\text{Li}^+\text{@C}_{60}$)^[3] has attracted much attention owing to its strong electron acceptability and unique ionic properties,^[4] and it has almost the same diameter as empty C_{60} . Here, we report the synthesis and characterization of ionic supramolecule $\text{Li}^+\text{@C}_{60}\text{C}=[10]\text{CPP}$ salt, and its notable properties induced by the specific intermolecular interaction between $\text{Li}^+\text{@C}_{60}$ and [10]CPP.

The complex $\text{Li}^+\text{@C}_{60}\text{C}=[10]\text{CPP}$ was immediately formed when $\text{Li}^+\text{@C}_{60}$ and [10]CPP were mixed in dichloromethane. The 1:1 complex of [10]CPP with $\text{Li}^+\text{@C}_{60}$ was unambiguously characterized by NMR, ESI-MS, UV-vis titration as well as X-ray crystal structure analysis (Figure 1). The complexation modulates the electronic state of [10]CPP and $\text{Li}^+\text{@C}_{60}$. UV-vis-NIR spectrum showed new absorption band due to the charge transfer interaction between $\text{Li}^+\text{@C}_{60}$ and [10]CPP. In addition, the complexation renders $\text{Li}^+\text{@C}_{60}$ less reducible, which indicates the increase of electron density of $\text{Li}^+\text{@C}_{60}$ induced by the electron transfer interaction. In the presentation, other interesting results such as photophysical property of the ionic complex will also be discussed.

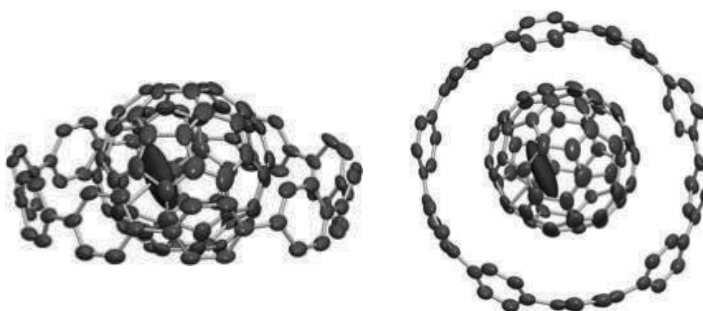


Figure 1. X-ray structure of $\text{Li}^+\text{@C}_{60}\text{C}=[10]\text{CPP}$ cation. Side view (left) and top view (right).

[1] Omachi, H. *et al. Acc. Chem. Res.* **2012**, *45*, 1378. [2] Iwamoto, T. *et al. Angew. Chem. Int. Ed.* **2011**, *123*, 8492.
[3] Aoyagi, S. *et al. Nature Chem.* **2010**, *2*, 678. [4] Ueno, H. *et al. Chem. Commun.* **2013**, *49*, 7376.

Corresponding Author: K. Itami

Tel and Fax: +81-52-789-5916, E-mail: itami@chem.nagoya-u.ac.jp

The Quantitative Importance of Purity on the Properties of Single Wall Carbon Nanotubes

○Naoyuki Matsumoto^{1,2}, Guohai Chen¹, Motoo Yumura^{1,2}, Don N. Futaba^{1,2}, Kenji Hata^{1,2}

¹ *Technology Research Association for Single Wall Carbon Nanotubes (TASC), Central 5, 1-1-1 Higashi, Tsukuba, Ibaraki 305-8565, Japan*

² *National Institute of Advanced Industrial Science and Technology (AIST), Central 5, 1-1-1 Higashi, Tsukuba, Ibaraki 305-8565, Japan*

No doubt surrounds the unique and exceptional properties of single-walled carbon nanotubes (SWCNTs); however, these properties pertain to the pristine SWCNTs, when in truth SWCNTs are never free from carbonaceous impurities. These impurities, both amorphous (sp^3) and graphitic (sp^2) in structure, are easily adsorbed to the outer surface of the SWCNTs during the synthesis process [1]. Fundamentally, through both theoretical and experimental reports, the clear understanding has been developed on the interaction of these impurities on SWCNTs to degrade these unique properties, such as electronic and thermal conductivity [2, 3]. These reports demonstrate that purity is undoubtedly important. However, question remains, how important? To date, due to our inability to quantify purity and our inability to develop purification processes that do not induce damage, the quantitative importance of carbonaceous impurities on the properties of SWCNTs remains unclear.

We quantitatively investigated the importance of purity on the application of SWCNTs by examining their effects on the electrical, thermal, mechanical, and dispersion properties for both the as-grown SWCNT forest, dispersion, and processed buckypaper. In contrast to previous reports, rather than using purification processes, we fabricated a family of SWCNT forests by the water-assisted (Super-growth) CVD method varying only in purity through post synthetic carbon deposition from nearly ideally pure (97%) to exceptionally dirty (38%). Our results showed that not only did nearly every property at every stage, from the as-grown SWCNT forest, dispersion, to the processed buckypaper, decrease, they decreased nonlinearly with the greatest fractional decrease (25-75%) occurring within the first 15% decrease in purity. For example, the SWCNT forest thermal diffusivity, the dispersability, and the buckypaper breaking strength decreased by 65, 45, 50%, respectively within this span. To add perspective on these results, SWCNTs with a purity of 85% (15% drop from ideal) would still possess a specific surface area of over 800 m²/g.

Furthermore, as SWCNT the synthetic structural control further advances, these results demonstrate that purity is as important as crystallinity, length, and diameter, on improving properties and should not be neglected as it can offset any improvement due to other structural improvements.

[1] S. Yasuda *et al.* Nano Lett. **9**, 2585 (2009)

[2] P. R. Bandaru J. Nanosci. Nanotech. **7**, 1 (2007)

[3] J. Hone *et al.* J. Phys. Chem. B, **59**, R2514 (1999)

Corresponding Author: Don N. Futaba

Tel/Fax: +81-29-861-4851

E-mail: d-futaba@aist.go.jp

MD simulation on RBM frequency of bundled SWNTs

○A. Beniya¹, N. Homma¹, S. Chiashi², Y. Homma¹, T. Yamamoto³

¹Department of Physics, Tokyo University of Science, Tokyo 162-8601, Japan

²Department of Mechanical Engineering, The University of Tokyo, Tokyo 113-8656, Japan

³Department of Liberal Arts, Tokyo University of Science, Tokyo 162-8601, Japan

Radial Breathing Mode (RBM) is one of the most important vibrational modes of single-walled carbon nanotubes (SWNT), because the measurement of RBM frequency ω_{RBM} allows us to uniquely assign the chirality to an individual SWNT by resonant Raman scattering. It is known that ω_{RBM} responds sensitively to surrounding environment around an SWNT. Recently, we showed both experimentally and theoretically that ω_{RBM} of an *individual* SWNT is up-shifted when the SWNT is exposed to water vapor [1]. On the other hand, an SWNT embedded in bundled SWNTs is not exposed to ambient air, but it receives van der Waals force from the surrounding SWNTs. Thus, we can expect that ω_{RBM} of bundled SWNTs is also up-shifted in comparison to that of an SWNT in vacuum. In this paper, we quantitatively analyze the up-shift of ω_{RBM} of bundled SWNTs using molecular dynamics (MD) simulation.

In order to estimate ω_{RBM} of bundled SWNTs, we prepare an SWNT bundle consisting of six (13,0) SWNTs as shown in Fig.1, and calculate the vibrational spectrum of an SWNT located at the core of bundled SWNTs. The obtained ω_{RBM} was $\sim 228 \text{ cm}^{-1}$ and it is $\sim 6 \text{ cm}^{-1}$ higher than ω_{RBM} of an individual SWNT in vacuum. This ω_{RBM} shift is comparable to the shift in the case of an individual (13,0) SWNT in water vapor we previously obtained [1]. In this symposium, we present MD simulation results of ω_{RBM} for various chirality types of bundled SWNTs, and discuss the diameter dependence of ω_{RBM} shift.

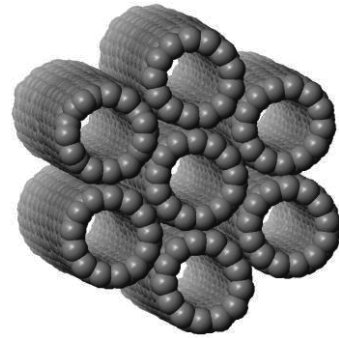


Fig.1: Bundled SWNTs

Reference

[1] Y. Homma, *et al*, *Phys. Rev. Lett.* **110**, 157402-1-4 (2013)

Corresponding Author: Takahiro Yamamoto

Tel: +81-3-5876-1486, Fax: +81-3-5876-1486,

E-mail: takahiro@rs.tus.ac.jp

Molecular structure of chalcogen encapsulated in single-walled carbon nanotubes studied by molecular dynamics simulations

○¹Yutaka Sato, ²Yosuke Kataoka, and ^{1,2,3}Hironori Ogata

¹ Graduate School of Science and Engineering, Hosei University, Koganei 184-8584, Japan

²Department of Faculty of Bioscience and Applied Chemistry, Hosei University, Koganei, 184-8584, Japan

³Research Center for Micro-Nano Technology, Hosei University, Koganei 184-0003, Japan

Single-walled carbon nanotubes(SWNTs) have a hollow space in the nanometer size that can be encapsulated various functional molecules. The confined environments of nanotubes permit the formation of various kinds of unique encapsulated low dimensional structures with unusual properties compared with the bulk materials. Recently, synthesis of sulfur encapsulated SWNTs(DWNTs) and one-dimensional sulfur structures have been reported by Fujimori *et al.* [1]. They also reported that these one-dimensional sulphur chains show the conducting character under ambient pressure. In this study, we report the effects of chirality and tube diameter of SWNTs on the local structure of the sulfur and selenium by using molecular dynamics(MD) simulations.

MD simulations were conducted by using SCIGRESSVer2.3.0(Fujitsu). We used the GEAR method of the fifth order in the numerical integration and the speed scaling method in the temperature control. One SWNT and arbitrary number of sulfur atoms were set in a rectangular cell. First, the relaxation calculation were conducted at 1K with the NVT ensemble for the encapsulation of sulfur. Stable structure at 297 K was calculated after the relaxation calculation at 800 K.

Figure1 shows one example of the structure of sulfur encapsulated in (6 , 6) SWNT at 297K. Sulfur encapsulated in SWNT took one-dimensional chain structure. The detailed systematic results will be presented.

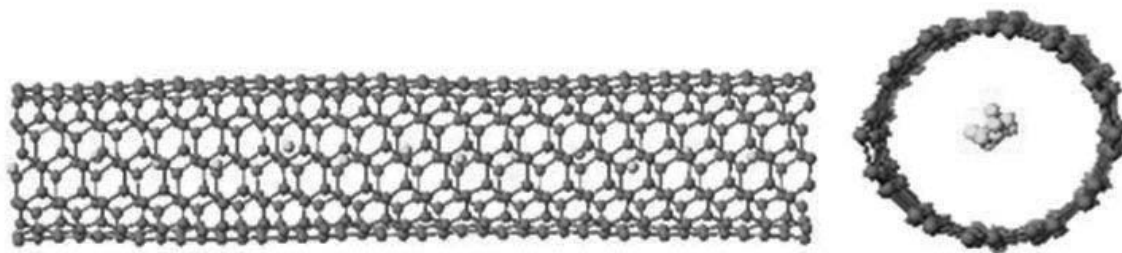


Figure 1. The structure of S@SWNT at 297K

[1] Toshihiko Fujimori *et al.* *Nature Commun.* **4**(2013)2162.

[2]Frank H.Stillinger *et al.* *J.Phys.Chem.*, **85**(1986)6460.

[3]Frank H.Stillinger *et al.* *J.Phys.Chem.* 1987, 91 (19), pp4899-4907

Local structure and properties of the alkali halides encapsulated in single-walled carbon nanotubes studied by molecular dynamics simulations

○Eita Yokokura¹, Yosuke Kataoka² and Hironori Ogata^{1,2,3}

¹ Department of Faculty of Bioscience and Applied Chemistry, Hosei University, Koganei, 184-8584, Japan

² Graduate School of Engineering, Hosei University, Koganei, 184-8584, Japan

³ Research Center for Micro-Nano Technology, Hosei University, Koganei, 184-0003, Japan

Single-walled carbon nanotubes (SWNTs) have a hollow space in the nanometer size that can be encapsulated various functional molecules. The confined environments of nanotubes permit the formation of various kinds of unique encapsulated low dimensional structures with unusual properties compared with the bulk. Synthesis of alkali halide encapsulated SWNTs and their structures have been reported[1-2]. However, the systematic studies on the local structure and some properties(ion conductivity, melting point *etc.*) encapsulated in SWNTs with different diameters and chirality have not been reported. In this study, we report the effects of the diameter and chirality of SWNTs on the local structure and melting point of the encapsulated alkali halides by using molecular dynamics (MD) simulations.

In our MD simulations, we used the Born-Mayer-Huggins-Tosi-Fumi intermolecular potential between the alkali halide ions and the Dreiding potential between carbon atoms in SWNT. One SWNT and any number of alkali halide ions around SWNT were set in a rectangular cell as initial configuration. Stable structure at 298 K was calculated with the NVT ensemble after the relaxation calculation at 1100 K. The relaxation calculation was conducted after temperature was increased by 10 K from 298K.

Figure 1 shows the local structures of the potassium iodide (KI) encapsulated in (a)(8, 8) tube and (b)(10, 10) tube at 298 K. KI are oriented in units of 2x2 crystallites in vertical along the longitudinal axis of the tube. The detailed systematic results will be presented.

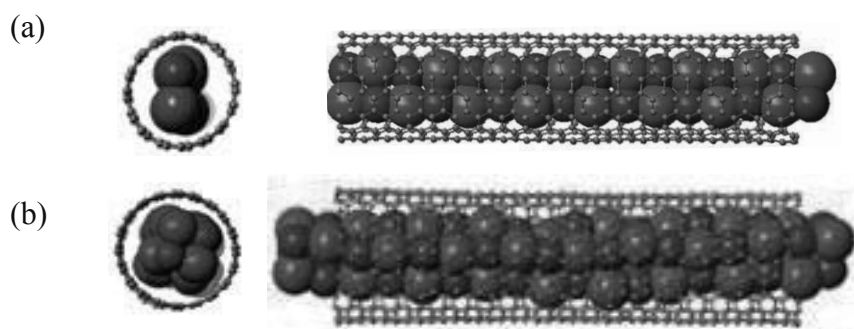


Figure1. Local structure of KI crystals encapsulated in (a),(b)(8,8) and (10,10) SWNT.

References

[1] J. Sloan, M. C. Novotny, S. R. Bailey et al., *Chem. Phys. Lett.* **329**(2000)61.

[2] R. R. Meyer, J. Sloan, R. E. Dunin-Borkowski, A. I. Kirkland, M. C. Novotny, S. R. Bailey, J. L. Hutchison, and M. L. H. Green, *Science* **289**(2000) 1324.

Tel: +81-42-387-6229, Fax: +81-42-387-6229, E-mail: hogata@hosei.ac.jp

Ultralow mode-volume photonic crystal nanobeam cavities for high-efficiency coupling to individual carbon nanotube emitters

○H. Machiya¹, R. Miura¹, R. Ohta², S. Imamura¹, A. Ishii¹, X. Liu¹, T. Shimada¹,
S. Iwamoto², Y. Arakawa², Y. K. Kato¹

¹ *Institute of Engineering Innovation, The University of Tokyo, Tokyo 113-8656, Japan*

² *Institute of Industrial Science, The University of Tokyo, Tokyo 153-8505, Japan*

The unique emission properties of single-walled carbon nanotubes are attractive for achieving increased functionality in integrated photonics. In addition to being room-temperature telecom-band emitters that can be directly grown on silicon, they are ideal for coupling to nanoscale photonic structures. Here we discuss high-efficiency coupling of individual air-suspended carbon nanotubes to silicon photonic crystal nanobeam cavities [1]. Photoluminescence images of dielectric- and air-mode cavities reflect their distinctly different mode profiles and show that fields in the air are important for coupling. We find that the air-mode cavities couple more efficiently, and estimated spontaneous emission coupling factors reach a value as high as 0.85. We also describe our recent efforts on optimizing the designs of air-mode cavities and their fabrication processes. Our results demonstrate advantages of ultralow mode-volumes in air-mode cavities for coupling to low-dimensional nanoscale emitters.

This work was supported by SCOPE, KAKENHI (24340066, 24654084, 26610080, 26870167), Asahi Glass Foundation, Canon Foundation, KDDI Foundation, as well as the Project for Developing Innovation Systems and the Photon Frontier Network Program of MEXT, Japan. A.I. is supported by MERIT and JSPS Research Fellowship. The devices were fabricated at the Center for Nano Lithography & Analysis at The University of Tokyo.

[1] R. Miura, S. Imamura, R. Ohta, A. Ishii, X. Liu, T. Shimada, S. Iwamoto, Y. Arakawa, Y. K. Kato, *Nature Commun.* **5**, 5580 (2014).

Corresponding Author: Y. K. Kato

Tel: +81-3-5841-7702, Fax: +81-3-5841-7772

E-mail: ykato@sogo.t.u-tokyo.ac.jp

Characteristic variation of thin-film transistors based on purified semiconducting carbon nanotubes

○Jun Hirotani¹, Ryotaro Matsui¹, Shigeru Kishimoto¹, and Yutaka Ohno^{1,2}

¹Graduate School of Engineering, Nagoya University, Nagoya 464-8603, Japan

²EcoTopia Science Institute, Nagoya University, Nagoya 464-8603, Japan

Carbon nanotubes (CNTs) provide great potential for high-performance flexible devices [1,2] because of exceptional intrinsic electrical, mechanical, and thermal properties. Though great efforts have been made to achieve high-performance CNT thin-film transistors (TFTs), one of critical issues for practical applications is device-to-device variation in their electrical characteristics [3]. Characteristic variation of CNT TFTs depends on the uniformity of CNT networks which can be improved by increasing number density of CNTs but also affected by fabrication process. Though theoretical [4] and experimental [5] studies have been conducted, further investigations are necessary both for reducing the variation and for enhancing the yield of devices.

In this work, we have investigated electrical performance and characteristic variation of CNT TFTs as changing number density of CNTs in the channel. We used high-purity (~95%) semiconducting single-walled CNTs to avoid a formation of short paths of metallic SWNTs in a high-density CNT film. The CNT film was formed on a SiO₂/Si substrate by the vacuum filtration and transfer method. An SEM image of the CNT film and schematic structure of back-gate CNT TFT are shown in the insets of Figure. The channel length and width are 100 μm.

More than a hundred CNT TFTs were measured for each CNT densities, and Figure shows transfer characteristics for a CNT density. The typical on/off ratio was 10⁵ ~ 10⁶, and ON-current variation was ~20% in terms of a standard derivation divided by average ON-current. Our results show that as the CNT density increases, the variation in ON-current tend to be eliminated, while the variation is still larger than predicted by simulation.

Acknowledgements: The semiconducting SWNTs were provided by TASC. This work was partially supported by Grant-in-Aid by MEXT, JST/SICORP, and JST/ALCA.

[1] Q. Cao *et al.*, Nature **454**, 495 (2008).

[2] D.-M. Sun *et al.*, Nature Nanotechnol. **6**, 156 (2011).

[3] A. E. Islam, Electronics **2**, 332 (2013).

[4] N. Pimparkar *et al.*, IEEE Trans. Electron Devices **54**, 637 (2007).

[5] M. Shimizu *et al.*, Appl. Phys. Exp. **6**, 105103 (2013).

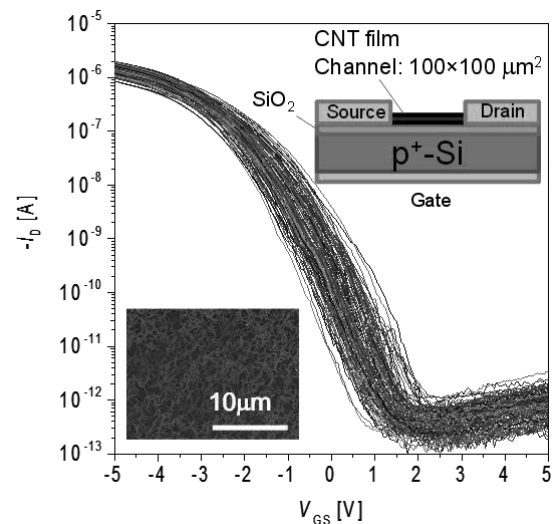


Figure. Transfer characteristics of 124 CNT TFTs. Insets: schematic device structure and an SEM image of channel.

Corresponding Author: Yutaka Ohno, Tel & Fax: +81-52-789-5387, E-mail: yohno@nagoya-u.jp

Thermoelectric power of carbon nanotubes from first principles

○ N. T. Hung, R. Saito

Department of Physics, Tohoku University, Sendai 980-8578, Japan

Carbon nanotubes as one-dimensional (1-D) structures can have either semiconducting or metallic properties dependent on their chiral vectors, which are denoted by two integers (n, m) [1]. This opens up a promising candidate for high-performance thermoelectricity with large thermoelectric power (TEP). In this work, the TEP of a series of semiconducting single-walled carbon nanotubes (s-SWNTs) is investigated from first principles calculations by using the density functional theory (DFT) [2, 3] and the Boltzmann transport equation. The Wannier function-based interpolation (Wannier90 code) [4] techniques are applied to compute all the ultra-dense electronic structure. We did not use the constant relaxation time approximation commonly practiced in the literature because it cannot explain the transport properties of s-SWNTs [5]. Instead, we calculate the relaxation time directly from electron-phonon interaction. Since the large number of atoms in the s-SWNTs is expensive to calculate full phonon dispersions within the DFT framework, here we utilize the extended tight-binding model (ETB) [5, 6] based on the DFT to obtain the electron-phonon matrix elements. The Seebeck coefficients are found to be in good agreement with recent theoretical studies using non-equilibrium Green's function method [7, 8]. A comparison with the experimental TEP of the s-SWCNTs films samples [9] is also provided. The results show that the TEP is strongly dependent on the band-gap and temperature. In other words, the thermoelectricity of CNTs can be controlled by their geometrical structure.

References:

- [1] R. Saito, G. Dresselhaus, M. S. Dresselhaus, "Physical properties of carbon nanotubes", Imperial college press (1998).
- [2] P. Hohenberg et al., *Phys. Rev.* **136**, B864 (1964).
- [3] W. Kohn et al., *Phys. Rev. A* **140**, A1133 (1965).
- [4] N. Marzari et al., *Rev. Mod. Phys.* **84**, 1419 (2012).
- [5] J. Jiang et al. *Phys. Rev.* **71**, 045417 (2005).
- [6] J. Jiang et al. *Phys. Rev.* **72**, 235408 (2005).
- [7] X. Tan et al., *Nanoscale Research Lett.* **7**, 116 (2012).
- [8] J. W. Jiang et al., *J. Appl. Phys.* **109**, 014326 (2011).
- [9] K. Yanagi et al. *Nano Lett.* **14**, 6437 (2014).

Corresponding Author: Nguyen Tuan Hung

TEL: +81-22-795-6442, FAX: +81-22-795-6447

E-mail: nguyen@flex.phys.tohoku.ac.jp

Effect of TiO₂ coating on field emission properties of carbon nanotube by in-situ transmission electron microscopy

Masahiro Matsuda, Hitoshi Nakahara, Koji Asaka and Yahachi Saito

Department of Quantum Engineering, Nagoya University, Furo-cho, Nagoya 464-8603

Field emission characteristics from a multiwall carbon nanotube (MWNT) are influenced by their tip structures and materials deposited on its surface. In order to clarify the role of TiO₂ deposition on MWNT, we studied field emission properties of TiO₂-coated MWNT emitters by in-situ transmission electron microscopy (TEM).

Amorphous TiO₂ was deposited on MWNTs attached to an edge of a gold plate by electron beam deposition, as shown in Fig.1. A gold-coated tungsten tip was used as an anode. Emission current - electric field characteristics and emission stability of TiO₂-coated emitter were measured in an electron microscope.

Fig. 2 shows thickness vs threshold field and emission area. The distance between the anode and a MWNT emitter was 300 nm. When thickness of TiO₂ was 0.3 nm, the threshold field (field required to give a current of 10 nA) was the lowest (271 V/μm). Possible reasons for the decrease in

the threshold field are the decrease in work function 4.0 eV for TiO₂, 4.5 eV for MWNT and enlargement of the emission area (from 7.6 nm² without TiO₂ to 1696.4 nm² for 0.3 nm TiO₂ derived from Fowler-Nordheim plots). Further increase in TiO₂ thickness made the threshold field higher than that in the uncoated MWNT. This may be caused by the decrease in the electric field concentration due to the increase in tip radius.

Emission fluctuation, which is defined by standard deviation divided by average current, is employed to evaluate emission stability. The fluctuation values were 0.46 and 0.19 for uncoated and 1.6 nm TiO₂-coated MWNT, respectively, showing that the TiO₂ coating improves emission stability. It is considered that adsorption and desorption of residual gases may be suppressed by TiO₂ and the enlarged emission area averages out the local instabilities.

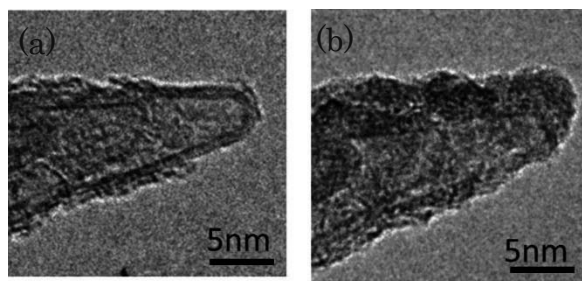


Fig.1 before (a) and after (b) 0.5nm TiO₂ coating on MWNT

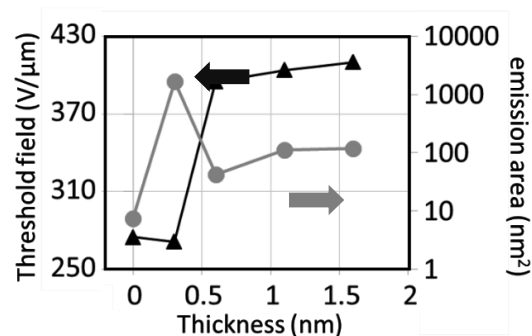


Fig.2 thickness - threshold field and emission area

Light-emitting Electrochemical Cell with Few-Walled Carbon-Nanotube Electrodes

○Ko Nakayama¹, Hiroyuki Shirae², Suguru Noda², Tomo Sakanoue¹,
Taishi Takenobu^{1,3,4}

¹ Department of Applied Physics, Waseda University, Tokyo 169-8555, Japan

² Department of Applied Chemistry, Waseda University, Tokyo 169-8555, Japan

³ Department of Advanced Science and Engineering, Waseda Univ., Tokyo 169-8555, Japan

⁴ Kagami Memorial Laboratory, Waseda University, Tokyo 169-0051, Japan

Recently, touch screens become core components of mobile terminal devices and transparent conductive films of ITO (indium tin oxide) are inevitable for device fabrication. However, due to their rarity and inflexibility, flexible transparent conductive films without rare materials have been strongly required for the next generation flexible electronics. Although carbon-nanotube film is expected to be one of the candidates for flexible transparent conductive films, the demonstration of flexible device is still seriously limited. Therefore, in this paper, we tried to apply few-walled carbon-nanotube (FWCNT) films into electrodes of light-emitting devices.

For this purpose, we fabricated the light-emitting electrochemical cell (LEC), which has very simple layered structures [1]. As shown in Fig.1, firstly, we prepared few-walled carbon-nanotube films on flexible PET (polyethylene terephthalate) films. The light-emitting layer of LEC is the mixture of fluorescent organic polymer and electrolyte, and, in this research, we selected Super Yellow (PDY-132) and ionic liquid ($P_{88812}BF_4$), respectively. The mixture with weight ratio of 4 (polymer) : 1 (ionic liquid) was spin-coated on flexible FWCNT films. Finally, the aluminum electrode was thermally deposited. The fabricated devices emitted yellow light and the luminance reached 1300 cd/m^2 at 10V with the efficiency of 5.36 cd/A , which is higher than that of similar LECs with ITO electrodes (1.09 cd/A). This result shows the potential high performance of nanotube films as flexible conductive films.

[1] T. Sakanoue, T.T et al., APL, 100, 263301 (2012)

Corresponding Author: T. Takenobu

Tel/Fax:+81-3-5286-2981, E-mail: takenobu@waseda.jp

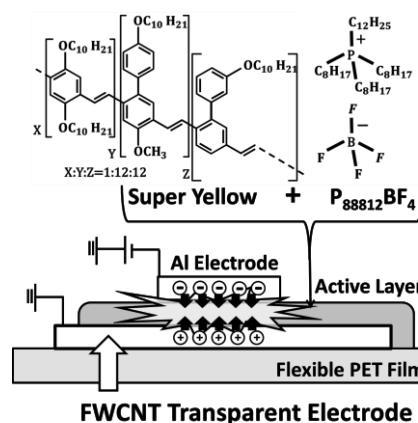


Fig.1. Device structure of LEC



Fig.2. Photo of LEC with FWCNT

Synthesis of Single-Walled Carbon Nanotubes from Rh Catalysts by Alcohol Gas Source Method in high Vacuum

○Akinari Kozawa¹, Takahiro Saida², Shigeya Naritsuka¹, Takahiro Maruyama^{1,2}

¹ Department of Materials Science and Engineering, Meijo Univ., 1-501 Shiogamaguchi, Tempaku, Nagoya 468-8502, Japan

² Department of Applied Chemistry, Meijo Univ., 1-501 Shiogamaguchi, Tempaku, Nagoya 468-8502, Japan

Single-walled carbon nanotubes (SWNTs) have been anticipated for application in a lot of future nanodevices. To fabricate SWNT devices, it is important to grow SWNTs with uniform chirality and diameter. So far, we have been reporting SWNT growth using Pt catalysts by CVD under a low ethanol pressure and succeeded in obtaining SWNTs with small diameters below 1.2 nm [1]. This suggests that metal catalysts with a high-melting point are effective to grow SWNTs with small and uniform diameters. In this study, we attempted to grow SWNTs using Rh as catalysts since the melting point of Rh (1966°C) is higher than Pt, and it might have advantage to form SWNTs with narrow chirality.

Using Rh catalysts, SWNTs were grown on SiO₂/Si substrates by the alcohol gas source method in the UHV chamber, a type of cold-wall CVD equipment [2]. The growth temperature was set between 500 and 700°C, and the ethanol pressure was varied between 1×10^{-5} and 1×10^{-2} Pa. The grown SWNTs were characterized by FE-SEM and Raman spectroscopy.

Fig. 1 shows the Raman spectra of SWNTs grown from Rh catalysts on SiO₂/Si substrates. The growth temperature and ethanol pressure were 700°C and 1×10^{-3} Pa, respectively. A sharp G-band and RBM peaks were observed, indicating that SWNTs were grown from Rh catalysts. It should be noted that D band intensity was very weak and that G/D ratio was more than 20, showing that the quality of SWNTs were fairly good. Our results showed that Rh is a useful catalyst to grow high-quality SWNTs. We will also discuss the difference between Rh and Pt catalysts in the SWNT growth.

[1] T. Maruyama *et al.* Mater. Express **1** (2011) 267.

[2] H. Kondo *et al.* Jpn. J. Appl. Phys. **52** (2013) 06GD02.

Corresponding Author: T. Maruyama

Tel: +81-52-838-2386, Fax: +81-52-832-1179,

E-mail: takamaru@meijo-u.ac.jp

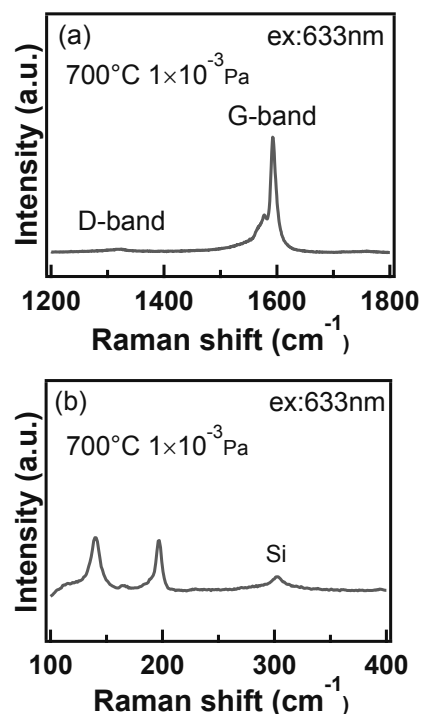


Fig.1 (a) High-frequency region and (b) RBM region of Raman spectra of SWNTs grown at 700°C.

Relationship between Chirality Control of Single-Walled Carbon Nanotube and Wavelength of the Irradiated Free Electron Laser

○Keisuke Yoshida, Yusaku Tsuda, Daiki Kawaguchi, Tomoko Nagata,
Nobuyuki Iwata and Hiroshi Yamamoto

*Department of Electronic Engineering, College of Science & Technology, Nihon University,
7-24-1 Narashinodai, Funabashi, Chiba 274-8501 Japan*

Single-walled carbon nanotube (SWNT) is one of the candidates for future applications in nanoelectronic devices due to its high mobility and high current-carrying capacities. As the electric properties of SWNTs are metallic or semiconducting depending on their chirality, the chirality control is required. We have succeeded in growing chirality controlled SWNTs by irradiating 800 nm free electron laser (FEL) during growth process using cold-wall chemical vapor deposition (CVD) method¹⁾. All grown SWNTs were semiconductor having 1.12 nm in diameter, which was revealed from multi excited laser Raman analysis. In this study we report chirality control as the wavelength of the FEL is varied. The process of chirality control is as follows: i) investigation of optimized CVD condition to grow SWNTs with specific diameter, ii) selection of resonantly absorbed wavelength of the FEL, iii) selective growth of SWNTs with specific chirality.

The SWNTs were prepared by alcohol CVD method. The SWNTs were grown at 650°C for 10 min under ethanol flow at 2kPa with Co/Mo catalysts deposited by dipping technique. FEL was irradiated during the growth.

Figure 1 shows the Raman spectra of the SWNTs grown with or without 700 nm FEL irradiation. The SWNTs diameters were 0.90 nm and 1.08 nm with FEL, while only 1.08 nm diameter SWNTs grew without FEL. As the chirality of SWNTs depends on the band gap, Raman spectra indicate that FEL irradiation enhance the SWNTs growth having the specific chirality. We expect that various chirality is selectively grown using various wavelength of the FEL. More detailed results will be discussed.

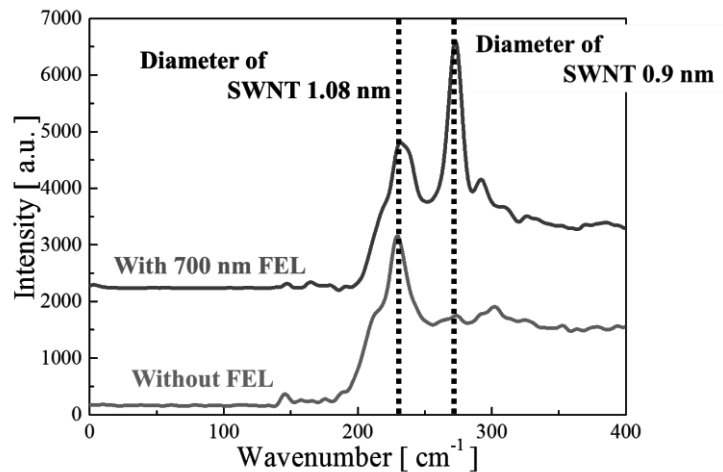


Fig.1 Raman spectra of the SWNTs grown with the 700 nm FEL.

Used excitation laser was 532 nm.

[1] K.Sakai, *et al.*, IEICE TRANS. Electron, **E94-C** (2011) 1861.

Synthesis of single walled carbon nanotubes by using sputtered Co/Cu and Co/W as catalyst

○Hua An, Kehang Cui, Rong Xiang, Taiki Inoue, Shohei Chiashi, Shigeo Maruyama

Department of Mechanical Engineering, The University of Tokyo, Tokyo 113-8656, Japan

Ever since their discovery, single walled carbon nanotubes (SWNTs) have attracted intensive attention because of their special electronic properties and potential applications. Unfortunately, the as-grown SWNTs are always a mixture of various chiralities, which limits their application in nanoelectronics. Since the chirality determines the structure of SWNTs, diameter control and chirality control are the prerequisite to obtain SWNTs with homogeneous properties. Extensive researches have focused on the diameter-control and chirality-control growth of SWNTs. However, it is a critical challenge to grow single-chirality SWNTs. Recently, tungsten-based bimetallic nano-clusters have been used as catalysts to grow SWNTs with a single chirality of (12, 6), resulting in an abundance higher than 92%[1].

In this study, we used two exotic bimetallic combinations Co/Cu and Co/W as catalysts to grow SWNTs by alcohol catalytic chemical vapor deposition (ACCVD) [2]. The catalysts were prepared on silicon substrates by a simple sputtering method. The SWNTs were characterized by scanning electron microscopy (SEM), Raman spectroscopy, optical absorption spectroscopy and transmission electron microscopy (TEM). We found that SWNTs obtained from Co/Cu catalyst have much smaller diameter than those grown from conventional Co or Co/Mo [3]. Temperature-dependent studies clearly proved that the introduction of copper facilitated the growth of small-diameter SWNTs at low temperatures. Meanwhile, high-quality and uniform SWNTs were obtained when we used Co/W to grow SWNTs. The chirality distribution and growth mechanism will be presented.

[1] F. Yang *et al.*, *Nature* **510**, 522 (2014).

[2] S. Maruyama *et al.*, *Chem. Phys. Lett.* **360**, 229 (2002).

[3] R. Xiang *et al.*, *ACS Nano* **6**, 7472 (2012).

Corresponding Author: Shigeo Maruyama

Tel: +81-3-5841-6421, Fax: +81-3-5800-6983

E-mail: maruyama@photon.t.u-tokyo.ac.jp

Control of In-Plane Orientation and Chirality of Single-Walled Carbon Nanotubes using Hot-Walled Chemical Vapor Deposition Method and Free Electron Laser

○Daiki Kawaguchi¹, Keisuke Yoshida¹, Yusaku Tsuda¹
Tomoko Nagata¹, Nobuyuki Iwata¹ and Hiroshi Yamamoto¹

¹ Department of Electronics & Computer Science, College of Science & Technology, Nihon University, 7-24-1 Narashinodai, Funabashi, Chiba 274-8501 Japan

Single-walled carbon nanotube (SWNT) has many advantages for application, such as high conductance, maximum allowable current density and mechanical strength. However, SWNTs can be both metal and semiconductor, depending on their chirality. Thus the control of the chirality is required. The in-plane orientation of the SWNTs are also essential for the electric devices.

We have succeeded in controlling the chirality and obtained all semiconductive SWNTs by irradiation of free electron laser (FEL) during growing process on SiO₂/Si substrate^[1]. The irradiation of FEL may enhance the growth of SWNTs having specific bandgap, which corresponds to the photon energy of the FEL. We also succeeded in growth of *in-plane* aligned SWNTs on crystal quartz. In this study, we report the simultaneous control of the chirality and in-plane orientation.

The SWNTs were grown by alcohol catalyst chemical vapor deposition (ACCVD) method on ST-cut quartz substrate for the *in-plane* orientation. The catalyst was evaporated Co/Fe nano-particles. Fig. 1(a) shows the dynamic force microscope (DFM) image. Well-oriented SWNTs were observed. Fig. 1(b) shows the Raman spectrum. Radial breathing mode (RBM) signals indicates the growth of SWNTs having 1.00 nm and 1.06 nm diameters.

The simultaneous control of the chirality and *in-plane* orientation will be reported in the presentation.

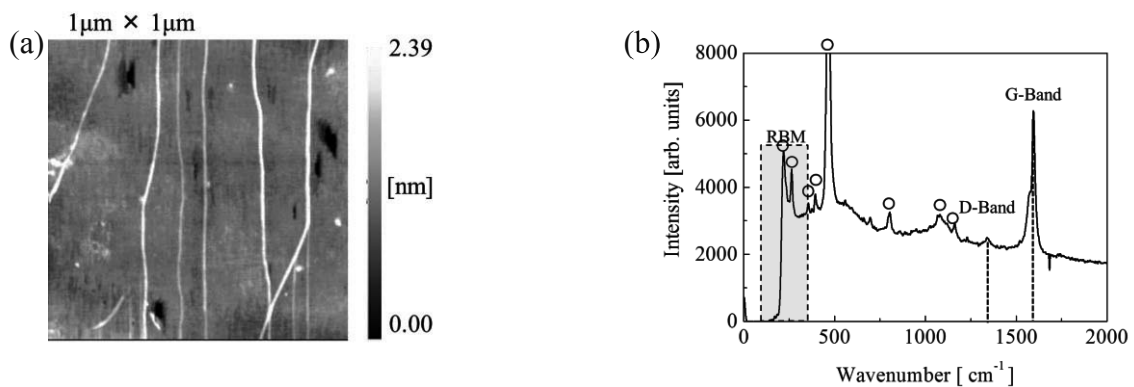


Fig. 1 (a) DFM image and (b) Raman spectra. Open circles indicate the peak arising from the substrate.

[1] K. Sakai *et al.* IEICE Trans. Electron. **E94-C**, 1861 (2011)

Corresponding Author: N. Iwata

Tel: +81-47-469-5457, Fax: +81-47-469-5457,

E-mail: iwata.nobuyuki@nihon-u.ac.jp

The Effects of Hydrogen Atom on Cobalt Clusters in the Reaction with H₂O Investigated by FT-ICR Mass Spectrometer

○Yuta Tobari¹, Kazuki Ogasawara², Yoshinori Sato², Makoto Saito², Shohei Chiashi², Shigeo Maruyama², Toshiki Sugai¹

¹ Department of Chemistry, Toho University, Funabashi 274-8510, Japan

² Department of Mechanical Engineering, The University of Tokyo, Tokyo 113-8656, Japan

In the carbon nanotube growth, reduction processes with H₂ on Co-related materials have been widely used to prepare catalysts or Co clusters. However after the preparation of the catalysts, H₂ have not been thought to play crucial roles on Co clusters but to react with nascent nanotube precursors directly. Here, we present salient differences between cobalt clusters, Co_n⁺, and hydrogenated cobalt clusters, Co_nH⁺, in the reaction with H₂O, which was performed by Fourier transform ion cyclotron resonance (FT-ICR) mass spectrometer.

The details of the experiment have been described elsewhere [1]. Co_n⁺ and Co_nH⁺ were produced by a laser vaporization cluster source with a Co metal plate and a supersonic He jet. These precursor clusters were trapped within an ICR cell and were then exposed to H₂O at 1.2×10⁻⁴ Pa and at room temperature for 4 s. The product ions were mass analyzed after the exposure.

Figure 1 shows the mass spectra of the precursor and the product ions. The intensity ratio between Co_n⁺ and Co_nH⁺ was almost constant in the entire size range (Fig. 1a). After the exposure to H₂O, all Co_n⁺ were mainly converted into simple adsorption products of Co_n(H₂O)⁺ without any size dependence (Fig. 1b). On the other hand, Co_nH⁺ were converted into Co_n(OH)⁺ in the smaller size range (9 ≤ n ≤ 13) indicating that the hydrogen on the Co clusters act as a promoter to break H₂O. The larger Co_nH⁺ clusters (13 ≤ n ≤ 18) were converted into simple adsorption products of Co_nH(H₂O)⁺. This enhancement effect of a hydrogen atom on Co clusters has also been reported in the reaction with NO [2]. The observed salient difference between Co_n⁺ and Co_nH⁺ suggests that the role of hydrogen should be investigated not as simple hydrogen gas but as the catalyst system with Co clusters.

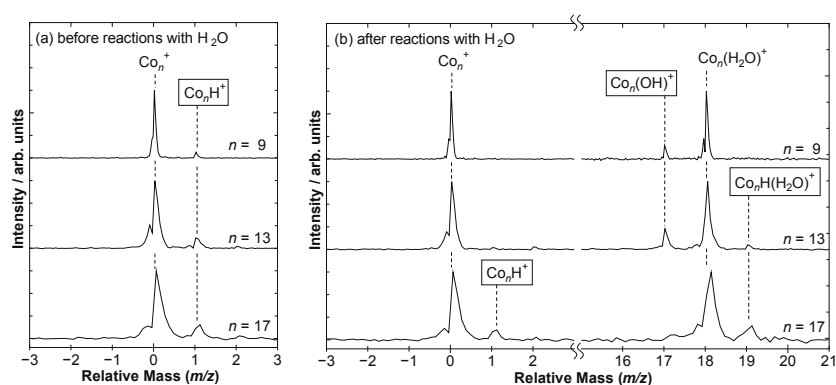


Fig. 1 High-resolution mass spectra of Co_n⁺ and Co_nH⁺ (a) before and (b) after reactions with H₂O.

Horizontal axes show mass difference between Co_n⁺ and product ions.

[1] S. Maruyama, *et al.* Rev. Sci. Instrum. **61**, 3686 (1990).

[2] T. Hanmura, *et al.* J. Phys. Chem. A, **111**, 422 (2007).

Corresponding Author: T. Sugai, Tel: +81-47-472-4406, E-mail: sugai@chem.sci.toho-u.ac.jp

Synthesis of carbon nanotubes by means of “molecular template epitaxial growth” approach

○Liu Hong^{1,2}, Akira Takakura^{1,2}, Lawrence T. Scott³, Yuhei Miyauchi^{1,2,4}, Kenichiro Itami^{1,2,5}

¹ Graduate School of Science, Nagoya University, Nagoya 464-8602, Japan

² JST-ERATO Itami Molecular Nanocarbon Project, Nagoya University,
Nagoya 464-8601, Japan

³ Merkert Chemistry Center, Boston College, Chestnut Hill, Massachusetts 02467, USA

⁴ Institute of Advanced Energy, Kyoto University, Uji 611-0011, Japan

⁵ Institute of Transformative Bio-Molecules (WPI-ITbM), Nagoya University,
Nagoya 464-8602, Japan

Carbon nanotubes have been considered as promising nanomaterials in various fields including chemistry, electronics, photonics and biologic science. The past two decades have seen a rapid development in the production strategy of carbon nanotube, which includes arc discharge, laser ablation and chemical vapor deposition (CVD), etc. Though mass production of carbon nanotubes has been realized, several shortcomings are still required to be overcome. First, metal catalysts are normally needed. Second, high temperature is necessary. Third, control of diameter and chirality of synthesized carbon nanotube is difficult. How to synthesize structure-controlled carbon nanotubes with metal-free processes at low temperature remains a challenge.

Here, we report our progress on “growth from template” approach, namely molecular template epitaxial growth (MTEG), in producing carbon nanotubes without using any metal catalyst. The template molecules used in this study are carbon nanoring ([9]cycloparaphenylene, [9]CPP) and molecular end-cap of nanotube ($C_{50}H_{10}$), both of which have been seen as precursors of carbon nanotube (Fig.1).^[1,2] Template molecules were dispersed on c-plane sapphire by spin-casting, and ethanol was used as carbon source gas in the CVD process. In the case of [9]CPP, the temperature of reaction could be as low as 450 °C, which offered carbon nanotubes with a diameter range of 0.8-2 nm (estimated from radial breathing mode of Raman spectra, Fig.2). As a contrast, we found that $C_{50}H_{10}$ -synthesized nanotubes owned much less distribution of chirality and diameter range. Details of the results will be discussed in the conference.

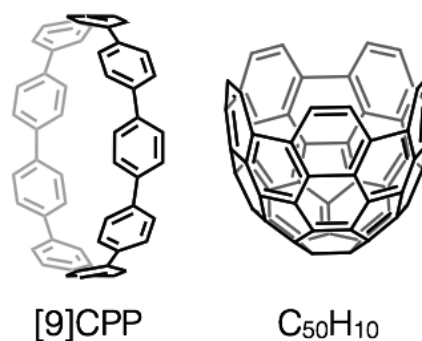


Fig.1 Chemical structure of [9]CPP and $C_{50}H_{10}$

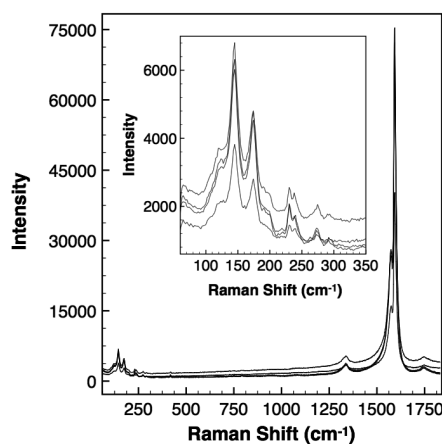


Fig.2 Raman spectra (excitation wavelength: 532 nm) of [9]CPP-synthesized carbon nanotubes measured at different locations. Inset: radial breathing mode region.

[1] H. Omachi *et al.* Nat. Chem. **5**, 572 (2013)

[2] L. T. Scott *et al.* J. Am. Chem. Soc. **134**, 107 (2012)

Corresponding Author: K. Itami, Y. Miyauchi

Tel/Fax: +81-052-788-6098 (K. I) +81-052-789-5916 (Y. M)

E-mail: itami@chem.nagoya-u.ac.jp (K. I) miyauchi.yuhei@d.mbox.nagoya-u.ac.jp (Y. M)

Hybridization of Semiconducting-Single-Walled Carbon Nanotubes and Fullerene-Carrying Carbazole-Fluorene Copolymers

○Fumiyuki Toshimitsu¹, Hiroaki Ozawa¹, Naotoshi Nakashima^{1,2,3}

¹ Department of Applied Chemistry, Kyushu University, Fukuoka 819-0395, Japan

² WPI-ICNER, Kyushu University, Fukuoka 819-0395, Japan

³ JST-CREST, Chiyoda-ku, Tokyo 102-0075, Japan

The combination of single-walled carbon nanotubes (SWNTs) and fullerenes is one of the most desirable systems for the development of nanotube-based electronics, such as organic photovoltaic and optoelectronic devices. Highly purified semiconducting-SWNTs (sem-SWNTs) are suitable for such applications, because the efficiency of the sem-SWNT-based optoelectronic devices has been limited due to the coexistence of the metallic-SWNTs. In addition, random molecular orientations between the sem-SWNTs and acceptors prevent the formation of efficient conducting pathways. Although hybrid materials of covalently modified SWNTs and fullerenes with high power conversion efficiencies (PCE) have been developed,^[1] the covalent nanotube modification lowers the intrinsic properties of the SWNTs, thus leading to lower efficiency than the theoretical value. Recent reports on hybridizing such components using bulk-hetero-junction method^[2] address the sem-SWNT purity and homogeneous composition issues simultaneously, yet the interaction between fullerenes and the SWNTs is only a Van-der-Waals interaction, which is too weak to fix the molecular orientation of the fullerene moieties on the surfaces of the SWNTs for the better performance of this class of composites.

Strategically developed conjugated polymers are one of the key techniques to enhance sem-SWNT properties. Here we report the design and synthesis of new copolymers **1–3** that are composed of fullerene-carrying carbazole and fluorene units with fluorene/carbazole composition ratios of 1:1, 5:1, and 10:1 (for **1–3**, respectively; Fig. 1). Solubilization of SWNTs by using these copolymers was examined by using atomic force microscopy (AFM), photoluminescence (PL), and Vis-NIR absorption and Raman spectroscopic analysis, and was found that 1) all these copolymers acted as sem-SWNT solubilizers and 2) the amount of the solubilized sem-SWNTs depended on the copolymer composition ratios. Furthermore, we propose optimized molecular structures and orientations between the fullerene moieties, copolymer main chains, and the sem-SWNTs based on molecular-mechanics calculations.

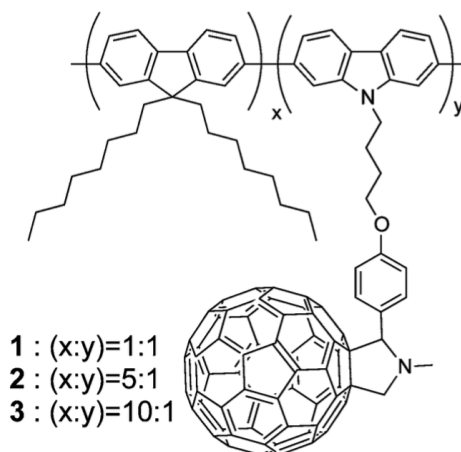


Figure 1. Chemical structures of copolymers 1–3.

[1] T. Umeyama, et al., *Adv. Mater.* **2010**, *22*, 1767–70.

[2] D. J. Bindl, et al., *Nano Lett.* **2011**, *11*, 455–60.

Corresponding Author: N. Nakashima

Tel: +81-92-802-2845, Fax: +81-92-802-2845,

E-mail: nakashima-tcm@mail.cstm.kyushu-u.ac.jp

Cytotoxicity of Carbon Nanohorns Enhanced by Too Much PLPEG

○Maki Nakamura¹, Yoshio Tahara^{1*}, Shinsuke Fukata¹, Minfang Zhang¹, Sumio Iijima^{1,2},
Masako Yudasaka¹

¹ National Institute of Advanced Industrial Science and Technology (AIST), 1-1-1 Higashi,
Tsukuba 305-8565, Japan

² Meijo University, 1-501 Shiogamaguchi, Nagoya 468-8502, Japan

(*Current address: Torii Pharmaceutical Co., LTD. Sakura, Chiba 285-0808, Japan)

In biological studies of nanocarbons, their dispersion in the aqueous solution is requisite. Various dispersants have been tested for nanocarbons, in which phospholipid polyethylene glycol (PLPEG) is one of the good and non-toxic dispersants, having been used in the application studies of nanocarbons to therapy and diagnosis. The coverage of PLPEG molecules on single-walled carbon nanohorn (CNH) surface is saturated at the monolayer level as estimated from the PLPEG quantities adsorbed on CNHs and size measurements with dynamic light scattering method [1]. Under the mono-coverage condition, CNH cytotoxicity is low [1]. On the other hand, it was found that cytotoxicity increased when the excess amount of PLPEG was used [2]. In this report, we discuss the reason for this abnormal toxicity results caused by the excess dose of PLPEG.

The CNHs were dispersed in phosphate buffer saline (PBS) with PLPEG (1,2-distearoyl-*sn*-glycero-3-phosphoethanolamine-*N*-[amino(polyethylene glycol) 2000] (ammonium salt)). PLPEG: CNH quantity ratios were 0.25, 0.5, 1, 2, and 3. These dispersion solutions were added in dishes where RAW264.7 macrophage was cultured at 37 °C in air contacting CO₂ (5%). The dispersion solution and cell culture medium were mixed by rolling the dishes. The final concentrations of CNHs were 0.01, 0.03, 0.1 and 0.3 mg/mL. To discuss the toxicity mechanism, the quantities of CNHs engulfed by RAW264.7 were estimated by measuring 700-nm light transmittance of the cell lysates. The cells were lysed with CellLytic M in the presence of protease inhibitor. After the centrifuge, aliquot of the supernatant was used for the protein assay to estimate the cell numbers, and the remaining lysate was sonicated with a surfactant, Triton X. The obtained dispersion solutions were subjected to the 700-nm light transmittance, and the CNH quantities were estimated by using absorbance-quantity calibration line. The particle sizes of CNHs remained in the cell culture medium were measured with dynamic light scattering.

The results showed that when PLPEG : CNH = 2 or 3, the macrophage uptake quantity of PLPEG-CNH was enhanced, leading to the decrease of cell viability. The mechanism of higher uptake of PLPEG-CNH in larger PLPEG quantity could be ascribed to the PLPEG-CNH agglomeration sizes in the cell culture medium increased at PLPEG : CNH = 3. The reason for this agglomeration size increase will be discussed in the presentation.

[1] M. Yang, M. Wada, M. Zhang, K. Kostarelos, R. Yuge, S. Iijima, M. Masuda, M. Yudasaka. *Acta Biomaterialia*, 9 (2013) 4744–4753.

[2] M. Nakamura, Y. Tahara, S. Iijima, M. Yudasaka, 1P-43, 42nd F-NT-G Symposium, 2012.

Corresponding Authors: M. Nakamura, M. Yudasaka, Tel: +81-29-861-6290, Fax: +81-29-861-6290,

E-mail: ma-ki-nakamura@aist.go.jp, m-yudasaka@aist.go.jp

Electrochemical properties of boron- and nitrogen-doped carbon nanohorn aggregates

○Ryota Yuge¹, Shunji Bandow², Masako Yudasaka³, Kiyohiko Toyama¹, Sumio Iijima⁴,
Noriyuki Tamura¹, and Takashi Manako¹

¹*Smart Energy Research Laboratories, NEC Corporation, Tsukuba 305-8501, Japan*

²*Department of Applied Chemistry, Meijo University, Nagoya 468-8502, Japan*

³*Nanotube Research Center, National Institute of Advanced Science and Technology (AIST),
Tsukuba, 305-8565, Japan*

⁴*Faculty of Science & Technology, Meijo University, Nagoya 468-8502, Japan*

Single-wall carbon nanohorns (SWNHs) [1] are a type of nano-carbon materials such as carbon nanotubes and graphenes, which are attractive having the high electrical conductivity, high dispersibility, and large specific surface area. Recently, it has been reported that nanocarbons and nitrogen- and/or boron-doped nanocarbons indicate the good performance as electrocatalysts for oxygen reduction reaction (ORR) [2-4]. These are potentially low cost catalysts for the fuel cell application because noble metals are not contained [2]. In this study we prepared the nitrogen and/or boron doped SWNHs and controlled the doping concentrations. We also investigated their electrochemical oxygen reduction activity.

SWNHs were prepared by CO₂ laser ablation of a graphite and/or boron-contained graphite target at room temperature in the continuous-wave mode. The gas pressure in the growth chamber was sustained at 760 Torr by controlling the evacuation rate while the flow rate of buffer gas of N₂ or Ar was kept at 10 L/min. Boron and nitrogen doping concentrations were controlled by adjusting the boron quantities contained in target and the flow rate ratio of Ar and N₂ buffer gases. The boron-, nitrogen-, and boron/nitrogen-doped SWNHs are denoted as B-, N-, and BN-SWNHs, respectively. The non-doped SWNHs are denoted as Ar-SWNHs.

Ar-SWNHs and N-SWNHs indicated the aggregate structure with dahlia type morphology. On the other hand, B-, and BN-SWNHs indicated the petal-dahlia type aggregate structure. The amount of petals (= thin graphene sheets) increased in B- and BN-SWNHs, probably because the boron acted as the graphite formation catalyst. In oxygen-saturated 0.1 molar potassium hydroxide solution, electro-catalytic activity of BN-, B-, and N-SWNHs were superior to that of Ar-SWNHs. Their electrocatalyst activities were also compared with those of the conventional carbon materials. The details will be shown in the presentation.

[1] S. Iijima *et al.* Chem. Phys. Lett. **309**, 165 (1999).

[2] K. Gong *et al.* Science **323**, 760 (2009).

[3] Y. Li, *et al.* Nature Nanotech. **7**, 394 (2012).

[4] Y. Zhao *et al.* J. Am. Chem. Soc. **135**, 1201 (2013).

Corresponding Author: R. Yuge

Tel: +81-29-850-1566, Fax: +81-29-856-6137, E-mail: r-yuge@bk.jp.nec.com

Selective formation of zigzag-edges in graphene cracks

○Miho Fujihara¹, Ryosuke Inoue²,
Yutaka Maniwa², Hisanori Shinohara¹, Yasumitsu Miyata^{2,3}

¹ Department of Chemistry, Nagoya University, Nagoya 464-8602, Japan

² Department of Chemistry, Tokyo Metropolitan University, Hachioji 192-0397, Japan

³ JST, PRESTO, Kawaguchi, 332-0012, Japan

Graphene edges have attracted much attention due to their unique electrical and magnetic properties. To understand these properties, it is highly desired to prepare clean, smooth, and structure-controlled edges. Recently, such clean and smooth edges with armchair and zigzag structure were realized by tearing suspended graphene under electron beam irradiation [1]. However, structure selective preparation of zigzag or armchair edges has not been achieved yet. In contrast, molecular dynamics (MD) simulations has predicted that uniaxial in-plane stress selectively produces the cracks with zigzag edges [2].

Here, we report the selective formation of graphene edges aligned in the zigzag orientation by cleavage with thermally-assisted tensile stress (Fig. 1a). Graphene grains were grown from methane on copper foil by using chemical vapor deposition at 1075 °C. After cooling to room temperature, we occasionally observed zigzag-shaped cracks in graphene (Fig. 1b). Considering the grain edges which have the zigzag face, these cracks are found to propagate parallel to the zigzag edges. Statistical analysis of the crack direction suggests that uniaxial tension is applied to the notched of graphene grains around Cu grain boundary (Fig. 1c). The origin of tension is probably due to the non-uniform lattice strain of graphene induced by thermal shrinking of Cu substrates as supported by Raman strain mapping. Furthermore, we demonstrate the carrier tuning around graphene edges by applying the electric field to the cracks (Fig. 1d). Our findings pave the way for the fabrication and applications of smooth, long zigzag edges of graphene and other two dimensional materials.

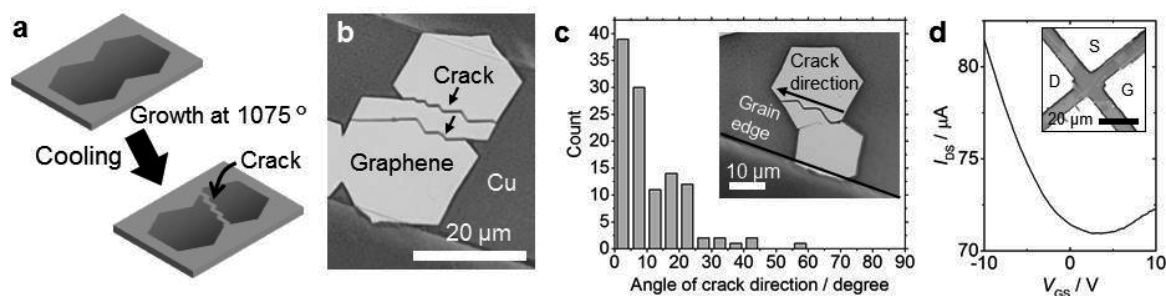


Fig.1 (a) Schematic illustration of tearing graphene during the post-growth cooling process. (b) Optical image of graphene with zigzag-shaped cracks on Cu foil. (c) Histogram of angles between the crack direction and Cu grain edges. Inset: optical image of graphene on Cu foil. (d) I_D - V_{GS} curve of a side gate field-effect transistor (FET) using the graphene with a straight crack. Inset: optical image of the side gate FET.

[1] K. Kim *et al.* Nature Commun. **4**, 2723 (2013).

[2] B. Zhang *et al.*, Appl. Phys. Lett. **101**, 121915 (2012)

Corresponding Authors: Y. Miyata, H. Shinohara

Tel: +81-42-677-2508, +81-52-789-2482, E-mail: ymiyata@tmu.ac.jp, noris@nagoya-u.jp

The synthesis of graphene by thermal CVD process without flowing gas containing carbon

○Shiyo Morisako , Marina Tsujimoto , Masaru Tachibana

*Department of Materials System Science, Yokohama City University,
Yokohama 236-0027, Japan*

Graphene is one of the nano-carbon materials and has two-dimensional sheet structure of Sp² carbon. Many studies have shown high carrier mobility and transmittance of graphene. Because of such properties, graphene is expected to use as thin-film electrodes such as Indium Tin Oxide (ITO). One of the most useful synthesis of graphene is Chemical Vapor Deposition (CVD), which needs high temperature and carbon sources like methane [1] or ethanol [2,3]. Using this synthesis, it is expected that a large amount of graphene used for industrial fields can be provided easily.

We synthesized graphene by using simple alcohol CVD process which use ethanol as carbon sources. As a result, we succeeded to synthesize mono or few layer graphene efficiently on copper foils. Interestingly, graphene was also synthesized without ethanol. It seems that the reason of formation of graphene is remaining vapor of alcohol in CVD chamber or dissolving carbon in a copper foil essentially as impurity. To investigate the factor of formation of graphene, we applied to two methods. At first, we annealed a copper foil substrate for an hour without ethanol after cleaning inside of chamber by flowing argon gas (900 sccm) to remove remaining absorbates. Subsequently, we washed the substrate and then annealed it again to investigate the effect of dissolving carbon. At all experiments, the formation of graphene was observed by Raman spectroscopy.

Recently, similar results were reported in H₂ plasma treatment without carbon sources [4]. The origin of synthesis might be also similar to that in our synthesis as mentioned above. In this work, we determined the main factor of segregation of graphene by annealing without ethanol. In addition, we measured optical property of graphene synthesized by annealing without ethanol.

[1] Xuesong Li et al. Science. 324 (2009) 1312-1314

[2] H Shinohara et al. Appl. Phys. Lett. 96 (2010) 263105

[3] A. Omukai. Trans. Mater. Res. Soc. Jpn. 36(3) (2011) 359-362

[4] R. Kato et al. Carbon. 77 (2014) 832-828

Corresponding Author: M. Tachibana

Tel: +81-45-787-2307

E-mail : tachiban@yokohama-cu.ac.jp

Highly Uniform Bilayer Graphene on Cu-Ni Alloy Films

○Yuichiro Takesaki¹, Hiroki Hibino², Masaharu Tsuji^{1,3}, Hiroki Ago^{1,3,4}

¹Graduate School of Engineering, Sciences, Kyushu University, Fukuoka 816-8580, Japan

²NTT Basic Research Laboratory, NTT cooperation, Kanagawa 243-0198, Japan

³Institute for Materials Chemistry Engineering, Kyushu University, Fukuoka 816-8580, Japan

⁴PRESTO, Japan Science and Technology Agency, Saitama 332-0012, Japan

Controlling the number of layers is important for future applications of graphene, because the number of layers strongly influences the electrical and thermal conductivities as well as mechanical strength of graphene. In particular, for semiconductor applications, bilayer graphene (BLG) is more promising than monolayer graphene, because the tunable bandgap is realized by applying a vertical electric field to BLG [1]. Recently, chemical vapor deposition (CVD) using a Cu catalyst has been widely used for the growth of monolayer graphene due to its low carbon solubility. On the other hand, in order to synthesize few-layer graphene, a transition metal with high carbon solubility, such as Ni and Co, is added to Cu catalyst [2-4]. However, BLG grown by CVD are generally not uniform, and the growth mechanism and the stacking order are not well understood.

Here, we studied the growth of highly uniform BLG by ambient pressure CVD using Cu-Ni binary metal films sputtered on c-plane sapphire substrates. Effects of the CVD temperature, cooling profile, CH₄ and H₂ concentrations, and Cu-Ni ratio were thoroughly investigated. We succeeded in growing highly uniform BLG (93% coverage), as shown in Fig. 1. In particular, the CVD temperature profile was found to increase the BLG area. From the low-energy electron microscope (LEEM) analysis, we clarified that the second layer grows underneath the first layer. We think that the first layer is catalyzed by the Cu-rich metal surface, while the second layer segregates from the bulk Cu-Ni alloy (Fig. 2). Moreover, the LEEM revealed that there are four types of orientations in our BLG. We will also discuss on the stacking order of BLG and its electrical property. Our work is expected to contribute to future development of graphene-based electronic devices.

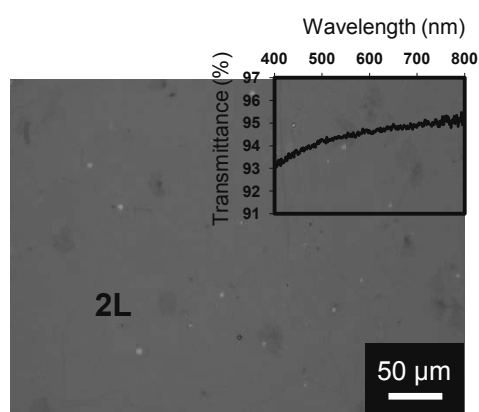


Fig. 1 Optical micrograph of transferred graphene mainly consisting of BLG. Inset shows the optical transmittance.

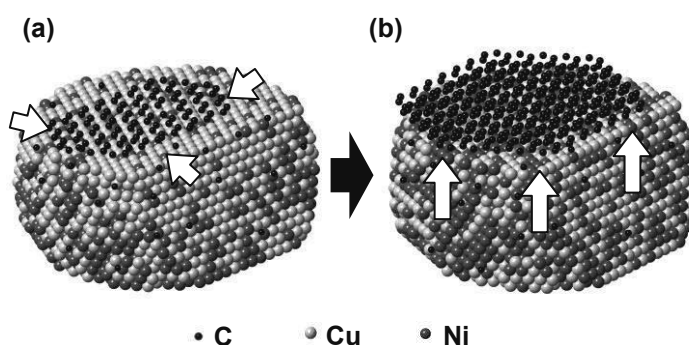


Fig. 2 Growth mechanism of BLG. (a) The first layer is grown on Cu-rich surfaces. (b) The second layer is segregated from the Cu-Ni below the first layer.

[1] Y. Zhang *et al.*, *Nature*, **459**, 820 (2009). [2] Y. Wu *et al.*, *ACS Nano*, **6**, 7731 (2012).

[3] Z. Sun *et al.*, *ACS Nano*, **6**, 9790 (2012). [4] W. Liu *et al.*, *Chem. Mater.*, **26**, 907 (2014).

Corresponding Author: Hiroki Ago, Tel&Fax: +81-92-583-7817, E-mail: ago@cm.kyushu-u.ac.jp

Annealing time dependence of precipitation of high-quality multilayer graphene using Al₂O₃ barrier and Au capping layers

○Jumpei Yamada¹, Manabu Suzuki¹, Yuki Ueda¹, Takahiro Maruyama², and Shigeya Naritsuka¹

¹Department of Materials Science and Engineering, Meijo University,
Nagoya 468-8502, Japan

²Department of Applied Chemistry, Meijo University, Nagoya 468-8502, Japan

Electrical wire is one of the prospective applications of graphene, whose property is thought to be improved by the use of graphene. To realize excellent graphene-wire, it is important to grow a high-quality graphene with large domains. However, the growth of graphene with large-domain is still challenging in the state-of-the-art growth technique. Multilayer graphene is necessary to flow a large current. The use of Al₂O₃ barrier and Au capping layers was helpful to improve the quality of multilayer graphene grown by precipitation method [1]. In this paper, the annealing time is varied to study the precipitation mechanism of multilayer graphene in the precipitation method.

Au(20nm) / Ni(300nm) / Al₂O₃ (2nm) / a-C(5nm) layers were deposited on a sapphire using electron-beam deposition for preparing the samples. The annealing time was varied from 30 to 60 minutes during the precipitation at 900°C in vacuum.

It is found from Fig.1 that multilayer graphene with very low D peak was successfully grown by the precipitation method. As shown in Fig.2, the thickness of the graphene increased with increasing the annealing time. While the proportion of 2-layers graphene was 80% at the annealing time of 30 min, 5-layers graphene occupied 60% of the whole surface at the time of 60 min. In addition, the D/G ratio improved with the thickness, and it finally reached to the excellent value of 0.024 on the sample annealed for 60 min. The precipitation mechanism of multilayer graphene using both Al₂O₃ barrier and Au capping layers will be discussed on the conference site.

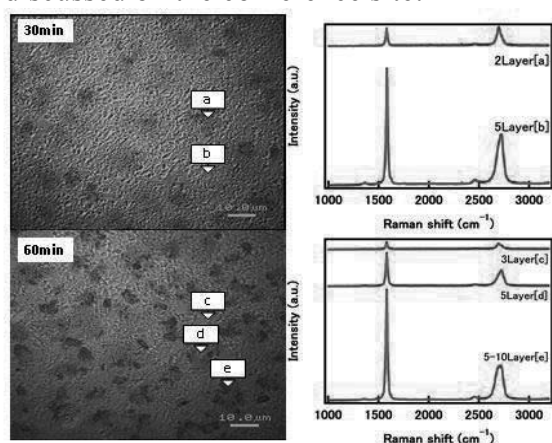


Fig.1 Surface optical microscope images and, Raman spectra of precipitated graphenes annealed for 30 and 60 minutes.

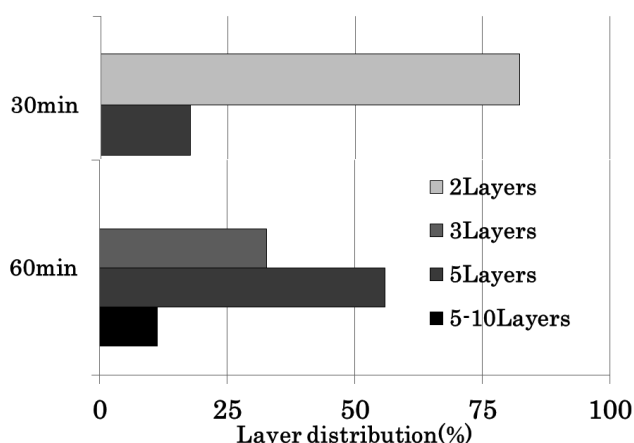


Fig.2 Layer distribution of precipitated graphenes annealed for 30 and 60 minutes.

Reference: [1] M. Suzuki et al., 2014 MRS Fall Meeting & Exhibit, Boston, MA, USA, Nov. 31st-Dec. 5 (2014) K20.28.

Acknowledgement: This work was partly supported by Grant-in-Aid for Specially Promoted Research (No.25000011) from the Ministry of Education, Culture, Sports, Science and Technology of Japan and JSPS Grand-in-Aid for Scientific Research on Innovative Areas (No.26105002).

Corresponding Author: J. Yamada **Tel:** +81-52-838-2387 **E-mail:** 100425324@ccalumni.meijo-u.ac.jp

Evaluation of magnetism of chemically active sites in graphene oxide / nanographene

○Tomoki Yamashina¹, Takuya Isaka², Kadumi Inoue², Yoshiaki Matsuo³, Kazuyuki Takai^{1,2,4}

¹ Graduate School of Science and Engineering, Hosei University, Tokyo 184-8584, Japan

² Department of Chemical Science and Technology, Hosei University, Tokyo 184-8584, Japan

³ Graduate School of Engineering, University of Hyogo, Hyogo 671-2280, Japan

⁴ Research Center for Micro-Nano Technology, Hosei University, Tokyo 184-0003, Japan

The introduction of functional groups, edges, defects or strain is typical method for giving chemical activity to graphene. For example, the edge structure gives graphene the half-filled edge states with a large density of states near the Fermi level, where the spin magnetism and chemically activity emerge as the singly occupied molecular orbital (SOMO) of aromatic molecules. The oxygen-containing functional groups also give graphene a catalytic activity in various reaction systems [1], where the stabilized radical states take an important role. In this study, the correlation between the spin magnetism and chemical activity for graphene oxide (GO) and activated carbon fibers (ACFs) which is assembly of nanographene with a lot of edges was investigated by the XRD, XPS, the magnetic susceptibility and GC-MS.

GO samples were synthesized by Brodie [2] and Hummers [3] methods. An oxidation reaction from benzyl alcohol to benzaldehyde was carried out by using ACFs and GO as catalyst to evaluate their chemical activities. The results of magnetic susceptibility are shown in **Table 1**, where N_{spin} , and χ_{const} are the spin density, and the temperature-independent term, respectively. The smaller χ_{const} for Hummers GO (HGO) and Brodie GO (BGO) than that of ACFs indicates the vanishment of π -electron by oxidation. HGO exhibits extremely large N_{spin} in spite of tiny spin magnetism of BGO, suggesting the artifact by the contribution of the Mn impurity originating from oxidant reagent. Judging from the N_{spin} , ACFs should contain the larger amount of the chemically active sites than that of BGO. This is supported by the larger GC-MS yield for oxidation of benzaldehyde by using ACFs than that by BGO. However, the reaction by using HGO catalyst results in even larger yield for benzyl alcohol than those with ACFs and BGO, where dibenzyl ether appears as major product, and benzaldehyde is obtained as byproduct. Thus, the presence of Mn impurity also significantly influences both the magnetism and the chemical activity of GO.

Table 1 Parameters of spin magnetism

Sample	N_{spin} (g ⁻¹)	χ_{const} (emu·g ⁻¹)
BGO	2.1×10^{18}	-4.6×10^{-7}
HGO	6.5×10^{20}	-3.3×10^{-7}
ACFs	3.9×10^{19}	-1.0×10^{-6}

[1] C.Su, M.Acik, K.Takai et al, *Nat. Commun.*, **3**, 1298 (2012)

[2] B. C. Brodie, *Phil. Trans. R .Soc. Lond.*, **149**, 249-259 (1859)

[3] D. C. Marcano et al, *ACS Nano*, **4**, 8, 4806–4814 (2010)

Corresponding Author: Kazuyuki Takai

Tel: +81-42-387-6138, Fax: +81-42-387-7002,

E-mail: takai@hosei.ac.jp

Acid-treatment minimizes unintentional strain and doping of single-layer graphene on SiO₂ substrate in aqueous environments

Katsuya Masuda and Masahito Sano

Department of Polymer Science and Engineering, Yamagata University
Yonezawa, Yamagata, 992-8510, Japan

Graphene is a zero band gap semiconductor which can be electron- and hole-doped easily due to a linear band dispersion at the Dirac point. It also has an atomically flat, planar surface that is chemically stable in air and liquid. These properties make graphene a very attractive material as a platform for electrochemical- and bio-sensing applications.

On the other hand, the same properties cause a problem that the electronic properties of graphene are easily affected by supporting substrates. It is well known that graphene on SiO₂/Si is unintentionally strained and hole-doped in air. Strain and doping levels differ from sample to sample as well as position within a single graphene flake. It is also important that the liquid environment does not affect the electronic properties. Various amine compounds are known to act as electron donors against single-walled carbon nanotubes. In particular, tris(hydroxymethyl)aminomethane (Tris), a compound that commonly used as buffer in biochemical studies, is shown to reduce proteins by electron transfer through nanotubes [1]. For stable and reliable operation of graphene electronic devices, minimization of unintentional strain and doping caused by both substrates and liquid is highly desirable.

In this study, we show that simply dipping the graphene on SiO₂/Si in either acid or alkali solution beforehand reduces the sample variation, improves stability against Tris, and brings the graphene close to the state of freestanding using Raman microscopy.

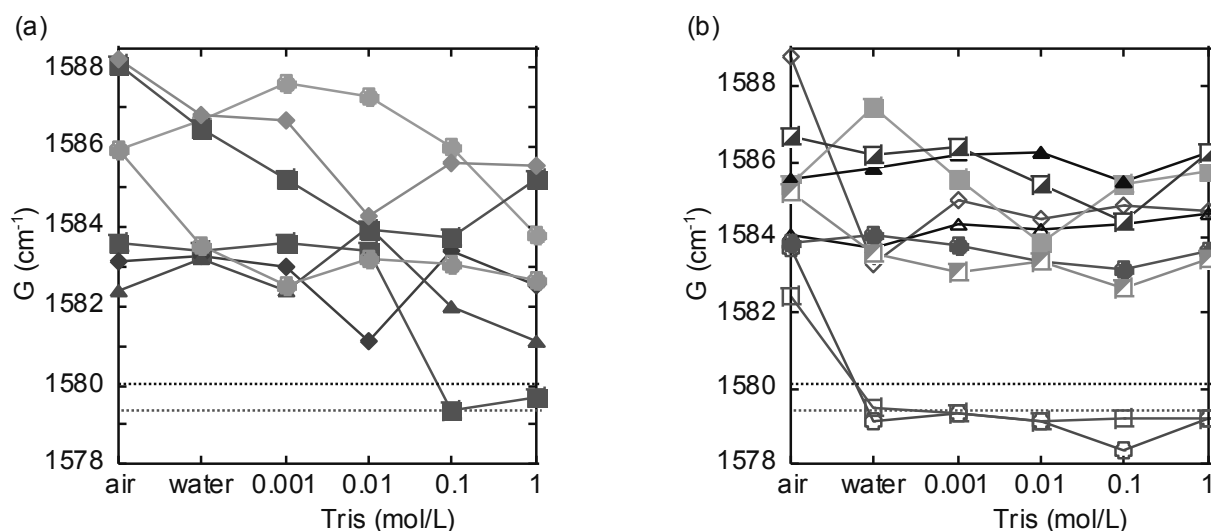


Fig. 1. The G center frequency in air, water and various Tris concentrations for (a) the untreated samples, (b) the acid- and alkali-treated samples with rinsing (filled marks) and without rinsing (empty marks). The black and red dashed line correspond to the values of graphite and freestanding graphene, respectively.

[1] T. Nakashima, M. Sano *J. Phys. Chem. C* **115**, 20931 (2011).

Corresponding Author: M. Sano

Tel: +81-238-26-3072 E-mail: mass@yz.yamagata-u.ac.jp

Electric Double Layer Light-emitting Diodes of Monolayer WSe₂

○Jiang Pu¹, Taiyo Fujimoto², Jing-Kai Huang³, Lain-Jong Li³,
Tomo Sakanoue¹, Taishi Takenobu^{1,2,4}

¹ Department of Advanced Science and Engineering, Waseda Univ., Tokyo 169-8555, Japan

² Department of Applied Physics, Waseda University, Tokyo 169-8555, Japan

³ Physical Sciences and Engineering Division, KAUST, Thuwal 23955-6900, Saudi Arabia

⁴ Kagami Memorial Laboratory, Waseda University, Tokyo 169-0051, Japan

Monolayer transition metal dichalcogenides (TMDCs) have emerged as potential candidates for optoelectronic applications because of their unique optical properties [1]. Owing to their spin-valley coupled system, TMDCs exhibited circular polarized photoluminescence and electroluminescence (EL), which provide possibilities for realizing novel functionalities. Recently, light-emitting diodes/transistors based on monolayer WSe₂ have demonstrated [2,3]. Although these devices enable EL capabilities, they typically need split-gate architecture or operate at lower temperature to obtain EL. Therefore, exploring new types of device configuration which can commonly generate excitonic EL is highly required for further advances. In order to achieve this goal, both formation of p-n junction and injection of high current density need to be realized simultaneously at room temperature. In this paper, we propose unique light-emitting structure, electric double layer light-emitting diodes (EDLEDs), fabricated with WSe₂ monolayers. The EDLEDs can self-organize dynamic p-n junction at room temperature due to ion alignment when we applied lateral electric field to materials.

The large-area WSe₂ films were synthesized on sapphire substrates through chemical vapor deposition [4]. The gold electrodes were patterned on film surface, and then ion gels, gelation of ionic liquids, were spin-coated to form EDLEDs. When we applied the lateral potential gradient which is larger than bandgap of WSe₂, the p-n junction is electrostatically formed in channel, which consequently yielded clear EL spectrum from fabricated WSe₂ EDLEDs (Fig. 1). In addition, we can inject high current density (>10 kA/cm²) into these devices at room temperature, resulting in direct observation of EL image from WSe₂ channel. Our proposed EDLEDs offer significant advantages for future TMDC-based optoelectronic devices.

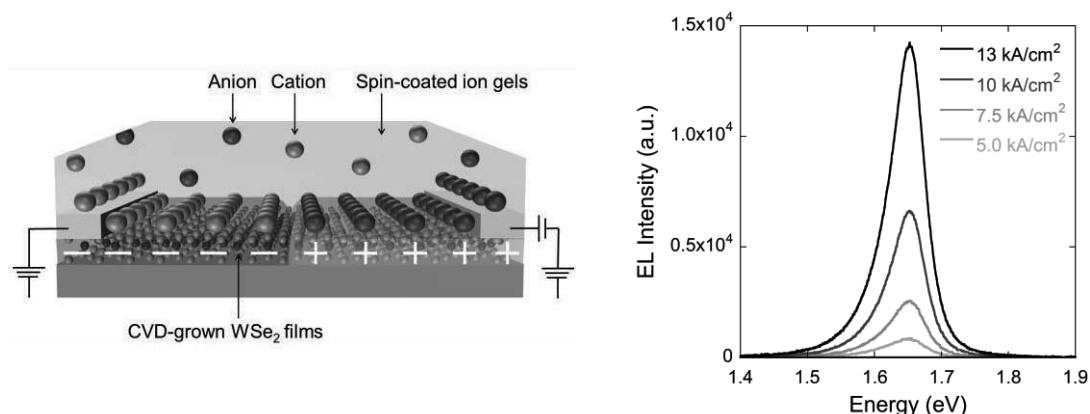


Fig. 1 The schematic depiction (left) and EL spectrum (right) of a WSe₂ EDLED

[1] Q. H. Wang, *et al.* Nat. Nanotechnol. **7**, 699 (2012).

[2] J. S. Ross, *et al.* Nat. Nanotechnol. **9**, 268 (2014).

[3] Y. J. Zhang, *et al.* Science. **344**, 725 (2014).

[4] J. K. Huang, J. Pu, *et al.* ACS. Nano. **8**, 923 (2014).

Corresponding Author: T. Takenobu

Tel/Fax: +81-3-5286-2981

E-mail: takenobu@waseda.jp

Effect of hydrazine adsorption on Graphene FET characteristic

○Taichi Umehara¹, Kazuyuki Takai^{1,2,3}

¹ Graduate School of Science and Engineering, Hosei University, Tokyo 184-8584, Japan

² Department of Chemical Science and Technology, Hosei University, Tokyo 184-8584, Japan

³ Research Center for Micro-Nano Technology, Hosei University, Tokyo 184-0003, Japan

The introduction of guest species to graphene has been extensively studied, since the electronic properties of atomic membrane are easily modulated by the surface adsorption [1]. Especially, molecular materials are promising adsorbate to modify graphene because of its capability in material design in comparison with metal adsorbate. Hole doping has been achieved by oxygen adsorption as a consequence of complex electrochemical processes, resulting in novel gate-tunable kinetics of the charge injection to graphene [2]. However, electron doping is poorly studied in the field of molecule adsorption of graphene. In this study, effect of the adsorption of hydrazine having electron-donating nature on graphene is investigated in terms of the transport properties.

Hydrazine monohydrate ($\text{N}_2\text{H}_4 \cdot \text{H}_2\text{O}$) was dropped to the channel region of graphene field effect transistor prepared by exfoliation on SiO_2 substrate, followed by drying under ambient condition.

The gate voltage dependence of the electrical conductivity for graphene before and after $\text{N}_2\text{H}_4 \cdot \text{H}_2\text{O}$ adsorption is shown in Fig. 1. Before $\text{N}_2\text{H}_4 \cdot \text{H}_2\text{O}$ adsorption, a p-type conduction caused by resist residue and ambient gases appears without hysteresis. After $\text{N}_2\text{H}_4 \cdot \text{H}_2\text{O}$ adsorption, a n-type conduction is clearly shown with a large hysteresis. The reducing nature of hydrazine successfully induces the charge transfer to graphene in spite of hysteresis by the presence of water having large electric dipole. Interestingly, the large amount of electron doping remains even after drying process. $\text{N}_2\text{H}_4 \cdot \text{H}_2\text{O}$ is liquid phase in bulk with higher vapor pressure (boiling point 387 K) compared to molecules often used in carrier doping (TCNQ etc.). It is suggested that hydrazine is not bonded to graphene with form of physisorption by simple van der Waals forces but chemisorption including the ionic bonding.

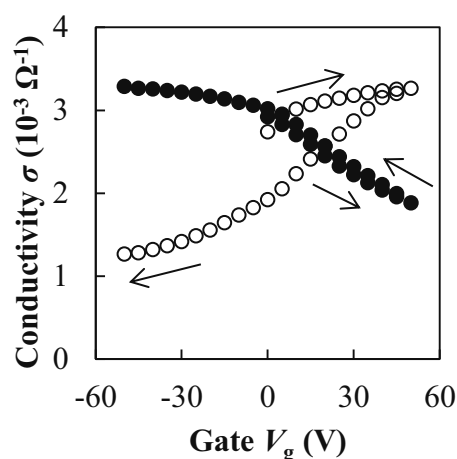


Fig. 1 Backgate-voltage dependence of the conductivity. Closed circles and open circles denote data under ambient condition, and after hydrazine treatment, respectively.

[1] S. Xiao et al, *Phys. Rev. B* **82**, 041406 (2010)

[2] Y.Sato, K.Takai, T.Enoki, *Nano Lett.* **11** 3468 (2011)

Corresponding Author: Kazuyuki Takai,

Tel: +81-42-387-6138, Fax: +81-42-387-7002,

E-mail: takai@hosei.ac.jp

Kohn anomaly meets Fano resonance in G and G' bands Raman spectra of graphene

○ Eddwi H. Hasdeo, Ahmad R.T. Nugraha, Riichiro Saito

Department of Physics, Tohoku University, Sendai 980-8578, Japan

The interplay between electron-phonon and electron-electron interactions in graphene for the G band ($\sim 1600\text{ cm}^{-1}$) and G' band ($\sim 2600\text{ cm}^{-1}$) is investigated theoretically. Around these phonon frequencies, the presence of gapless linear energy bands (Dirac cones) in graphene strongly affects the phonon energies, spectral broadening factors, and spectral lineshapes. One of the related phenomena is the Kohn anomaly, in which the phonon energy (lifetime) becomes lower (shorter) due to the interaction between a phonon and an electron-hole pair in the linear energy band [1]. Another important phenomenon is the appearance of the asymmetric spectral lineshape of the phonon spectra, known as the Fano resonance, which has long been observed in metallic nanotubes [2] and recently is observed in graphene as a function of Fermi energy [3]. The detailed mechanism behind those two phenomena have been a long standing question for more than a decade.

Here we show that the Fano resonance in graphene originates from the interference between the phonon spectra and the electronic Raman scattering (ERS) spectra [4,5]. Furthermore, the Kohn anomaly and the ERS should correspond to the same electron-hole pair excitation in the Dirac cones of graphene. Taking both effects into account, we are able to reproduce the experimentally observed Fermi energy dependence of frequency shift, spectral linewidth, and spectral asymmetry of the G band Raman spectra [5]. We extend this theory for the G' band of graphene and we expect to explain the behavior of frequency shift and spectral linewidth as a function of Fermi energy for the G' band, which is opposite to that of the G band.

[1] A. Jorio et al., "Raman spectroscopy in graphene related systems", Wiley (2011).

[2] S. D. M. Brown et al., Phys. Rev. B 63, 155414 (2001).

[3] D. Yoon et al., Carbon 61, 373-378 (2013).

[4] E. H. Hasdeo et al., Phys. Rev. B 88, 115107 (2013).

[5] E. H. Hasdeo et al., Phys. Rev. B 90, 245140 (2014).

Corresponding Author: E. H. Hasdeo

TEL: +81-22-795-6442, FAX: +81-22-795-6447, E-mail: hasdeo@flex.phys.tohoku.ac.jp

Surface plasmon excitations in graphene

○ M. Shoufie Ukhtary, Eddwi H. Hasdeo, Ahmad R.T. Nugraha, Riichiro Saito
Department of Physics, Tohoku University, Sendai 980-8578, Japan

Collective oscillations of electrons can be excited on the surface of metal and these oscillations are known as surface plasmons (SPs). The existence of SPs can be depicted by their dispersion relation showing the relation between the plasmon frequency and wavevector. This relation can be obtained by solving Maxwell's equation on the surface (semiclassical model) or by using random phase approximation (RPA) of quantum mechanics. In the case of graphene, the SP dispersion for doped graphene has been studied by some researchers using both the semiclassical model [1] and also the RPA method [2], and these prove that doped graphene can sustain the SPs. However, to take an advantage of the SP properties of graphene, we have to design a realistic system consisting of graphene and layered dielectric materials so that the SPs have a possibility to be excited.

Excitation of SPs can be realised by applying light with a certain frequency onto the designed system. The wavevector of the light needs to match the SP wavevector of in order to have SPs excited, which might be achieved by utilizing total internal reflection of light [3]. A special arrangement of graphene and the dielectric materials is necessary to create the total internal reflection. Analysis of the excitation process is done by the transfer matrix method to obtain the electric field profile across the system and then we can extract the absorption or reflection spectra from the field profile. By considering several layer arrangements, we find that a much larger absorption of light by graphene could be obtained rather than the famous 2.3% absorption of light, especially when we apply THz radiation to the system. This phenomenon seems to depend on the doping level or Fermi energy of doped graphene and thus the light absorption in graphene might be controllable.

[1] X. Luo et al., *Material Science and Engineering R* **74** (2013).

[2] E. H. Hwang and S. Das Sarma, *Physical Review B* **75** 205418 (2007).

[3] S. A. Maier. *Plasmonics*. Springer (2007).

Corresponding Author: M. Shoufie Ukhtary

TEL: +81-22-795-6442, FAX: +81-22-795-6447, E-mail: shoufie@flex.phys.tohoku.ac.jp

Interlayer exciton in atomically thin heterostructures of transition metal dichalcogenides

○Daichi Kozawa¹, Ivan Verzhbitskiy², Alexandra Carvalho², A. H. Castro Neto², Kazunari Matsuda¹, Goki Eda²

¹*Institute of Advanced Energy, Kyoto University, Uji, Kyoto 611-0011, Japan*

²*National University of Singapore, 2 Science Drive 3, 117542, Singapore*

Heterostructure of monolayer transition metal dichalcogenides (TMDs) possesses atomically sharp interface between the two layers and forms intrinsic p-n junction. Photoexcited electron-hole pairs spontaneously separate into the two layers, resulting in formation of interlayer exciton (Fig. 1a and b). This charge transfer is extremely fast process that take place within 50 fs[1]. The TMD-based heterostructures are promising particularly in optoelectronics such as photo sensing and photovoltaic applications taking advantage of the efficient charge transfer and strong light-matter interactions[2]. Here, we report photocarrier relaxation in the heterostructures using photoluminescence (PL) and PL excitation spectroscopy.

Heterostructure MoSe₂/WS₂ bilayer was fabricated on a quartz substrate using dry transfer process of upper layer onto the bottom layer with PDMS elastic polymer. In PL spectra of MoSe₂/WS₂ heterostructure (Fig. 1c), PL peak of the interlayer exciton lies below the band edge emission of isolated MoSe₂ by ~ 35 meV because of the intrinsic band offset (Figure 1b). The redshift of the PL peak and smaller PL intensity suggest the observation of the interlayer exciton. We further conduct PL excitation spectroscopy for the heterostructure to examine the relaxation of the interlayer exciton. We will discuss the detailed mechanism of the photocarrier relaxation in the heterostructures.

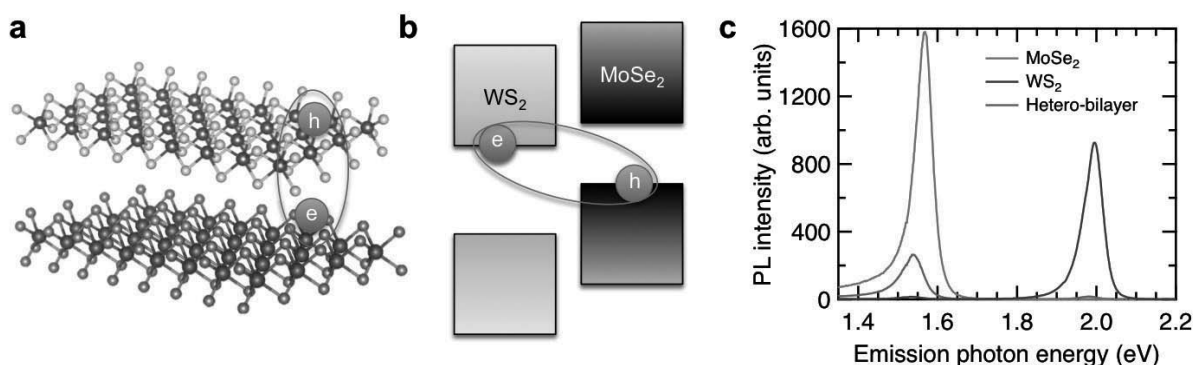


Fig.1 **a,b**, Schematic atomic structure and energy diagram of the MoSe₂/WS₂ heterostructures with interlayer exciton. **c**, PL spectra of MoSe₂/WS₂ heterostructure measured at room temperature. PL spectra of isolated monolayers MoSe₂ and WS₂ are also shown for comparison.

[1] X. Hong *et al.*, Nat. Nanotechnol. **9**, 682 (2014).

[2] D. Kozawa *et al.*, Nat. Commun. **5**, 4543 (2014).

Corresponding Author: D. Kozawa

Tel: +81-774-38-3465

E-mail: d-kozawa@iae.kyoto-u.ac.jp

Optical characteristic of CVD grown monolayer WSe₂ under high-density carrier doping

○Keiichiro Matsuki¹, Jiang Pu², Kazunari Matsuda³, Lain-Jong Li⁴, Taishi Takenobu^{1,2,5}

¹ Department of Applied Physics, Waseda University, Shinjuku 169-8555, Japan

² Department of Advanced Science and Engineering, Waseda Univ., Tokyo 169-8555, Japan

³ Institute of Advanced Energy, Kyoto University, Uji 611-0011, Japan

⁴ Physical Sciences and Engineering Division, KAUST, Thuwal 23955-6900, Saudi Arabia

⁵ Kagami Memorial Laboratory, Waseda University, Tokyo 169-0051, Japan

Monolayer transition-metal dichalcogenides (TMDCs), such as MoS₂ and WSe₂, are attracting interest due to their direct band gap in monolayers, large binding energy of exciton, and spin-valley coupled system. Although their optical properties have been already reported well, the effect of high-density carrier doping, which might lead to many-body effects, has not yet been investigated. Recently, we have succeeded in the CVD-growth of large-area samples and their application into the electric double layer transistors (EDLTs), in which one can accumulate extremely high density carriers ($> 10^{20}/\text{cm}^3$) [1-4]. Therefore, in this research, we tried to measure optical properties of WSe₂ monolayers under high-density carrier doping.

Figure 1 shows the device structure of WSe₂ EDLTs. Large-area monolayer WSe₂ was synthesized by CVD method on a sapphire substrate and Au/Ni electrodes were thermally deposited on it. As the electrolyte, we selected the ion gel, which is the mixture of ionic liquid ([EMIM][TFSI]) and organic polymer (PS-PMMA-PS). As shown in Fig. 2, we successfully accumulated both hole and electron carriers, and controlled the resistance of WSe₂ monolayer by gate voltage application, which is the signature of carrier doping and estimated highest carrier density is approximately $2 \times 10^{20}/\text{cm}^3$.

For optical characteristics, we used 532-nm incident light and collected photoluminescence (PL) spectra at room temperature in vacuum. The spectra were measured under both hole and electron carrier accumulation. Figure 3 reveals PL spectra at different gate voltages and we observed clear spectral changes under high-density carrier accumulation. However, these PL peaks are not simply explained by exciton or charged exciton. The mechanism will be discussed at the meeting.

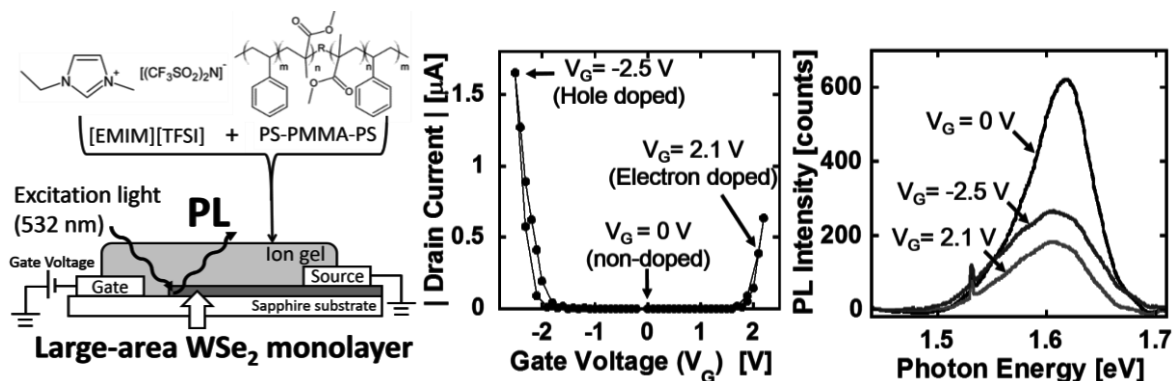


Fig.1. Device structure

Fig.2. Transistor characteristics

Fig.3. PL characteristics

[1] A. M. Jones *et al.*, Nature Nanotech. **8**, 634 (2013), [2] K. F. Mak *et al.*, Nature Nanotech. **12**, 207 (2013)

[3] J. K. Huang *et al.* ACS Nano. **8**, 923(2014), [4] J. Pu *et al.*, Nano Lett. **12**, 4013(2012)

Corresponding Author: Taishi Takenobu, Tel&Fax: +81-3-5286-2981, E-mail: takenobu@waseda.jp

Photon energy dependence of angle resolved photoemission spectroscopy in graphene

○ Pourya Ayria¹, Eddwi H. Hasdeo¹, Ahmad R.T. Nugraha¹, Shin-ichiro Tanaka² and Riichiro Saito¹

¹*Department of Physics, Tohoku University, Sendai 980-8578, Japan*

²*The institute of Scientific and Industrial Research, Osaka University, 8-1 Mihogaoka, Ibaraki, Osaka 567-0047, Japan*

The dependencies of angle-resolved photoemission spectroscopy (ARPES) for different photon energies and light polarization near Dirac point of graphene are studied theoretically. Recently, Tanaka *et al.* showed an interesting ARPES results in which polarization dependent on ARPES intensity changes its character as a function of photon energy [1]. Near the K point of graphene, along of the $\Gamma - K$ direction π^* band is brightened by s-polarized light (s-branch), while along the $K - M$ direction π^* band is brighten by p-polarized light (p-branch) due to the interference between carbon atom A and B wavefunctions [2]. The experimental observation reveals that the intensity of p-branch compared with s-branch becomes dominant for specific photon energy even though for various linear light polarizations. The origin of this dependency in ARPES can be explained by the concept of electron-photon matrix elements effect in which the final state of photoelectron has the crucial impact on observation ARPES intensity [3].

Therefore, in this work, we study the electron-photon matrix elements effect in ARPES of graphene theoretically. In order to find out the impact of the matrix elements, the final states energy and wavefunction of the excited electron are expanded by the first principle calculation [4]. Changing incident photon energy allows us to access different final state energy. However, electron-photon dipole selection rule imposes that transition to some final states are allowed and some are not. Therefore, by considering these conditions, the theoretical calculation reproduces the experimental observation. Moreover, the calculation of the electron-photon dipole vector for various final energies clarifies the origin of the dramatic increase of ARPES intensity in the p-branch. We find that the number of the final states which results in dipole vector in y direction along the $\Gamma - K$ direction for the π^* band is less than the number of the final states with x direction along the $K - M$ direction particularly for a specific region of band energy. Hence, the contribution of dipole vector in x direction compared with y direction at this region in ARPES intensity has crucial effect on increasing ARPES intensity of the p-branch.

[1] Shin.ichiro.Tanaka *et al.*, [private communication]

[2] C. Hwang *et al.*, Phys. Rev. B. 84, 125422 (2011).

[3] A. Damascelli *et al.*, Rev. Mod. Phys. 75, 155414, 473 (2003).

[4] Paolo Giannozzi *et al.*, J. Phys. Cond. Matt. 21, 395502 (2009).

Corresponding Author: P. Ayria

TEL: +81-22-795-5719, FAX: +81-22-795-5719, E-mail: pourya@flex.phys.tohoku.ac.jp

Local electric field effects on nearly free electron states of graphene nanoribbons

○Ayaka Yamanaka, Susumu Okada

*Graduate School of Pure and Applied Sciences, University of Tsukuba, Tennodai, Tsukuba
305-8577, Japan*

Electric field occasionally affects the electronic structure of graphene and graphite. In the case of bilayer graphene under the normal electric field, the metal-semiconductor-metal transition occurs with increasing the electric field. Similar electronic structure modulation also found in the graphene nanoribbon under the lateral electric field. In the case, we found that the lateral electric field basically opens or increases the energy gap of the ribbons [1]. Moreover, under the strong lateral electric field, we found that the nearly free electron (NFE) state shifts downward and crosses Fermi level [2]. In this work, we study the detailed electric-field dependence of NFE state of graphene nanoribbons based on the density functional theory with combining the effective screening medium method.

We consider the graphene nanoribbons under parallel ($\theta=0$ degree) to perpendicular ($\theta=90$ degree) electric field as shown in Fig. 1. Figure 2 shows the eigen value of NFE states of graphene nanoribbons as a function of the external electric field. In the parallel electric field, NFE state at the ribbon side rapidly shift downward with increasing the electric field, while the NFE state distributed above and below the ribbon is insensitive to the field. In the normal electric field, both NFE states are insensitive to the electric field. These results imply that the electric field concentration around the ribbon edges enhances the decrease the electrostatic potential around the edge atomic site. Thus, the mutual arrangement and shapes of graphene nanoribbons with respect to the electric field is important to control the energy of NFE states.

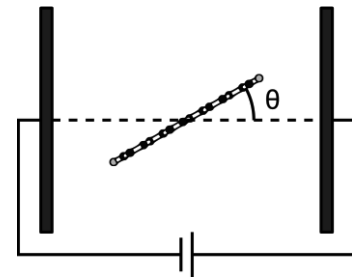
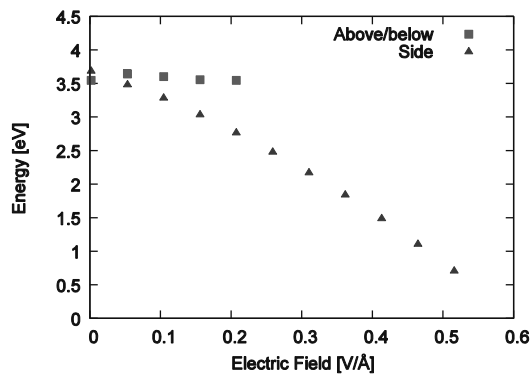


Fig.1 Structural model of rotated nanoribbons under an electric field.

(a) Parallel electric field ($\theta=0$)



(b) Normal electric field ($\theta=90$)

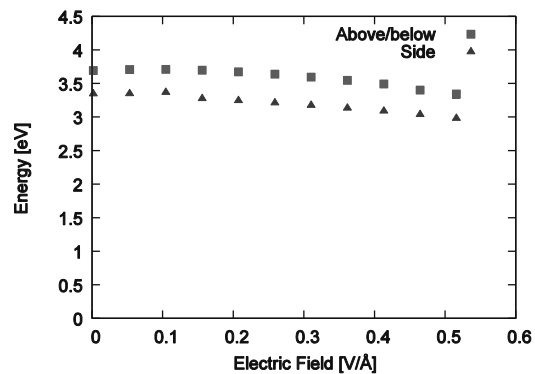


Fig.2 Eigen value of NFE state of graphene nanoribbons

[1] A. Yamanaka and S. Okada, *Jpn. J. of Appl. Phys.* 53, 06JD05 (2014).

[2] A. Yamanaka and S. Okada, *Appl. Phys. Express* 7, 125103 (2014).

Corresponding Author: A. Yamanaka

Tel: +81-29-853-5600 (ext. 8233), Fax: +81-29-853-5924,

E-mail: ayamanaka@comas.frsc.tsukuba.ac.jp

Evaluation of Graphene Quality by Raman Rapid Chemical Imaging

○Mamoru Komatsu, Kaori Umeyama, Noriaki Nishikawa, Mark H. Wall*

Thermo Fisher Scientific K.K., Chemical Analysis Division, Yokohama 221-0022, Japan

Graphene holds great potential for use in a variety important areas that include electronics, energy storage, high strength composites and sensing technologies, to name a few. Graphene has demonstrated exceptional barrier properties, being impenetrable to even helium. Coupled with the fact that the material is also optically transparent this behavior has attracted intense interest in the material science area towards using graphene as a barrier layer in a variety of applications. In this poster, we show how Raman imaging can be used to gain important insight with respect to critical parameters and mechanisms that govern the nucleation and growth of graphene via chemical vapor deposition (CVD) (Fig 2 & 3). This poster also



Fig 1. DXRxi Raman Imaging Microscope

presents preliminary work investigating the protective capabilities of graphene employing the use of rapid Raman imaging (Fig 4-6).

Additionally, this poster introduces the latest tool available to obtain Raman imaging of grapheme, the Thermo Scientific™ DXR™xi Raman imaging microscope(Fig 1).

Raman chemical imaging of graphene samples

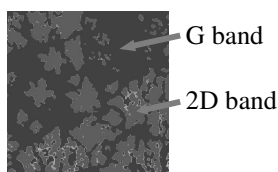


Fig 2: Raman chemical image of island growth of monolayer graphene grown on Cu and transferred to SiO₂/Si. Peak-height-ratio was used to generate the image. Red regions represent 2D band peak (2700-2800cm⁻¹), and the blue regions represent G band peak (1580-1590cm⁻¹).

- 50 × 50 micron area
- 10 co-addition scans
- Collection time: 16.7 minutes.

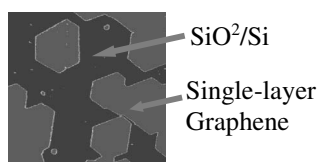


Fig 3: Raman chemical image of hexagonal graphene islands that has been transferred to SiO₂/Si. MCR was applied to generate the image. Red regions are single-layer graphene and the blue regions are SiO₂/Si.

- 175 × 175 micron area
- 10 co-addition scans
- Collection time: 3.4 hours.



Fig 4: Optical image of single layer graphene coated Cu

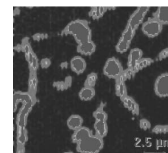


Fig 5: Raman chemical image of intensity scale associated with 642cm⁻¹ band of CuO_x

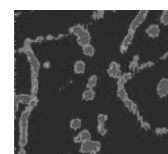


Fig 6: Raman chemical image of intensity scale associated with 1370cm⁻¹ band (D band)

*Corresponding Author: Dr. Mark H. Wall
Thermo Fisher Scientific, Madison, WI, U.S.A.
E-mail: mark.wall@thermofisher.com

CVD synthesis of high-quality h-BN films for heterostructure devices

Yuki Uchida,¹ Tasuku Iwaizako,¹ Masaharu Tsuji,^{1,2} and Hiroki Ago^{1,2,3}

¹Graduate School of Engineering Sciences, Kyushu University, Fukuoka 816-8580, Japan

²Institute for Materials Chemistry and Engineering, Kyushu University, Fukuoka 816-8580, Japan

³PRESTO, Japan Science and Technology Agency, Saitama 332-0012, Japan

Recently, heterostructures of various layered materials have attracted a great deal of interest due to their unique properties and promising applications in electronics and photonics. Among them, hexagonal boron nitride (h-BN), a honeycomb lattice of boron and nitrogen atoms, is a good candidate as an atomically thin insulating material. Its atomically smooth structure, the absence of charge impurities, and large band gap (5.9 eV) make h-BN a promising material for heterostructure devices. It has been demonstrated that in graphene field-effect transistors (FETs) the insertion of an exfoliated h-BN flake in the interface between single-layer graphene and SiO₂ dramatically increases the carrier mobility of the graphene [1,2]. However, for practical applications, development of large-area growth of h-BN sheets is essential. Here, we present our study on chemical vapor deposition (CVD) growth of large h-BN sheets on heteroepitaxial Cu(111) films.

A thin film of Cu(111) was sputtered onto c-plane sapphire substrate at 250 °C to improve the Cu crystallinity. h-BN was then grown on the Cu surface by ambient pressure CVD at 1050 °C using ammonia borane (NH₃BH₃) as a precursor in the flow of H₂ and Ar gasses. Figure 1 shows optical microscope images of the Cu surface reacted with ammonia borane for 50 min. The film of h-BN completely covered the center of the Cu surface, while isolated triangular h-BN domains can be seen at the edges of the Cu surface. We found that that the triangular h-BN domains are oriented in two directions (Figure 1C), suggesting the epitaxial growth of h-BN on the Cu(111) surface. When increasing the CVD time to 60 min, the whole Cu surface (1 cm²) was fully covered with h-BN. Comparison of graphene FETs measured with and without h-BN sheet will be also shown at the Symposium.

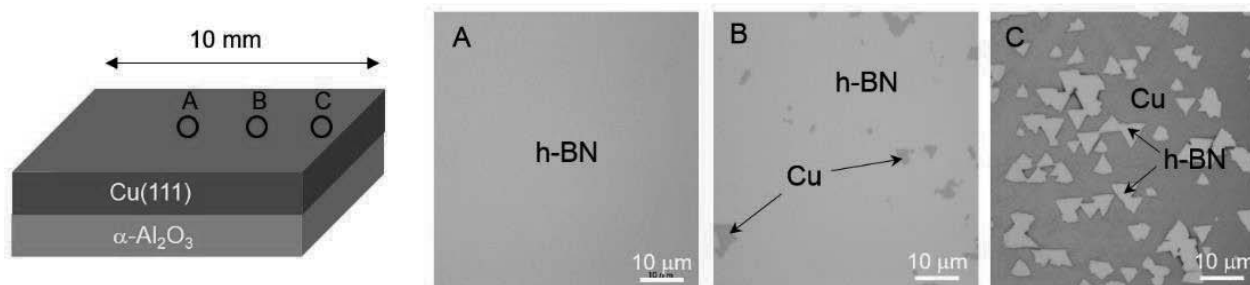


Fig. 1 Optical micrographs of the Cu surface taken at three positions. To visualize h-BN sheets, the Cu substrate was baked in air which makes clear contrast due to slight oxidation of the Cu surface.

[1] J. B. Oostiga *et al.*, *Nat. Mater.*, **7**, 151 (2008). [2] C. R. Dean *et al.*, *Nat. Nanotech.*, **5**, 722 (2010).

Corresponding Author: Hiroki Ago, Tel&Fax: +81-92-583-7818, Email: ago@cm.kyushu-u.ac.jp

Electric field control of thermoelectric properties in WSe₂

○Takahiko Iizuka¹, Masaro Yoshida¹, Sunao Shimizu², Yoshihiro Iwasa^{1,2}

¹ *Quantum-Phase Electronics Center (QPEC) and Department of Applied Physics,
The University of Tokyo, Tokyo 113-8656, Japan*

² *RIKEN Center for Emergent Matter Science (CEMS), Wako 351-0198, Japan*

Layered transition metal dichalcogenides (TMDs) have attracted growing interest in remarkable electric transport and optical properties. However, the experimental researches of thermoelectric properties are limited although theoretical predictions imply high thermoelectric performance especially in mono or few-layer systems [1-3].

Thermoelectric figure of merit (ZT) is expressed as $S^2/\rho\kappa$, where ρ , S , κ are the electrical resistivity, the Seebeck coefficient, and the thermal conductivity. These are in a relation of trade-off as a function of carrier density and thus the optimization against the carrier density is desired for all materials. In this sense field effect carrier control, in particular, using electric-double-layer transistors (EDLTs) offers a powerful means for this purpose, because it enables us the continuous tuning of carrier density simply changing gate voltages.

In this presentation, we report the electric field control of thermoelectric properties in Tungsten diselenide (WSe₂), which is an archetypal member of semiconducting TMDs. Single crystals of WSe₂ can be easily mechanically exfoliated and the atomically flat surface is one of the ideal platforms for EDLT technique [4]. We made a micro EDLT-device of exfoliated WSe₂ thin flake and measured its gate voltage dependence of the Seebeck coefficient S and the electrical resistivity ρ . For the Seebeck coefficient measurement, an electrode separated from the flake is used as a heater creating a temperature gradient. Two electrodes attached to the flake are used as local resistance thermometers with four-terminal method. Those electrodes are also used as voltage probes while they are used as source and drain terminals for the electrical conductivity measurement.

We observed the ambipolar FET operation and large evolution of the Seebeck coefficient including the sign change. This is the first observation of the Seebeck coefficient in the electron doped WSe₂ thin flake. We also estimated the power factor $P = S^2/\rho$, which is crucial for thermoelectric performance, and found peaks as a function of gate voltage both for electron- and hole-doping. The optimized power factor reached 2000 $\mu\text{W}/\text{mK}^2$, implying that WSe₂ is a promising thermoelectric material.

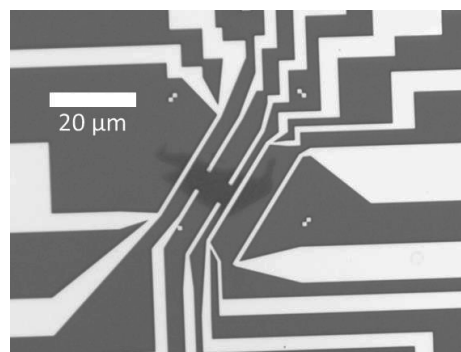


Fig.1 An optical microscope image of a WSe₂ EDLT-device

[1] J. Wu *et al.*, Nano Lett. **14**, 2730–4 (2014).

[2] D. Wickramaratne *et al.*, J. Chem. Phys. **140**, 124710 (2014)

[3] W. Huang *et al.*, Phys. Chem. Chem. Phys. **16**, 10866–74 (2014)

[4] Y. Zhang *et al.*, Science **344**, 725–8 (2014)

Corresponding Author: T. Iizuka

Tel: +81-3-5841-6822, Fax: +81-3-5841-6822,

E-mail: iizuka@mp.t.u-tokyo.ac.jp

Influence of Electric Double Layer Carrier Injections on Optical Absorption Spectra of CVD synthesized Multi-layered MoS₂ and WS₂ thin films

○Kotaro Homma, Hideki Kawai, Kazuhiro Yanagi

Department of Physics, Tokyo Metropolitan University, Minami-Osawa 192-0397, Japan

Transition metal dichalcogenides (TMDCs) are atomically thin two dimensional semiconducting crystals. TMDCs have a strong spin-orbit coupling originated from the *d* orbitals of the heavy metal atoms, which is distinct characteristic from graphene and carbon nanotubes.¹ The conduction and valence-band edges are located at the K points of the 2D hexagonal Brillouin zone, and the strong spin-orbit coupling induces the spin splitting at the valence band top. In the case of their monolayer and 3R phase crystals², the inversion symmetry is broken in the samples. As a result, spin and valley are coupled, leading various approaches to manipulate the valley degree of freedom of carriers.¹

For the manipulation of electronic states of TMDCs, electric double layer carrier injection techniques are widely used, and various physical properties have been manipulated, such as superconducting states and circular polarized light emissions.³ However, whether the carrier injection can selectively inject holes on the one of the splitting electronic states has not been clarified yet. Such selective carrier injection will contribute to the valleytronic applications. Previously we have tuned optical absorption and thermoelectric properties of single-wall carbon nanotubes using electric double layer carrier injections.⁴ To clarify the above question, in this study, we investigated the influence of electric carrier injections on optical absorption spectra, especially A and B exciton optical absorption bands, which are caused by the spin splitting, of multi-layered MoS₂ and WS₂ thin films, which were synthesized by chemical vapor deposition methods.

Figure 1 shows the optical absorption spectra of multi-layered MoS₂ thin films as a function of potential shift. As shown in the figure, the A and B exciton optical absorption bands are clearly identified. When the electrons are injected to the bottom of conduction bands, we found that the A and B exciton bands are disappeared at the same time, which in agreement with the electronic structures. However, although we tried to extract electrons from the top of the valence bands, as shown in the figure, nothing has changed in the optical absorption spectra. The result indicates that electrons cannot be extracted from our CVD grown MoS₂ due to the presence of defects, suggesting importance to prepare a film with high crystallinity.

Reference: [1] Xiao *et al.*, *PRL* 108 196802 (2012), [2] Suzuki *et al.*, *Nat. Nanotech.* 9, 611 2014, [3] Zhang *et al.*, *Science* 344 725 (2014), Zhang *et al.*, *Nano Lett.* 12 1136 2012, Ye *et al.*, *Science* 338 1193 (2012) [4] Yanagi *et al.*, *Adv. Mater.* 23 2811 (2011), *PRL* 110 86801 (2013), *Nano Lett.* 14 6437 (2014)

Corresponding Author: K. Yanagi

Tel: +81-42-677-2494,

E-mail: yanagi-kazuhiro@tmu.ac.jp

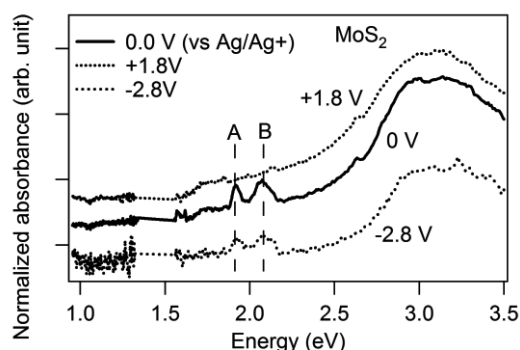


Fig. 1 Influence of Electrochemical doping on optical absorption spectra of CVD grown multilayered MoS₂ thin film.

Preparation of Nb₂O₅-Graphene Nanocomposites and Kinetics for Photocatalytic Degradation of Organic Dyes

Hae Soo Park, ○Jeong Won Ko and Weon Bae Ko

Department of Chemistry, Sahmyook University, Seoul 139-742, South Korea

Niobium pentoxide (Nb₂O₅) nanoparticles were synthesized using niobium (V) chloride and pluronic F108NF as the precursor and templating agent, respectively. The Nb₂O₅-graphene nanocomposites were placed in an electric furnace at 700 °C and calcined under Ar atmosphere for 2 h. The morphology, crystallinity, and photocatalytic degradation activity of the samples were characterized by X-ray diffraction, transmission electron microscopy, scanning electron microscopy, and UV-vis spectroscopy. The Nb₂O₅-graphene nanocomposites were worked as a photocatalyst in the photocatalytic degradation of organic dyes under 254 nm UV light; the organic dyes used were methylene blue (MB), methyl orange (MO), rhodamine B (RhB), and brilliant green (BG). The photocatalytic degradation kinetics for the aforesaid dyes were determined in the presence of the Nb₂O₅-graphene nanocomposites.

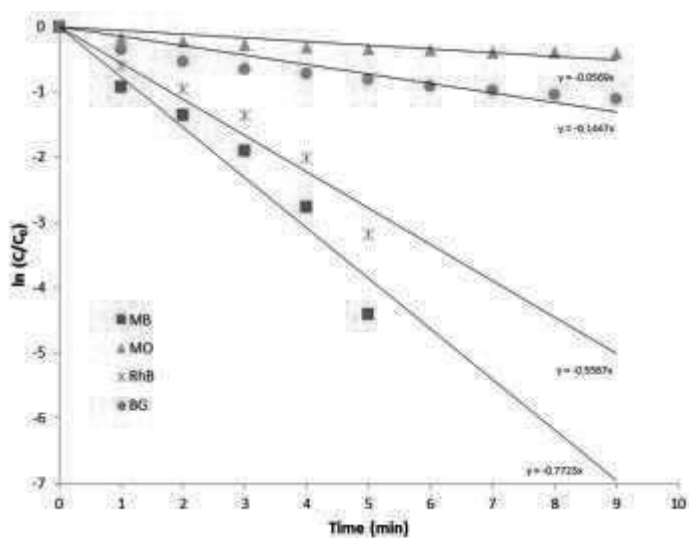


Fig.1 Kinetics of the degradation of (a) MB, (b) MO, (c) RhB and (d) BG with the synthesized Nb₂O₅-graphene nanocomposites

[1] F. Hashemzadeh, R. Rahimi and A. Ghaffarinejad, *Ceram. Int.*, **40**, 9817 (2014).

[2] S. K. Hong, J. H. Lee and W. B. Ko, *J. Nanosci. Nanotechnol.*, **11**, 6049 (2011).

Corresponding Author: Weon Bae Ko

Tel: +82-2-3399-1700, Fax: +82-2-979-5318

E-mail: kowb@syu.ac.kr

発表索引
Author Index

Author Index

< A >

Abe, Shigeaki 1P-12
 Abe, Yurika 2P-41
 Achiba, Yohji **1-1**, 2-7, 2P-8,
 2P-41
 Ago, Hiroki 2P-28, 3P-27, 3P-40
 Aikyo, Yusuke **1P-26**
 Airya, Pourya 1P-2
 Akabori, Masashi 3-2
 Akasaka, Takeshi 2P-5, 3P-4, 3P-5
 Akashi, Ryosuke 3-7
 Akatsu, Takashi 2P-38
 Akiyama, Kazuhiko 2-5
 Akizuki, Naoto 1P-5, 2P-11
 An, Hua **3P-18**
 Ando, Tsuneya 2-10
 Anisimove, Anton 2-1
 Aonuma, Shuji 2P-15
 Aota, Shun **1P-5**
 Aoyagi, Shinobu 2P-1
 Arai, Miho **3-4**
 Arakawa, Yasuhiko 3P-11
 Araki, Takuma **2P-20**
 Arita, Ryotaro 3-7
 Asaka, Koji 3P-14
 Ayria, Pourya **3P-37**

< B >

Balch, Alan L. 2P-5, 3P-4
 Badow, Shunji 1P-44, 3P-24
 Bégin-Colin, Sylvie 1-8
 Beniya, Atsushi **3P-8**
 Bianco, Alberto 1-8
 Bordacs, Sandor 3-7
 Braam, Daniel 1P-26

< C >

Carlson, Robert M. K. 2P-26
 Carvalho Alexandra 3P-35
 Castro Neto, A. H. 3P-35
 Chechetka, Svetlana 1-8
 Chen, Guohai 3P-7
 Chen, Xiao **3-8**
 Chen, Zhongming 1P-15
 Chiashi, Shohei 1P-11, 1P-18, 2-2,
 2P-22, 3-8, 3P-8,
 3P-18, 3P-20
 Chiba, Kazuki **2-5**

Chiba, Takaaki 2-1, **2-2**
 Cui, Kehang 2-1, 3P-18
 Cuoug, Nguyen Thanh 2P-35
 Czank, Thomas **1P-2**

< D >

Dahl, Jeremy E. P. 2P-26
 Dao Duy, Thang 1P-26
 Dong, Baojuan 1P-43
 Dresselhaus, M. S. 1P-41

< E >

Eda, Goki 1P-29, 3P-35
 Endo, Hitomi 2-7, **2P-8**, 2P-41
 Ezawa, Motohiko 1P-33, 1P-34, 1P-35

< F >

Fernández-Lázaro, Fernando 2P-4
 Fokina, Natalie A. 2P-26
 Font-Sanchis, Enrique 2P-4
 Fujigaya, Tsuyohiko **1-5**
 Fujihara, Miho **3P-25**
 Fujii, Shunjiro 1-4, 1P-14, **3P-3**
 Fujimoto, Taiyo 3P-31
 Fujimoto, Yoshitaka 2-9
 Fujiwara, Akihiko 2P-42
 Fukata, Shinsuke 3P-23
 Fukumaru, Takahiro 1-5
 Fukuzawa, Masashi **1-3**
 Fukuzumi, Shunichi 2P-4
 Furuta, Hiroshi 2P-19
 Futaba, Don 3P-7

< G >

Gao, Xiang 2P-2
 Guo, Huaihong **1P-41**, 1P-43

< H >

Hara, Hideyuki 2-4
 Harada, Yusaku 1P-17
 Haruta, Naoki **2-6**, 2P-31
 Haruyama, Junji 1P-33, 1P-34, 1P-35,
 1P-36
 Hasdeo, Eddwi H. 2-11, **3P-33**, 3P-34
 Hasdeo, Hesky 1P-31, 3P-37
 Hasegawa, Kei 1P-10, 1P-15, 1P-17,
 1P-19, 1P-21
 Hashimoto, Kenro 1-1

Hasobe, Taku	2P-4	Ishiyama, U	1P-8
Hata, Kenji	3P-7	Itami, Kenichiro	3P-6, 3P-21
Hatakeyama, Kazuto	1P-37	Ito, Masahiro	2-8
Hatta, Akimitsu	2P-19	Ito, Takahiro	3-2
Hattori, Yoshiyuki	1P-38	Ito, Yusuke	2-8
Hayase, Shohei	1-6, 3-10	Itoh, Chihiro	2P-20
Hayashi, Hironobu	2S-5	Iwahara, Naoya	2P-43
Hayashi, Yutaro	1P-24	Iwaizako, Tasuku	3P-40
Hibino, Hiroki	2P-28, 2P-32, 3P-27	Iwaki, Ryoma	1P-35
Higashide, Noriyuki	2P-17	Iwamoto, Satoshi	3P-11
Hiraiwa, Atsushi	2-3	Iwasa, Yoshihiro	2P-42, 2P-44, 3-3, 3-7, 3P-41
Hirakawa, Takuya	1P-14		
Hirano, Atsushi	1-4, 1P-14, 2P-18	Iwata, Nobuyuki	1P-24, 3P-17, 3P-19
Hirano, Kazutaka	2P-21	Izumiyama, Akinori	1P-28
Hirano, Yu	1P-9, 2-3		
Hiroshiba, Yasuhiro	1P-1	< J >	
Hirotani, Jun	3P-12	Jeon, Il	2-1
Homma, Kotaro	3P-42	Jiang, Ming	2P-16, 2P-17
Homma, Naoki	3P-8	Jinnouchi, Ryota	1P-1
Homma, Yoshikazu	2-8, 3P-8	Jippo, Hideyuki	2P-36
Honda, Atsushi	2P-20	Juhasz, Gergely	2P-12
Honda, Shiro	1S-2		
Hong, Liu	3P-21	< K >	
Honma, Tomohiro	1P-36	Kako, Masahiro	2P-5, 3P-5
Hoshino, Ryo	1P-24	Kamijo, Junichi	1P-33
Huang, Jing-Kai	3P-31	Kanahashi, Kaito	2P-35
		Kanbara, Takaki	1P-26
< I >		Kanda, Shouhei	2P-14
Ichihashi, Toshinari	1-7	Karousis, Nikolaos	3P-4
Iijima, Sumio	1-7, 2P-29, 3P-23, 3P-24	Katagiri, Yoto	1P-34
Iizuka, Takahiko	3P-41	Katagiri, Yuto	1P-33
Iizumi, Yoko	1-7, 2P-29	Kataoka, Yosuke	3P-9
Ikehara, Yuzuru	1-7	Kataoka, Yousuke	3P-10
Ikuma, Naohiko	3P-2	Kataura, Hiromichi	1-4, 1P-5, 1P-14, 2P-18, 3P-3
Ikuta, Taro	1P-13		
Imai, Kentaro	1P-24	Kato, Hiroki	2-8
Imai, Yasuhiko	2P-42	Kato, Sho	1S-3
Imamura, Saneyuki	3P-11	Kato, Tateaki	1P-33
Imazu, Naoki	1S-2	Kato, Yuichi	1-3
Inaba, Masafumi	1P-9, 2-3	Kato, Yuichiro K.	1P-4, 1P-7, 2S-6, 2-12, 2-13, 2P-16, 2P-17, 3P-11
Inoue, Kadumi	3P-29		
Inoue, Naoko	2P-44	Katumoto, Shingo	1P-33, 1P-34
Inoue, Ryosuke	2P-30, 3P-25	Kauppinen, Esko I.	2S-4, 2-1, 2-2
Inoue, Taiki	1P-11, 3P-18	Kawabata, Kosuke	1P-15
Isaka, Takuya	3P-29	Kawaguchi, Daiki	3P-17, 3P-19
Ishii, Akihiro	1P-4, 2-12, 2-13, 2P-16, 2P-17, 3P-11	Kawahara, Kenji	2P-28
		Kawai, Hideki	2P-14, 3P-42
Ishii, Satoshi	1P-26	Kawakami, Hiroki	2P-1
Ishikawa, Ryo	1P-41	Kawano, Saki	3P-1

Kawarada, Hiroshi	1P-9, 2-3	Li, Yan	1S-1 , 1P-6, 1P-16
Kawashima, Yuki	2P-4	Li, Zong-Jun	2P-2
Kigure, Shota	2P-6	Liu, Gang	3-11
Kikuchi, Ryo	1P-36	Liu, Hsiang	1P-31
Kim, Dong Young	1P-10	Liu, Xuqing	3P-11
Kimura, Masato	3P-4	Lorke, Axel	1P-26
Kimura, Ryoya	1P-24		
Kimura, Shigeru	2P-42	< M >	
Kimura, Takahide	2P-15, 3-11	Machida, Tomoki	3-4
Kishimoto, Ken	2P-39	Machiya, Hidenori	3P-11
Kishimoto, Shigeru	3P-12	Maeda, Yutaka	3P-4
Kisoda, Kenji	2P-20	Makino, Tatuya	1P-34
Kitamura, Yoshimasa	2P-14	Manako, Takashi	3P-24
Kitaura, Ryo	1P-27, 2P-23, 2P-26, 2P-40, 3S-9	Maniwa, Yutaka	1P-22, 1P-25, 2P-14, 2P-30, 2P-32, 3P-25
Ko, Jeong Won	3P-43	Manuel Blas-Ferrando, Vicent	2P-4
Ko, Weon Bae	3P-43	Maria, Kazi Hanium	1P-20
Kobayashi, Keita	2P-25	Maruyama, Mina	3-9
Kobayashi, Yoshihiro	3-2	Maruyama, Shigeo	1P-11, 1P-18, 2-1, 2-2, 2P-22, 3-8, 3P-18, 3P-20
Kobayashi, Yu	2P-32		
Kodama, Takeshi	1-1, 2-7, 2P-8, 2P-41	Maruyama, Takahiro	3P-16, 3P-28
Kodama, Takuya	1-1	Masubuchi, Satoru	3-4
Kogane, Kennta	1P-38	Masuda, Katsuya	3P-30
Koinuma, Michio	1P-37	Matsubayashi, Hironobu	1P-1
Koirala, Sandhaya	2P-34	Matsuda, Kazunari	1P-5, 1P-29, 2P-11, 2P-34, 3S-8 , 3-5, 3P-35, 3P-36
Kokubo, Ken	3P-2		
Komatsu, Mamoru	3P-39	Matsuda, Masahiro	3P-14
Komatsu, Naoki	2P-15, 3-11	Matsui, Katsuma	3P-6
Konabe, Satoru,	3-6	Matsui, Ryotaro	3P-12
Kondo, Takahiro	1P-26	Matsuki, Keiichiro	3P-36
Koretsune, Takashi	2-9	Matsumoto, Jun	2-7, 2P-8, 2P-41
Kosugi, Yuta,	1P-44	Matsumoto, Naoyuki	3P-7
Koyata, Miho	1P-36	Matsumoto, Shogo	1P-37
Kozawa, Akinari	3P-16	Matsumoto, Yasumichi	1P-37
Kozawa, Daichi	1P-29, 2P-34, 3-5, 3P-35	Matsuo, Yoshiaki	3P-29
		Matsuo, Yutaka	2-1, 2P-1, 2P-2
Kubuki, Shiro	2-5	Mieno, Tetsu	1P-20
Kumamoto, Yusuke	2-12, 2P-16	Mikie, Tsubasa	3P-2
Kuriya, Masaaki	1P-17	Mimuro, Kazuki	1P-1
Kushida, Soh	1P-26	Minami, Kazuya	3P-5
Kusuda, Hiroyuki	1P-44	Miura, Ryohei	3P-11
Kusunoki, Michiko	1P-9, 2-3	Miyabe, Kyosuke	2P-5
Kuwabara, Junpei	1P-26	Miyako, Eijiro	1-8 , 2P-29
Kuwahara, Yuki	2P-9	Miyamoto, Yoshiyuki	2P-33
		Miyata, Yasumitsu	1P-22, 1P-25, 2P-23, 2P-30, 2P-32, 3P-25
< L >			
Lee, Chih-Yu	1P-9, 2-3	Miyauchi, Yuhei	1P-5, 1P-29, 2P-11, 2P-34, 3P-21
Li, Lain-Jong	2P-35, 3P-31, 3P-36		
Li, Shu-Hui	2P-2		

Mizorogi, Naomi	2P-5	Nishino, Hidekazu	1S-2
Mizuno, Masashi	2P-37	Noda, Suguru	1P-10, 1P-15, 1P-17,
Mizuno, Seigi	2P-28		1P-19, 1P-21, 3P-15
Mizutani, Akitaka	1P-42	Nomura, Kumiko	1P-35
Mori, Hatsumi	2-4	Norimatsu, Wataru	1P-9, 2-3
Mori, Shohei	1P-22 , 2P-32	Nouchi, Ryo	3-1
Morisako, Shiyo	3P-26	Nugraha, Ahmad R. T.	1P-31, 2-11 , 3P-33,
Morisawa, Yusuke	2-7		3P-34, 3P-37
Moriya, Rai	3-4		
Moriyama, Hiroshi	2-4	< O >	
Motomiya, Kenichi	2P-21	Ochi, Masayuki	3-7
Mouri, Shinichiro	1P-5, 1P-29 , 2P-34,	Ogasawara, Kazuki	1P-18 , 3P-20
	3-5	Ogata, Hironori	1-6, 2P-3, 3-10,
Murakami, Toshiya	2P-20		3P-1, 3P-9, 3P-10
Myodo, Miho	1P-9, 2-3	Ohata, Chika	1P-34 , 1P-35, 1P-36
		Ohfuchi, Mari	1P-3 , 2P-36
< N >		Ohkubo, Kei	2P-4
Nagao, Tadaaki	1P-26	Ohmori, Shigekazu	2P-9
Nagase, Shigeru	2P-5, 3P-4, 3P-5	Ohno, Yutaka	1P-10, 3P-12
Nagashima, Dai	2P-43	Ohta, Hiromichi	2P-35
Nagashio, Kosuke	3S-7	Ohta, Ryuichi	3P-11
Nagata, Tomoko	1P-24, 3P-17, 3P-19	Ohta, Yujiro	2P-28
Nakada, Kyoko	1P-40	Oi, Takashi	1S-2
Nakagawa, Takafumi	2P-2	Okada, Hiroshi	2P-1
Nakahara, Hitosi	3P-14	Okada, Susumu	1P-8, 1P-32, 2P-6,
Nakai, Yusuke	2P-14		2P-7, 2P-35, 2P-36,
Nakamoto, Keisuke	2P-38		2P-39, 3-6, 3-9,
Nakamura, Junji	1P-26		3P-38
Nakamura, Keisuke	2P-15	Okazaki, Toshiya	1-7, 2P-29
Nakamura, Maki	1-7, 3P-23	Olmstead, Marilyn M.	2P-5, 3P-4
Nakamura, Takashi	3-5	Omachi, Haruka	2P-6, 2P-23, 2P-26
Nakamura, Taketomo	1P-33, 1P-34	Onga, Masaru	3-3
Nakanishi, Takeshi	2-10	Ortiz, Javier	2P-4
Nakanishi, Yudai	1P-35	Ōsawa, Eiji	1-9, 1P-39
Nakanishi, Yusuke	2P-26	Osawa, Toshio	1P-15, 1P-19
Nakashima, Naotoshi	1-3, 1-5, 2P-11,	Oshima, Yuki	2P-14
	2P-12, 2P-24, 3P-22	Otsuka, Keigo	1P-11
Nakayama, Ko	3P-15	Ozawa, Hiroaki	3P-22
Namba, Natsuki	1P-40	Özyilmaz, Barbaros	1P-33
Narita, Kohei	1P-32		
Naritsuka, Shigeya	3P-16, 3P-28	< P >	
Nasiblin, Albert G.	2-2	Pander, Adam	2P-19
Nasibulin, Albert	2-1	Park, Hae Soo	3P-43
Natsume, Yuhei	2P-13	Pichon, Benoit	1-8
Negishi, Ryota	3-2	Popert, Alexander	1P-7
Nihey, Fumiyuki	2P-9	Pu, Jiang	2P-35, 3P-31 , 3P-36
Nishihara, Taishi	3P-6		
Nishikawa, Jumpei	2P-10	< Q >	
Nishikawa, Noriaki	3P-39	Qin, Hongmei	2P-15
Nishimura, Tomoaki	1-6		

< R >		Sorimachi, Jun-ya	2P-7
Rao, Apparao	1P-36	Sota, Masaki	3-8
Ryan, James	2P-2	Suda, Yoshiyuki	1P-42
		Suenaga, Kazu	1-2
< S >		Sugai, Toshiki	1P-1 , 1P-18, 1P-23, 3P-20
Saeki, Akinori	3P-2	Sugiura, Takeshi	3P-5
Saida, Takahiro	3P-16	Suzuki, Kazuma	1P-9, 2-3
Saiki, Ayano	1P-44	Suzuki, Manabu	3P-28
Saiki, Koichiro	1S-3	Suzuki, Mitsuaki	2P-5, 3P-4
Saito, Makoto	1P-18, 3P-20	Suzuki, Motoyuki	1S-2
Saito, Riichiro	1P-2, 1P-31, 1P-41, 1P-43, 2-11, 2P-37, 3P-13, 3P-33, 3P-34, 3P-37	Suzuki, Ryuji	2P-42, 2P-44, 3-7
		Suzuki, Shoji	2P-40
Saito, Susumu	2-9 , 2P-10	< T >	
Saito, Takeshi	2P-9	Tabata, Kenichi	1P-26
Saito, Yahachi	3P-14	Tachibana, Masaru	3P-26
Saito, Yu	2P-44	Tagmatarichis, Nikos	3P-4
Sakaguchi, Takahiro	2-2	Taguchi, Yuki	2-7, 2P-8, 2P-41
Sakai, Hayato	2P-4	Tahara, Yoshio	3P-23
Sakanoue, Tomo	3P-15, 3P-31	Takada, Tomoya	1P-12
Sano, Masahito	3P-30	Takada, Yukihiro	1P-40
Sano, Yoshiaki	2P-3	Takagi, Yukai	2P-22
Sasaki, Shogo	1P-25 , 2P-32	Takahashi, Misaki	1P-23
Sasaki, Yuki	1P-27	Takai, Kazuyuki	1P-28 , 1P-38, 2P-38, 3P-29, 3P-32
Sastre-Santos, Ángela	2P-4	Takakura, Akira	3P-21
Sato, Kenichi	1S-2	Takashima, Kengo	1P-30
Sato, Kumiko	2P-5, 3P-5	Takatsuka, Takayuki	1P-13
Sato, Tohru	2-6, 2P-31 , 2P-43	Takenobu, Taishi	1P-10, 2P-35, 3P-15, 3P-31, 3P-36
Sato, Yoshinori	1P-18, 2P-21, 3P-20	Takesaki, Yuichiro	3P-27
Sato, Yutaka	3P-9	Takikawa, Hirofumi	1P-42
Schreiner, Peter R.	2P-26	Takizawa, Rina	2P-28
Scott, Lawrence	3P-21	Tamura, Noriyuki	3P-24
Segawa, Yasutomo	3P-6	Tanaka, Kazuyoshi	2-6, 2P-31, 2P-43
Seki, Shu	3P-2	Tanaka, Shin-Ichiro	3P-37
Senga, Ryosuke	1-2	Tanaka, Takeshi	1-4, 1P-5, 1P-14, 2P-18, 3P-3
Shi, Wu	2P-44	Tanaka, Toshihiko	1-9
Shibuya, Megumi	1P-9, 2-3	Taniguchi, Takaaki	1P-37
Shimada, Takashi	2P-16, 3P-11	Taniguchi, Takashi	2P-32
Shimizu, Kazuki	1P-42	Terasawa, Tomo-o	1S-3
Shimizu, Sunao	3P-41	Thendie, Boanerges	2P-23
Shimomura, Yuuki	1P-11	Tobari, Yuta	1P-18, 3P-20
Shinohara, Hisanori	1P-27, 1P-34, 1P-35, 2P-6, 2P-23, 2P-26, 2P-40, 3P-25	Tohji, Kazuyuki	2P-21
		Tokura, Yoshinori	3-7
Shirae, Hiroyuki	1P-10 , 3P-15	Toshimitsu, Fumiyuki	1-3, 2P-24 , 3P-22
Shiraishi, Tomonari	2P-11 , 2P-12	Touhara, Hidekazu	1P-38
Shiromaru, Haruo	1-1, 2-7, 2P-8, 2P-41	Toyama, Kiyohiko	3P-24
Siregar, Syahril	1P-31		

Tsuda, Yusaku	3P-17	Yamada, Syunya	1P-36
Tsuji, Masaharu	2P-28, 3P-27, 3P-40	Yamaguchi, Kohtaro	1P-21
Tsujimoto, Marina	3P-26	Yamaguchi, Mai	1P-19
Tsukagoshi, Kazuhito	1P-41	Yamaguchi, Masanori	2P-20
Tsushima, Kohei	3-8	Yamamoto, Hiroshi	1P-24, 3P-17, 3P-19
Tsuzuki, Mayumi	1-4, 1P-14	Yamamoto, Mahito	1P-41
Tuan Hung, Nguyen	3P-13	Yamamoto, Shohei	2-4
		Yamamoto, Takahiro	1P-30, 3P-8
< U >		Yamamoto, Yohei	1P-26
Uchida, Yuki	3P-40	Yamanaka, Ayaka	3P-38
Uda, Takushi	1P-4 , 2P-17	Yamanoi, Ryoko	1-9, 1P-39
Ue, Hitoshi	1P-42	Yamashina, Tomoki	3P-29
Ueda, Chihiro	3P-4	Yamashita, Hiroki	2P-27
Ueda, Mako	1P-37	Yanagi, Kazuhiro	2P-14, 3P-42
Ueda, Yuki	3P-28	Yang, Feng	1P-6, 1P-16
Ueno, Hiroshi	3P-6	Yang, Juan	1P-6, 1P-16
Ueno, Keiji	1P-41, 3-4	Yang, Teng	1P-41, 1P-43
Ukhtary, Shoufie	3P-34	Yasuda, Hidehiro	2P-25
Umeda, Yoshito	1P-42	Ye, Jianting	2P-42, 2P-44
Umehara, Taichi	3P-32	Yokoi, Hiroyuki	1P-37
Umemura, Kazuo	2-8	Yokokura, Eita	3P-10
Umeyama, Kaori	3P-39	Yokoyama, Akio	2-12
		Yokoyama, Koji	2P-21
< V >		Yomogida, Yohei	1-4 , 1P-14
Verzhbitskiy, Ivan	3P-35	Yoshida, Keisuke	3P-17 , 3P-19
		Yoshida, Masahiro	1P-4, 1P-7, 2-12 , 2-13, 2P-16, 2P-17
< W >		Yoshida, Masaro	2P-42 , 2P-44, 3P-41
Wada, Yoriko	2-7, 2P-43	Yoshikawa, Ryo	2P-22
Wakabayashi, Tomonari	2-7 , 2P-8, 2P-41, 2P-43	Yoshitake, Haruhiko	1-6, 3-10
Wall, Mark	3P-39	Yoza, Kenji	2-4
Wang, Qing	2P-40	Yudasaka, Masako	1-7, 1-8, 2P-29, 3P-23, 3P-24
Wang, Wei-Wei	2P-5, 3P-4	Yuge, Ryota	1-7, 3P-24
Wang, Xiao	1P-16	Yumura, Motoo	3P-7
Wang, Zhipeng	1-6, 3-10	Yumura, Takashi	2P-27
Watanabe, Kenji	2P-32		
Watanabe, Osamu	1S-2	< Z >	
Watanabe, Yoshio	3-2	Zhang, Daqi	1P-6 , 1P-16
Wei, Xiaojun	1-4, 1P-5, 1P-14	Zhang, Hong	2P-33
		Zhang, Minfang	1-7, 1-8, 2P-29 , 3P-23
< X >		Zhang, Yijin	2P-42, 2P-44, 3-3
Xiang, Rong	2-2, 3-8, 3P-18	Zhang, Zhidong	1P-41, 1P-43
		Zhao, Li	2P-15
< Y >		Zhou, Lin	1P-41
Yabuki, Naoto	3-4		
Yabushita, Yuhei	2P-20		
Yamada, Hiroko	2S-5		
Yamada, Jumpei	3P-28		
Yamada, Michio	3P-4		
Yamada, Shoji	3-2		

複写をご希望の方へ

フラーレン・ナノチューブ・グラフェン学会は、本誌掲載著作物の複写に関する権利を一般社団法人学術著作権協会に委託しております。

本誌に掲載された著作物の複写をご希望の方は、(社)学術著作権協会より許諾を受けて下さい。但し、企業等法人による社内利用目的の複写については、当該企業等法人が社団法人日本複写権センター((社)学術著作権協会が社内利用目的複写に関する権利を再委託している団体)と包括複写許諾契約を締結している場合にあつては、その必要はございません(社外頒布目的の複写については、許諾が必要です)。

権利委託先：一般社団法人学術著作権協会

〒107-0052 東京都港区赤坂 9-6-41 乃木坂ビル 3階

URL : <http://www.jaacc.jp/> E-Mail : info@jaacc.jp

電話 : 03-3475-5618 FAX : 03-3475-5619

注意：複写以外の許諾（著作物の引用、転載・翻訳等）に関しては、(社)学術著作権協会に委託致しておりません。直接、フラーレン・ナノチューブ・グラフェン学会へお問い合わせください。

Reprographic Reproduction outside Japan

- Making a copy of this publication
Please obtain permission from the following Reproduction Rights Organizations (RROs) to which the copyright holder has consigned the management of the copyright regarding reprographic reproduction.
- Obtaining permission to quote, reproduce; translate, etc.
Please contact the copyright holder directly.

Users in countries and regions where there is a local RRO under bilateral contract with Japan Academic Association for Copyright Clearance(JAC) are requested to contact the respective PROs directly to obtain permission.

Users in countries or regions in which JAC has no bilateral agreement are requested to apply for the license to JAC.

Japan Academic Association for Copyright Clearance (JAC)
Address : 9-6-41 Akasaka, Minato-ku, Tokyo 107-0052 Japan
URL : <http://www.jaacc.jp/> E-mail : info@jaacc.jp
Phone : +81-3-3475-5618 FAX : +81-3-3475-5619

2015年2月21日発行

第48回フラーレン・ナノチューブ・グラフェン総合シンポジウム 講演要旨集

《フラーレン・ナノチューブ・グラフェン学会》

〒113-8656 東京都文京区本郷 7-3-1

東京大学大学院工学系研究科 機械工学専攻
丸山研究室内

Phone/Fax : 03-3830-4848

E-mail : fntg@photon.t.u-tokyo.ac.jp

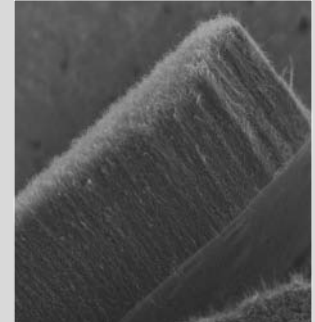
URL : <http://fullerene-jp.org>

印刷 / 製本 (株)創志企画

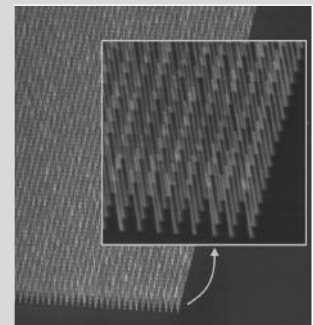
AIXTRON

アイクストロン社

カーボンナノチューブ&グラフェン成長用CVD装置 Black Magic



Dense CNT



Horizontal SWCNT



Graphene

- 装置導入後、スピーディに希望のCNTやグラフェンを成長可能
- オリジナルレシピ付き「Thermal CVDとPlasma CVDの2モードに対応」
(シングルCNT用、ダブルCNT用、マルチCNT用、グラフェン用、横方向CNT用、低圧カプロセス用、高速成長CNT用など)
- あらゆる基板サイズに対応 (研究用2"、4"、6"モデルから量産用最大300mmモデルまで)
- プラズマによる簡単なクリーニングと高メンテナンス性
- 世界中の大学・研究所・企業へ多数納入実績あり

アイクストロン株式会社 www.aixtron.com

〒140-0001 東京都品川区北品川1-8-11 Daiwa品川Northビル 9F
E-mail: JAPANINFO@aixtron.com

Tel: 03-5781-0931 Fax: 03-5781-0940

販売代理店: 丸文株式会社 www.marubun.co.jp

〒103-8577 東京都中央区日本橋大伝馬町8番1号
E-mail: kagaku@marubun.co.jp

Tel: 03-3639-1336 Fax: 03-3662-1349

Thermo
SCIENTIFIC

Cover more ground, easily

ナノサイエンスや地質学、バイオなど、ラマン分光の技術をもっと活用できる分野は多岐にわたります。Thermo Scientific™ DXR™xi イメージング顕微ラマンは、高度な性能を視覚的に操作することにより、初心者から熟練者まで分析業務をとてシンプルにすることができるケミカルイメージング装置です。これであなともラマンのエキスパート。広大なエリアを秒単位で探索し、確実にターゲットを捉えます。

革新的ラマンイメージング

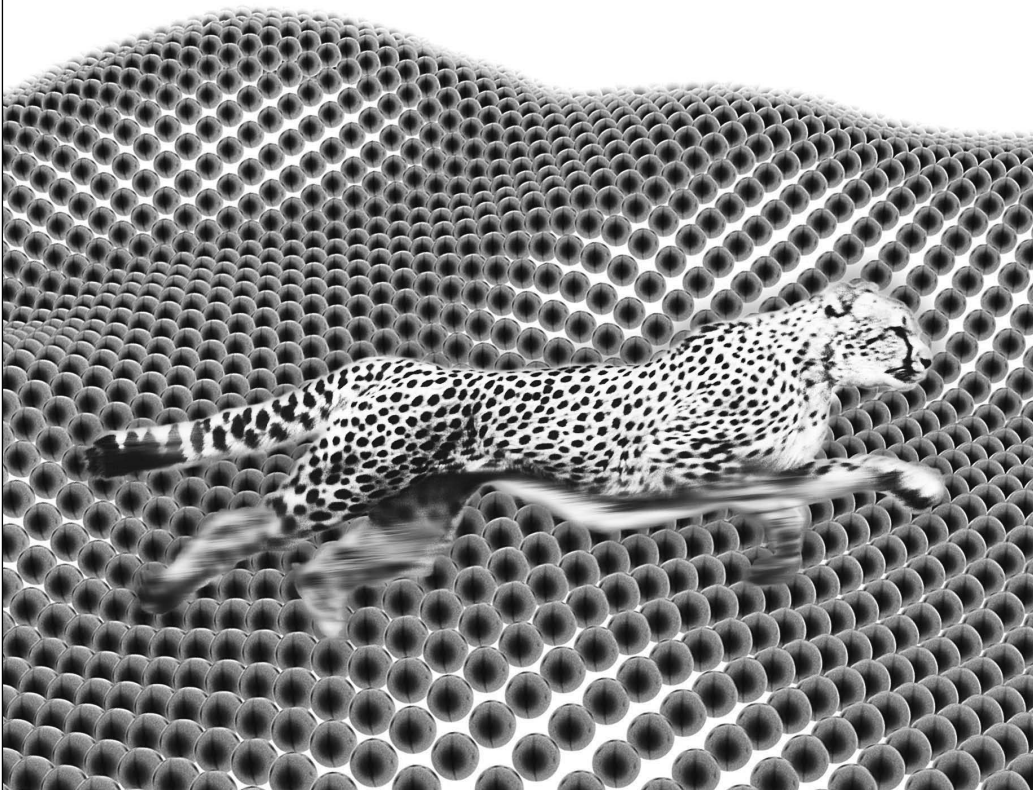
• www.thermoscientific.jp/DXRxi/



DXRxi イメージング顕微ラマン
一体型・高性能ラマン
イメージングシステム



Thermo Scientific OMNIC™xi
ラマンイメージングソフトウェア
一体型・高性能ラマン
イメージングシステム



サーモフィッシャーサイエンティフィック株式会社

TEL.0120-753-670 FAX.0120-753-671

〒221-0022 横浜市神奈川区守屋町 3-9

Analyze.jp@thermofisher.com www.thermoscientific.jp

須藤彰三・岡 真 監修

《基本法則から読み解く物理学最前線 ⑤》



フラーレン・ ナノチューブ・ グラフェンの科学

齋藤理一郎 著

ナノカーボンの世界

本書は、ナノカーボンという新しい炭素材料を紹介した本である。ナノカーボンとは、グラフェン、フラーレン、カーボンナノチューブという新物質をまとめて呼ぶ名前であり、いずれも新素材として注目を集めている。

この本の使命は、ナノカーボンの科学がどんなものであるかを物理学の研究者が紹介する本であり、必要な知識が詳細に書かれた教科書ではない。またいろいろな知識が整理されたハンドブックでもない。異国の地(ナノカーボンの世界)へ案内する旅のガイドブックである。

本書は高校生から大学院生、研究者、一般へと幅広い読者を想定した、式のあまりない本である。他の分野の人も予備知識なしで理解できるように専門用語の説明を加えている。ナノカーボンについて、あらかじめ知っている中堅の研究者にも気楽に読める本である。

【A5判・並製本・180頁・本体2,000円(税別)】

主要目次

- 第1章 ナノカーボンの世界
- 第2章 ナノカーボンの発見
- 第3章 ナノカーボンの形
- 第4章 ナノカーボンの合成
- 第5章 ナノカーボンの応用
- 第6章 ナノカーボンの電子状態
- 第7章 ディラックコーンの性質
- 第8章 グラフェンとナノチューブのラマン分光
- 第9章 未来への課題



ナノ構造の科学とナノテクノロジー

—量子デバイスの基礎を学ぶために—

Edward L. Wolf 著・吉村雅満・目良 裕・重川美咲子・重川秀実訳 海外で評価の高いテキスト『Nanophysics and Nanotechnology: An Introduction to Modern Concepts in Nanoscience 2/e』の翻訳書。ナノ物理の基礎から工学への応用まで幅広い分野を網羅し、学生、研究者、技術者に向けての最適な内容構成としている。 B5判・並製本・294頁・本体6,000円(税別)



ナノの本質 —ナノサイエンスからナノテクノロジーまで—

T. Pradeep 著・木村啓作・八尾浩史・佐藤井一訳 本書はナノサイエンス、ナノテクノロジーについて数式を排除し、多くの図と写真で理解できるよう工夫された『NANO: The Essentials』の翻訳書。業界用語・専門用語もできるだけ日常語で表現する、化学式を用いずに化合物名で表わすなど、そこかしこに細かい工夫がみられる。この分野に出てくる必要な実験技法を網羅しており、本書一冊で完結する記述となっている。巻末にはナノ関連の用語集がついており、ナノ関連のハンドブックとしても有用である。 菊判・上製本・534頁・本体6,500円(税別)

〒112-0006 東京都文京区小日向4-6-19
TEL. 03-3947-2511/FAX. 03-3947-2539

共立出版



<http://www.kyoritsu-pub.co.jp/>
<https://www.facebook.com/kyoritsu.pub>



COSMOSIL

誘導体化フラーレン用HPLCカラム

COSMOSIL[®] Buckyprep-D

- 誘導体化フラーレン用HPLCカラム
- トルエン移動相中で誘導体化フラーレンが分離可能

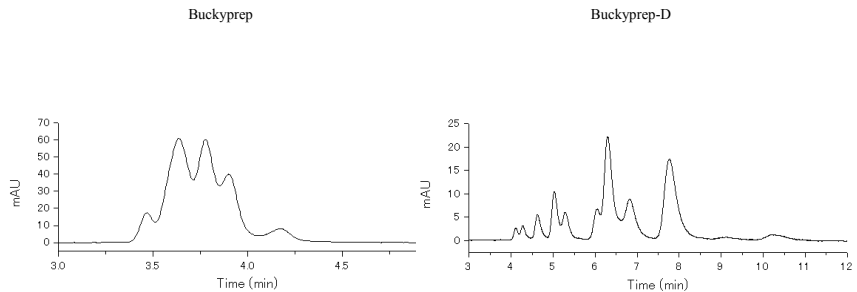
■C60インデン付加体の分析例

C₆₀インデンは誘導体化フラーレンの一種であり、有機薄膜太陽電池のn型半導体材料として注目されている化合物です。コスモシル Buckyprep-Dを用いることにより高い分離性能が得られます。

COSMOSIL Application Data

Column: Buckyprep
 Column size: 4.6mmI.D.-250mm
 Mobile phase: Toluene
 Flow rate: 1.0 ml/min
 Temperature: 30°C
 Detection: UV 325nm

Sample: C₆₀ [Indene]₂ (1.0mg/ml)
 Inj. Vol.: 1.0μl



Data courtesy of Yusuke Tajima, Dr. Sci. Organic Optoelectronics Laboratory, RIKEN (Institute of Physics and Chemistry)

NACALAI TESQUE, INC

■Buckyprepシリーズの用途

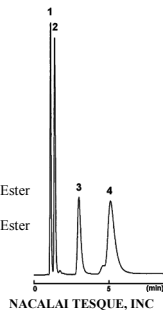
- フラーレン分離のスタンダードカラム → COSMOSIL Buckyprep
- 誘導体化フラーレンの分離 → COSMOSIL Buckyprep-D
- 金属内包フラーレンの分離 → COSMOSIL Buckyprep-M

・ 誘導体化フラーレン (Buckyprep-D)

COSMOSIL Application Data

Column: Buckyprep-D
 Column size: 4.6mmI.D.-50mm
 Mobile phase: Toluene
 Flow rate: 1.0 ml/min
 Temperature: 30°C
 Detection: UV325nm

Sample: 1; C₆₀ (0.125mg/ml)
 2; C₇₀ (0.250mg/ml)
 3; [6,6]-Phenyl-C₆₁ Butyric Acid Methyl Ester [PCBM] (0.125mg/ml)
 4; [6,6]-Phenyl-C₇₁ Butyric Acid Methyl Ester [[70]PCBM] (0.375mg/ml)
 Inj. Vol. 1.0μl

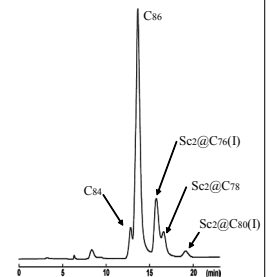


・ 金属内包フラーレン (Buckyprep-M)

COSMOSIL Application Data

Column: Buckyprep-M
 Column size: 4.6mmI.D.-250mm
 Mobile phase: Toluene
 Flow rate: 1.0 ml/min
 Temperature: 30°C
 Detection: UV312nm

Sample: Sc₂@C₇₆(I)
 Sc₂@C₇₈
 Sc₂@C₈₀(I)
 C₈₆



Sample courtesy of Prof. H. Shinohara, Department of chemistry, Nagoya University

NACALAI TESQUE, INC

詳しい情報はWeb siteをご覧ください。

ナカライテスク株式会社

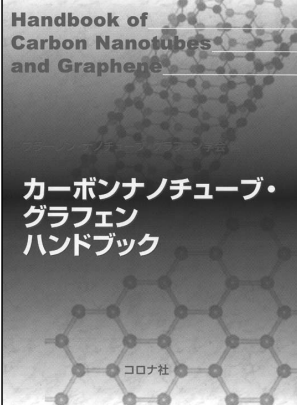
〒604-0855 京都市中京区二条通烏丸西入東玉屋町498

価格・納期のご照会 フリーダイヤル 0120-489-552
 製品に関するご照会 TEL:075-211-2746 FAX:075-211-2710
 Web site :<http://www.nacalai.co.jp>

書籍のご案内

◆定価は本体価格+税です。

カーボンナノチューブ・ グラフェンハンドブック

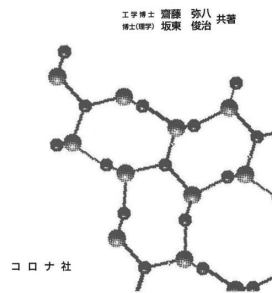


フラーレン・ナノチューブ・
グラフェン学会 編
B5判/368頁
本体10,000円

本ハンドブックでは、カーボンナノチューブの基本的事項を解説しながら、エレクトロニクスへの応用、近赤外発光と吸収によるナノチューブの評価と光通信への応用の可能性を概観。最近囁目のグラフェンやナノリスクについても触れた。

カーボンナノチューブの基礎

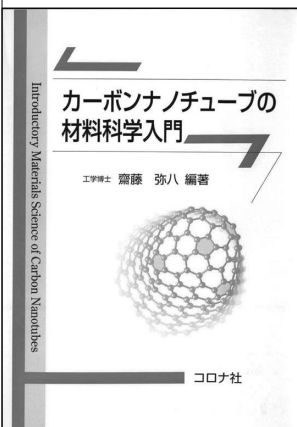
カーボン ナノチューブの基礎



齋藤弥八・坂東俊治
共著
A5判/220頁
本体2,800円

カーボンナノチューブはC₆₀フラーレンに次ぐ新しい炭素材料であり、エレクトロニクスやエネルギー分野への応用が注目されている。本書は、ナノチューブとその関連物質の作製法、構造、物性および応用を平易に述べた入門書である。

カーボンナノチューブの 材料科学入門



齋藤弥八 編著
坂東俊治・中山喜萬・
春山純志・久保佳実
共著
A5判/250頁
本体3,400円

材料科学に新分野を創出し、エレクトロニクスからエネルギー分野まで広範囲な応用が期待されるナノテクノロジー材料の典型物質「カーボンナノチューブ」について、その製法から物性、実用の可能性までを解説した。

関連書籍のご案内

熱刺激電流による電気電子材料評価 —基礎と応用—

岩本光正・田口大 共著/A5判/192頁/本体3,000円

ナノ構造エレクトロニクス入門

土屋英昭 著/A5判/268頁/本体3,600円

基礎からわかるナノデバイス

日本学術振興会「未踏・ナノデバイステクノロジー
第151委員会」編/A5判/252頁/本体3,400円

現代電気電子材料

山本秀和・小田昭紀 共著/A5判/204頁/本体2,600円

太陽エネルギー社会を築く

材料テクノロジー

(I)—材料・デバイス編—

(II)—材料プロセス編—

名古屋大学MBTセンター 編/各巻A5判/

(I)224頁/本体3,000円/(II)196頁/本体2,600円

AFM-ラマン装置

AFM-ラマンの用途

Applications of AFM-Raman

① AFM/ラマン同一領域測定

- AFM：形状、電気・磁氣的性質、機械特性、熱特性などの可視化
- ラマン：有機物、無機化合物、結晶性などの化学情報

② TERS分析

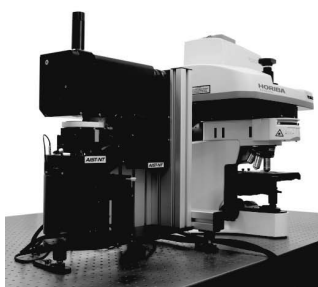
- 回折限界を超える測定空間分解能 (数 10 nm～) によるラマン測定
- ※TERS：Tip Enhancement Raman Spectroscopy

AFM-ラマンの特長・仕様

Advantages and Specifications

■ 仕様・特長

1. ラマン光に干渉しない IR AFM ダイオード
2. ヘッドの移動を必要としないチップ交換
3. カンチレバーのオートアライメント
4. TERS 用 高 NA 対物レンズ (0.7 NA)



Smart SPM + XploRA



Combscope + XploRA INV

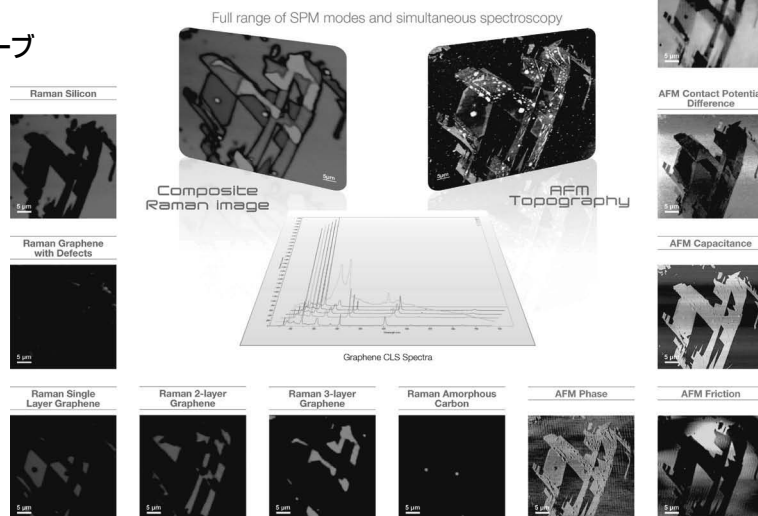
アプリケーション例

Application Examples

■ 主なアプリケーション

- カーボンナノチューブ
- 生物構造
- グラフェン
- ナノワイヤ
- ポリマー
- SERS 基板
- 半導体

Raman-AFM

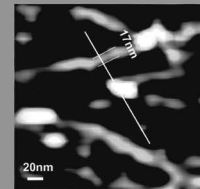


Data courtesy of Prof. Hiroshi Uji of KU Leuven

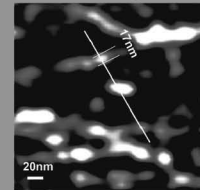
TERS

Label-free chemical characterization with nanoscale resolution

SWCNT STM Image



SWCNT TERS Image G Band



株式会社 堀場製作所

本社 〒601-8510 京都市南区吉祥院宮の東町2番地 TEL: (075)313-8121 <http://www.horiba.com/jp/scientific/>
 ●東京(03)6206-4717 ●名古屋(052)936-5781 ●大阪(06)-6390-8011 ●福岡(092)292-3593

●製品の技術的なご相談をお受けします。 [カスタマーサポートセンター](#) フリーダイヤル 0120-37-6045

Action for innovation

ELIONIX

ナノテクノロジーの進化を支える

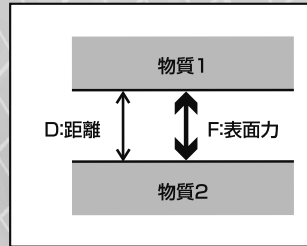
新製品

表面力測定を新たな領域へ
“高い再現性”を実現

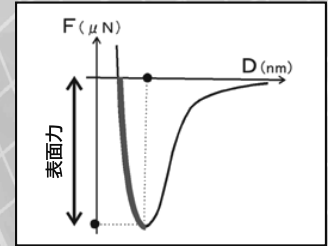


ESF-5000 表面力測定装置

表面力とは、接触した2つの物質表面を引き離すために必要な力。



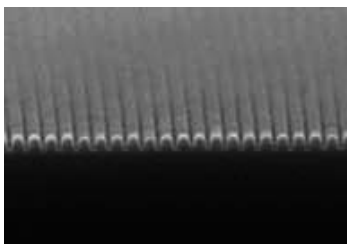
表面力の概念図



2つの物質表面の間に働く力と距離

世界をリードするエリオニクス の 微細加工技術と精密測定技術

超高加速電圧 125kV
超微細、高速描画を実現



4nm 極細線 Pitch 35nm



ELS-F125 超高精細高精度電子ビーム描画装置

<http://www.elionix.co.jp>

株式会社 エリオニクス

[本社・工場・ショールーム] 〒192-0063 東京都八王子市元横山町3-7-6
TEL.042-626-0611 FAX.042-626-6136

[ナノテクシステムセンター] 〒192-0012 東京都八王子市左入町279
TEL.042-692-0610(代表) FAX.042-692-0690

[西日本営業所] 〒563-0025 大阪府池田市城南1丁目9-22グリーンプラザ2F
TEL.072-754-6999(代表) FAX.072-754-6990





インテル® Parallel Studio XE 2015

シミュレーションを高速化

バージョン 2015 より、インテル® Composer XE、インテル® Parallel Studio XE、インテル® Cluster Studio XE が統一され、『インテル® Parallel Studio XE』ブランドとして生まれ変わりました。

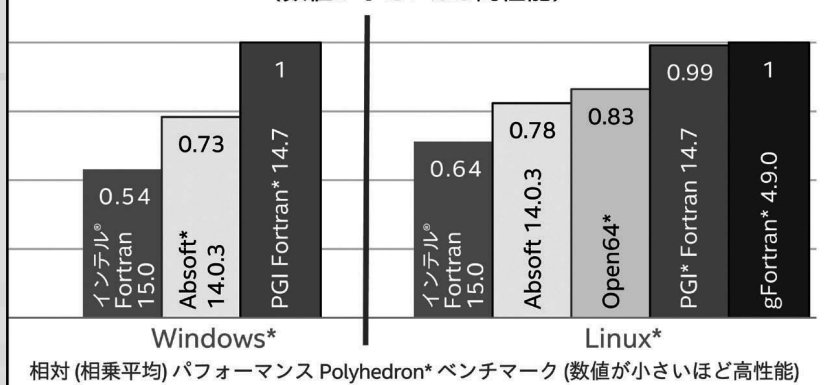
開発のニーズにあわせて、3 種類のエディションを提供します。

コンパイラ ライブラリー	▶ Composer Edition (旧名称: インテル® Composer XE)	▶	<ul style="list-style-type: none"> 最新プロセッサの性能を最大限に引き出せるように、最適化されたバイナリを自動生成する Fortran、C/C++ コンパイラ 最適化されたパフォーマンス・ライブラリーと並列化モデル
解析	▶ Professional Edition (旧名称: インテル® Parallel Studio XE)	▶	Composer Edition の機能に加え、パフォーマンス分析、マルチスレッド化のアドバイス、高度なメモリー/スレッド・エラー・チェック機能を提供
MPI	▶ Cluster Edition (旧名称: インテル® Cluster Studio XE)	▶	Professional Edition の機能に加え、最適化された MPI ライブラリー、MPI アプリケーションのエラーチェックおよびチューニング機能を提供

インテル® Parallel Studio XE 2015 の主な新機能

- 新しい標準規格に対応 (C++11、Fortran 2003/2008、MPI-3.0、OpenMP 4.0)
- インテル® グラフィックス・テクノロジーの解析に対応
- メモリー使用量の増減を解析しグラフ表示
- インテル® Xeon Phi™ コプロセッサに対応した並列化アドバイスツール

インテル® Fortran コンパイラによる優れた Fortran アプリケーション・パフォーマンス – Windows*/Linux* (数値が小さいほど高性能)



システム構成: ハードウェア: インテル® Core™ i7-4770K プロセッサ @ 3.50GHz, ハイバースレディング無効, 16 GB RAM; ソフトウェア: インテル® Fortran コンパイラ 15.0, Absoft* 14.0.3, PGI* Fortran* 14.7, Open64*, gFortran* 4.9.0; Linux* OS: Red Hat® Enterprise Linux® Server release 6.4 (Santiago), カーネル 2.6.32-358.el6.x86_64; Windows* OS: Windows* 7 Enterprise SP 1; Polyhedron Fortran ベンチマーク (www.polyhedron.com)

性能に関するテストに使用されるソフトウェアとワークロードは、性能がインテル® マイクロプロセッサ用に最適化されていることがあります。SYSmark* や MobileMark* などの性能テストは、特定のコンピューター・システム、コンポーネント、ソフトウェア、操作、機能に基づいて行われたものです。結果はこれらの要因によって異なります。製品の購入を検討される場合は、他の製品と組み合わせた場合の本製品の性能など、ほかの情報や性能テストも参考にして、パフォーマンスを総合的に評価することを勧めます。*その他の社名、製品名などは、一般に各社の表示、商標または登録商標です。ベンチマークの典拠: インテル コーポレーション

最適化に関する注意事項: インテル® コンパイラは、互換マイクロプロセッサ向けには、インテル製マイクロプロセッサ向けと同等レベルの最適化が行われない可能性があります。これには、インテル® ストリーミング SIMD 拡張命令 2 (インテル® SSE2)、インテル® ストリーミング SIMD 拡張命令 3 (インテル® SSE3)、ストリーミング SIMD 拡張命令 3 補足命令 (SSSE3) 命令セットに関連する最適化およびその他の最適化が含まれます。インテルでは、インテル製ではないマイクロプロセッサに対して、最適化の提供、機能、効果を保証していません。本製品のマイクロプロセッサ固有の最適化は、インテル製マイクロプロセッサでの使用を目的としています。インテル® マイクロアーキテクチャーに非固有の特定の最適化は、インテル製マイクロプロセッサ向けに予約されています。この注意事項で対象としている特定の命令セットに関する詳細は、該当製品のユーザーズガイドまたはリファレンス・ガイドを参照してください。改訂 #20110804

無料評価版はこちら ➡

<http://www.xlsoft.com/intel>

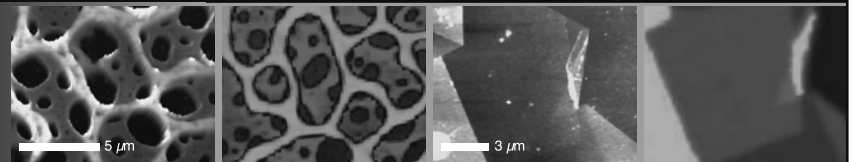
製品の詳細に関するお問い合わせ先:

XLISOFT エクセルソフト 株式会社

〒108-0073 東京都港区三田 3-9-9 森伝ビル 6F
Tel: 03-5440-7875 Fax: 03-5440-7876 E-mail: intel@xlsoft.com

インテル® ソフトウェア製品のパフォーマンス / 最適化に関する詳細は、<http://software.intel.com/en-us/articles/optimization-notice/#opt-jp> を参照してください。
Intel、インテル、Intel ロゴ、Intel Xeon Phi、VTune は、アメリカ合衆国および / またはその他の国における Intel Corporation の商標です。* その他の社名、製品名などは、一般に各社の表示、商標または登録商標です。
© 2015 Intel Corporation. 無断での引用、転載を禁じます。
XLsoft のロゴ、XLsoft は XLsoft Corporation の商標です。Copyright © 2015 XLsoft Corporation.

AFM/共焦点ラマン顕微鏡 alpha300AR



ガラス上のブレンドポリマー 左: AFM形状像 右: 共焦点ラマン像 Si基板上のグラフェン箔 左: AFM形状像 右: 共焦点ラマン像

WITec (ビーテック) 社がAFMと共焦点ラマン顕微鏡を複合した、
全く新しいコンセプトの顕微鏡をご提供いたします。
AFMで微細な表面形状を観察し、ラマンイメージングで表面特性を
マッピングすることができます。

